CARDIFF SCHOOL OF ENGINEERING
CARDIFF UNIVERSITY

EXPERIMENTAL COMPARISON OF BRICKWORK BEHAVIOUR AT PROTOTYPE AND MODEL SCALES

ABBA-GANA MOHAMMED

BEng, MSc

THESIS SUBMITTED TO CARDIFF UNIVERSITY IN CANDIDATURE FOR THE DEGREE OF DOCTOR OF PHILOSOPHY

SEPTEMBER 2006

ProQuest LLC
789 East Eisenhower Parkway
P.O. Box 1346
Ann Arbor, MI 48106-1346

Declaration

This work has not previously been accepted in substance for any degree and is not concurrently submitted in candidature for any degree.

Signed..... (Candidate) Date..19/12/06

Statement 1

This thesis is the result of my own independent work/investigation, except where otherwise stated. Other sources are acknowledged by explicit references.

Signed..... (Candidate) Date..19/12/06

Statement 2

I hereby give consent for my thesis, if accepted to be available for photocopying and for inter-library loan, and for the title and summary to be made available to outside organisations.

Signed..... (Candidate) Date..19/12/06

Acknowledgements

All praise is due to God for all His mercies to us, may He continue to guide us, ameen. I would like to thank Prof. Tim Hughes for his assistance and encouragement all through the research programme. Thanks are also due to the technical staff of Cardiff School of Engineering, particularly Des, Harry, Brian, Len, Mal, Carl and Andrew for all their assistance with my work.

The part sponsorship of my studies by the PTDF in Nigeria is gratefully acknowledged. My appreciation also goes to my erstwhile colleagues in the masonry research group, Richard and Mahmood for their encouragement and support during the course of the work.

I am also grateful to the family of Dr Gana for all their support and friendship during my study in Cardiff. Thanks are also due to Bukar, Suleiman, Dr Junaidu and their families for making our stay here enjoyable. The companionship of the brothers and sisters at the Maktaba is also gratefully appreciated.

Finally I would like to thank my family for their moral and financial support and particularly my wife and kids for their constant and enduring support.

Abstract

A programme of masonry tests has been undertaken at prototype and model scales with a view to comparing their behaviour and strength under various conditions of loading. Characterisation tests were carried out to determine the principal behaviour of the units and mortar before the main programme of masonry test. The testing regime was in two parts: in the first category of tests; compressive, shear, flexural, bond and diagonal tensile strength tests were carried out on prototype, half, fourth and sixth scale models. While in the second category of tests; the effect of different joint thickness, increasing mortar strength and different sand gradings were tested on the compressive, shear, flexural, bond and diagonal tensile strengths of sixth scale model masonry.

The size effect laws for quasi-brittle materials from fracture mechanics were also applied to the test data in order to find out their suitability to masonry model studies.

The knowledge gained on the model scale behaviour of masonry was then applied to a prototype study involving the effect of eccentricity on the compressive strength of masonry as it relates to masonry arches. The sixth model scale was used for this study using four different eccentricities.

On the whole, the model tests showed similar behaviour to the prototype. While there was no discernable scale effect in the shear, flexural, bond and diagonal tensile strength test, the compressive strength tests showed a noticeable scale effect. The parametric study at sixth scale also showed it is possible to use a sixth model to determine the effect of the increasing mortar strength and different grading of sands on masonry strength. However, the effect of increasing joint thickness was difficult to quantify. Indications from the size effect analysis of test data were also encouraging.

The experimental data from the different tests were generally found to be in good agreement with the size effect laws of fracture mechanics. The application study was found to agree with the prototype investigation for low eccentricities but does not correspond well for higher eccentricities. Overall the results showed that it was possible to use model tests to provide masonry strength properties that could be used to determine the structural behaviour real life structures from numerical studies.

Table of Contents

LIST OF TABLES

TABLE OF FIGURES

TABLE OF PLATES

1 Introduction

1.1 Background

Recent programmes of research undertaken using a geotechnical centrifuge on sixth and twelfth scale masonry arch bridges as well as various other model studies on masonry-infilled frames, walls and other masonry components and structures has necessitated further investigation into the small scale experimental structural behaviour of masonry. This recent interest in masonry modelling has arisen because of the need to assess and maybe strengthen existing historic masonry structures like bridges and buildings. For instance there are over 40,000 masonry arch bridges in the UK. Most of these bridges are over 100 years old, while some are as old as 500 years. Increasing traffic speeds and weights have made assessing both the ultimate and serviceability requirements of these bridges necessary.

There is also the need to understand the structural behaviour of masonry structures under extreme natural events like windstorms, floods, earthquakes etc, since some of these events, like flooding have become recurrent actions posing danger to thousands of people inhabiting or working in masonry structures. For example in January 2005, up to £250m worth of damage was caused by flooding due to very heavy rainfall in Carlisle, England[1]. In Iran an earthquake in Bam killed about 35,000 people and flattened about 90% percent of the city's mainly masonry houses[2]. Because of the issues associated with the cost implications of full size masonry tests, coupled with the danger of instrumentation destruction at failure, repeatability and difficult boundary conditions it has become increasingly necessary to carry out such tests at reduced scales.

Small scale centrifuge studies have ranged from investigation into soil/masonry structure interaction by Taunton[3], to a parametric study of the factors that influence the strength of masonry arches by Burroughs[4], as well as studies into modelling repair techniques of masonry arches by Baralos[5] and Miri[6]. In these investigations, a centrifuge was used as a means of simulating full scale gravity stresses on the reduced scale models. But, it is the case that most model studies are undertaken

without recourse to a centrifuge, bearing in mind there are only a few in the UK. Such other studies have shown that it is possible to model masonry behaviour at model scale.

The need therefore arose for a small scale experimental testing programme of masonry with a view to understanding its structural behaviour under a variety of conditions as will be detailed in the next section.

1.2 Objectives

In general the investigation was aimed at understanding of the model scale structural behaviour of masonry structures by testing masonry components to determine the masonry structural behaviour and properties under various conditions, looking at;

- Comparison of masonry behaviour at prototype and model scales under different loading conditions.
- Parametric study of factors affecting masonry behaviour at a suitable model scale.
- Application of size effect laws from fracture mechanics to masonry test results.
- Application of small scale masonry model testing to a prototype investigation.

1.3 Layout

In Chapter 1, reasons for the need of the research as well as the main objectives have been presented.

Chapter 2 contains the literature review and starts with discussion on the strength properties of masonry and factors affecting it. This is followed by a review of small scale modelling of masonry. Discussion also focuses on size effect issues from the fracture mechanics perspective and finally the chapter finishes with a look at factors affecting size effects.

Chapter 3 focuses initially on the considerations that went into the design of the research programme, looking at the choice of materials, method of construction, scales considered etc. Discussion on the constituent materials used in the programme is included as well as the tests on the materials.

In Chapter 4, the different categories of tests undertaken at four scales are presented here. Issues like instrumentation at model scale and fabrication of tests rigs are discussed.

Chapter 5; the results of the masonry tests conducted at different scales are presented and discussed here. The masonry structural behaviour at the different scales is compared for each category of test, while also looking at the effect of scale on the particular strength property like shear or bond. An analysis of the masonry test data with respect to the size effect laws of fracture mechanics is also presented.

Chapter 6 discusses a parametric study on a number factors like joint thickness, mortar strength etc, that affect sixth model scale masonry strength under a variety of conditions.

In Chapter 7, small scale modelling at sixth scale is applied to a real prototype problem. The results from the model scale are presented and compared to the prototype test.

Chapter 8 concludes on the most important findings of the investigation and recommendations for further study are also detailed.

2 Literature Review

Masonry is a composite material, with the constituents having distinct strength and deformation characteristics. However even though masonry has been used for thousand of years it is yet not as well understood as it should be, because of the different properties of its components as well as its failure mechanisms.

Before going into the mechanics of masonry behaviour under different loading conditions, it is necessary to first look at those factors that influence masonry behaviour whatever the loading condition. Because it is these factors that ultimately determine how good or bad a composite, a particular masonry assembly is. It is the interaction between the stiff brick and the less stiff mortar bed that largely determines the overall properties of the masonry assembly under the condition to which they are subjected.

2.1 Some important properties of the units

Masonry consists of individual units of brick, block or stone bound with a jointing material usually mortar. Bricks and blocks are made of fired clay, calcium silicate or concrete. Clay bricks as used in this study are a type of ceramic formed by burning clay or shale at very high temperatures. Physically they are hard, brittle, non-ductile and highly temperature resistant. They are made up of varying composition of silicates and metallic oxides like alumina, kaolinite, mica etc, which are chemically stable and therefore make clay bricks suitable as a construction material.

2.1.1 Suction rate and moisture content of the unit

During the manufacture of bricks, some pores are formed during firing because of the combustion of organic matter. This makes them porous with relatively high suction. According to Sneck[7] the suction rate of the masonry units is the most important extrinsic parameter affecting the fresh mortar, and consequently the properties of the hardened mortar and ultimately the properties of the whole masonry assembly. This is because water suction from mortar by the brick affects the mortar bed as a whole and

the properties of the interface between the unit and the mortar. The suction rate of the units depends also on a number of factors; the water absorption of the unit, rate of absorption and the capillary suction force. The water absorption of the masonry unit gives a measure of the quantity of water that can be removed from the mortar, while the absorption rate gives a measure of how rapidly water is removed from the mortar. The capillary suction force could be important in cases where the unit is made up of material with very fine pores like sand-lime units.

The importance of the amount of water in the mortar cannot be over emphasised, because it is that which determines the rate of hydration of the cement particles, and ultimately the strength of a joint and its adhesion to the unit. To underscore this point Brocken et al[8] under took a Nuclear Magnetic Resonance study of water extraction from mortar during bricklaying and found that, using a particular fired-clay brick most of the water was extracted from the mortar in about 3 minutes. In addition they found that prewetting the same brick by 50% of its saturation value hardly affects the extraction process. It is only when the bricks are nearly fully saturated that all extraction of water from the mortar stops. Closely related to the suction rate is the moisture content of the bricks. The importance of this parameter on masonry behaviour as stated by Harvey[9] is firstly in the expansion/contraction of the masonry units as they come into equilibrium with their surroundings. And secondly in the effect the moisture content of the unit has on the all known physical properties of masonry. Therefore, for the same type of brick, because of the smaller exposed surface area in a model unit compared to prototype unit, it could have a faster rate of coming into equilibrium with the surroundings which could result in a faster suction rate.

2.1.2 Strength and stiffness of the unit

The compressive strength of masonry units is obviously the most important strength parameter from the structural perspective. But due to their high porosity and brittleness, bricks are generally weak in tension and stronger in compression. Their compressive strength varies over a wide range depending on the porosity of the brick. Generally, the more porous is the brick the lower is the compressive strength. With the same brick, the compressive strength of bricks can vary considerably, consequently a coefficient of variation of between 15 and 20% is typical for a

particular sample[10]. The stiffness of clay bricks is approximately 300 times the compressive strength[11] and because of their brittle nature the stress/strain relationship remains linear almost up to the point of fracture. As with all ceramics the strength and stiffness properties of bricks are mainly determined by minute flaws or cracks in their structure. There is usually a random distribution of such flaws in various sizes, and the largest of these will be responsible for the fracture of a solid[12]. According to the Griffith concept, the less surface area there is present, the stronger the material should be, since there is less chance of flaws occurring[13]. This implies that for brittle materials like clay masonry, reduced scale models could be stronger than the prototypes because of this phenomenon.

2.2 Some important properties of mortars

Mortars are used to bed and join masonry units giving them the continuity required for stability and exclusion of weather elements[10]. The proportion of the different constituents is usually determined by how the masonry is to be used, which is governed by the strength requirement of the application, degree of resistance to movement required, degree of frost resistance and rain penetration required etc. Traditionally lime is usually added to sand to make mortar, but nowadays cement-lime-sand, masonry cement–sand or cement-sand with plasticizer are normally used as mixtures for mortar. Lime is added to cement mortar to improve the workability, water retention and bonding properties[14].

2.2.1 Water retentivity

Water retentivity allows mortar to resist the suction of dry masonry units and maintains moisture for proper curing and ensures that hydration of the cement can take place. It quantifies the mortar's ability to retain its plasticity when in contact with the absorptive masonry units. If enough water is not retained by a mortar, hydration will suffer resulting in a poor bond between the brick and mortar[14]. This property of mortar is closely related to the suction rate of a brick, in that, a less absorptive brick and very retentive mortar will not form a good composite, just as a highly absorptive brick and mortar with low retentivity will result in a poor bond. This is very important for model scale masonry because of their relatively thin joints and model masonry assemblies may therefore require a more retentive mortar than a prototype, to ensure that there is sufficient water for hydration of the cement.

2.2.2 Strength and stiffness of mortars

The main agent responsible for the setting and strength development of cement mortars is the cement hydration process. Consequently the higher the cement content in mortar the higher its strength. But because adequate cement hydration only takes place in the presence of sufficient water, the water/cement ratio of mortar becomes one of the most important factors that affect the compressive strength of mortars[14]. There are many parameters that influence mortar strength apart from the water/cement ratio and they include; cement volume, workability and sand grading. The effect of sand grading on the compressive strength has shown a higher strength yield in mortars with coarse sands. While the effect of sand grading on the tensile bond properties of mortars has been discussed by Anderson and Held [15], who found that the finer the grading of sand, the lower the bond strength of the masonry. This suggests that, since very fine sands have to be used in relatively small brickwork models because of the thin joints, the bond strengths of such models may show lower bond strengths to a comparable prototype because of this reason. And generally the higher the cement content of mortar the stronger is the bond while the converse is true for the water to cement ratio.

The stiffness properties of mortar are also important because they greatly influence the stiffness properties of brickwork as well as its strength[10]. The stress/strain relationship in mortars usually shows distinct plastic characteristics.

2.3 Properties of the composite

2.3.1 Compression

Masonry is usually loaded in compression in most situations under which it is used. Under an axial compressive stress on a masonry assembly as shown in Figure 2.1, the softer mortar expands laterally because of the Poisson effect, but because of the bond and friction between the mortar and unit, it is confined and unable to expand freely which results in a state of lateral tension in the unit and triaxial compression in the mortar[16]. It is this state of stress that causes the vertical tensile splitting cracks in masonry observed in many situations. In some cases failure of masonry can be due to shear failure along some line of weakness, this type of failure is usually as a result of the mechanical properties of the mortar being similar , or even greater than that of the unit[17]. In the verification of a theoretical approach to the modelling of masonry

behaviour and its elastic properties, McNary and Abrams[18] found that the strength and deformation of stack bonded masonry specimens were influenced primarily by the mortar, but that was not the limiting failure criteria. They concluded that even though failure of the masonry was as a result of the lateral tensile strength of the unit, it is the mortar that induces the tensile stresses.

A variety of factors affect the compressive strength of masonry as shown in Table 2.1. Some of these factors, like the unit characteristics are determined in the manufacturing process, while others like mortar properties are influenced by variation in constituent materials, proportioning and mixing[19]. Even though masonry strength is not directly proportional to the mortar strength it does however still increase with increasing mortar stiffness. This is because as detailed above the tensile stresses in the unit are due to the mortar. An inherent property of the unit that plays a very important role in determining the compressive strength is the tensile strength of the units. This is influenced by the clay quality, firing temperature, porosity etc[17].

Hendry[19] reported that compressive strength of masonry varies roughly as the square root of the unit strength and the third or fourth root of the mortar strength. Apart from the strength of the unit, the other properties of the unit that have important influences on the masonry characteristics include the bed joint thickness and the unit height. An increase in the former has been reported by Francis et al[20] to decrease the compressive strength of four unit high stack bonded masonry made with perforated clay units. Tests by Porto et al[21] have also shown that the compressive strength of clay block masonry wallettes made with thin layer mortar of 1.3mm average thickness were 20% more than those made with mortar of 12mm average joint thickness. This implies that model masonry with very thin joints could show a stronger strength due to thinness of the joint alone. Hendry[14] also states that the compressive strength of masonry decreases with increasing unit height due to platen restraint. The influence of the unit compressive strength on that of the masonry compressive strength suggests that the Griffith concept as detailed in section 2.1 would also be applicable to masonry strength which could result in a higher compressive strength in small scale masonry models.

Various empirical relations have been developed by different authors to determine masonry strength from the properties of the unit and the mortar. A review of which

can be found in Hendry [19]. One of such formulae for the characteristic strength of masonry provided by Eurocode 6 (EC 6)[22] is given as Equation 2.1

$$f_k = Kf_b^{0.65} f_m^{0.25} \quad N/mm^2 \qquad (2.1)$$

Where K is a constant taken as 0.6 for group 1 masonry units, f_b is the normalised compressive strength of masonry units in N/mm^2 and f_m is the mean compressive strength for general purpose mortar.

The normalised compressive strength of the masonry units f_b, is obtained by multiplying the mean compressive strength of the samples by a conversion factor of 1.2 to get it to an equivalent to the air–dry condition, which is a requirement before being multiplied again by the shape factor δ of 0.85 from the table of shape factors in EC 6.

From the findings of McNary and Abrams[18], they also found that the theoretical model they used to predict the compressive strength of masonry from the tests they carried out, underestimated the actual strength from the test results by about 35%. This they attributed to among other things, the assumption of uniform lateral strain conditions at the brick-mortar interface. This assumption does not of course reflect the unique property of the interface.

The deformation properties of masonry seem to be determined mainly by the softer mortar bed, therefore masonry stiffness increases with increasing mortar strength. However masonry stiffness is still often directly related to brick strength[23]. The influence of mortar in determining the stiffness properties of masonry is best illustrated from the findings of Lenczner[10], which showed that there was almost no change in the stiffness of masonry made with 1: 1/4:3 mortar using units with very dissimilar strengths; one with a mean strength of 32.6 N/mm^2 and the other 90.2 N/mm^2. The stiffness properties of masonry are different in the two orthogonal directions because of the anisotropy of the unit[24-26]. This could be due to way the clay brick is extruded and then fired. This further illustrates the difficulties in accurately modelling the properties of masonry.

Equations for the determination of masonry stiffness show that some of these relations are dependent on unit strength, like that of Plowman[23], while others are dependent on

the masonry strength as those reported by Sahlin[11] and the ones used in BS 5628[27] and Eurocode 6 (EC 6)[22]. Brooks and Baker[26] use an analytical approach to propose a formula shown as Equation 2.2 that estimates masonry stiffness, E_{wy} depending on the unit strength, f_{by}, and mortar strength, f_m, as well as a coefficient that takes into account the water absorption properties of the unit, γ_{wa}.

$$\frac{1}{E_{wy}} = \frac{2.15}{f_{by}} + \frac{0.175}{\gamma_{wa}} \tag{2.2}$$

An empirical relation from EC 6[22] for the masonry stiffness uses a very simple approximation given as Equation 2.3

$$E = 1000 f_k \tag{2.3}$$

Where f_k is as previously defined. Knutsson and Nielsen[28] observed that it is rather too simplistic to use this approximation, since the stiffness and strength are not uniquely related for different types of masonry.

2.3.2 Shear

The shear strength of masonry is of significance when designing for lateral forces on walls. Resistance of a wall to horizontal shear increases as the normal load it is subjected to, is increased. Many authors[10, 11] have found the relationship between the shear strength, τ and the precompression force follows a Coulomb type relationship given by Equation 2.4.

$$\tau = \tau_0 + \mu\sigma_C \tag{2.4}$$

where τ_0 is the shear strength at zero precompression, μ is an apparent coefficient of friction and σ_C is the normal compressive stress. This relationship holds up to a certain value of the normal precompressive stress beyond which joint failure between the unit and mortar is replaced by cracking through the units. The limiting value for the normal compressive stress for clay brick masonry has been determined to be around 2.0 N/mm^2 [14]. For higher values of the compressive stress, cracking through the units is further replaced by crushing failure of the masonry. The entire failure envelope for the different failure stages is shown in Figure 2.2 according to the failure theory developed by Mann and Muller[19] in Hendry[19]. This failure envelope is

slightly different to the one proposed by Riddington and Ghazali [29], in their case at higher compressive stresses of above 2.0 N/mm^2, tensile failure of the mortar is replaced by a joint slip failure as determined using triplet specimens. Their findings also showed that the average bond shear strength of masonry reduces as the degree of bending, to which the specimens were subjected, is increased. The degree of bending in the specimens was varied by moving the support from a position that is just close to the joints to the edge of the two outer units, while the loading condition were kept constant. Set up of the triplet test will be discussed in Chapter 4.

In reporting on some aspects of a programme of tests involving about 1300 triplets, Jukes and Riddington[30] found that the degree of bending as defined earlier plays an important role in the shear strength of masonry. They recommended a test arrangement as in BS EN 1052-3[31] that minimises the effects of bending on the specimen. This is because bending causes a deviation from the normal Coulomb criterion for shear failure, which is that of linear shear stress/precompression stress. This finding would be more critical for model tests since the boundary conditions for minimum bending in such tests would be relatively difficult to achieve than for a prototype test.

2.3.3 Flexural strength

When masonry is required to withstand out of plane lateral loads knowledge is needed of its flexural strength. In most situations because of the way masonry is built, it is the flexural strength normal to the bed joints, σ_{normal} that structural engineers are interested in. However if masonry is supported on its vertical edges, by say columns, but free at its upper and lower edges, its flexural strength parallel to the bed joints, $\sigma_{parallel}$ also becomes important. The flexural strength in this direction is usually about 3-6 times more than the flexural strength normal to the bed joints[11].

If the brick-mortar bond is good, the flexural strength parallel to the bed joint is limited by the modulus of rupture of the units. But if the adhesion is poor, the limiting factor is the shear strength of the unit mortar interface in the bed joints[14]. In the first instance the failure takes the form of a crack through the perpend joints and units. While in the second case failure is in the form of a zigzag through the bed joints and perpend joints[32].

The limiting factor in the flexural strength normal to the bed joints is either the bond strength or the tensile strength of the mortar. Failure is usually occasioned by failure in the mortar joint, or in the interface between the mortar bed joint and the unit or sometimes partly in the mortar and unit[11]. Many factors affect the flexural strength in this direction, some of which, as discussed by Sise et al [33], include the moisture characteristics of the unit and mortar composition, as well as the joint thickness and curing conditions. But they concluded that the joint thickness was the single most important factor affecting the flexural strength normal to the bed joints. Their findings also showed that there is an optimum moisture content in the units for good bond development, beyond which the flexural bond strength begins to drop. This is corroborated from findings by Fried and Li[34], who also found that the flexural bond strength increases slightly when the units were fully saturated. However in a recent paper by Reda Taha et al[35], they found that the volume of cement in the mortar is the most important parameter governing bond strength in masonry. There appears to be no unanimity on the factor that has the most influence on bond strength so far, probably because there are many variables involved and the test methods and curing conditions are also different. However because of the thin joints in small scale masonry models, the flexural strength normal to the bed joint could be lower due to findings by Anderson and Held [15] (section 2.2.2) that mortar with fine grained sand result in a lower bond strength.

2.3.4 Tensile strength

Direct tensile stresses in masonry are mainly due to in-plane loading effects caused by wind, eccentric gravity loads, and thermal/moisture movements or by foundation movement[14]. The tensile strength of masonry is generally controlled by the tensile bond strength at the brick-mortar interface. This is influenced by many characteristics of the units and mortars as discussed by Groot [36], who found the moisture content/suction of the unit as one of the main variables affecting the tensile bond strength, as well as the mortar composition (including sand grading).

The nature of the bond is mechanical-chemical as reported in a paper by Shrive and Reda Taha[37] from findings by Dubovoy and Ribar[37]. The chemical nature of the bond is due to the covalent or Van der Waals bond between the unit and cement hydrates. While the mechanical bond is due to the mechanical interlocking of the

hydration products transferred into the surface pores of the unit. However, it was argued that the mechanical bond is much stronger than the chemical bond.

Various methods have been used for the determination of the bond strength of masonry, and can be divided into; direct tensile bond methods like the couplet test and the flexural bond strength methods like the bond wrench test. The former use direct tensile principles to test the joints under consideration while in the latter, bond strength is determined by subjecting the specimen to some form of bending stress. In a review of bond strength test methods by Jukes and Riddington[38], the authors were of the view that a direct tensile bond test method is more appropriate for testing the in-plane bond strength of masonry. While the bond wrench test is ideal for testing the out-of-plane bond strength of masonry, in their view the flexural bond strength tests measure the bond strength of the edge of a joint, which could be different to that at the centre. However, whatever the deficiencies of the bond wrench test, it provides an easy and repeatable way to determine the bond properties of masonry as evidenced in its recent adoption in the British Standards as a test method for determining the bond strength of masonry; BS EN 1052-5:2005[39].

2.4 Structural models

A structural scale model is any structural element or assembly of structural elements built to a reduced scale (in comparison with full size or prototype structures) which is to be tested, and for which laws of similitude must be employed to interpret the results.[40]

Structural modelling involves a broad range of studies on full scale structures, also called prototypes, in virtually all fields of physical engineering under a variety of loading conditions including; static, dynamic, seismic, wind, zero gravity etc.

2.4.1 Classes of structural models

Models can be classified into different categories based upon their intended purpose. Questions that arise in model application studies decide which class of model is suitable for a particular research. Such questions could be whether an elastic response is sufficient or a complete loading behaviour is necessary to understand the mode of failure of the model.[41]

2.4.2 Elastic model

Elastic models as the name suggests are types of models that are used for studies in the elastic range only. The homogenous elastic material for the model may not necessarily have any semblance to the prototype material but the model still has a direct geometric correlation to the prototype. The post cracking behaviour of masonry or concrete and the post yield behaviour of steel cannot be predicted with this type of model.

2.4.3 Indirect model

An indirect model is a type of elastic model that is used to obtain influence diagrams for reactions, shearing forces, bending moments, axial forces etc. Load application in such models has no direct bearing to the actual loads expected on the prototype, since load effects are determined from superposition of the influence values. Thus these models do not have a direct physical resemblance to the prototype. Their application is less today as computers are now used for purely elastic calculations.

2.4.4 Direct model

A direct model is a geometrically similar model to the prototype in all ways, and load application in this model is the same as in the prototype. Strains, deformations, and stresses in this model for a particular loading condition are typical of similar quantities in the prototype for the corresponding loading condition. An elastic model can also be a direct model.

2.4.5 Strength model

A strength model is also called an ultimate strength, realistic or replica model; it is a direct model that is made of materials that are similar to the prototype materials such that the models will predict prototype behaviour for all loads up to failure. The models under investigation in this research project would be looking at strength behaviour as well as other effects.

Other model types include wind effects models, dynamic models, design models, photomechanical models etc.

2.5 Brick masonry modelling

In the last century, the first small scale masonry model test was perhaps the one carried out by the Road Research Laboratory (now TRL) under the auspices of the RAF. The aim of the test was to predict the effect of bombing specific German dams during the Second World War. 5 million bricks of approximately 5mm by 7.5 mm by 10 mm were used to represent the dam at a scale of 1:50. The model test showed that a breach could be produced by a bomb from an aircraft at some predetermined distance from the crest of the dam. This proved to be the case when the Moehne and Eder dams were breached by RAF planes bombardment in 1943.[42]

2.5.1 Uniaxial and biaxial strength tests on piers and walls

H. Vogt [43] carried out a series of tests in the 1950's, on fourth scale model bricks of size 60mm by 29mm by 20mm assembled in the form of pillars, of cross section 60mm by 60 mm and 300mm high (about 12 courses). The pillars consisted of two model bricks with the joints at 90° in alternate courses. 8 pillars were tested in 4 groups, with 2 pillars in each group. Group 1 pillars had cement mortar joint; Group 2 had lime-cement mortar, Group 3 lime mortar, while Group 4 had cardboard strips as joints. The results showed that, the mortar strength exhibited a decreasing trend from Group 1 to 3, Group 1 being the strongest. Similarly the compressive strength of the pillars also showed this decreasing trend from Group 1 to 3. The pillars in Group 4 remarkably had strength of about 50% more than that of Group 3. Based on the results the author concluded that the tensile strength of the joint material played an important role in the overall strength of the pillars. Further tests carried out on reinforced pillars in a second programme of tests, led the author[43] to conclude that it was feasible to carry out test on model scale bricks with some degree of confidence.

A testing programme conducted by Hendry et al [44], concluded that it was possible to reproduce the strength of full scale brickwork strengths from tests on model brickwork. The model tests on one third and sixth scale model bricks consisted of replicating tests carried out on full scale masonry specimens, by other researchers, in three categories of tests. The first series of tests were concerned with the relationship between strength of brickwork and mortar strength. In the second series the effects of eccentricity and slenderness were considered. Lastly, in the final programme of tests the effect of elastic restraint afforded by slabs to wall connections was investigated. In

the first category of tests, square piers consisting of 2 bricks per course laid at right angles to the bricks in the next course in an alternate fashion and 11 courses high, were tested in compression. Both third and sixth scale piers were tested in this manner using mortars of different mixes and strengths. The variation of brickwork strength against mortar strength using 25.4mm (1 inch) cubes showed good correspondence between the model and full scale results although there was considerable scatter in the results. The strength axes were normalised with respect to the brick strength to give dimensionless scales to allow for comparison of the full scale and model scale results. The failure pattern in both full and model tests also was similar with the brickwork failing under horizontal tension. Mortar strengths obtained from 25.4mm (1inch) cubes were found to be more appropriate for the model scale in place of the traditional 70.6mm (2.78) inch cubes.

To investigate the effect of eccentricity and slenderness in the second group of tests, piers of both third and sixth scale models of varying heights were tested with knife edge loads at various eccentricities. The results again showed acceptable agreement between the full scale and model scale results even in their mode of failure, which was mainly by buckling.

In the last batch of tests sixth scale model walls loaded between reinforced concrete slabs were modelled. As was the case with the full scale tests, the model walls generally failed by vertical splitting, showing good correspondence between the two tests in terms of the failure pattern. Because of the difference in the brick strengths in the full scale and model scale tests, it was necessary to adjust the full scale brick strengths by application of factor using a relationship derived by Davey and Thomas[44] in Hendry et al [44], in order to allow for comparison between the two scales. From these adjustments it was seen that there was good agreement between the brickwork strength in the model and full scales. One area of divergence in the test results was in the modulus of elasticity of the model walls which was about half the value at full scale. No explanations were given by the authors for that behaviour and as such no comparisons were drawn in that regard.

Sinha and Hendry[45] investigated the effect of brickwork bond on sixth scale model brick walls and concluded that the different bonds considered did not affect the brickwork strength in any significant measure. A note was also made of the failure

mode of the walls, which was typically by vertical splitting, underlying the importance of the tensile strength of the brick, in the behaviour of the brickwork in compression.

In another study by Sinha and Hendry[46] the relationship between brickwork strength under compression and brick crushing and tensile strengths was explored using sixth scale models walls and piers along with other parameters. Generally it was observed that brickwork strength increased with the compressive strength of the brick used but not in direct proportion. In contrast, the relationship between the brickwork and tensile strength was reasonably linear, probably due to the failure of the brickwork by tensile splitting. Thus it was suggested by the authors that the tensile strength of bricks appeared to be a better indicator of brick performance in brickwork than the conventionally used compressive strength test.

Khoo and Hendry[47] carried out a series of tests on third scale model bricks in order to establish a failure criterion for brickwork in compression. The basis of their failure theory was that an element of brick under uniform vertical compression within a masonry panel is influenced by a combination of vertical compression and bilateral tension. The latter as result of differential lateral strain between the brick element and mortar bed. The horizontal mortar joint is therefore in a state of triaxial compression, comprising a vertical compression and a pair of lateral compressions. According to the authors, this interplay of forces causes a slightly concave bi-axial compression-tension failure envelop for brick as the results of their investigation showed, indicating a greater interaction of compression –tension than the theoretical curves of other researchers. The main draw back of the earlier theoretical failure theories on masonry is their over simplification of the interaction between the brick and mortar under stresses, which may not be elastic because of the heterogeneity of the mortar.

In an investigation to determine the strength of brickwork under biaxial tensile and compressive stress by Samarasinghe and Hendry[48], the authors used sixth scale model bricks for their research. Panels measuring 150 x 150 x 18mm and 230 x 240 x 18mm were used for the investigation. From their results the authors concluded that the biaxial strength of brickwork cannot be represented wholly by a two dimensional relationship between the principal stresses without considering a third variable; the bed joint in relation to the principal stresses. Thus the failure surface of brickwork in

biaxial stress must be defined by a three dimensional surface namely; the major principal stress, a minor principal stress and their orientation relative to the bed joint. Using the results of this study the authors developed a finite element model to simulate the in-plane behaviour of brickwork[49]. By the use of shear wall tests to validate the model, they showed that the crack pattern and associated stress levels can be predicted, so also could the load condition at failure which could be estimated provided that there was no extensive cracking at the base of the wall.

Page [50] investigated the biaxial compressive strength of brick masonry using half scale model bricks. The results showed that masonry exhibits directional properties that require the use of a three dimensional surface in terms of the two principal stresses and their orientation to the bed joint as highlighted in the preceding paper[49]. The author concluded that the bed joint orientation did not play a significant role in the failure mode of the masonry panels except in cases where one of the principal stresses was dominant. He also found that for most principal compressive stress ratios, the uniaxial panel strength with the load normal to the bed joint underestimated the biaxial compressive strength irrespective of the bed joint orientation.

Egermann et al[51] undertook a testing programme to compare the strength and stiffness relationship of brick masonry at different scales. Tests were carried out at full scale, half scale and fourth scale in order to compare the strength- stiffness behaviour at these scales. The results were correlated with those of an earlier study by Hendry and Murthy[44], and both showed that model brickwork strengths can be reasonably used to predict prototype brick strengths for the same brick type. However the stiffness of the model walls was observed to decrease in proportion to the scale. This according to the authors could be due to poorer compaction of the mortar bed in the model walls and or to the size of the walls (to use the analogy of soils, where the larger particles have a higher stiffness ratio.)

In a recent research carried out to investigate the behaviour of brickwork at small scale, Hughes and Kitching[52] found that using sixth scale model bricks cut from full scale bricks, it was possible to replicate prototype strength behaviour in line with previous authors. However the sixth scale model specimens were about 50 % as stiff as the prototype specimens to support the point made in the last paper and first raised

by Hendry and Murthy[44], that the deformation and stiffness behaviour of full scale brickwork is not properly modelled at model scale.

2.5.2 Shear strength tests

One storey height, 3 bay, brick wall panels in the form of cross walls made of sixth scale model bricks were tested by Murthy and Hendry[53] in order to determine the correlation between the shear strength of the panels and the vertical compressive stress they were subjected to. The horizontal shear force was applied at the floor slab level through a hydraulic jack. Results obtained from the model tests compared well with the shear resistance calculated from the coefficient of friction of a pair of bricks under vertical stress, with a mortar bed in between them. The mortar bed was prevented from making a bond in between the bricks by separating them during setting with a thin film of paper. A modified soil mechanics shear box was used for the determination of the coefficient of friction, and was found to be approximately 0.72.

Further tests[53] on sixth scale 3 storeys, 3 bay, cross wall structures were carried out to investigate how the rigidity of shear panels affected the ultimate strength of the structure. The lateral loading was applied at right angles to the cross-walls, and the dead load of the structure increased six fold in order to achieve correct scaling of the dead load stresses. By adding the shear walls in stages in the bays, their effect on the rigidity of the structure was observed to vary considerably from 15.7 times with one bay infilled to 104 times with infill in all three bays compared with the initial structure without infill. The ultimate load was determined with all the bays infilled. The results established the reliability of model scale results even though no direct comparisons were made to full scale tests.

In similar work by Kalita and Hendry[54], on lateral loading of a sixth scale model cross wall structure of 5 storeys, they concluded that the model results showed reasonable agreement with finite element analyses of the same structure, provided that the shear modulus of the brickwork was varied with the level of precompression.

Sinha et al[55] carried out model and full scale tests on five storey cross wall structures under lateral loading to simulate wind type loading conditions. The model structure was made of sixth scale bricks and loaded with a purpose built frame for the

application of the loads, while the full scale tests were undertaken on a five storey building in a disused quarry, where the horizontal loads were applied by jacking the structure against the quarry face. The deflection results of the two tests showed good agreement at low stresses but were considerably greater for the model structure at higher stresses.

2.5.3 Lateral and flexural load tests

One third model scale wall panels were used by Baker[56] to investigate their behaviour under wind type loads. All the panels were 27 courses high and 10, 15 or 20 bricks long, giving aspect ratios of 1, 1.5 and 2 respectively. In order to achieve uniformity in the wall construction the panels were laid on their sides and mortar vibrated into the joint spaces while the bricks units were clamped in position on a flat base over a vibrating table. This ensured uniformity of the joints in the walls and a rapid construction time of 10 minutes for each wall. Testing was also carried out in this orientation; that is with the panels cast horizontally on their sides and then loaded through a water bag that exerted an upward pressure on the walls. Thus the effect of gravity is missing both in the actual construction of the specimens and the testing. Since the paper was focused mainly on highlighting the manufacture and testing of the wind panels nothing significant was reported on the findings from the test results, apart from a mention that the test provided an accurate and simple reading of data.

Duarte and Sinha[57] investigated the effect of lateral pressure on half scale model brickwork panels with openings in the middle in order to understand the real behaviour of brickwork cladding with window openings, as found in buildings. The lateral load was applied until failure via an air bag placed in between the panels and the loading frame. Different aspect ratios and boundary conditions were explored in the testing regime, but in each case the opening was positioned in the centre of the panels. The results of the experimental programme were compared to a yield line analysis and an elastic analysis using a standard computer program, with the former giving results that were in reasonable agreement to the experimental investigation. The results also showed that the flexural tensile strengths of the specimens normal and perpendicular to the bed joint were similar.

In out of plane loading tests for the investigation of the influence of size on the flexural strength masonry, Lourenco and Barros[58] tested a number of block masonry

panels of varying height, ranging from 100mm to 300mm. The results showed that there was a reduction in the flexural strength as the specimen height was increased. In concluding the authors suggested that the masonry codes should include provisions for making the flexural strength dependent on specimen height.

2.5.4 Reinforced masonry

Suter and Keller[59] used third model scale brickwork to determine the ultimate shear strength of reinforced brickwork lintels and compared the results to three other tests on full scale lintels. All the specimens were five courses high while the width varied from just a single brick to two bricks separated by a grouted and reinforced cavity. The specimens were tested by a two point loading arrangement to bring about a shear failure. Overall the results of the third scale and full scale tests showed good agreement, and therefore, the authors concluded that it was possible to use small scale bricks to model the shear behaviour of full scale lintel beams.

2.5.5 Prestressed masonry

Third model scale bricks were utilised for an investigation of the behaviour of post tensioned brickwork fin walls by Daou and Hobbs[60]. The 1.52m model cross walls were constructed on a reinforced concrete base and were tested while held in position at the bottom in the form of a cantilever. Prestressing and load testing were carried out on the same day to eliminate time dependent prestress losses. A lateral loading system was used to stimulate earth pressures as obtained in retaining walls. Variables in the testing programme were prestress force, steel area and the arrangement of the lateral loading system. The data obtained provided useful knowledge on the understanding of how the variables interacted.

2.5.6 Seismic effect studies

Reduced scale models of masonry buildings have been used to study the effect of earthquakes because of their relative ease of construction and testing compared to full size buildings. In this area, shaking table tests have been extensively employed to investigate the response of masonry models of different forms construction.

Qamaruddin et al[61] used fourth scale models to test the suitability of a so called sliding building model concept for earthquake zones before half scale models were later employed in the actual testing programme. The authors found that lintel bands

and steel at the corners and junctions of walls, as well as at the jambs of openings were adequate in giving the required strength and energy absorbing capacity even for the severest of earthquakes. Other shaking table tests by various authors[62-65] have shown that scale models can be conveniently used to undertake seismic effect investigations of masonry buildings.

2.5.7 Centrifuge modelling

The use of a centrifuge for modelling of masonry structures at small scale was perhaps pioneered by Taunton[3], who used one to study the soil/masonry structure interaction as it related to arch bridges. Using a geotechnical centrifuge to accurately scale up the gravity stresses of a sixth scale model of an arch bridge, the results showed good correlation with documented failure mechanism of similar full scale arches and good modelling of peak loads. Other results of distorted twelfth and eighteenth scale models having the same width as the sixth scale model but with correctly scaled ring thickness and span length did not show good correspondence to the prototype tests. The author attributed this to defects in the construction of the models because of their very small sizes. Of particular importance was the observance of the separation of the arch ring in the centrifuge model tests, a phenomenon hitherto induced only by artificial means in conventional small scale model tests. This finding in addition to the repeatability of modelling peak loads led the author to the conclusion that a centrifuge can be effectively used for small scale modelling of masonry arch behaviour.

Hughes et al[66] have discussed the advantages of using a centrifuge to undertake small scale modelling of masonry. The paper highlighted the areas centrifuge modelling could be used in like seismic effects on masonry, blast action on structures, masonry arch bridge modelling etc. They concluded that the main benefit in using the centrifuge lies in accurately scaling gravity stresses while carrying out the tests in highly controlled environment and flexible conditions.

Sicilia[67] undertook a study of a 3D masonry arch at Ponypridd, Wales (built by William Edwards) using both a 1/55 centrifuge model and FE analysis. His research confirmed that centrifuge modelling can be used to produce repeatable results on complex masonry arch structures. Further research explored the small scale modelling of the repair techniques of arch bridges using a centrifuge. Work by Barolos[5] showed

the feasibility of using a centrifuge to model different repair techniques in arch bridges. These included the use of steel bars, dowels and meshes within grout and microconcrete in damaged arches.

Another investigation by Burroughs[4] looked into the parameters that influence the strength of masonry arches using a centrifuge. A series of 1/12 scale models with full size spans of 6m were made and tested for the effect of arch barrel thickness, masonry strength, loss of mortar etc under serviceability and ultimate loads. On the whole the findings gave new insights into the behaviour of masonry arches behaviour under ultimate and serviceability loads.

2.6 Models and size effects

Historically the value in scale models lies in being able to predict the behaviour of a prototype model from the scale model. Presently small models are usually used to validate numerical models which will then be used to predict the structural behaviour of whole structures like model arch bridges and buildings. However for a researcher to be able to predict this with some degree of confidence, knowledge is required of the effect of size or scale on the model material. This becomes more important in the case of composites like masonry where the constituent brick and mortar have different properties. Therefore an appreciation is needed of the effect of size or scale on the model material, if reliable model studies are to be made.

2.6.1 Size effect

Scale effect is a phenomenon related to the change, usually an increase in strength that occurs when the specimen size is reduced [41]. The importance of this effect cannot be overemphasised as more and more reduced scale model studies are being undertaken for the prediction of various aspects of prototype behaviour and design strengths (that is in codes and standards). Correct understanding of size effects is also necessary for the accurate interpretation of material properties tests of various sizes and shapes in different parts of the globe.

2.6.2 History

The subject of size effect of objects was discussed by Leonardi da Vinci as early as the 1500's, and concluded that "among cords of equal thickness the longest is the least strong". He also added that a cord "is so much stronger ... as it is shorter"[68].

After more than a century Galileo, in 1638, rejected Leonardo's exaggerated rule and argued that cutting a long cord at various points should not necessarily make the remainder stronger. However he added that a size effect is seen because large animals have relatively bulkier bones than small ones, which he referred to as the "weakness of giants".

Some decades later Mariotte experimented with ropes, paper and tin and concluded that "a long rope and a short one always support the same weight except that in a long rope there may happen to be some faulty place in which it will break sooner than in a shorter (one)" He suggested that this is as a result of the principle of "the inequality of matter whose absolute resistance is less in one place than (in) another". In effect he had put the foundations of the statistical theory of size effect, two and half centuries before Weibull.

Griffith's [68]famous work in 1921 followed, which founded the theory of fracture mechanics and also introduced fracture mechanics into study of size effect. Griffith concluded from his observations that "the weakness of isotropic solids... is due to the presence of discontinuities or flaws. The effective strength of technical materials could be increased 10 or 20 times at least if these flaws could be eliminated". His work in effect provided an experimental basis of Mariottes's statistical concept of size effect rather than a discovery of a new type of size effect[68]. Weibull then completed the statistical size effect initiated by Mariotte in a series of papers over 17 years from 1939-1956[68]. Most of the studies thereafter until the 1980s dealt with the purely statistical origin for size effect on the strength of quasi-brittle materials, therefore until the mid 1980's size effect on strength was thought of as having a statistical origin. This is seen in Sabnis's review[69] of studies in the area in which he only discussed the known statistical concepts at that time of bundled strength and weakest link. The most notable of the statistical concepts was the latter, which holds that, the presence of a single severe defect in any of the constituent elements is adequate to cause failure of the whole material. Consequently the failure strength of a specimen subjected to uniform stress is determined by the strength of the weakest element present. The most prominent exponent of this theory was Weibull [69].

2.6.3 The energetic and deterministic size effect

In Linear Elastic Fracture Mechanics (LEFM), where the failure criterion is expressed in terms of the energy consumed per unit crack length increment. The fracture process is assumed to occur at one point, the crack tip, which exhibits the strongest possible size effect. In this case the nominal strength is inversely proportional to the square root of structure size [70]. But this is only true if the cracks are large and there is a sudden failure at the start of cracking. This theory can therefore, only be true for very large structures in which failure occurs immediately after crack initiation. However it has been observed that concrete test data do not follow LEFM criteria, neither do they obey strength theory, in which there is no size effect. Therefore there is need for a non-linear form of fracture mechanics that takes into account the stable crack growth and the large micro-cracked zone of the fracture surface. This criteria or law as shown in Figure 2.3, bridges the zero size effect of the strength criterion and the size effect predicted by LEFM because it recognizes the large size of the micro-cracked zone of quasibrittle materials like concrete, rocks and clay bricks. It is seen from the figure that most structures lie in between the strength criterion (most laboratory tests) and LEFM (very large structures like dams). This figure suggests that there may not be a strong size effect for most tests conducted in laboratories with a relatively small size for a reference structural size D (as defined below). This could apply to this investigation since the tests would be on small masonry assemblies and not large masonry structures.

The size effect derived by Bazant[71] is based on the theory of stress redistribution and fracture energy release. It is assumed that the length of a crack at maximum load is proportional to a reference structure size D (say beam depth) while the size (width) of a fracture process zone at maximum load is constant, related to the heterogeneity of the material. The fracture energy, G_f is defined as a material property representing the amount of energy required to propagate a unit area of crack, then the energy used and released by fracture is proportional to $G_f D$[68]. Because the energy required to produce a unit fracture extension is approximately independent of the structural size, the nominal stress at failure of a larger structure is lower than for a smaller one, so that the energy release would exactly match the energy required for the fracture formation[72].

The size effect on structural strength is taken as the effect of the characteristic structure size (say D) on the nominal strength σ_N of the structure when geometrically similar structures are compared. This size effect in two dimensions is defined in terms of a nominal stress at failure in Equation 2.5

$$\sigma_N = C_n(P_u/bD) \tag{2.5}$$

Where P_u = maximum (ultimate) load, b = thickness of specimen or structure, D = characteristic dimension, and C_n = dimensionless constant. This is rewritten in terms of size effect of fracture mechanics type in the form of Equation 2.6

$$\sigma_N = \frac{B_o f_t}{\sqrt{(1+\beta)}},\ \beta = D/D_o \tag{2.6}$$

Where f_t = is a measure of material strength introduced to make B_o non-dimensional and B_o and D_o are empirical constants; coefficients B_o and D_o represent specimen shape and size. This assumes that the thickness b = constant for different D and also the specimen proportions are constant for all sizes. When the specimen is small, plasticity is also small, size effect does not manifest at these smaller values of β, and effectively results in a horizontal curve as seen in Figure 2.3. At intermediate values, there is a smooth transition and in the case of LEFM at large sizes ($\beta \rightarrow \infty$) at which case size effect is very pronounced it approaches the asymptote with slope of 1:2[41].

Equation 2.6 can be transformed to a linear plot in the form of Equations 2.7 and 2.8

$$Y = AX + C \tag{2.7}$$

$$\text{Where } X = D,\ Y = \frac{1}{(\sigma_N)^2},\ A = \frac{1}{D_o B_o^{\,2} f_t^{\,2}},\ \text{and } C = AD_o \tag{2.8}$$

The intercept C and slope A can be determined through linear regression analysis of data.

Some criticisms abound in the literature regarding the applicability of the law to unnotched structures. Carpenteri and Chiaia[73] observed that in deriving the formula the energy dissipated to cause fracture in a notched specimen is proportional to $G_f D$, and D is proportional to the crack length. But for unnotched specimens the length of the characteristic flaw responsible for crack propagation is independent of specimen

size, which therefore causes the anomalous behaviour of Bazant's formula. However Bazant[74] argues it is misleading to use Equation (2.6) for unnotched specimens since its modification has been derived to cater for unnotched specimens as given in Equation 2.9;

$$\sigma_N = k\sigma_0\left(1+\frac{rD_b}{D}\right)^{1/r} \tag{2.9}$$

Equation (2.9) was derived for the modulus of rupture of a notchless concrete beam, where $\sigma_0 = (2D/3L)f_t$ and D_b is the thickness of the boundary layer of cracking are both constants because the ratio D/L is constant for geometrically similar structures. D and L are the beam depth and length respectively, r and k are positive constants (usually $k = 1$ and $r = 1$ or 2)[75].

2.6.4 The theory of Crack Fractality or the Multifractal Scaling Laws (MFSL).

Theory of crack fractality or the Multifractal scaling Laws (MFSL) can be of two types;

1. Invasive fractality of the crack surface; referring to the fractal nature of surface roughness.
2. Lacunar fractality; referring to the fractal distribution of microcracks.

This theory proposed by Carpenteri and his co workers[76-78] holds that the difference in fractal characteristics of cracks at different scales of observation is the main source of size effect in disordered materials. The nominal stress from this law is given by Equation 2.10

$$\sigma_U = f_t\left(1+\frac{l_{ch}}{b}\right)^{1/2} \tag{2.10}$$

where b is the characteristic dimension of the structure and l_{ch} is a characteristic length related to the material microstructure. The scaling relationship shown in Figure 2.4a is a two-parameter model, where the asymptotical value of the nominal strength f_t corresponding to the lowest tensile strength is reached only in the limit of infinite sizes. The dimensionless term $(1+ l_{ch}/b)$ in Equation 2.10 represents the variable influence of disorder, consequently quantifying the difference between the nominal

quantity measured at scale b and the asymptotic value. In the logarithmic plot shown in Figure 2.4b, the transition from the fractal regime to the homogeneous becomes clear. The threshold of this transition is represented by point Q, whose ordinate and abscissa are $\log f_t$ and $\log l_{ch}$ respectively.

Some observations have been made by Bazant[68, 74] on the MFSL some of which are:

1. That the MFSL is identical to a special case of the energetic- statistical scaling law for failure at crack initiation (Equation (2.9)).
2. That the derivation of MFSL from fractal concepts includes problematic steps which invalidate it and that the MFSL does not follow mathematically from the fractal hypothesis made by its proponents.
3. That the MFSL cannot predict the dependence of size effect law parameters on the structure geometry. On the other hand, the energetic theories are able to predict their dependence.

It can be seen that taking $k = 1$ and $r = 2$ in Equation (2.9) gives

$$\sigma_N = \sigma_0 \left(1 + \frac{2D_b}{D}\right)^{1/2} \tag{2.11}$$

The remarkable similarity between Equations 2.10 and 2.11 is then apparent, and the constants in the equations can easily be obtained through statistical regression of test data as before.

2.6.5 Karihaloo's size effect formula for notched quasi-brittle structures

Karihaloo[79] used the concept of a fictitious crack model (FCM) to arrive at a size effect formula for the nominal strength of notched three point bend fracture specimens of concrete and other quasi-brittle structures defined as

$$\sigma_N = A\left(1 - \frac{B}{W}\right)^{1/2} \tag{2.12}$$

$$\text{Where } A = \sigma_\infty; \quad B = \frac{1}{2} l_{p\infty} \frac{g'(\alpha)}{g(\alpha)} \tag{2.13}$$

Where $l_{p\infty}$ and σ_∞ refer to the size of the fracture process zone in a very large specimen $(W \to \infty)$ and its nominal strength, while $g(\alpha)$ and $g'(\alpha)$ are a non-dimensional geometry factor and its first derivative, respectively. They depend on the notch to depth ratio $\alpha = a/W$. Deficiencies and refinements to Equation (2.12) have been discussed by Abdalla[80] and Karihaloo et al[81] and will not be covered here.

2.7 Fracture mechanics characterisation of masonry

Fracture mechanics characterisation of masonry properties has been carried out by a number of authors[82-84], and their studies has shown that fracture mechanics can be used for the determination of the fracture parameters like fracture energy of masonry from adaptations to the standard RILEM[85] test set up for the determination of fracture energy for concrete. Bocca et al[82] undertook a series of three-point bending tests on clay brick units of 20 by 40mm in cross section and 200mm long, including varying the notch lengths. Their findings showed that load-deflection curves with post-peak softening branches can be obtained by controlling the crack mouth opening displacement. This finding is significant as it implies that clay brick units show a process of crack growth as evidenced in the strain softening (from the load-deflection graphs) and can therefore be modelled by LEFM techniques. Numerical models can then be used to predict fracture properties of masonry as well as gain a further insight into the mechanics of the composite behaviour of masonry using LEFM concepts.

Carpenteri et al[84] carried out perhaps the first test for the determination of the fracture parameters of a complete masonry assembly. Three-point bending tests were carried out on five notched masonry walls of different sizes (same thickness but varying span and depth) by controlling the crack mouth opening displacement. The load-deflection diagrams show a softening branch, an indication of strain softening and stable crack growth. From the diagrams, the fracture energy of the specimens was calculated and analysis with respect to the MFSL using fractal fracture mechanics concepts. Also carried out was the analysis of the nominal strength from the tests according to the MFSL. The normal log-log plot of the nominal strength and reference structure size showed good agreement of the test data with the MFSL.

In a further study by Olivito and Stumpo[83] to characterise the mechanical behaviour of masonry using fracture mechanics concepts, they concluded that masonry can

support low tensile stress conditions and exhibits a bimodular behaviour which must be defined individually, because it is related to masonry composition and texture. Their results also show that masonry exhibits a strain softening behaviour caused by the start and growth of cracking. The fracture specimens were masonry walls built in the form of a beam of two different sizes; (length x height x thickness) 720 x 225 x 120mm and 720 x 225 x 60mm. Instead of cutting a notch on the masonry, the central mortar perpend joint in the lowest brick row was left unfilled in order to initiate cracking in the central part of the specimens.

Using numerical simulations to model size effect in masonry structures, Lourenco[86] found that, for a masonry pier subjected to a point load in which failure was mainly due to a tensile failure mechanism, there is evidence of a size effect for the range of sizes simulated. The observed size effect closely followed the MFSL law as well as the size effect law (Equation 2.6), but more in agreement with the former. The reason for that, as has been discussed previously, is that the comparison should have been made to Bazant's other law for crack initiation from a smooth surface (Equation 2.11), which is identical to the MFSL (Equation 2.10). In the simulations for a shear wall with an opening and open on the top edge, in which a shear or sliding failure was dominant, no size effect was seen. The analysis was not conclusive about another configuration of shear walls tested that were restrained on the top edge in which a compressive failure was dominant.

2.8 Factors affecting size/scale Effect

A number of factors affect the strength properties and ultimately the overall behaviour of quasi-brittle materials. Some of the strength properties include compressive, tensile, tensile, bond and fatigue strengths, and various dimensional changes including creep. The materials affected by size effect range from naturally occurring rock, timber etc to man made materials like concrete, steel etc and even composites like masonry.[87]

Random strength

Random strength describes the effect random distribution of flaws has in a heterogeneous material. It plays an important role in the micro mechanisms

determining the strength of materials. Thus a larger specimen should have more flaws and consequently less strong than a smaller specimen with fewer flaws[41].

Compaction

Generally smaller specimens of mortar or concrete will tend to achieve better compaction and higher density and thus a higher strength because of their smaller volumes. This is especially the case when standard compaction procedures are employed through vibration for a given time or specific number of tampings[41].

Curing and drying

Curing is an important variable influencing mortar strength. Two specimens of different sizes will cure differently because the surface to volume ratio increases with decrease in specimen size. The strength of the material will vary from the surface of the specimen to its centre, depending on its size, since hydration may not be uniform throughout the specimen at the time of testing[41].

Drying of the specimen will also influence the gain in strength as a result of the surface to volume ratio, which varies inversely with the specimen size[41].

Loading rate and state of stress

The rate of loading influences the strength of specimens, because higher loading rates lead to higher strengths. The stress of stress, for example compression, tension, and flexure, also influences the strength of the specimen. For instance the strength of compressive specimens depends on the accuracy of the loaded ends, and on parallelism, if rotating heads are not used. It is also possible to achieve a higher level of capping accuracy in smaller specimens, which will result in higher strength[41].

Testing machine and loading platens

Properties of the testing machine such as the stiffness of the loading platens have a profound effect on test results. Stiff end plates tend to apply uniform strain conditions to the specimen under test, thus resulting in a higher strength than if thinner plates were used[41].

Compaction of mortar bed by masonry units

Because of the heavier masses of larger masonry units, they tend apply more pressure on the mortar bed than smaller units. This observation was made by Egermann et al[51] as a possible cause for the decrease in stiffness as masonry model size is reduced.

Unit characteristics	Mortar characteristics	Masonry	Workmanship factors
Strength	Strength:	Bond	Incorrect proportioning and mixing of mortar
Type and geometry:	mix	Direction of stressing	
solid	water/cement ratio	Local stress raisers	Incorrect adjustment of suction rate of units
perforated	water retentivity		
hollow	Deformation properties		Incorrect jointing
height/thickness ratio	Relative thickness		Disturbance of units after laying
Absorption properties			
			Unfavourble curing conditions

Table 2.1- Factors affecting masonry strength[19].

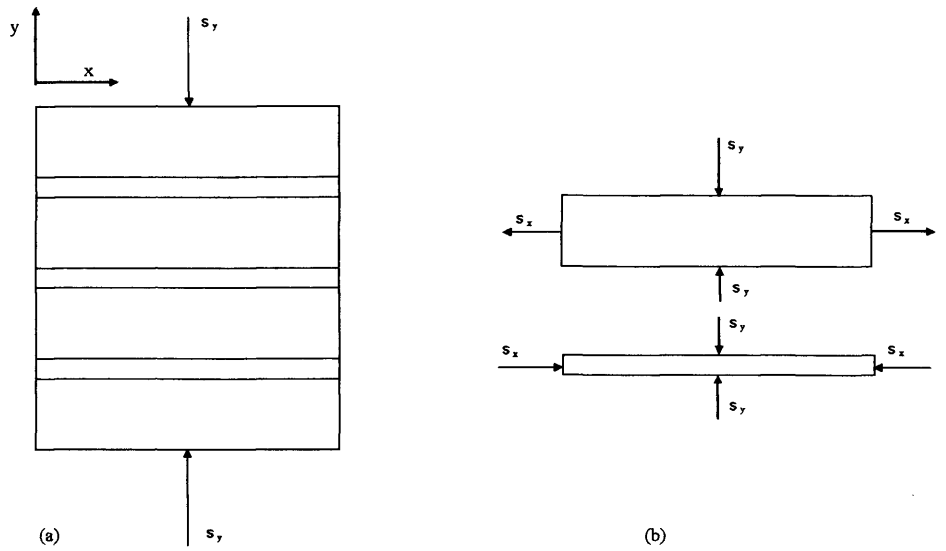

Figure 2.1- (a) Masonry specimen under axial force, (b) Stress states for brick and mortar elements.

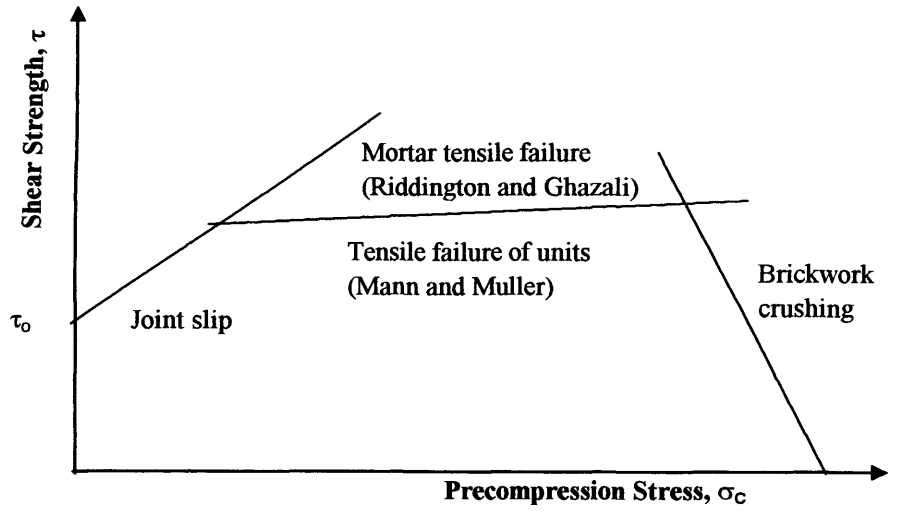

Figure 2.2- Failure modes of masonry in shear with precompression.

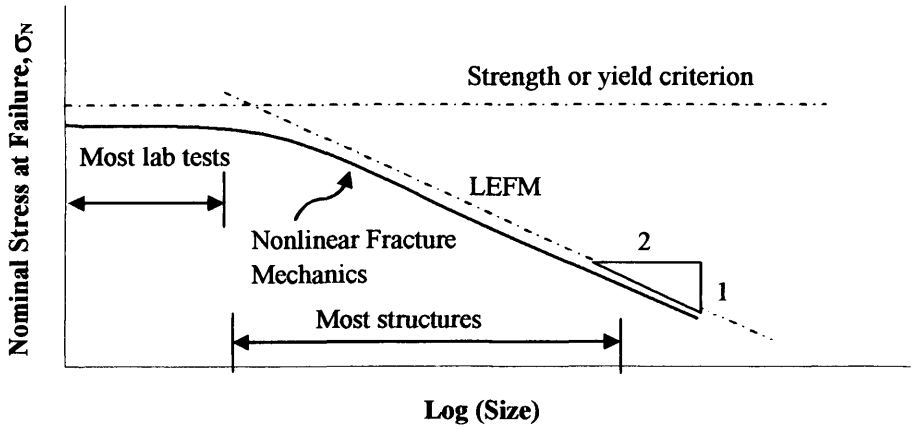

Figure 2.3- Size effect according to strength criteria, linear and nonlinear fracture mechanics.

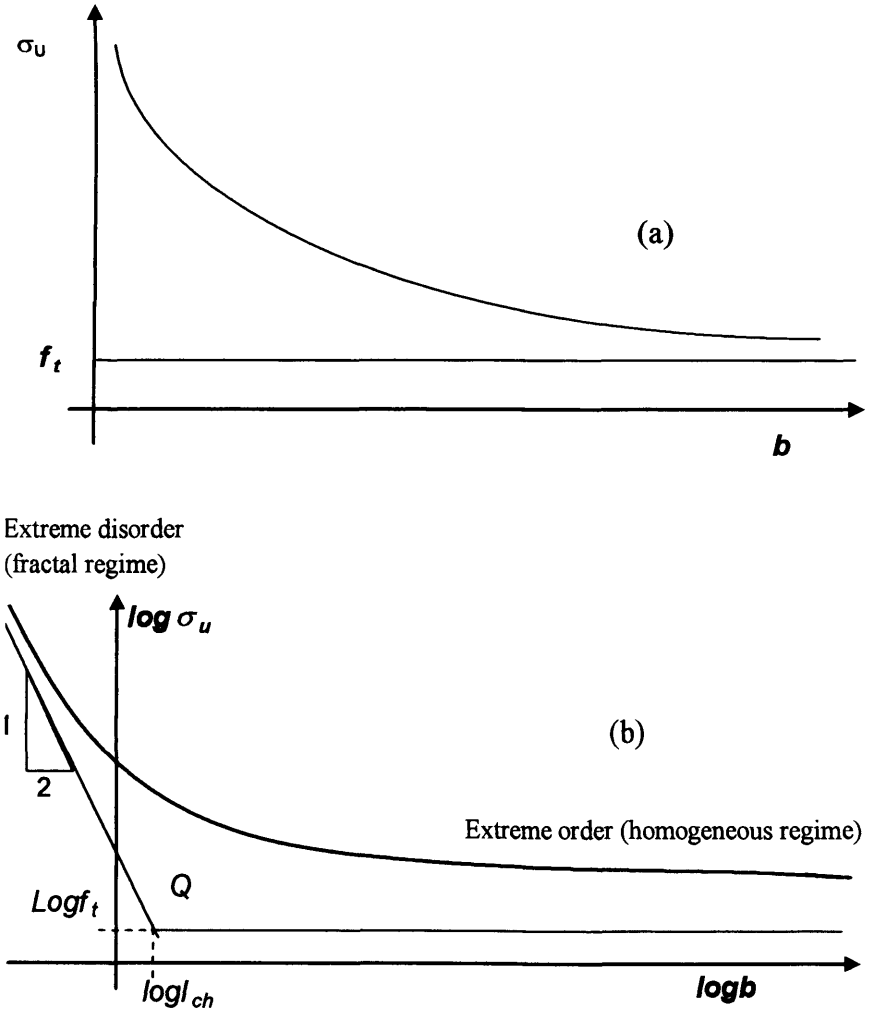

Figure 2.4- (a) Multifractal scaling law (MFSL) for tensile strength, (b) Bilogarithmic diagram for the same.

3 Experimental Design and Material Tests

3.1 Experimental design

The various factors taken into account in designing the composite masonry experimental programme are initially considered followed by a discussion of the tests to be undertaken on the constituent materials; the brick and mortar.

The aim of this research as it has been stated is to compare experimentally brickwork structural behaviour at prototype and model scales. Because of this, the research programme was divided into two parts; firstly looking at the effect of scale in the experimental structural behaviour of brickwork and secondly to further investigate opportunities for small scale modelling looking at the effects of some parameters like different joint thickness, sand grading and different mortar strengths. However a reference scale was needed that provides significant opportunities for modelling overall structural behaviour of for example arch bridges, whole buildings, retaining walls etc as well as for undertaking the parametric study. Taunton[3] has suggested twelfth scale as a limiting scale in small scale masonry modelling as discussed in section 2.5.7 while other authors[44, 51, 53] have reported reasonable model to prototype scale correspondence using half, third, fourth and sixth scale model masonry. An examination of the different factors led to the choice of the sixth scale as the benchmark model because it is most suitable for modelling whole masonry structures and components in a controlled laboratory environment. Two further scales of half and fourth scale were also investigated for the first programme of tests in order to get a complete picture of masonry behaviour across the range of scales. It was intended that material tests would be first carried out to determine the properties of the constituent materials that make up the masonry; the bricks and mortar e.g. compressive strength and flexural strength etc. Knowing the individual material properties will aid in understanding the composite behaviour of the masonry assembly; by determining how properties of the components contribute to overall brickwork behaviour under various conditions of loading.

In order to fully understand the composite behaviour of the masonry specimens, consideration was made of how best to capture the structural behaviour of a masonry structure, because in any masonry structure, its various elements are under the influence of a variety of actions. For instance a masonry wall could at any point be under a vertical compressive load, out-of-plane and or in-plane lateral forces, etc. Even though most of these forces act together, it is better to isolate each one to understand the mechanics of its action. Therefore to understand the fundamental behaviour of masonry, each of the actions was taking separately and considered for each of the chosen scales. Consequently in order to understand the behaviour of masonry under some of the most common actions to which it is subjected to, the following tests were chosen.

- Compressive strength test. Masonry is loaded in compression in the majority of the situations under which it is used. Therefore it is necessary to understand the mechanics of brickwork in compression for both prototypes and models. In addition to the compressive strength, the stiffness of the masonry under compression would also be investigated in order to compare the stiffness behaviour of prototype and model scale masonry. Various formats of specimens are used for compressive strength test; stack bonded units, wallettes and piers. Stack bonded units(prisms) tests are adopted as the standard for determination of the compressive strength of masonry in North America and Australia[19]. They provide a reliable estimate of masonry strength that is reasonably representative of masonry walls[88]. Hendry[19] suggests that an aspect ratio (height to width ratio) of 5 was necessary in order to eliminate platen effects in the testing of such specimens. But it was thought that, since comparable specimens would be used for the prototype and model tests, the end restrains would be similar and therefore a lower aspect ratio would still be acceptable for the purposes of comparison. Consequently it was decided to use a three brick high stack bonded triplet. It was also intended to use a wallette format that would allow for the determination and comparison of the lateral strains and Poisson effects in prototype and model scale masonry. Hence it was decided to use the wallette format complying with the specifications of BS EN 1052-1[89]. The triplet tests would be used for the prototype and three model scales since it would be easier to construct and test

while wallette tests would be used for the prototype and sixth benchmark model to allow for comparisons of lateral strain properties of masonry.

- Flexural strength test. The flexural resistance of masonry is important when masonry is loaded laterally due to for example wind, floods etc. For the flexural strength normal to the bed joints, which is a flexural bond strength, the different grading of the sands in the prototype and models could be important because as reported in the literature review, a lower bond strength could result due to a finer grading of sand (as is the case for the model scales) for comparable specimens. Many types of specimen formats are used for determining the flexural strength of masonry, a review by Fried and Anderson[90] has indicated that the following have been used; wallette specimens e.g. the BS 1052-2[91] wallettes, stack bonded piers tested as beams, crosses couplets, derivation of horizontal flexural resistance from vertical resistance and unit modulus of rupture (M of R). Some of the methods test every joint, while others test only the weakest joint in a specimen. However it was thought even though the wallette specimens would be relatively difficult to construct compared to the other formats, testing in four point bending would be relatively easier to undertake and the format is the most representative of a masonry wall. Hence it was concluded that the BS 1052-2[91] wallette specimen formats would be adopted for the determination of the flexural strength of the prototype and model specimen. However because of the variable loading arrangement in the four scales, undertaking the test in the vertical orientation as stipulated by the standard would have required different test set-ups for the four scales that would have resulted in significant challenges which would have been difficult to overcome within the duration of the testing programme. Therefore it was decided to undertake the test in the horizontal orientation by taking into account the contribution of the self weight of the specimens.
- Shear strength test. The shear resistance of brickwork is of significance when masonry walls are subjected to in-plane lateral loads. Two types of tests should be undertaken here; an initial shear strength test to determine the initial shear strength at zero precompression stress for masonry bed joints and a shear strength test on shear panels to determine the diagonal tensional shear strength at the centre of a masonry panel. A review of masonry joint shear strength tests by Jukes and Riddington[92] has indicated a wide range of tests, and concluded that a triplet test

with applied precompression and minimum bending was the most suitable because the specimens are easy to build, the apparatus not too complex and the results were shown to be consistent. Therefore the triplet test complying with provisions of BS 1052-3[31] was adopted for the determination of the initial shear strength for masonry bed joints. There are various formats for the diagonal shear strength test[19]; shear panels precompressed biaxially, with the shear load applied at the edges, diagonals etc. The RILEM recommendation for testing materials suggests a shear panel that is tested diagonally. This format is easier to test in the laboratory and is most suitable for model study investigation because of the simpler set up for the test. Therefore the RILEM recommendation LUMB6[93] for the diagonal tensile strength test was adopted for the investigation.

- Bond wrench test. As reported in the literature review the bond strength of masonry is important under the action of in-plane loads like wind, eccentric gravity loads etc. After due consideration of the relative advantages and disadvantages of the direct tensile test methods (like the Sheffield test) and the flexural bond strength test methods (like bond wrench test) in terms of the reliability of the test method, ease of fabrication and testing of the apparatus with regards to the range of scale being investigated, the bond wrench test was chosen. It provides a simple and reliable way of determining the bond strength for the range of sizes under consideration in this project. The test can be carried out on varying heights of stacks bonded units from couplets to eleven units high. Because of the need for the relative ease of handling and carrying out of the tests couplets were used in the prototype, half and fourth scales while triplets were used for the sixth scale. The couplet and triplet test are thought to be comparable since the second joint in a triplet would be tested as a couplet.

3.1.1 Bricks

The first consideration in the choice of the bricks was how many types of bricks to use. Since the main aim of the research was to investigate small scale modelling of brickwork it was thought that one brick type was suitable and adequate for meeting the aims of the study; because the same brick type can be used for the different scale study and the parametric study at sixth scale. The method of manufacture of the model bricks played a very important part in the choice of the prototype bricks. In work by Vogt [43] it was concluded that it was difficult to manufacture model bricks

through the usual firing process that will give the required accuracy at a particular model scale. The fourth scale model bricks manufactured for their testing programme had a noticeable curvature that greatly affected the dimensions of the bricks. In a more recent work by Egermann et al[51], full scale and half scale bricks produced from the same brickworks and extruder still left the model brick slightly stronger and more burnt than the full scale bricks because of the firing process. Even though the dimensional accuracies of the model bricks were not commented upon, a simpler, economical and more controllable way of manufacturing bricks is still desirable. Because of these issues and others regarding the making of small bricks as reported by Taunton[3], a cutting method which has been used successfully by other researchers [3, 52] was used for the production of the model bricks.

The following factors were considered in choosing the prototype brick.

- Strength. Because most masonry structures are or were generally built from low to medium strength bricks and in order to understand the behaviour of masonry it is necessary to use comparable models to the full size structures, it was decided that a brick with low to medium strength would be chosen.
- Absence of void. In order to allow for comparison between model and prototype, and since it may be difficult to accurately produce a model brick with perforations or frogs, solid bricks were preferable.
- Internal Structure. An internal structure of a brick that has relatively few internal cracks would be most ideal for the investigation. This would entail that cut model bricks will be most representative of the prototype brick.

Using the criteria set above for the selection of a suitable prototype brick, two types of brick were selected for consideration as the prototype brick; Ibstock Birtley Warwick Old English brick and Baggeridge Mellowed Red Stock brick. In the case of the former the initial model bricks produced from the first few prototype bricks were satisfactory but subsequently substantial flaws in their internal structure compromised the quality of the model bricks. Even though the former were easier to cut than the latter, the latter was chosen because of the stated problem. The Mellowed Red Stock was then chosen to produce all the model bricks and also to carry out the prototype tests. The average dimensions of the prototype and model bricks are given in Table 3.1.

3.1.2 Cutting method

As stated earlier the cutting method used here had been used by Taunton [3] to produce sixth, twelfth and eighteenth scale model bricks. It involves sawing a prototype brick into half to give two approximately square half bricks. Each half brick was then glued on the bedding face to a steel base plate to provide a way of securing it to the cutter. Another cut was made on the face opposite the bed face to remove the coarse wire-cut surface. Parallel cuts were then made as shown in the Figure 3.1, followed by another series of parallel cuts normal to the first series. The cut brick columns were then broke off for subsequent sizing to the correct length with a slit off saw. The sixth scale and fourth model bricks were produced in this manner, while the half was produced using a different technique. This was simply made by first trimming all the four sides of a prototype brick to make it 197 x 96 x 62 mm. Followed by a longitudinal cut through the brick at half its depth. Two other cuts were then made; one transverse across the brick at mid span and another longitudinal cut across the brick at half its width. This resulted in eight "half scale" bricks not exactly the required half scale dimension but sufficiently close at 1:2.22. The alternative to this would have been to get only one correctly sized half scale brick from one full scale brick because of the wastages resulting from the thickness of the cutting blade.

Tests undertaken by Taunton[3] to determine whether the firing process may have left the core of the brick less fired than the core concluded that there was no significant difference in strength between model bricks cut from the surface when compared to those cut from the core for a similar type of brick. Issues related to the effect of different frictional properties of sawn and prototype bricks have also been investigated by Taunton for a similar brick to the one used in this study and concluded that the surface finish does not significantly affect the angle of friction[3]. However the different surface finish of the prototype and cut model bricks could affect the flexural and bond strength of masonry since these have been shown to be affected by the surface finish of the units[94]. This point will be considered in the discussion of the results. There is also an inherent selection process in the cutting method during sawing of the model bricks by way of snapping of some of the cut bricks. However this is not deemed to be of great significance as there is also a selection process in the use of the prototype bricks, since only suitable bricks with no visible defects were considered suitable for the prototype tests.

3.1.3 Mortar

In the selection of an appropriate mortar for the tests, it was intended that a mortar that best compares to what is in use currently and in the past for masonry structures would be most suitable. The first consideration was whether to use a cement-sand mortar or cement-sand-lime mortar. Traditionally lime has been used in mortar to improve its workability and water retention properties. It was thought that both of these properties were desirable considering possible difficulties in adequately placing mortar in the bed joints of the model specimens and rapid suction of water from the model bed joints because of their small thickness. In the case of cement-sand mortars, plasticers are normally used currently in the construction industry to improve workability. However it was thought that since most historic masonry structures were made of lime based mortars, it was concluded that a cement-lime-sand mortar mix was most appropriate for this study.

For the prototype tests, it was intended to use a mortar that was comparable to ones used in practice, since this would best reflect the behaviour of a full size structure. Therefore normal building sand was chosen to make the prototype mortar. For the models scales the intention was to use two mortars that would be most suitable for the small bed joints in the model tests, but in order to achieve this, the sand for one of the mortars, a reference mortar, should be of fine grading to allow the mortar to be used for the parametric study involving different joint thicknesses. And of a strength that was appropriate to the aims of the investigation. Since low to medium strength mortar is used in most masonry structures from existing historic structures to new build, mortar designation iii, (BS 5628[95]) was chosen as the benchmark mortar made using HST95 Congleton sand with an average grain size of 130μm. While the second mortar was required to be of coarser grading in order to allow for the comparison of the effect different sand gradings on sixth scale masonry behaviour. Therefore it was concluded that Congleton HST95 and HST60 silica sands were most suitable for the investigation, after carrying out sieve analysis tests to determine their particle size distribution with reference to the grading limits of BS 13139, further discussion on the gradings of the three sands is reported in section 3.2.1.1. In order to further investigate the effect of increasing mortar strength at model scale, mortar designations (ii) and (iv) were also considered, in addition to the designation (iii). Therefore six mortar types were used in the sixth scale; that is three each for each of the two sand types.

While only one mortar designation; the benchmark model mortar was used for the half and fourth scales. Details of the different mortars used for the various scales are summarised in Table 3.2. The batching for the constituents of dry mortar was carried out in accordance with the guidance given in BS 4551[96] for the batching by weight of the three chosen mortar designations.

It has been reported by Hendry and Murthy [44] that is preferable to use 25mm mortar cubes instead of the standard 71mm cubes. In fact 25mm cubes have comparable strengths to the standard 100mm cubes as found from tests undertaken to compare their respective compressive strengths. Tests carried out using prototype mortar show that, the compressive strength of 25mm cubes was only 2% more than that of a 100mm cube [97]. In the case of the benchmark model mortar the compressive strength of the 100mm cube was just 4% more than that of the 25mm cube. Furthermore the 25mm cubes are judged to be most suitable for the small mortar mixes used in the research since using 100mm mortar cubes may not be representative of the actual mortar used for making the specimens. Therefore three, 25mm mortar cubes were adopted for the determination of mortar compressive strength for quality control purposes.

In summary the masonry tests would be undertaken in two categories; in the first category all the masonry tests detailed above would be carried out using one mortar type (designation iii, BS 5628[95]) to compare structural brickwork behaviour across the four scales. In the second category three mortar grades (designations ii-iv, BS 5628[95]) and two different sand types would be chosen to compare the effect of increasing mortar strength and different sand grading on the five masonry tests at sixth scale. Also the effect of different joint thicknesses (using model benchmark mortar) will also be investigated at this scale. In all there are eight different sub tests being undertaken for each of the five tests stated earlier at the sixth scale.

3.1.4 Masonry specimens

The first consideration here was the joint thicknesses, and using the recommendation in Eurocode 6 [98] that the prototype joint thickness for masonry made with general purpose mortar should be between 8-15mm because of the marked influence of joint thickness on the strength of masonry[20]; a joint thickness of 10mm was therefore adopted for the prototype specimens. In order to obtain the joint thickness for the

model scale specimens, the prototype joint thickness of 10mm was simply divided by the corresponding scale factor. Thus the corresponding joint thicknesses in the half, fourth and sixth scales were 5.0mm, 2.5mm and 1.6mm respectively. Two further joints thicknesses of 1.0mm and 2.5mm were also considered in the sixth scale in order to investigate the effect of varying joint thickness on masonry strength. In choosing the number of specimens for a particular test, the guidance given by the appropriate standard or recommendation was followed. Details of all the masonry tests undertaken are given in Table 3.3

Traditionally masonry is constructed by laying units on their bed faces and the brick or blockwork built vertically. However this method requires a lot of skill and is subject to very significant workmanship variations even when carried out by the same mason[19]. Another method of making masonry is to lay the units horizontally in special moulds before mortar is placed in the bed spaces to fill the joints. This method can be carried out under controlled conditions and is much faster to undertake. It is usually used to manufacture prefabricated masonry panels in the factory. Furthermore, the horizontal method of laying ensures uniformity of construction and eliminates the differential compaction of mortar joints by the different weights of units through the different scales. It may be argued here that the horizontal method of laying does not correspond with the normal way of laying bricks and therefore does not accurately model brickwork behaviour. However, firstly, it was necessary to minimise workmanship variations in this research project so that real structural behaviour of the specimens is not masked by material variability. This point has also been made by Baker[56] who used this method to make one-third scale masonry panels for wind loading tests. Secondly, since both the prototypes and models would be constructed in this way, there is a valid point for comparison. Hence after due consideration of all of the factors detailed above, the horizontal method of making masonry was adopted for the current research project. Plate 3.1(a) shows the preparation of a triplet specimen, the wooden spacers can be seen in between the bricks.

In the choice of materials for making the specimen mould for laying the sixth scale specimens, a material that offered very high dimensional tolerance was needed as well as being able to resist corrosion. The material also needed to be suitable for the large number of tests and different size specimens (because of the different joints) at the sixth scale. After consideration of the different factors, brass was chosen because it

offers the needed dimensional tolerance being a metal and will also resist corrosion. However, in the prototype, half and fourth scales the number of tests are less and the degree of dimensional tolerance required not as high as in the sixth scale. Therefore timber was preferred for the larger scales because it is lighter for handling purposes and could be reasonably used for the smaller number of tests. In the case of the sixth scale specimens the moulds were made is such a way as to accommodate the different joint thicknesses of the specimens.

However some issues could have arisen by using the horizontal laying method. This could have included the improper filling of the joints at the bottom of the end of a joint, segregation of the mortar constituents during compaction by vibration and differential curing of the exposed top face of the specimen in contrast to the covered bottom. In order to minimise the first and second problems it was intended to fill and compact the mortar joints gradually in stages. Since the intention was to cure the specimens while exposed at the ambient laboratory temperature, any effects of the differential curing on the top and bottom surfaces would be considered in the discussions of the results.

3.1.5 Adjustment of the suction rate of masonry units

The suction rate of masonry units is one the most important extrinsic factors affecting mortar, and hence, the properties of the hardened mortar and of the whole composite[7]. It has been established through nuclear magnetic resonance (NMR) tests that water extraction out of mortar during brick laying only slows down when the bricks are almost saturated[8]. But using fully saturated bricks could have its draw back when highly retentive mortars like lime-cement mortars are used. Also failure to adjust the suction rate usually leads to a weak mortar on setting resulting in a pillow shaped, weak mortar bed[14, 19].

In order to determine the water absorption characteristics of the brick used in this research, the water absorbed by five masonry units immersed in a tank of water was weighed at regular intervals over a period of 30 minutes and then weighed after a period of 24 hrs. From this it was observed that twenty minutes was the time needed for the units to reach 95% of their saturation value at 24 hrs. Figure 3.2 shows the graph brick weight against log of time. It is seen from the figure that for the first 20 minutes there is very rapid absorption of water characterised by a very steep slope, it

then steadies to a gentler slope. Therefore it was decided that 20 minutes was sufficient time to wet the bricks to an appreciable degree of wetness so that the suction rate of the brick units does not limit the water needed for the complete development of the strength properties of the mortar.

3.1.6 Preparation of specimens

Having determined 20 minutes as the time needed to appreciably wet the specimens, all masonry units (prototype and model scales) were wetted for that duration prior to being laid on their edge faces in their particular moulds. Spacers were used to define the joint thicknesses as well as to rigidly keep the units in place. Wooden spacers were used for making the prototype specimens while tile spacers of 1.0mm, 1.6mm, 2.5mm and 5.0mm thicknesses were used for the scale models. The mould and contents were placed on a vibrating table, mortar of standard consistence was then placed on top of the gaps between the units and vibrated gradually until all the joints were full of mortar and the spacers removed. The time taken to finish this procedure varies with the type of specimen and the scale. Moulds were left undisturbed for two days before demoulding and storing the specimens away for curing under normal laboratory conditions until they were tested. Plate 3.1(b) shows the preparation of a sixth scale wallette specimen, the plastic tile spacers can be seen separating the model bricks.

3.2 Materials and tests

This section details the different materials used and the various tests undertaken. The tests detailed here are those concerned with the mechanical properties of the materials, while the tests on the masonry assemblies are covered in the next chapter.

3.2.1 Materials

3.2.1.1 Sand

Three types of sand were used in this research. Ordinary building sand was used for tests involving prototype specimens while Congleton HST95 and HST60 silica sands were used for the model scale tests. In order to ensure the same sands were used throughout the study, all the sands were bought in one batch and of sufficient quantity to last the duration of the programme. The grading curves for the model sands and the ordinary building sand are shown in Figure 3.3, it shows that HST 60 sand and the

building sand lie within the grading limits of the code, but nearer the fine limit. The building sand is just coarser than the HST 60 sand. While the other model sand, HST 95, has a grading that is finer than the fine limit set by the code but straddles an assumed sixth scale coarse grading line. The two sixth scale grading lines were fitted by simply dividing the sieve sizes for the main grading limits set by a factor of 6. The grading of all the sands shows that they are within the limits set by BS EN 13139:2002[99] for aggregates used in mortar.

3.2.1.2 Cement

The cement used conforms to BS EN 197-1:2000[100]. It was acquired in different batches in order to ensure that the fresh qualities of the cement needed for strength build up are maintained during the duration of the testing programme.

3.2.1.3 Lime

Hydrated lime which conforms to BS EN 459-1: 2001[101] was acquired in one batch and used throughout.

3.2.1.4 Bricks

The Mellowed Red stock bricks used are solid, wire cut, frogless clay bricks made by Baggeridge Plc and supplied in one batch. They have a standard dimension of 215 x 102.5 x 65mm and conform to the requirements of BS 3921[102].

3.2.2 Tests on constituent elements; Brick units

In order to fully understand the behaviour of the units under load, some series of tests were proposed. These tests would be necessary in understanding the composite behaviour of masonry, since the unit and mortar react differently under load. They would be carried out to determine the most fundamental properties of the units that influence the composite behaviour of the assembly. The tests would be carried out on all the brick units; that is both prototype and model scales (unless stated otherwise).

- Compressive strength test. One of the most commonly quoted mechanical properties of a clay brick is its compressive strength. It is the main reason it is widely used as construction material. As with most brittle materials, the strength of clay bricks is determined by the natural distribution of flaws as it has been discussed already. Consequently, it is important to determine the compressive

strength for the prototype and model bricks because the effect of random strength predicts a higher strength for the model bricks.

- Modulus of elasticity. The deformation properties of masonry units are important because engineers need to predict the deflection of masonry under load. The intention is to understand the stress-strain relationship in the unit with a view to determining its contribution to that of the composite when the masonry tests are undertaken. The modulus of elasticity test would only be carried out on the prototype units because it would be difficult to carry out the test in the model scales because of the small size of the model units.

- Flexural strength test. When masonry is subjected to out-of-plane flexural stress in the direction of the bed joints, failure could either be through the perpend joints and units or through the units. In the former the flexural strength of masonry is governed by the modulus of rupture or flexural strength of the unit. Therefore it is essential to determine this parameter for the prototype and model units.

- Indirect tensile strength test. Even though clay masonry is primarily strong in compression and weak in tension, its failure under compressive stress is governed by the tensile strength of the units, consequently the determination of this parameter is necessary for the understanding of the failure mechanics of masonry.

- Water absorption test. The importance of the suction properties of the units in ensuring proper bond development and strength has already been discussed. This is a standard test aimed at comparing the water absorption characteristics of the prototype and model bricks.

- Fracture energy tests (prototype and half scale only). The mechanism of failure in a brick unit is mainly occasioned by fracture of the brick. This is due to the energy release characteristic of the material. Understanding the energy release mechanism of brick fracture should help in understanding the mechanics of the fracture formation in composite masonry.

3.2.2.1 Compressive strength test

The prototype units were tested in accordance to the requirements of BS EN 772-1:2000[(103)] in a compression testing machine at a loading rate of 6.6 kN/s until failure

occurred. Prior to being tested the units were immersed in water for a minimum of 24 hrs until just before testing. Plywood pieces 5mm thick were used as packing in the tests in order to minimise the platen restrain and also to ensure a level and flat surface for even load application.

All other compressive strength tests on the model bricks were tested in a compression testing machine at comparable strain rates using loading rates of 0.9kN/s, 0.4kN/s, and 0.2kN/s for the half, fourth and sixth scale units respectively. No stiffness tests were carried out on the model bricks because of the small size of the specimens.

Typical failure of units was by tensile cracks parallel to the direction of load application followed by splitting, which was followed by crushing of the specimens. The mean compressive strength of the prototype and model bricks are shown in Table 3.4, the mean compressive strength of the prototype units was determined to be 29.2 N/mm^2 with a Coefficient of Variation, (COV) of 14.3%. The COV indicates the inherent variability in the strength of kiln fired clay masonry probably due to the way bricks are extruded or pressed and subsequently fired in the kiln as has been reported by Jessop et al [25]. Figure 3.4 shows the variation of the compressive strength of the units with scale. It is seen that there is a noticeable increase in compressive strength of the units as the scale is reduced.

Consideration of Figure 3.4 shows that there is no uniform trend in the increase in strength as the scale is reduced, for example the half scale units' strength is only marginally higher than the prototype unit strength, while the fourth and sixth scale unit strengths are 43% and 63% higher than the prototype unit strength. It is seen from the results that, there exist some similarities in the strength of the prototype and half scale on one hand, and also in the strengths of the fourth and sixth scale units on the other hand. In order to further investigate the possible effect of the orientation of the model units in the prototype in relation to their orientations while being tested in compression, a test was devised as follows; three 50mm cubes specimens each were cut from a prototype brick and their faces labelled to show the orientation of the cut pieces in the parent material. Figure 3.5 shows the orientation of the model units in the prototype as well as how top, end and side are defined. Sixteen samples from six bricks were tested in the three different orientations. Results as shown in Table 3.5 show that there is about a 26-30% increase in strength for the specimens cut and

loaded in the side-side and end-end orientations than for the specimens cut and loaded in the top-bottom orientation. The side-side and end-end orientation coincides with the top-bottom orientation in the fourth and sixth scales. Showing that, there is a possible anisotropy with respect to the strength of a brick when considering the loading orientation as reported by Shrive and Jessop[37], who concluded that extruded clay units are anisotropic because of the manufacturing process.

Another reason for the higher strength in the fourth and sixth scale could be due to the effect of fracture mechanics of brittle materials as first suggested by Griffith, that the less the surface area of a brittle material is the stronger it is, since there is less probability of flaws occurring[13]. Therefore smaller brittle materials will show a higher strength than larger materials because of this. This may be true for the fourth and sixth scales but not for the half scale units. Since curiously there is no great strength difference between the prototype and half model scale units, possibly because they are tested in the same orientation the flaws in them are also embedded in a similar manner and would therefore behave similarly under stress. It would be interesting to see if the same effect would be seen in the masonry compressive strength tests, since the strength of masonry is primarily due to the unit strength.

3.2.2.2 Modulus of elasticity test

Five 200 x 60 x 60mm specimens were used for the determination of the modulus of elasticity of the units. These units were cut to size from standard prototype units and were tested end to end in the direction of their longitudinal axis. Four, Linear Variable Displacement Transducers (LVDT) were fitted (held with plastic padding) onto the faces of units; two LVDTs, one each on opposite faces were attached in the vertical orientation to measure the longitudinal deflection while the other two were attached horizontally at mid section to measure the lateral deflection. Plate 3.2 shows the set up for the test. Two pieces of Fibre board unit were used to cushion the platen effect on the specimens. Load was applied at a rate of 0.1kN/s through two loading cycles of up to a load of 40kN and then loaded to failure in the final lap. Failure was characterised by the vertical splitting and cracking of the specimens in the direction of loading followed by crushing of the units. Some units left pyramidal shaped masses on the platens after failure, a consequence of the platen effect.

In the identification system used for the tests, the first letter B refers to Brick, MOD refers to the type of test in this case modulus of elasticity, and the number refers to the specimen number. Where a number is followed by a letter A or B it refers to the deformation measurements both axial and lateral on either face of a brick. While a number followed by AV refers to the averaged axial or lateral strain (average of A and B) from two opposite deformation measurements. For example B-MOD-5A would refer to the strain measurement from one face of brick sample 5 in the modulus of elasticity test.

The brittle nature of the material is evident from the way they failed as shown in Figure 3.6, which shows stress/strain relationship in three of the specimens. They reveal that the units stress/strain relationship is linear up to the failure as evident from a lack of a plastic region in the curves. In Figure 3.7, a complete set of stress/strain curves for test B-MOD-5 is shown. The figure shows that there is minimal effect of bending during test and it is representative of most of the test undertaken.

The modulus of elasticity was calculated based on the strain readings at a third of the maximum stress reached for each of the units, as is common for masonry. An average value of 11500 N/mm^2 was obtained for the modulus of elasticity, with compressive strength of 25.6 N/mm^2 and a Poisson's ratio of 0.06. It is also seen from the results that the specimens used for the actual determination of the compressive strength were about 14% higher in strength than the slender ones used for the determination of the stiffness parameters; probably due to the greater effect of platen restraint in the former.

3.2.2.3 Flexural strength test

The flexural strength test also called the modulus of rupture was carried out in accordance with the requirements of LUM A2[104], which is the RILEM recommendation for the flexural strength test of masonry units. Since the units' span/ depth ratio is less than 4, three units were required to be joined together at their ends with an epoxy resin adhesive. The ends to be joined together were first grooved before the adhesive was applied in order to ensure effective bonding. The assembly was left to cure for a day before being immersed in water for a minimum period of 24 hrs. Testing was by a three point bending, and load was applied gradually until failure of the specimen in the central unit at a rate of 0.04kN/s in the case of the prototype

beam. Plate 3.3 shows the set up for the test, the position of the two joints in the specimen can be seen from the plate.

Epoxy resin was also used to glue the model scale units as mentioned earlier. Testing of the specimens was carried out in a 20kN testing machine at a displacement rate of 0.2mm/min for the half scale beam and 0.1mm/min for the fourth and sixth scale beams. Displacement rates were used in the smaller capacity machine because of problems in testing under load control. The displacement rates chosen were made to achieve failure within an average time that was comparable to the load controlled prototype tests.

The RILEM recommendation gives the modulus of rupture, S as Equation 3.1

$$S = M/Z \qquad (3.1)$$

where:

M = the bending moment at failure in Nmm, given as $Pl/4$,

Z = section modulus of test specimen in mm^3, given as $bd^2/6$,

P = maximum load at failure, N,

l = distance between supports,

b = mean width of beam cross-section at line of fracture,

d = mean height of beam cross-section at the line fracture. The average dimensions of the specimens used for the test is provided in Table 3.6.

Results and Discussions

Typical failure of the specimen was by tensile failure and cracking of the central unit in bending. From Table 3.4, it is seen that the mean modulus of rupture for the prototype specimens was determined to be 4.3 N/mm^2, with a COV of 21.2%, highlighting again the variability in the results. The modulus of rupture of the prototype units is about 15% of their mean compressive strength. This is within the range described by Nevader[11], that the modulus of rupture of solid bricks varies within the limits 14 to 32 % of their compressive strength for compressive strengths values of 20 to 51N/mm^2.

Figure 3.8 shows the modulus of rupture of the prototype and model units across the four scales. It is seen from the results, that the half scale model units have the highest modulus of rupture, followed by the prototype units while the fourth and sixth scales units have similar values. However it is seen that half scale value is about twice the fourth and sixth scale values. The expectation was for an increase in the flexural strength as the size is decreased, but it seems there is no clear scale effect from the prototype to the sixth scale. It would be interesting to see how modulus of rupture of the units affects the masonry flexural strength parallel to the bed joints when failure is governed by the flexural strength of the units.

3.2.2.4 Indirect tensile strength test

The indirect tensile test was also carried out in a load controlled machine according to the specifications of LUM A3[105], the RILEM recommendation for the indirect tensile strength test of masonry units. The units were first saturated in water for a minimum of 24 hrs before being tested. The load was applied at a constant rate of 0.25kN/s until the prototype units were split at the cross section under consideration. Each prototype unit was split at three points across the normal orientation of its long axis; initially at 42.5mm from one edge, then across its centre and finally 42.5mm from the other edge. While for the model scale units the splitting distance from either edge was 19mm, 11mm and 7mm respectively for the half, fourth and sixth scales.

The load rate of 0.02kN/s was used for the half scale test in a load controlled testing machine, while a displacement rate of 0.20mm/min and 0.15mm/min was used for fourth and sixth scale test respectively.

Results and Discussions

The results from Table 3.4 and Figure 3.9, which shows the variation of the mean indirect tensile strength across the four scales, indicates a trend of gradual increase in the tensile strength as the scale is reduced. It is seen that the prototype units have the least tensile strength of 1.9N/mm^2, while sixth scale units have the highest tensile strength. The sixth scale tensile strength is 26% more than the prototype tensile strength. The mean tensile strength is 7% of the compressive strength of the units in the prototype and 5% of the compressive strength in the sixth scale. This indicates a

possible linear relationship between tensile and compressive strength masonry units as shown in Figure 3.10.

3.2.2.5 Water absorption test

The units were tested according to the specifications of LUM A4[106], the RILEM recommendation for the water absorption and water porosity tests of masonry units. The units were weighed before and after saturation in a water tank for 24 hrs.

Results and Discussion

The mean water absorption of the prototype units as seen from Table 3.4 was determined to be 14.8%, this is about 11.5% less than the mean water absorption of the half scale units, which is the highest across the four scales. Figure 3.11 shows the variation of the water absorption across the scales, it reveals that there is a marginal increase in the water absorption as the scale is reduced. But this is no conclusive proof that there is definite scale effect, because the effect is marginal.

There is some debate about the appropriateness of this test as a measure of the absorption characteristic of brick masonry. As indicated by the preliminary tests on the suction property of the units; that in 20 minutes the units had reached 95% of their total saturation value, suggests that 24hrs of wetting as prescribed by the water absorption test is too long a time to highlight the critical phase of interaction between the unit and mortar.

On the other hand the Initial Rate of Absorption, IRA test (which has not been undertaken as part of this study) takes just one minute to carry out and is too short to capture the important period of interaction between the units and mortar. The Sorptivity test, as described by Reda Taha et al[107], seems to bridge the Water Absorption and the IRA test methods by putting forward a modified IRA test that takes about 25 minutes to complete with weighing done at regular intervals as described in the test for suction properties stated earlier.

3.2.2.6 Fracture energy test

The facture energy is defined as the amount of energy required to propagate one unit area of crack, and the area of crack is the projected area on a plane parallel to the main crack direction. Since there is no specific standard test for fracture energy of

masonry bricks, the RILEM recommendation, FMC 1[85] for the determination of the fracture energy of mortar and concrete was adapted. Two separate tests were carried out; one involving three brick units glued together (brick beam) and another consisting of only one unit. Three brick units joined together at their ends, as in the case of flexural energy test for brick units was tested in the first instance according to the procedures outlined in FMC 1. A central notch 5mm wide and cut to half of the unit height was made in the central unit of the specimens prior to being immersed in water for a period of 24hrs. The setup was then placed in the rig, where a transducer and a clip gauge were fitted to measure the vertical deflection at mid span and the crack mouth opening displacement (CMOD) respectively. The test was carried in the form of a three-point bending test and controlled by the CMOD gauge at a displacement rate of 0.0004mm/s. The measurements/readings were recorded on a data logger for later analysis. Plate 3.4 shows the set up for brick beam while Plate 3.5 shows the set up for the single unit test. It can be seen from the Plate 3.4 that while the LVDT for measuring the central mid span displacement was suspended from a jig mounted on the brick beam, the LVDT for the single brick test was supported from an attachment screwed into the unit. The drilling of the holes for the attachment of the screws in the unit, could have some undesired effect on the test even though it is difficult to quantify the exact effect.

A similar test was also undertaken using three half scale units glued together with a central 5mm wide, 10mm deep notch (1/3 of the unit height) in the middle unit. The test was also undertaken in the same machine at a displacement rate of 0.0002mm/s. Because of the expected low loads, a 250kgf Z-load cell was attached to the base of the loading platen to apply the load as well as to record it. With this set up, it was possible to use the 500kN capacity testing machine to measure loads to the accuracy of 0.1N. A set up for the test is shown in Plate 3.6 with the 250kgf Z-load cell on top of the specimen.

As stated earlier since there is no standard test for the fracture energy test for bricks, some authors like Baker[108] have used both brick beams and single units for brick fracture tests, while Bocca et al[82] used the single brick configuration for the their fracture tests. In order to compare the two tests, both single unit and brick beam configurations were used for the determination of the fracture energy in the current work

Calculations for the fracture energy were undertaken using Equation 3.2. This was done after determining the value of W_o, which is the area under the load- deflection graph calculated numerically on the PC using Equation 3.3.

$$G_F = \frac{(W_o + mgd_o)}{A_{lig}} \tag{3.2}$$

Where:

G_F = fracture energy in N/m;

W_o = area under load- deflection graph in N/m;

m = m1 + 2m2 in kg;

m1= weight of beam between supports in kg;

m2 = weight of loading arrangement not attached to machine in kg;

g = acceleration due to gravity in m/s^2;

d_o = deformation at the final failure of the beam in m;

A_{lig} = area of ligament, defined as the projection of the fracture zone on a plane perpendicular to the beam axis in m^2.

$$W_o = \sum_{i=1}^{n} (x_{i+1} - x_i).\frac{(y_i + y_{i+1})}{2} \tag{3.3}$$

Results and Discussions

Though the mean fracture energy from both the single brick and brick beam prototype tests are close; 50.7 N/m for the former and 47.4 N/m for the latter, the results from the single brick test are more variable with a COV of 54% compared with 10% for the brick beam tests. In the identification system used for the tests, B and FRC refer to Brick and Fracture test respectively, while BM and U refer to beam and single unit specimens respectively. The load/deflection curves for the brick beam tests are shown in Figure 3.12 while those for the single unit tests are shown in Figure 3.13. The figures reveal that the load/deflection response for the beam test is softer than that for the single unit test. Similar results have also been obtained by Baker[108]. The

difference is more noticeable when typical load/deflection curves for the two tests are combined on the graph as shown in Figure 3.14, it shows that the single beam tests have a sharper peak and steeper gradient than the beam tests which show a gentler slope and flatter peak. This may be due to the greater bending effect because of the increased span on the crack propagation process in the central unit in the case of beam, while in the case of the single brick there is no such effect and hence the sharper peak and more brittle response. Another advantage of the beam test could be that, because of the restraining effect, it stabilises the specimen and hence variability is reduced as is apparent in the results. For these reasons the prototype fracture energy results shown in Table 3.4 are those from the beam test.

From the combined flexural stress/deflection response for the prototype and half scale tests in Figure 3.15, it is seen that the half scale exhibits greater ductility than the prototype, as well as a capacity to withstand a marginally higher load. The mean fracture energy from the half scale test results was determined to be 58.2N/m, which is about 23% more than the prototype beam fracture energy. Therefore about 23% more energy is needed to propagate a unit area of crack in the half scale model unit compared to the prototype beam. The results have confirmed the findings in the literature[82] that load-deflection diagrams of clay units exhibit a softening branch that indicate strain softening and stable crack growth. This is significant since it implies that fracture mechanics concepts could be used to understand the process of crack propagation and failure in masonry.

3.2.3 Tests on constituent elements; Mortars

The primary function of mortar is to bed and join units, providing them with the continuity required for stability and the exclusion of weather elements[10]. The understanding of some important mechanical properties of mortar is essential for better understanding of its contribution to the composite action of masonry. Therefore the following tests were proposed in order to determine the important properties of masonry, namely;

- Compressive strength test. The strength of mortar as a jointing material is important for the overall strength of the composite masonry assembly. In situations where strong brickwork is required, it is also necessary to have a strong mortar in order to complement the strength of the unit. This test is needed, first to

understand the mechanics of mortar in compression in order to determine its contribution to masonry strength and secondly as a quality control tool to ensure that the specimens were made with mortar of comparable strengths for tests with the same mortar designations.

- Modulus of elasticity tests. The determination of the stiffness of mortar from modulus of elasticity tests is necessary since mortar stiffness has been shown to influence the stiffness and strength properties of masonry[10]. Therefore understanding the stress/strain relationship in mortar is important as it would aid in the understanding of the stiffness properties in masonry.

- Flexural strength tests. The aim of the flexural strength test is to determine the limiting tensile strength on mortar to cause cracking by a three point bending test. The knowledge of this for the different types of mortar in this investigation is important because mortar usually fails by crack propagation through the cement paste rather than failure of the aggregate[109].

- Fracture energy tests. The fracture energy tests are necessary so as to understand the mechanics of failure of the different types of mortar used for the study. Knowing that would help in the understanding of the overall behaviour of the mechanics of crack propagation in brickwork.

- Mortar consistency tests, dropping ball. Consistency tests are required to test the workability of mortar and ensure mortar of standard consistence was used for preparing the specimens.

- Water retentivity tests. Water retentivity tests would be carried in order to determine the water retentivity properties of the different mortars and see how they affect the final properties of the finished masonry.

3.2.3.1 Compressive strength test

Even though non standard moulds of 25mm cube were used for making the mortar specimens for the compressive strength test, nonetheless, the procedure outlined in BS EN 1015-11:1999[110] were followed in testing the specimens. The test was carried out under displacement control at a rate of 2mm/min. Three 25mm cube mortar samples from all masonry samples made were taken for the determination of their compressive

strength. Both the model scale and prototype mortar specimens for the compressive strength were made from the same moulds.

Results and Discussion

Typical failure of the mortar specimens was by shear cracks in the direction of loading. This tended to be triangular in shape originating from the sides of the specimen at the top slanting inwards, towards the centre at mid height and diverging again to the sides of specimen at the bottom. The final outcome of this is a pyramidal shaped mass at failure considered to be due to the platen restraint.

The average value of the compressive strength for different batches of 1:1:6 prototype mortars, (MP mortar) was 5.0N/mm^2, as seen from Table 3.7, which gives a summary of mortar test results. This value of compressive strength is higher than the expected minimum compressive strength of 3.6N/mm^2 from BS 5268$^{(95)}$ for mortar designation (iii), which is an indication that the batching, mixing and curing conditions used were appropriate for the attainment of the specified minimum strength.

From Figure 3.16, which shows the variation model mortar compressive strength as the mortar strength class is increased, it is seen that mortars made with HST 60 sand consistently had higher compressive strengths than those made with HST 95 sand. The strength class is the new nomenclature used in the EC 6 to differentiate the mortar types. Strength class M6, M4 and M2 correspond to mortar designations (ii), (iii), and (iv) respectively. The strength class was substituted for the mortar designations in the X- axis as it better illustrates the increase in strength. As expected it can be seen from Figure 3.16 that the relationship between compressive strength and strength class is a linear relationship. For designation ii, (class M6), there is a 58% difference between the compressive strength of the two mortar designations. While for designation iv, (class M2), there is only a difference of about 30%, indicating a convergence in the strength of the two mortars with decreasing mortar designation. Because of the coarser grading of the HST 60 sand, it has higher a bulk density and thus a lower water to cement (w/c) ratio than an equivalent weight of HST 95 sand, which subsequently increases the compressive strength of M60 mortars. The wider divergence at higher mortar grades could be attributed to the greater quantity of cement available for making a more cohesive mix in the case of HST 60 mortar, which has coarser grading of sand. Therefore there is better cohesion between the

coarse sand grains and finer cement grains. An investigation into the effects of grading on mortar properties by Anderson et al[15] also yielded similar results; the sand with coarsest grading within the BS EN 13139[111] limit gave higher compressive strength as a result of the lower w/c ratio. Since the prototype sands are coarser than the model sands, there is a possibility that the prototype tests could have higher mortar strength. However the influence of this on masonry strength might not be very significant as suggested by Hendry[19]; that halving of mortar cube strength only results in a 12% reduction in masonry strength for a medium strength brick. But the different grading of the sands could still have an effect on the flexural bond strength and shear bond strength tests which are more susceptible to changes in the grading characteristics of the sand in the mortar as reported by Anderson and Held[15].

The variation of compressive strength with w/c ratio as shown in Figure 3.17 shows a decrease in compressive strength with increasing w/c ratio. It is also seen from the plot that at about a compressive strength of 3.5 N/mm^2 (grade iii mortar) the two mortars have the same value of w/c ratio of around 2. The plot also shows that the mortars with coarser sand (M60) are affected more by changes in w/c ratio than mortars with finer sand (M95) mortars. This implies that the prototype tests could be more susceptible to changes in the w/c ratio than the model tests because of the coarser sands in the former.

3.2.3.2 Modulus of elasticity test

Prisms measuring 75 x 75 x 200 mm were used for determining the elastic properties of the prototype and model mortar modulus of elasticity tests. Four LVDT's were attached to each specimen as described for the brick specimens. Load was controlled at a rate within the range of 0.06-0.1kN/s. The specimens were tested through two loading cycles of up to a third of the expected maximum load for some of the tests, but most of the tests were carried out without load cycling after it was seen that there was no noticeable difference in the loading and unloading cycles in the earlier tests. The mortar strength calculations here were based upon the 75 x 75mm specimen and not the 25mm cubes. All the stiffness calculations were determined at a third of the maximum stress reached as a secant modulus.

Results and Discussion

Typical failure was by vertical cracks on the faces and splitting at the sides of the specimens. It is also seen in Figure 3.18 and 3.19, which compare the stress/strain curves for the axial strain and lateral strain respectively, that the M60-ii and M95-ii mortars were the stiffest and showed a more brittle response than the less stiff M95-iv and M60-iv. However from Table 3.7, the stiffness of M60-iv and MP-iii were found to be similar even though MP-iii is a designation (iii) mortar. The figures also reveal that the brick is more brittle in the stressed direction than the mortars as evident from the sharp drop in the curve as opposed to the gentle "peak plateau" of the mortar curves that show some ductility. It is also seen from the Figures 3.18 and 3.19 that there is almost a linear stress/strain relationship in the brick up to failure as opposed to the mortars, which show non-linearity at about half of the peak stress.

From the stiffness/strength plot in Figure 3.20 and the stiffness/strength class plot in Figure 3.21, it is seen that there is a much greater difference in the stiffness between the strength classes in the M60 mortar than in the M95 mortars. For instance there is a 51% percentage increase in stiffness between M95-iv and M95-ii, while the percentage increase in stiffness between M60-iv and M60-ii is 149%. This is similar to the greater effect the w/c ratio has on the strength of the M60 mortars than on the M95 mortar strength, as has been investigated in section 3.2.3.1. This indicates that even for suitable model sands, the stiffness and strength properties for the same designation of mortar could be different. Therefore, when modelling prototype behaviour at model scale, the grading of the model sand should be similar to that of the prototype even though the average grain size is smaller. The stiffness of MP-iii was determined to be 6700 N/mm^2; this is about 3% stiffer than M95-iii and 86% less stiff than M60-iii.

3.2.3.3 Flexural strength test

25mm x 25mm x 100mm moulds were used for the manufacture of the flexural strength test specimens. The load was applied as three point bending. This is slightly smaller than the recommended 40 x 40 x160mm mould prescribed by BS EN 1015[112] for the flexural strength. But because of the small volumes of mortar being used for the actual masonry construction it was thought that using the same moulds for both the small and prototype scale mortar was more appropriate. Testing was done in

accordance with the specifications of BS EN 1015-11: 1999[110] at a displacement rate of 2mm/min.

Results and Discussion

The average value for the flexural strength for the prototype mortar was found to be 1.8 N/mm^2, which is about 35% of its compressive strength. Failure of the specimen was occasioned by a single vertical crack at the mid section of the prism specimen.

Figure 3.22 shows the flexural strength/ strength class relationship for the model scale mortars, it is seen from the figure that there is a linear relationship between the parameters, characterised by an increase in the flexural strength as the strength class is increased. In this case however, the trend line for both the M60 and M95 mortars is similar, implying that the rate of increase of flexural strength across strength class for the two mortars types is identical. In the case of the relationship between flexural strength and the w/c ratio, it is seen from Figure 3.23 that, as in the case of the compressive strength, there is a decrease in flexural strength as the w/c ratio increases. It is also seen from the figure that there is a convergence in the trend lines for the two mortars at lower w/c ratios and a wider divergence for higher ratios. There is also a linear relationship between the compressive strength and flexural strength with increasing mortar strength for both types of mortars as shown in Figure 3.24.

3.2.3.4 Fracture energy test

The fracture energy test was carried out according to the recommendations of FMC 1[85], the RILEM recommendation for the fracture energy determination of mortars and concrete. The specimens were 100mm square in section and 500mm long with a notch 5mm wide at mid span, through half of the beam's depth. Load application was by three point bending at a displacement rate of 0.0003mm/s, while controlled by a CMOD gauge fitted on the specimen and all the set up is as described for the brick fracture test.

Results and Discussions

The average fracture energy for the 1:1:6 prototype mortar was determined to be 19.5 N/m (Table 3.7). The COV for the presented results was 8.3%, showing that there was less variability in the results compared with the brick specimens. The mean fracture

energy is based on an average of 3 specimens even though 5 were tested. The other two gave load deflection graphs with sharp almost vertical drops in the post peak portion, an indication that the deflection at the centre of the beam remained constant even with further application of load, they were therefore not used in the analysis. The load/deflection curves for the other three are shown in Figure 3.25, and they show a somewhat gentle post peak gradient compared with the graphs for the brick test, thus indicating that the brick specimens are more brittle than the mortar specimens. Since less energy is needed to propagate a unit area of crack in the mortar than in the brick, cracks normally develop from the weakest joint at the mortar/brick interface in masonry composites and then propagate through the brick.

Figures 3.26, 3.27, and 3.28 show the load/deflection or load/CMOD curves for the M95-iii, M95-ii and M95-iv model mortars, while Figures 3.29, 3.30 and 3.31 show the load/CMOD curves for M60-iii, M60-ii and M60-iv model mortars. The load/CMOD curves were used for some of the tests because for some unknown reason the computer did not log the measurements of the LVDT measuring the central deflection at mid span. And since it has been reported by Karihaloo[113], that the CMOD and central mid span deflection for a three point bend test are almost identical, the load/CMOD curves were used for the affected tests. The close agreement of the load/CMOD and load deflection curves can be seen from one of the tests unaffected by the anomaly in Figure 3.32. Barr et al[114] have suggested using of a correction factor given as Equation 3.4, for the correlation of the CMOD and mid-span deflection.

$$\delta = \frac{L}{4}\frac{1}{H}CMOD \qquad (3.4)$$

Where L is the loaded span, H the apparent depth over which the beam rotates and δ the mid-span deflection. By using Equation 3.4 the correlation factor was found to be 0.95, which indicates a very close correlation and therefore the load/CMOD curves were used for the analysis.

The load/deflection curves for the benchmark mortar, M95-iii reveal that the peak load in test M95-iii-3 is about half the peak load in the other two tests. As a result the post-peak softening branch for that test is not identical to those of the other two tests. No strong reason can be advanced for this. Not surprisingly the fracture energy for

this mortar from Table 3.6 comes out to be lower than expected; 9.9N/m which is even less than the fracture energy of the M95-iv mortar; 14.6N/m. In Figure 3.27, it is seen that the area under the curve for the M95-ii tests is greater than that in the M95-iii and MP-iii tests, an indication that more work is needed to create a unit area of fracture in the M95-ii mortar than in the M95-iii and MP-iii mortars. This is to be expected since the M95-ii is of higher strength class than the other two. The load/CMOD curves in Figure 3.28 for the M95-iv test show a more gentle post peak softening response than the M95-iii and M95-ii tests. This confirms the generally held view that designation (iv) mortars are better in accommodating movement than designation (ii) and (iii) mortars.

In Figures 3.29, 3.30 and 3.31, which show the load/CMOD curves for the M60 mortars, it is seen as expected that the area under the curves is largest in the M60-ii mortar followed by the M60-iii mortar and least in the M60-iv mortar. A combined plot of typical load/CMOD curves in Figure 3.33, for all the mortar tests, reveals that the areas under each of the three M60 curves are greater than the areas under the curves corresponding to the same mortar designation for the M95 mortars. This confirms that mortars with coarse sands generally have higher strength than those with finer sands because greater energy is required to propagate a unit area of crack.

Figure 3.34 shows the variation of the fracture energy in model mortars with respect to their strength class. It shows that the fracture energy increases linearly with increase in the strength of mortar. Probably because in the higher strength classes the proportion of the binder (cement) is higher, therefore more energy will be required to break the bond and create fracture. The fracture energy from the M60 mortar tests was also higher than the M95 tests as observed previously in the case of the compressive strength. In Figure 3.35, the flexural stress/deflection curves during fracture tests are shown for some selected mortar types as well as for the brick beam. It is seen from the figure that the brick is under a higher stress state than the mortars. In addition it has a sharper softening branch than the mortars, which is an indication of its more brittle nature. From the figure it can be seen that, the stress/deflection response in the pre peak region is almost linear for the brick while this is not the case for the mortars. However, the mean fracture energy for M60-ii mortar is higher than that of the brick beam by about 15%.

3.2.3.5 Mortar consistence test; Dropping Ball

The consistence of the mortar specimens was determined in accordance to BS 4551[115] and MR 2[116], the RILEM standard for the mortar consistence test. Consistence is defined by the Commission W3[117] as the property of a mortar by virtue of which it tends to resist deformation. This test was used to ensure a uniform consistence of all the mortar used by ensuring that the penetration value of the ball was within the prescribed limits.

3.2.3.6 Water retentivity and consistence retentivity Tests

The water retentivity and consistence retentivity tests were carried out in conjunction with the mortar consistence test mentioned above. Water retentivity measures the capacity of a mortar to retain part of its water content when it is in contact with an absorbent surface like brick. This is important because the properties of hardened mortar are largely affected by how much water is available for the complete hydration of cement in the mix.

Consistence retentivity is the measure of how much consistence a mortar retains when it is in contact with an absorbent surface like brick. Both tests were carried in accordance with the specification of BS 4551 Part 1: 1998. The values of these properties are summarised in Table 3.7.

The water retentivity of the prototype mortar, MP-iii was determined to be 84% and its consistence retentivity 55%. From Figure 3.36, which shows the consistence retentivity of the two model mortars across their respective strength classes, there does not seem to be a significant change in the consistence retentivity values for the M60 mortars. While for the M95 mortars there is decrease in consistence retentivity as the strength is increased. Also consistence retentivity of the M95-iii mortar is identical to that of the MP-iii mortar, while M95-iv had the highest consistence retentivity value of 60%. In terms of the water retentivity/strength class variation as seen from Figure 3.37; the M60 mortars had a marginally lower value of water retentivity than the M95 mortars.

It is expected that both prototype and model specimens would have similar properties with regards to bond formation between the unit and mortar, since the water retentivity of the prototype and benchmark model mortars are identical and their water

absorption properties similar. However the properties at the brick/mortar interface might be affected by the different surface textures of the prototype and model units. There could also be the effect of a faster drying rate of the thin model mortar joints because of their smaller surface area.

Scale	Length ,mm	Width, mm	Depth, mm
Prototype	215.0	102.5	65.0
Half	96.8	46.1	29.3
Fourth	53.8	25.6	16.3
Sixth	35.8	17.1	10.8

Table 3.1- Average dimensions of prototype and model bricks.

Mortar Type	Scale	Mortar designation and proportion	Sand
MP-iii	Prototype	(iii),1:1:6	Builder's sand
M95- ii	Sixth	(ii), 1:1/2:4	Congleton HST 95
M95- iii	Half, fourth, & Sixth	(iii),1:1:6	Congleton HST 95
M95- iv	Sixth	(iv),1:2:9	Congleton HST 95
M60- ii	Sixth	(ii), 1:1/2:4	Congleton HST 60
M60- iii	Sixth	(iii),1:1:6	Congleton HST 60
M60- iv	Sixth	(iv),1:2:9	Congleton HST 60

Table 3.2- Different mortar types used in the tests.

Test	Scale	Specimen Type	Quantity	Mortar Type	Sand Type	Bed Joint mm
Compressive Strength	Prototype	Wallette	5	MP-iii	Builder's sand	10
	Prototype	Triplet	5	MP-iii	Builder's sand	10
	Half	Triplet	5	M95-iii	HST95	5
	Fourth	Triplet	5	M95-iii	HST95	2.5
	Sixth	Triplet	5	M95-ii,M95-iii, M95-iv	HST95	1.6
	Sixth	Triplet	4	M60-ii,M60-iii,M60-iv	HST60	1.6
	Sixth	Triplet	4	M95-iii	HST95	1
	Sixth	Triplet	4	M95-iii	HST95	2.5
	Sixth	Wallette	5	M95-iii	HST95	1.6

Test	Scale	Specimen Type	Quantity	Mortar Type	Sand Type	Bed Joint mm
Shear Strength	Prototype	Triplet	15	MP-iii	Builder's sand	10
	Half	Triplet	12	M95-iii	HST95	5
	Fourth	Triplet	12	M95-iii	HST95	2.5
	Sixth	Triplet	12	M95-ii,M95-iii, M95-iv	HST95	1.6
	Sixth	Triplet	12	M60-ii,M60-iii,M60-iv	HST60	1.6
	Sixth	Triplet	12	M95-iii	HST95	1
	Sixth	Triplet	12	M95-iii	HST95	2.5

Test	Scale	Specimen Type	Quantity	Mortar Type	Sand Type	Bed Joint mm
Flexural Strength Normal and Parallel to bed joints	Prototype	Wallette	5 each	MP-iii	Builder's sand	10
	Half	Wallette	5 each	M95-iii	HST95	5
	Fourth	Wallette	5 each	M95-iii	HST95	2.5
	Sixth	Wallette	5 each	M95-ii,M95-iii, M95-iv	HST95	1.6
	Sixth	Wallette	5 each	M60-ii,M60-iii,M60-iv	HST60	1.6
	Sixth	Wallette	5 each	M95-iii	HST95	1
	Sixth	Wallette	5 each	M95-iii	HST95	2.5

Test	Scale	Specimen Type	Quantity	Mortar Type	Sand Type	Bed Joint mm
Bond Strength	Prototype	Couplet	9	MP-iii	Builder's sand	10
	Half	Couplet	9	M95-iii	HST95	5
	Fourth	Couplet	9	M95-iii	HST95	2.5
	Sixth	Triplet	8	M95-ii,M95-iii, M95-iv	HST95	1.6
	Sixth	Triplet	8	M60-ii,M60-iii,M60-iv	HST60	1.6
	Sixth	Triplet	8	M95-iii	HST95	1
	Sixth	Triplet	8	M95-iii	HST95	2.5

Test	Scale	Specimen Type	Quantity	Mortar Type	Sand Type	Bed Joint mm
Diagonal Tensile Strength	Prototype	Wallette	3	MP-iii	Builder's sand	10
	Half	Wallette	5	M95-iii	HST95	5
	Fourth	Wallette	5	M95-iii	HST95	2.5
	Sixth	Wallette	5	M95-ii,M95-iii, M95-iv	HST95	1.6
	Sixth	Wallette	5	M60-ii,M60-iii,M60-iv	HST60	1.6
	Sixth	Wallette	5	M95-iii	HST95	1
	Sixth	Wallette	5	M95-iii	HST95	2.5

Table 3.3- Details of all masonry tests.

Test	Prototype	Half	Fourth	Sixth
Compressive Strength, N/mm^2	29.2	30.6	41.9	47.4
COV, %	14.3	8.4	9.7	32.7
Flexural Strength, N/mm^2	4.3	6.3	3.7	4.4
COV, %	21.2	15.1	10.4	24.8
Indirent tensile strength, N/mm^2	1.9	2.1	2.2	2.4
COV, %	14.0	29.5	34.9	22.5
Water Absorption, %	14.8	16.5	15.3	16.3
COV, %	14.8	5.6	5.3	16.7
Modulus of Elasticity, N/mm^2	11500	-	-	-
COV, %	31	-	-	-
Fracture Energy, N/m	47.4	58.2	-	-
COV, %	10.5	25.8	-	-
Poisson's ratio	0.06	-	-	-
COV, %	48.1	-	-	-

Table 3.4- Mechanical properties of prototype and model bricks.

	Top	Side	End
	Strength,N/mm^2	**Strength,N/mm^2**	**Strength,N/mm^2**
1	24.3	27.1	31.3
2	31.4	35.4	31.9
3	24.9	35.4	29.3
4	22.8	31.8	38.8
5	24.2	32.7	31.1
6	21.7	26.1	31.9
Mean	**24.9**	**31.4**	**32.4**
COV%	**13.6**	**12.7**	**10.1**
% increase	**0**	**26**	**30**

Table 3.5- Effect of loading orientation on brick strength.

Scale	Total length mm	Length of support, l mm	b mm	d mm
Prototype	670.0	570.0	130.0	67.0
Half	292.0	252.0	46.1	29.6
Fourth	463.0	143.0	25.7	16.5
Sixth	109.0	96.0	17.2	10.8

Table 3.6- Average dimension of flexural tensile strength specimens.

	HST95ii	HST95iii	HST95iv	HST60ii	HST60iii	HST60iv	MP
Mortar Designation	ii	iii	iv	ii	iii	iv	iii
Vol. Proportions	1 : 1/2 : 4	1 : 1 : 6	1 : 2 : 9	1 : 1/2 : 4	1 : 1 : 6	1 : 2 : 9	1 : 1 : 6
W/c ratio	1.25	1.8	2.58	1.11	1.41	2.20	1.55
Water retentivity,%	83	86	85	83	83	81	84
Consistence retentivity,%	40	55	60	40	42	40	55
Comp. Str. N/mm^2	6.3(3.3)	4.7(8.5)	1.8(8.1)	10.0(4.6)	7.1(8.8)	2.3(3.1)	5.0(1.8)
Flexural Str. N/mm^2	3.3(5.1)	2.3(5.3)	0.8(5.5)	3.5(0.21)	2.5(6.0)	0.9(1.9)	1.8(11.8)
Fracture Energy, N/m	42.0(19.8)	9.9(20.2)	14.6((36.2)	54.7(0.3)	43.3(14.0)	18.8(27.4)	19.5(8.3)
Modulus of Elasticity,	12900(7.9)	6500(8.7)	4500(12.7)	17000(2.96)	12500(5.22)	6800(5.51)	6300(17.8)
Poisson's ratio	0.10	0.10	0.09	0.12	0.11	0.10	0.12

Table 3.7- Properties of prototype and model mortars (COV in brackets).

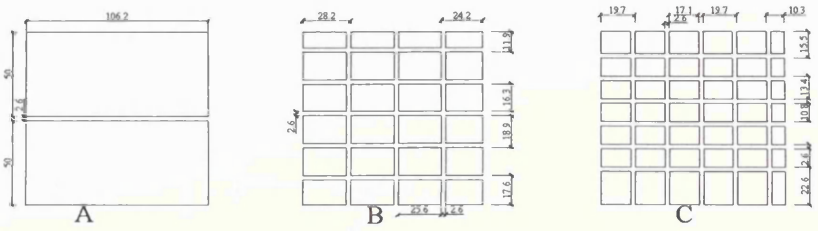

Figure 3.1- Drawing plans showing the cutting dimensions in the half, fourth and sixth model units respectively.

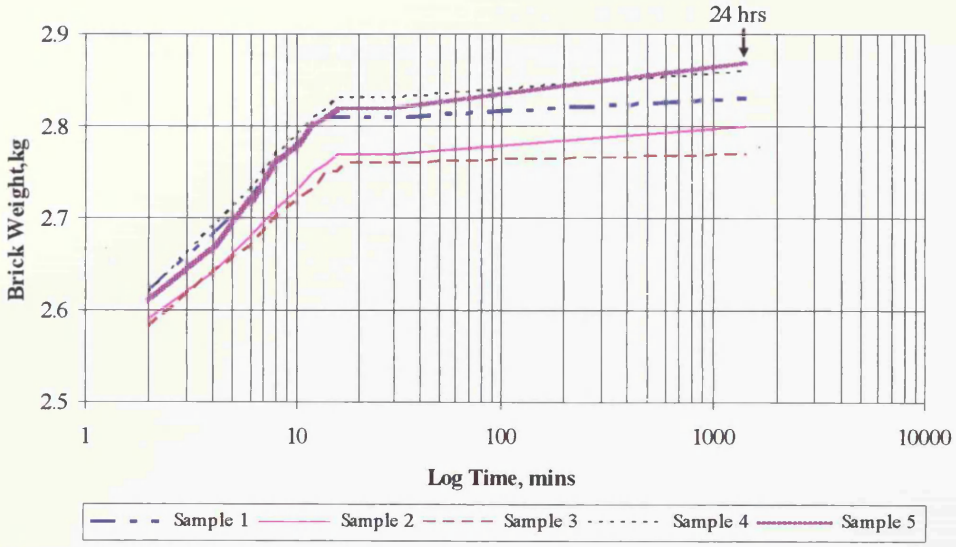

Figure 3.2-Water absorption characteristics of the prototype brick.

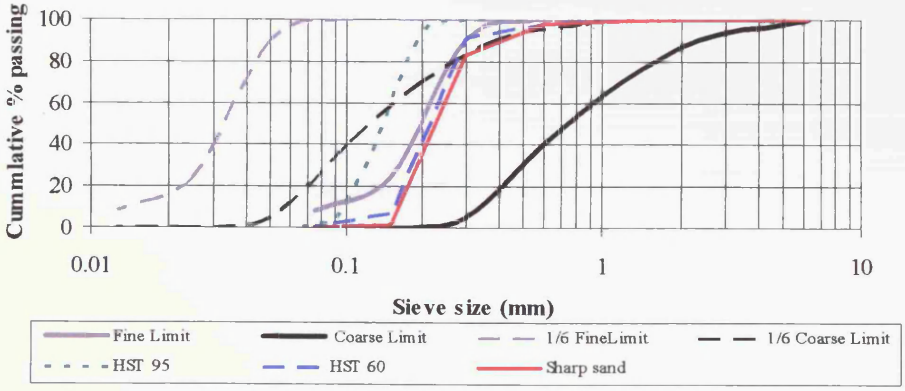

Figure 3.3- grading curves for prototype and model sands within the BS limits.

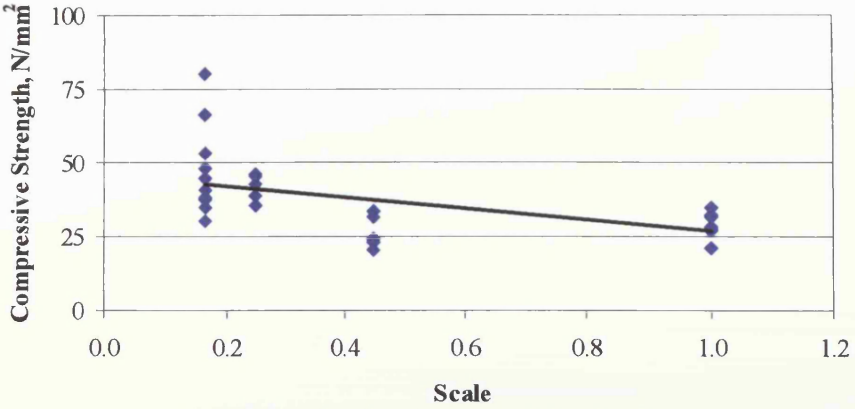

Figure 3.4- Unit compressive strength in the four scales.

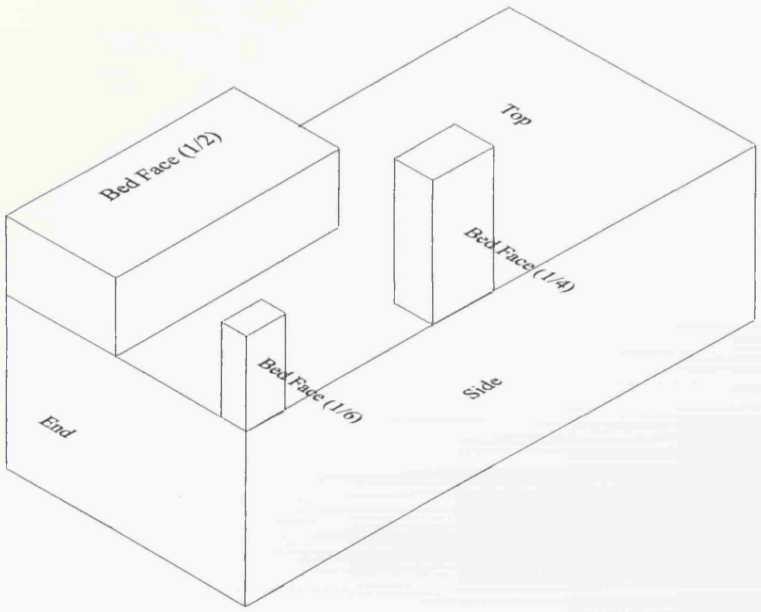

Figure 3.5- Orientation of model units in a prototype brick.

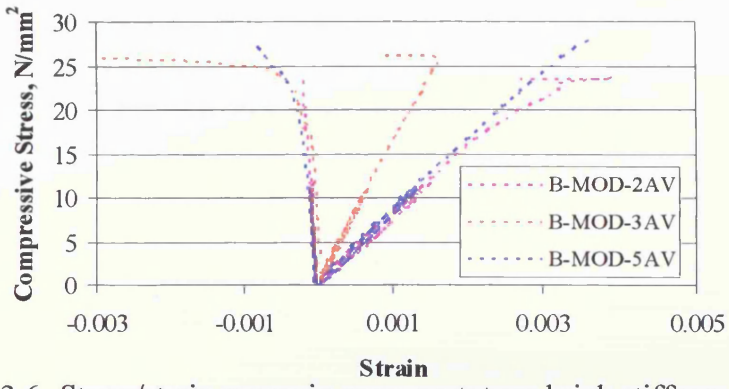

Figure 3.6- Stress/strain curves in some prototype brick stiffness tests.

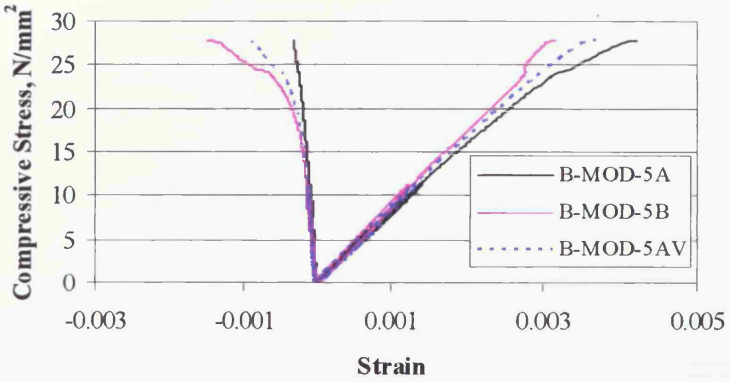

Figure 3.7-Typical stress/strain relationship in prototype brick.

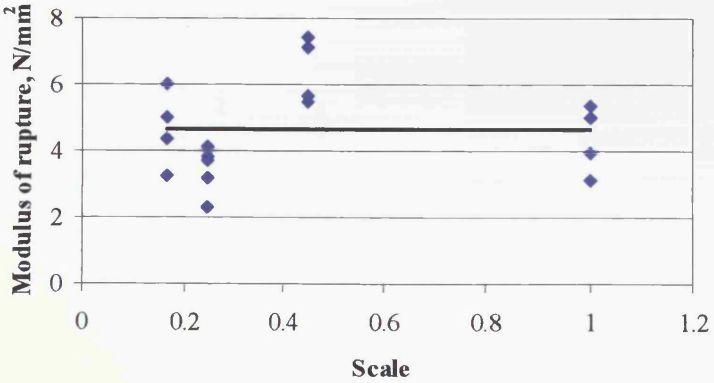

Figure 3.8- Modulus of rupture of prototype and model scale units

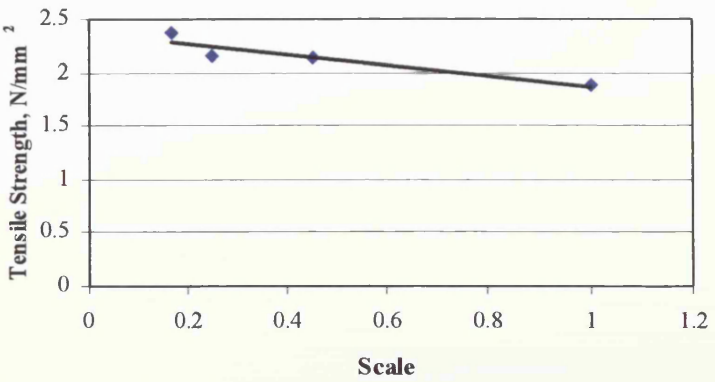

Figure 3.9- Indirect tensile strength of prototype and model scale units.

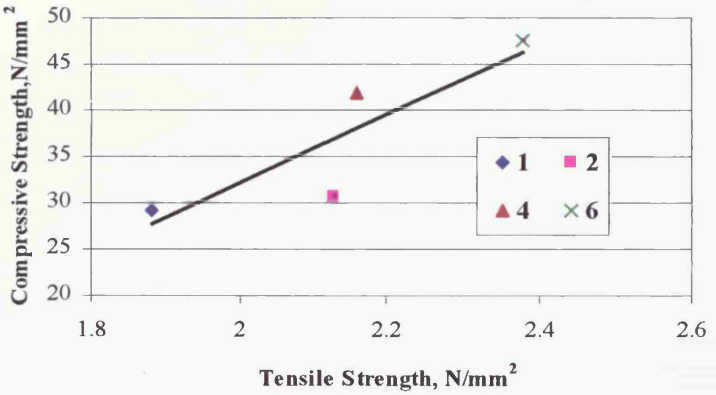

Figure 3.10- Compressive strength/tensile strength relationship for prototype and model units.

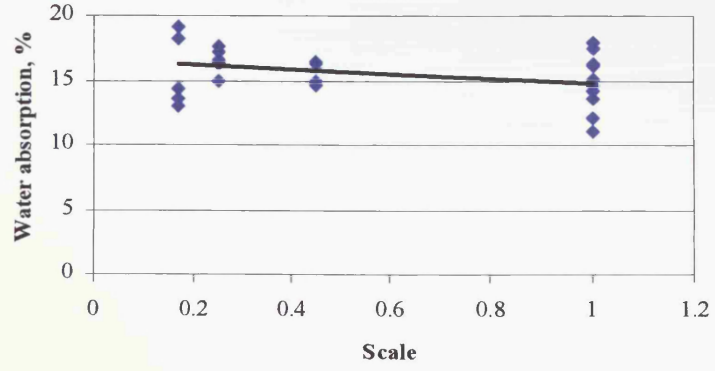

Figure 3.11- Water absorption of units across the four scales.

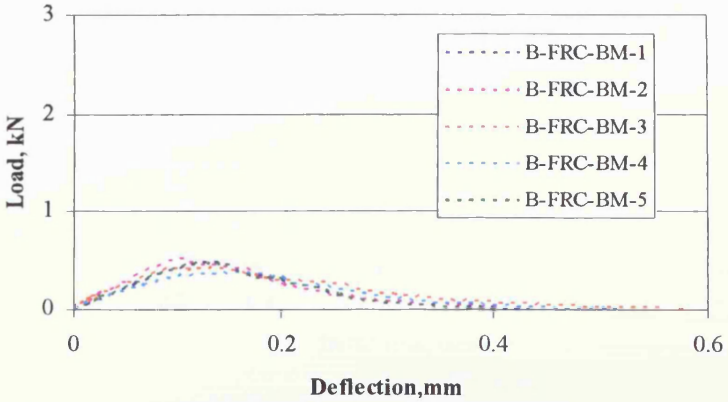

Figure 3.12- Load/deflection curves for prototype brick beam fracture test.

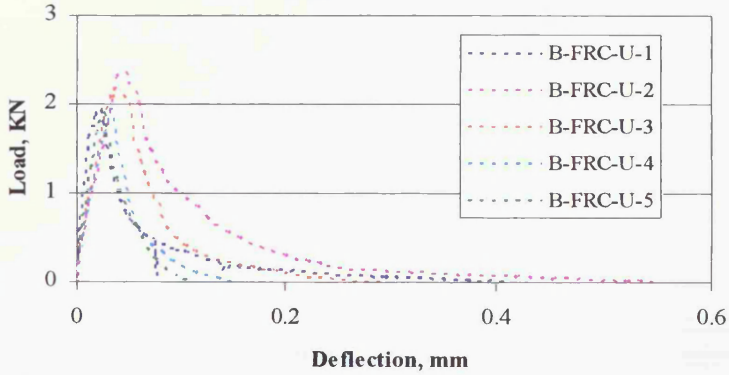

Figure 3.13- Load/deflection curves for prototype unit fracture test.

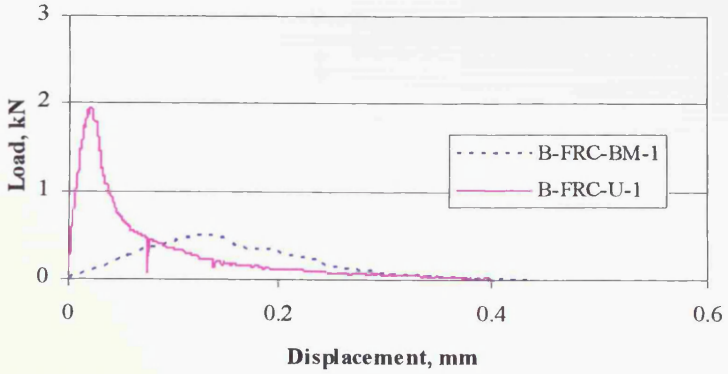

Figure 3.14- Typical load/deflection response for beam and single unit prototype fracture energy tests.

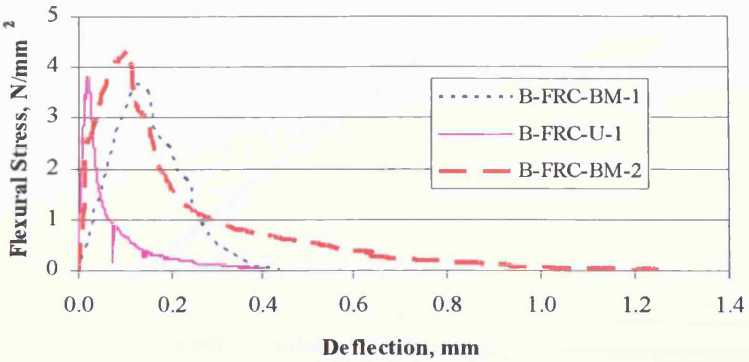

Figure 3.15- Flexural stress/deflection response for prototype and half scale unit Fracture Energy tests.

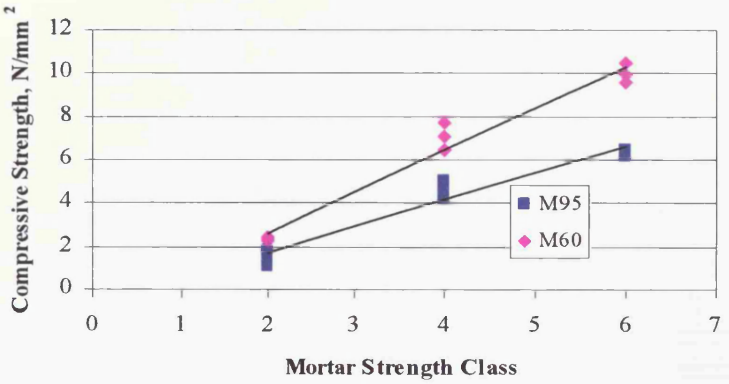

Figure 3.16- Compressive strength of model mortars/strength class relationship.

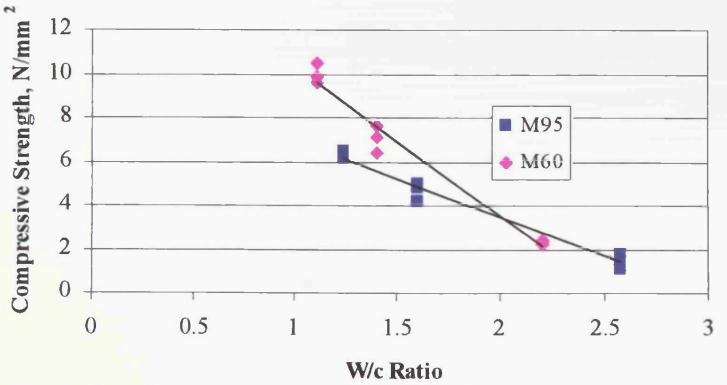

Figure 3.17- Variation of compressive strength of model mortars with w/c ratio.

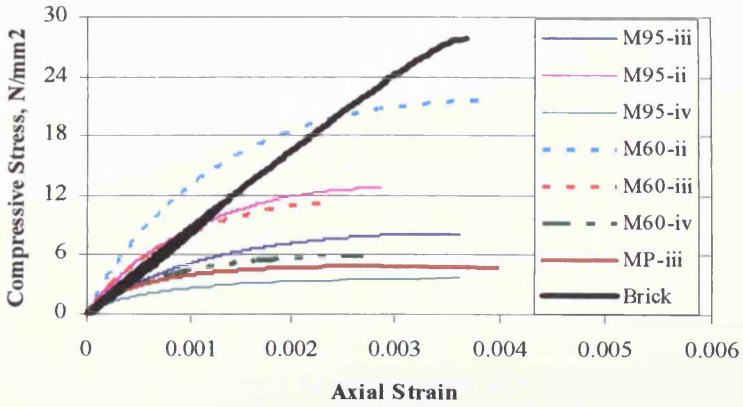

Figure 3.18- Comparison typical stress/ axial strain plot for prototype and model mortars.

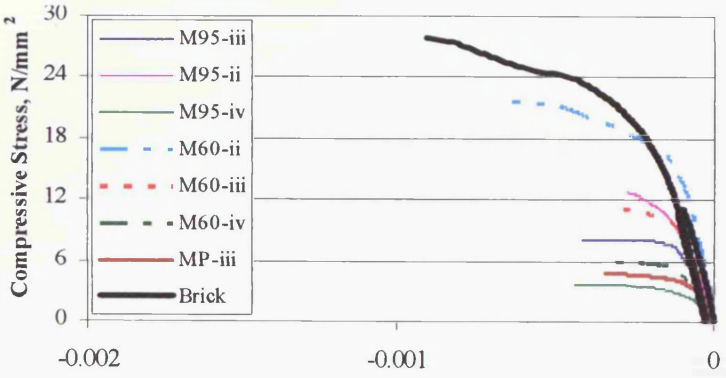

Figure 3.19- Comparison of typical stress/lateral strain plot for prototype and model mortars.

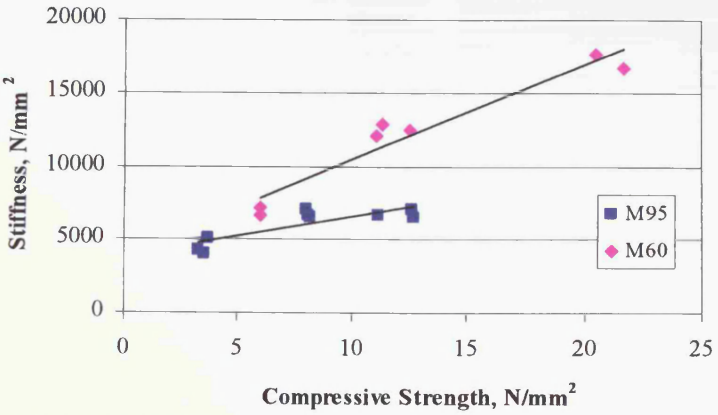

Figure 3.20- Variation of stiffness with strength for model mortars.

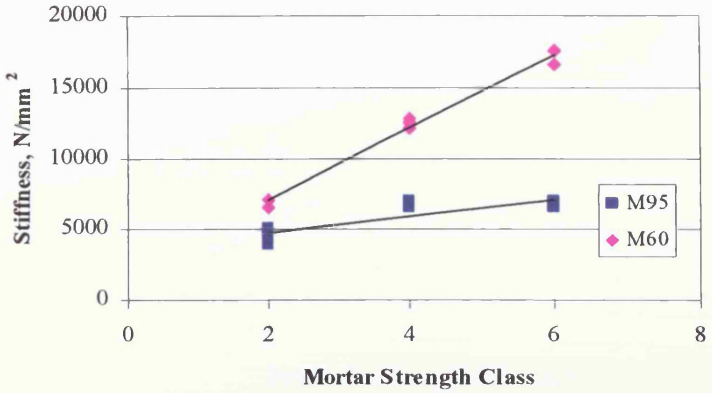

Figure 3.21- Variation of stiffness with strength class for model mortars.

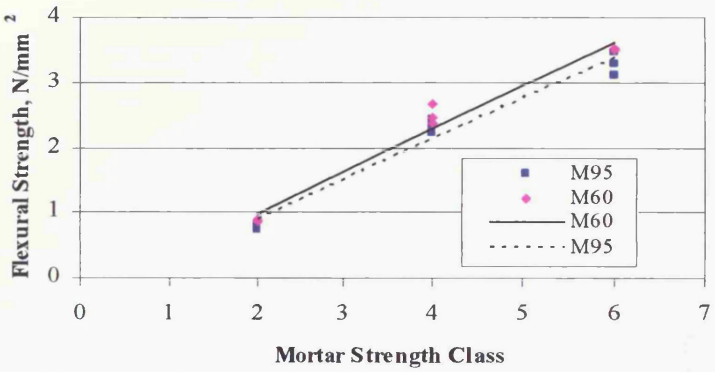

Figure 3.22- Flexural strength of model mortars/strength class relationship.

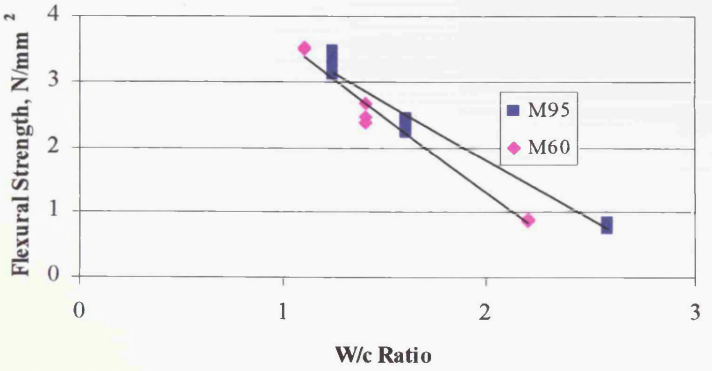

Figure 3.23- Variation of flexural strength of model mortars with w/c ratio

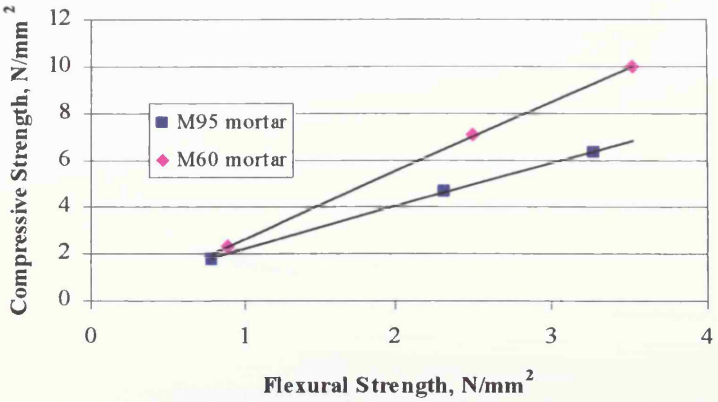

Figure 3.24- Mean compressive strength/ mean flexural strength relationship for model mortars.

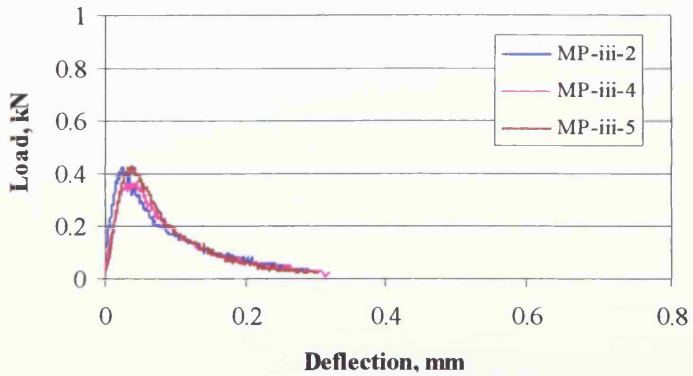

Figure 3.25- Load/deflection graphs for prototype mortar fracture tests.

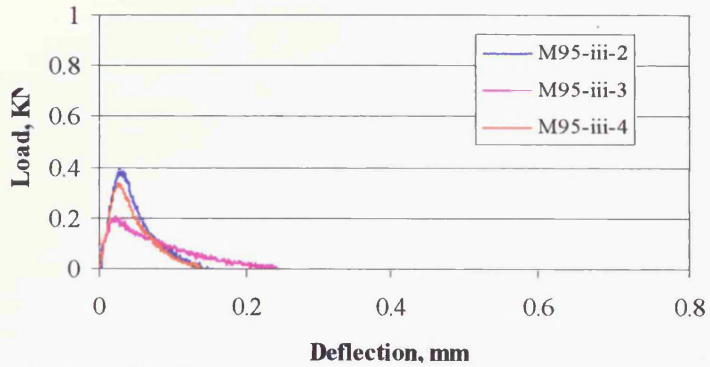

Figure 3.26- Load/deflection graphs for benchmark mortar fracture test.

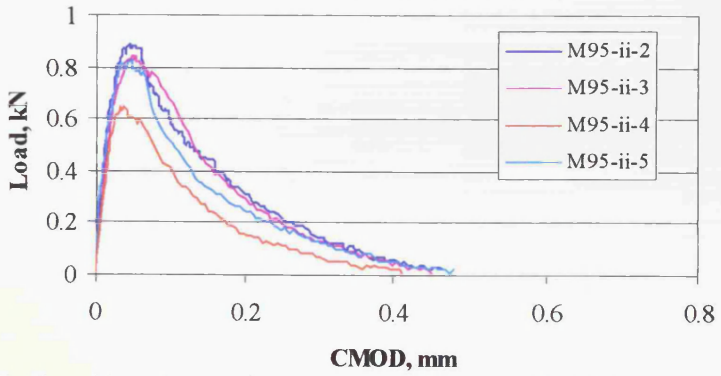

Figure 3.27 - Load/crack mouth opening deflection, CMOD for M95-ii mortar fracture test.

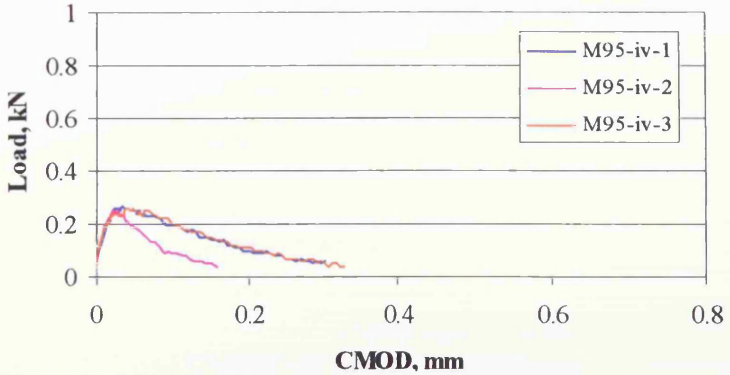

Figure 3.28- Load/CMOD curves for M95-iv mortar fracture test.

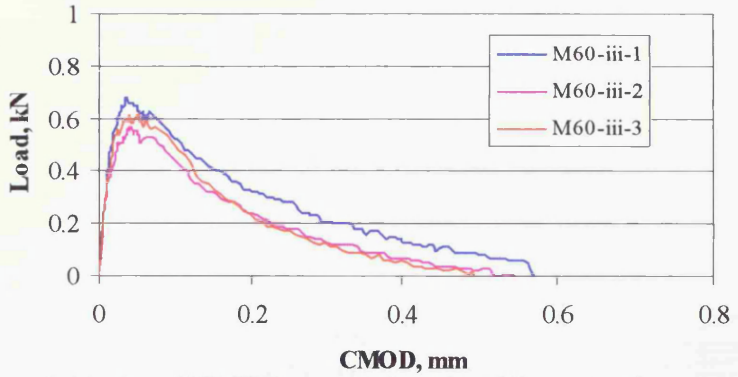

Figure 3.29- Load/CMOD curves for M60-iii mortar fracture test.

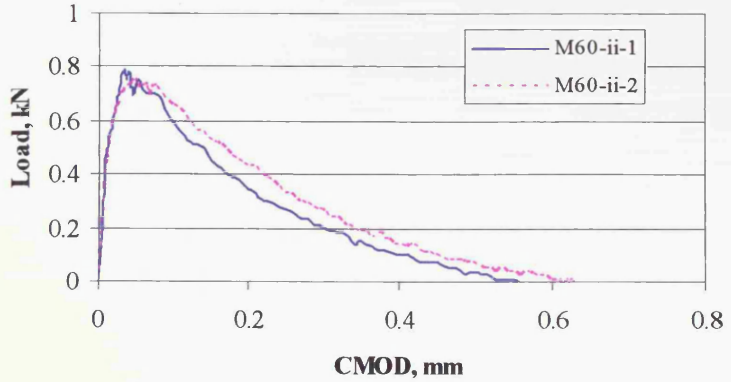

Figure 3.30- Load/CMOD curves for M60-ii mortar fracture test.

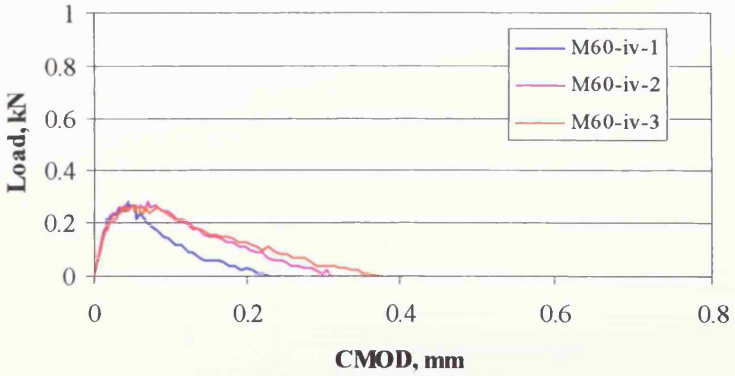

Figure 3.31- Load/CMOD curves for M60-iv mortar fracture test.

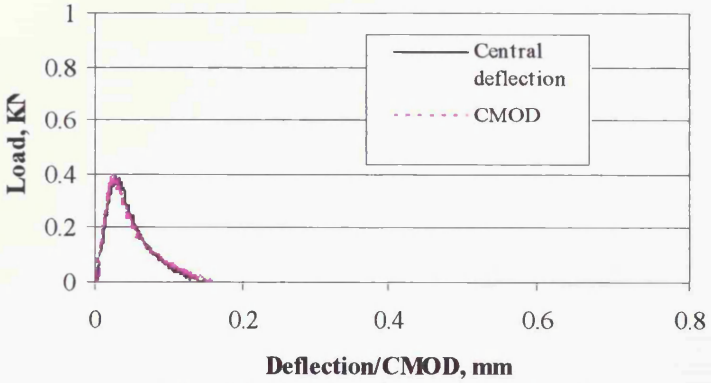

Figure 3.32- Comparison of Load/CMOD and central deflection at mid span for M95-iii fracture test.

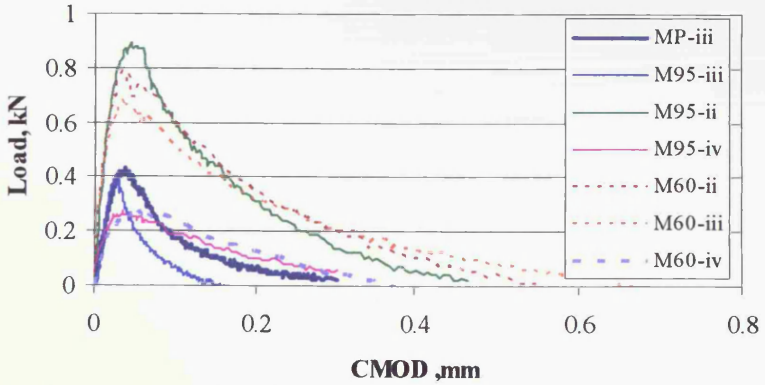

Figure 3.33- Comparison of typical load/CMOD curves from mortar fracture test

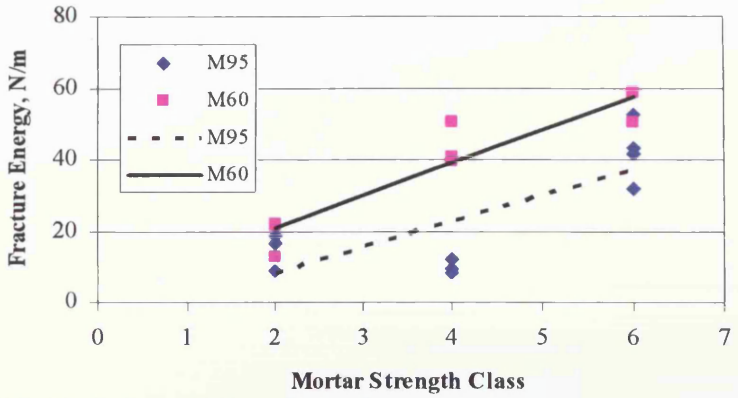

Figure 3.34- Variation of fracture energy with mortar class in model mortars.

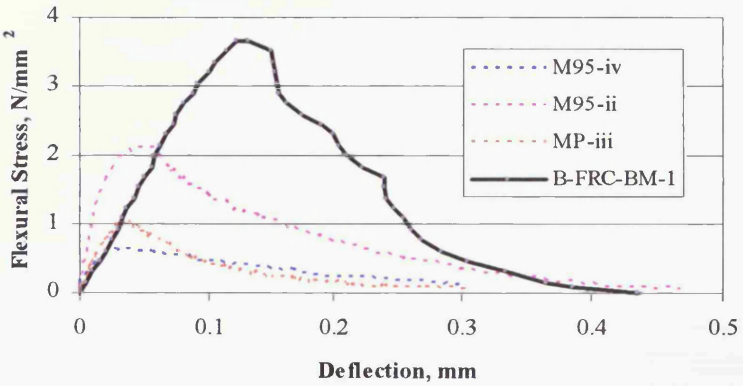

Figure 3.35- Comparison of flexural stress/deflection curves for some mortars and prototype brick during fracture tests.

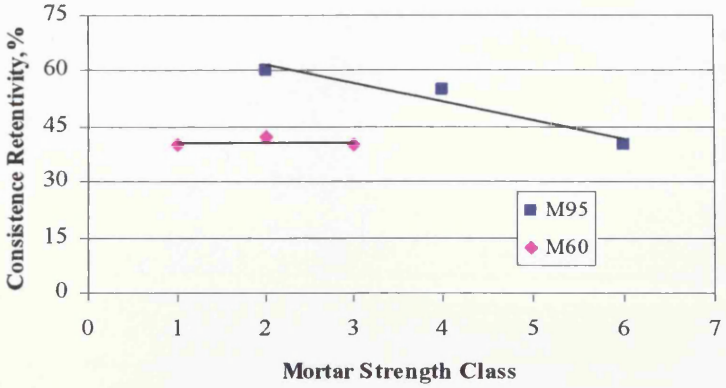

Figure 3.36- Variation of consistence retentivity in model scale mortars.

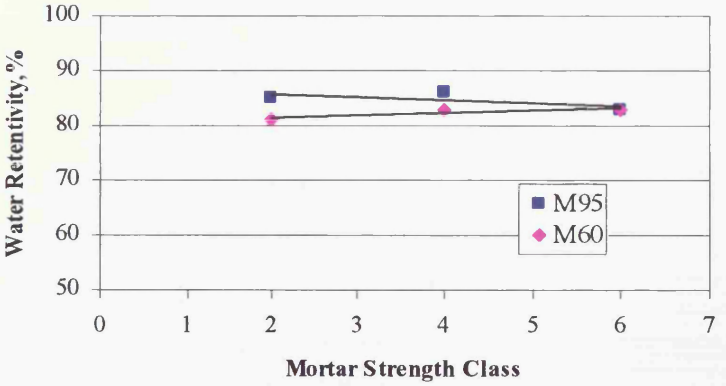

Figure 3.37- Variation of water retentivity in model scale mortars.

Plate 3.1(a)- Triplet masonry specimen in preparation.

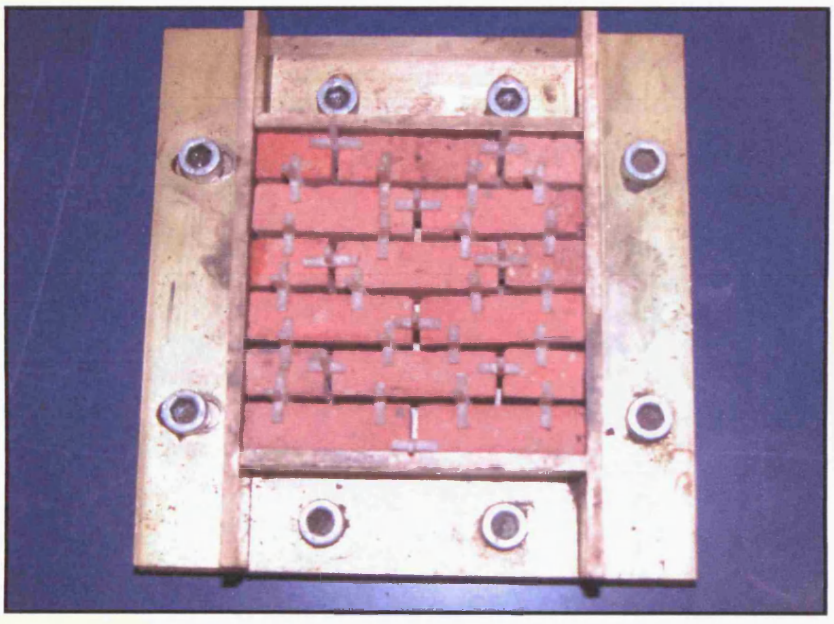

Plate 3.1(b)- Sixth scale wallette specimen in preparation.

Plate 3.2- Set up of brick modulus of elasticity test.

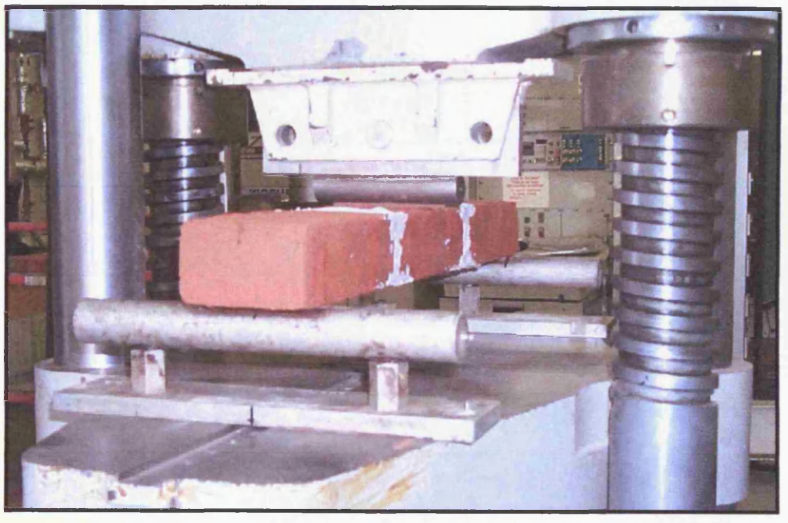

Plate 3.3- Set up of prototype brick flexural strength test.

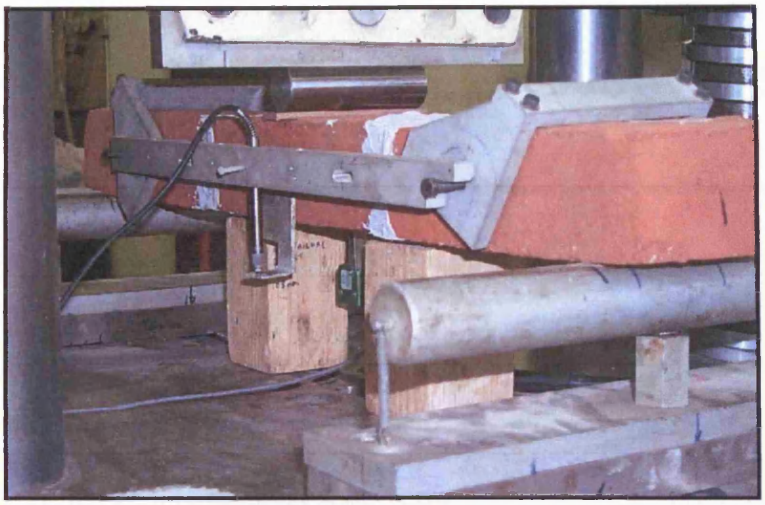

Plate 3.4- Set up for brick beam fracture energy test.

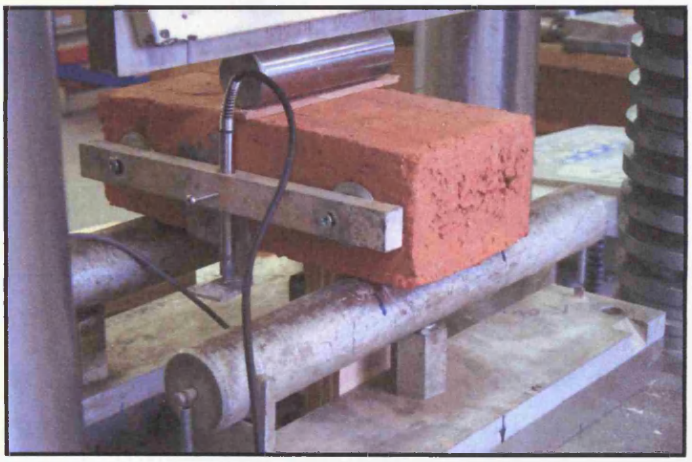

Plate 3.5- Set up for single brick unit fracture energy test.

Plate 3.6- Set up for half scale model unit fracture test.

4 Masonry Assemblies and Tests

The details of the various masonry tests and their instrumentation are presented in this chapter. Most of the tests are derived from standard masonry tests from the codes, and performed on small specimens for example wallettes and triplets. The detail of the development of the testing programmes has been given in Chapter 3.

The five masonry tests undertaken as part of the current study were the; compressive strength test, initial shear strength test, flexural strength tests, bond wrench test and diagonal shear strength test. All the five tests were carried out on each of the four scales namely; prototype, half, fourth and sixth scale.

Loading rate

In general the tests were carried out under load control as specified by most of the standards and their recommendations used. For example in the compressive strength a loading rate of 0.15N/(mm^2.min) for low strength units to 1.25N/(mm^2.min) for high strength unit was specified by BS EN 1052-1[89]. Since the units used in this investigation are of medium strength (29N/mm^2 for the prototype and 46N/mm^2 for the sixth scale) a loading rate of 0.5N/mm^2/min was used for the tests. For the prototype and half scale triplet tests this works out as 0.18kN/s and 0.04kN/s respectively. The same procedure was used to determine the loading rates for the scales and tests. However in some of the model tests involving low loads where a 20kN capacity testing machine was used, testing in load control was not achievable and a constant rate of displacement was used for the affected tests. In such cases a trial test was first carried out in displacement control to determine the time taken to reach maximum load in a test, from which a suitable displacement rate was determined that would achieve failure in a time comparable to the time taken to reach failure in the tests with load control. Maurenbrecher[118] has reported that compressive strength tests on extruded stack bonded masonry units tested at 9.5N/mm^2 and 0.3N/mm^2 loading rates showed a reduction of only 4% in strength for the slower test. Therefore it was concluded that using a constant displacement rate instead of constant

load rate for the smaller model tests should not significantly alter the outcome of the tests.

4.1 Compressive strength test

Prototype

Two specimen formats were tested at this scale; a 2 brick wide by 6 brick high wallette specimen as shown in Figure 4.1(a) and a three brick high triplet as shown in Figure 4.2. Both specimen types were made with the MP mortar. The former were tested in accordance with the requirements of BS EN 1052-1[89] in a testing machine at a loading rate of 0.4kN/s while the latter were tested at a loading rate of 0.18kN/s until failure occurred. Three 25mm cubes were collected from each batch of mortar made and were tested at 28 days for the determination of their compressive strength for quality control purposes.

In the case of the 2 x 6 wallette specimens, the positions of the LVDTs are as shown in Figure 4.1(a), while Figure 4.2 shown the positions of the LVDTs in the triplet specimens. The LVDTs were fitted in order to measure the deformations of the specimens under compressive loading for the determination of the stiffness properties of the masonry. In both instances, the LVDTs were fitted on both the front and back faces of the specimens (top and bottom in relation to how the bricks were laid in the mould) to identify any bending effects. Fibreboard pieces were used as packing to ensure a flat level surface in case of the prototype specimens. However it was thought that using fibreboard pieces would not be necessary for the testing of model scale specimens since their surfaces were already flat. Furthermore it has been reported by Templeton and Edgell[119] that the compressive strength of clay bricks with mortar capped surfaces are only about 8% more than those with ground surfaces for low to medium strength bricks. While Edgell et al[120] have found that mortar capped masonry wallettes are only about 2% stronger in compression than plywood capped wallettes. From the forgoing it was therefore concluded that using fibreboard capped prototype specimens would still be comparable to uncapped surfaces of the model specimens.

Instrumentation

Four LVDT's, two on either face were used to measure vertical deformations on the prototype wallettes. The range of these vertical transducers was ±15mm while the range of the transducers used for measuring the horizontal deformations were ±10mm. One each of these transducers was used on either face of the wallettes. Measurements were monitored and recorded on a data logger together with the output from the load cell.

In the case of the triplet specimens at half, fourth, and prototype scales, LVDT's with a range of ±5mm were used for recording the vertical deflections under the applied loading. All measurement were monitored and recorded on a data logger connected to both the transducers and the load signal.

Because of the small sizes of the sixth scale specimens, specially made gauges called model masonry clip gauges (MMCG's) were used for the deformation measurements. These gauges were made for an earlier project involving sixth scale models [52] and they consist of a central 6mm wide spring steel clip, 0.5mm thick as shown in Plate 4.1. The figure shows the ends of the steel clip which carry two M3 caphead bolts, one at each end at a distance of 30mm apart. Fastened to the end of these bolts are two aluminium arms with 1.0mm holes for attaching to drawing pins. A thin steel plate was finally attached to one end to carry the wire connectors and also to secure the wires. Mounted on the spring steel are four electrical resistance gauges, two aligned orthogonally on each side. The gauges were manufactured by Micromeasurements Group, UK and were of type CEA-06-UN-350. They were wired in a full bridge strain gauge circuit and were made to locate on two standard drawing pins, placed 25mm apart. This corresponds to the distance between the centres of the units in three courses of sixth scale masonry. To ensure uniformity in laying the pins, small gauge bars were used to position the pins at the required spacing of 25mm apart. Plate 4.2 shows the specimens fitted with the MMCGs for the sixth scale triplet and wallet stiffness test

Half Scale

Three brick high triplet specimens were tested in compression in this case. Load was applied at a rate of 0.04kN/s until failure occurred. Two transducers; one on each side, were fitted longitudinally on opposite sides of the specimen for measurement of the

deformation of the specimen under the applied load. The mean of five specimens was used for determining the compressive strength at this scale. Plate 4.3 shows all four triplet specimens from the four scales side by side.

Fourth scale

Three brick triplet specimens similar to those in the other scales detailed were tested in compression in a load control machine at a load rate of 0.02kN/s until failure occurred. The specimens were fitted with one transducer each on opposite sides of the specimen to measure the longitudinal deformations in the direction of loading.

Sixth Scale

Two specimen formats were tested as in the prototype test. Designation (iii) mortar prepared with HST 95 sand (benchmark mortar) was used in this instance for both specimen formats, while only triplet specimens were made with the other mortar types shown in Table 4.1 and for the different joint thickness tests. The wallette specimens were tested in accordance with the requirements of BS EN 1052-1[89] with displacement control at a constant displacement rate of 0.005 mm/s until failure occurred. While the triplet specimens were tested in displacement control at a constant displacement rate of 0.06mm/min until failure of the specimens. MMCG's were used to measure the deformations of the specimens under the applied loading; Figure 4.1(b) shows how the gauges were fixed to both sides of the wallette specimens.

Stiffness

The modulus of elasticity of the wallette specimens was calculated according to the recommendations of BS EN 1052-1[89], which stipulates that it should be determined as a secant modulus from the mean of the strains of all four measuring positions at a third of the maximum stress reached. In the case of the triplet specimens, the stiffness was also determined from the mean strains of the two measuring points occurring at a third of the maximum stress. Plate 4.4 shows the set up for the prototype modulus of elasticity tests.

Calculations

Strength

From BS EN 1052-1[89], the compressive strength of masonry, f_i was determined from Equation 4.1

$$f_i = \frac{F_{max}}{A_i} \quad \text{N/mm}^2 \qquad (4.1)$$

Where F_{max} is the maximum load reached on an individual masonry specimen and A_i is the loaded cross-section of an individual masonry specimen.

Also from the same code, the characteristic compressive strength of masonry is given as $f_k = f/1.2$ or $f_k = f_{i,\min}$ (4.2)

Where, $f_{i,\min}$ is the smallest compressive strength of an individual masonry specimen and f is the mean compressive strength of the masonry.

Modulus of elasticity

The modulus of elasticity of an individual masonry specimen was evaluated as a secant modulus from the mean of all the measuring positions (two for the triplet specimens and four for the wallet specimens), occurring at a stress equal to one third of the maximum stress reached according to the provisions of BS EN 1052-1[89] using Equation 4.3.

$$E_i = \frac{F_{max}}{3.\varepsilon_i.A_i} \qquad (4.3)$$

Where ε_i is the mean strain in an individual masonry specimen at one third of the maximum strength achieved.

4.2 Shear strength test

Prototype

The shear strength test for the prototype was carried out in accordance with the provisions of BS EN 1052-3[31] the standard for the determination of initial shear strength of masonry specimens. The set up dimensions for the initial shear strength test are shown in Figure 4.3, which shows a triplet specimen supported on two rollers. A special test rig was fabricated and used for the testing of the triplet specimens using the general provisions of the standard. The rig is shown in Plate 4.5, which shows that

it made up of a four 25 x 25mm square Rectangular Hollow Section (RHS) welded to 15mm steel plates at either end. A 100kN load cell was bolted on one of steel plates while a hydraulic ram was mounted on to the other. The supports consisted of two 12mm steel plates on to which 12mm diameter bars were welded while the load was applied through two 12mm diameter bars held on to 12mm steel plate with plasticine.

The specimens were placed within the frame on the supports against 15mm steel plates that push against the load cell on one end and the hydraulic ram on the other. Fibre board pieces were put in between the specimen and steel plates to even out surface irregularities on the bottom and top faces of the specimens. The ram was controlled through an air regulator while the exerted pressure was read through a Gemini universal signal conditioning unit. The experiments were carried out at three precompression stress levels of $0.2N/mm^2$, $0.6N/mm^2$ and $1.0N/mm^2$ while the shearing load was applied at a loading rate of 0.15kN/s using a load controlled machine. Four specimens were tested at each precompression level making a total of 12 specimens.

Half Scale

A similar frame to the one used in the prototype test was used for testing the specimen in this case. The only difference in the two frames was the size; apart from that they were similar in every respect. The support bars were 6mm in diameter, which were welded to 6mm steel plates as in previous case. The same hydraulic ram was used to exert the precompression force needed for the test, while a 20kN load cell was used to measure the applied precompression force. Instrumentation was as described in the last section and load was applied at a loading rate of 0.02kN/s via the same testing machine.

Fourth and sixth Scale

A specially constructed rig was used for testing the specimens in the fourth and sixth scales. Plate 4.6 shows a picture of the set up for the sixth scale test. At one end of this rig is a pneumatic ram attached to a 50kgf Z-load cell via a steel bolt, at the other end is a rigidly bolted steel block. The specimen sits against this block and another that is free to move horizontally and connected to the Z-load cell by means of a steel ball. Compressed air was passed through an air regulator into the inlet valve of the

ram, this in turn pushes the Z-load cell and exerts a force that compresses the specimen between the two steel blocks. The specimens were supported on 6mm bars fixed to 5mm steel plates for the fourth scale test while a 5mm bar and 5mm steel plate was used for the sixth scale test.

The force exerted on the load cell was read via a data logger, where it was monitored and controlled by means of the regulator. The shearing load was applied at a rate of 0.01kN/s via the testing machine until the shear failure of the specimens.

Calculations

The individual shear strength, f_{shi} and precompression stress, f_{pi} for each specimen were calculated from Equations 4.4 and 4.5 respectively

$$f_{shi} = \frac{F_{i\max}}{2A} \tag{4.4}$$

$$f_{pi} = \frac{F_{pi}}{A} \tag{4.5}$$

where F_{imax} and F_{pi} are the maximum shear load reached and the maximum precompression force respectively. While A is the cross- sectional area of the specimen parallel to the bed joints.

The initial shear strength was evaluated from the plot of f_{shi} against f_{pi} as the intercept of the linear regression line of the plots on the vertical axis, while the gradient represents the co-efficient of friction.

4.3 Flexural strength test

Prototype

The test specimens were in accordance with the specifications of methods of tests for masonry-Part 2: determination of flexural strength, BS EN 1052-2[91], however the actual test was carried out whilst the specimens were supported and loaded in a horizontal orientation while the code recommends a vertical loading arrangement. Two specimen formats were tested; a 2 units wide by 10 courses high rectangular specimen for the determination of the masonry flexural strength across the bed joints

and a 4 units wide by 4 courses high wallette for the determination of the flexural strength parallel to the bed joints. The load was applied at a load rate of 0.5kN/s until the failure of the specimens while the panels were supported on two roller supports of 40mm diameter and loaded by two rollers of the same diameter. Plate 4.7 shows the set up for the flexural strength parallel to bed joints test. Fibreboard pieces were put in between the roller surfaces and specimen to ensure all round contact between them. A steel panel carrying a swivel head was placed on the rollers to eliminate any unevenness of the specimen surface so as to ensure uniform load application through both loading rollers. Figure 4.4 shows the set up dimensions for the flexural strength parallel to the bed joints while Figure 4.5 shows the set up dimensions for the flexural strength normal to the bed joints in all four scales.

Half Scale

The two specimen formats were tested using a load controlled testing machine, in this case at a loading rate of 0.05kN/s. Steel rollers of 19mm diameter were used to support the specimens while loading rollers of the same diameter were used. The load was applied through a swivel placed on top of a rigid steel plate as in the previous case to ensure uniform load application through both rollers.

Fourth Scale

The flexural strength test was also carried out in a load controlled testing machine at a load rate of 0.03kN/s. The specimens were supported on 12mm diameter steel rollers and loaded in four point bending through rollers of similar diameter. A swivel head was used to apply the load as in the previous cases.

Sixth Scale

A small capacity testing machine was used to carry out the flexural strength tests at this scale. Load was applied via displacement control at a rate of 0.3mm/min until failure of the specimens. Steel rollers of 9mm diameter were used to support and load the specimens in four point bending. As in the other scales load was applied through a swivel head, formed by placing a steel ball in between two steel plates with rounded centres. The set up for the test is shown in Plate 4.8.

Calculation

The flexural strength of masonry, f_i was determined from Equation 4.6.

$$f_i = \frac{3(F_{max}+W)(l2-l1)}{2Bt^2} \qquad (4.6)$$

where F_{max} is the maximum load reached, W is the self weight of a specimen and t is the width of masonry unit. B, $l2$ and $l1$ are as defined in Figures 4.4 and 4.5.

4.4 Bond wrench test

Prototype

Couplet specimens were made for the determination of the bond strength of masonry using the bond wrench method and tested in accordance with the specifications of the RILEM standard LUMB3[121]. Plate 4.9 shows a picture of the test set up, which consist of a lever clamped to the upper unit in the assembly and another clamp applied to the lower unit, restraining the assembly from movement whilst load was applied to the end of the upper lever. Load was applied via a load controlled testing machine at a load rate of 0.07kN/s. The load was applied at a distance of 335mm from the longitudinal centre of the assembly. Figure 4.6 gives the set up dimensions for the four scales.

Half, fourth and sixth scales

A similar arrangement to the one used in the prototype tests were also used in the case of the half, fourth and sixth scale models. The tests were however carried out in a smaller capacity testing machine at displacement rates of 1mm/min, 0.6mm/min and 0.3mm/min corresponding to the rates in the half, fourth and sixth scale specimens respectively. The load was applied at a distance of 175mm, 105mm and 43mm from the longitudinal centre of half, fourth and sixth scale specimens respectively. Plate 4.10 shows the set up for the sixth scale test.

Calculations

The bond strength, S was calculated from Equation 4.7.

$$S = \frac{M}{Z} - \frac{W}{bd} \qquad (4.7)$$

Where M = bending moment at failure in Nmm,

Z = section modulus in mm^3 (given as $bd^2/6$),

W= maximum compressive load applied to the joint, N,

b and d are mean width and depth respectively of joint at line of fracture.

4.5 Diagonal tensile strength test

Prototype

The diagonal tensile strength test was carried in a testing machine according to the provisions of the RILEM recommendation for the determination of the diagonal tensile strength of small wall specimens, LUMB6[93]. The specimens were 4 units wide and 12 units high as shown in Figure 4.7, which shows dimensions of the test specimens in all four scales. The specimens were required to be as reasonably square as possible as recommend by the code; 940 x 905 mm was achieved for the prototype specimens. This was because of variations in the dimensions of the units resulting from the manufacturing process.

Because of the significant weight of the specimens, measures were taken to facilitate handling of the specimen after construction as well as to put them in position for testing. Firstly, the base of the wooden mould for constructing the specimens was oiled and laid with a strong plastic sheet. The specimens were then constructed in the usual way (as per this research) and left to cure for about a week before demoulding. During demoulding the specimens were slid from the mould with the aid of the plastic sheet where they were taken for storage until they were tested.

In order to position them in the rig for testing, the specimens were sandwiched between two wooden panels, as shown in Plate 4.11. The panels have channel shaped aluminium section screwed along the diagonals, so that they could be lifted up using a crane from a bolt holding the two sections together. Fibreboard pieces made to the size of the specimens were used in between the specimens and wooden panels to cushion the effect of the clamping force. The two wooden boards were then bolted together securely before the whole assembly was lifted by an overhead crane onto the testing machine.

The specimens were then gently lowered onto specially made steel V-blocks for testing the specimens diagonally. Another steel V-block was placed on the opposite corner of a specimen before they were positioned, centred and plumbed prior to the fixing of transducers for the measurement of the deformations. Fibreboard pieces where used to even out surface irregularities on top and below the loaded diagonals. Load was applied at a constant displacement rate of 0.01mm/s until failure of the specimens. A constant displacement rate was used in this test to enable safe stoppage of the testing machine at failure so that the LVDTs were not damaged. Two transducers were placed on the compression and tension diagonals on each side to measure the deformations. The lengths of the transducers are given in Figure 4.7. All the transducers were calibrated LVDTs with a range of ±15mm. A different transducer, with a range of ±25 was used to record the vertical deflection at the centre of the panel. The measurements from the five transducers and the load signal were fed to and monitored on a data logger, for later analysis. The set up for the test is shown in Plate 4.12.

Half Scale

The half scale diagonal tensile strength test was also carried out in a testing machine at a load rate 0.04kN/s until failure of the specimens. The specimens were loaded via two brass V-blocks glued to the corners of the diagonals. Plastic padding epoxy resin was used to glue the V-blocks and the specimens aligned and centred while the glue was setting. The specimens were also fitted with transducers as discussed in the case of the prototype specimens and the length of the gauges are set out in Figure 4.7. Plate 4.13 shows the set up for the test.

Fourth Scale

The diagonal tensile strength test at fourth scale was carried out in a testing machine at a load rate of 0.01kN/s until the failure of the specimens. The specimens were also loaded diagonally through two brass V-blocks glued to the top and bottom diagonals using plastic padding. Two transducers, one each on the compression and tension diagonals were used to measure the deformations of the panel under compression. This was done for both the front and back (top and bottom) faces of the panel in order to cancel out bending effects. Five specimens were tested in this way.

Sixth Scale

The diagonal tensile strength test in this case was carried out in a testing machine at a displacement rate of 0.07mm/min. The gauges were fitted, as discussed for the other scales and load was applied through two brass V-blocks glued to the top and bottom of either diagonal. Strain measurement were recorded and monitored on an Orion logger before being retrieved for subsequent analysis. Even though the sizes of the specimens are different for the different joints test, a uniform gauge length as shown Figure 4.6 was used for all the sixth scale tests. Plate 4.14 shows the set up for the test.

Discussion

The difficulties posed by constructing and testing relatively large prototype specimens is seen from this test and the advantage of model tests has further been highlighted. All the model specimens were relatively easy to construct and test therefore less time and effort was expanded in their testing because the challenges seen in the prototype test were not seen.

Calculations

The diagonal tensile strength, S_{pt} (shear strength) was evaluated from Equation 4.8

$$S_{pt} = \frac{0.707P}{A_n} \tag{4.8}$$

Where P is the load at failure

A_n is the net area of the specimen $= \dfrac{(L+B)tn}{2}$ (4.9)

t is the wall thickness and L and B the face dimensions, n is the fraction of the gross area of the specimen that is solid.

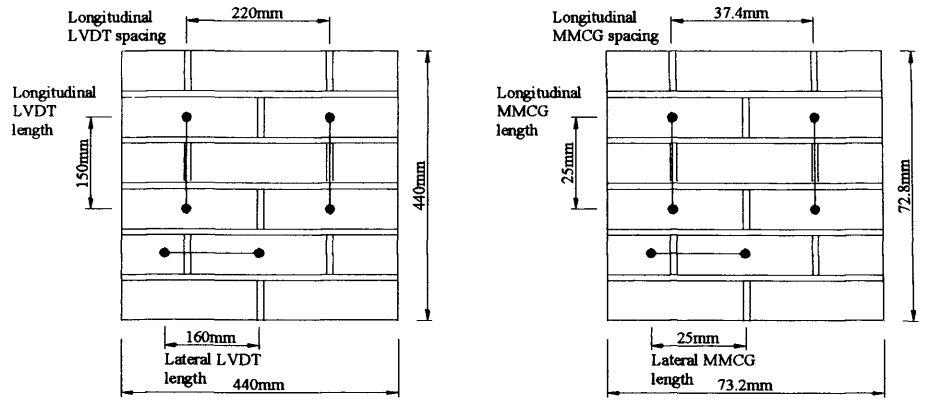

(a) Prototype (b) Sixth Scale

Figure 4.1- Position of transducers in wallette specimens.

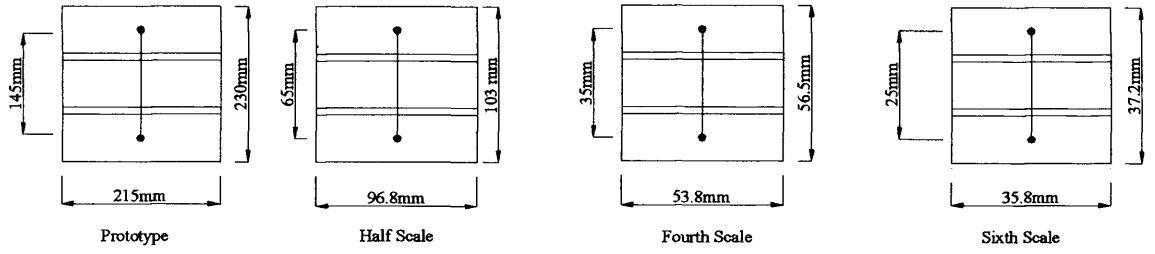

Figure 4.2- Position of transducers in triplet specimens.

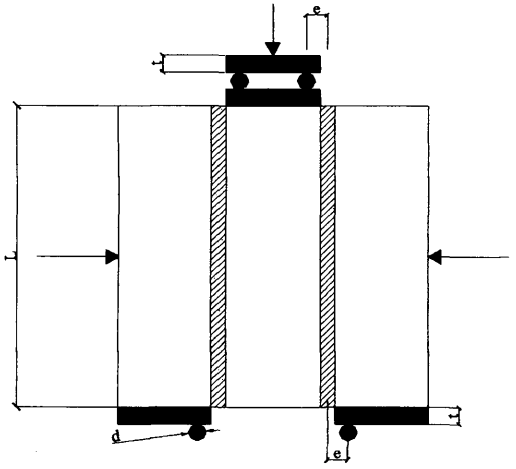

	L, mm	e, mm	d, mm	t, mm
Prototype	215	14.5	12	12
Half	96.8	6.5	6	6
Fourth	53.8	3.5	6	5
Sixth	35.8	2.5	5	5

Figure 4.3- Set up dimensions for shear strength tests.

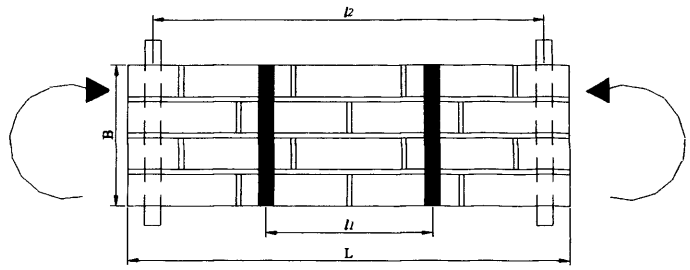

	Length, L	Width, B	Support Span, $l2$	Loading Span, $l1$
Prototype	895	305	795	430
Half	400	135	350	155
Fourth	225	75	200	85
Sixth	148	47	131	58

Figure 4.4 - Set up dimensions (mm) for flexural strength parallel to bed joint tests.

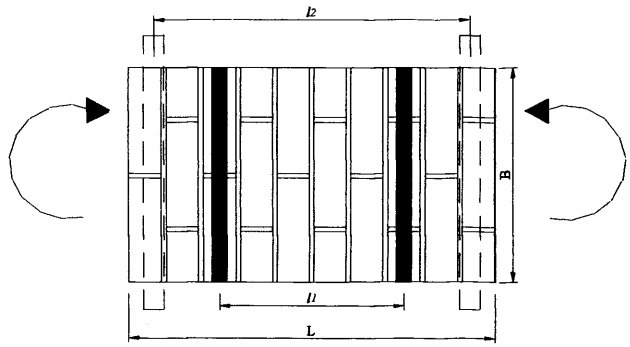

	Length, L	Width, B	Support Span, $l2$	Loading Span, $l1$
Prototype	775	445	675	400
Half	345	200	295	177
Fourth	180	110	155	90
Sixth	122	73	105	60

Figure 4.5- Set up dimensions (mm) for flexural strength normal to bed joint tests.

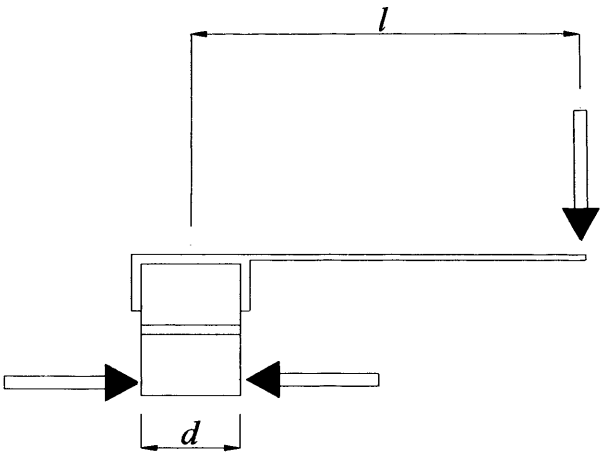

	Depth, *d*	Moment arm, *l*
Prototype	103	335
Half	46	175
Fourth	26	105
Sixth	17	43

Figure 4.6- Set up dimensions (mm) for bond strength test using the bond wrench.

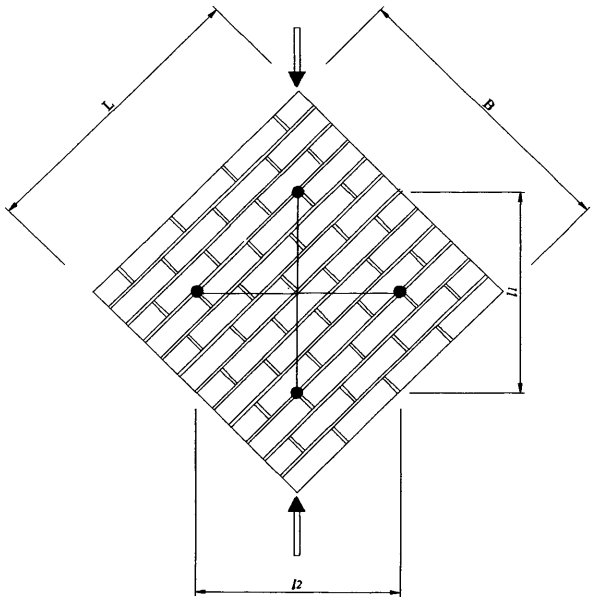

	Length, *L*	Width, *B*	*l1*	*l2*
Prototype	940	905	950	950
Half	410	405	220	220
Fourth	228	224	100	60
Sixth	148	145	90	90

Figure 4.7- Set up dimensions and transducer lengths (mm) for diagonal tensile strength tests.

Plate 4.1- MMCG used for deformations measurements in the sixth scale.

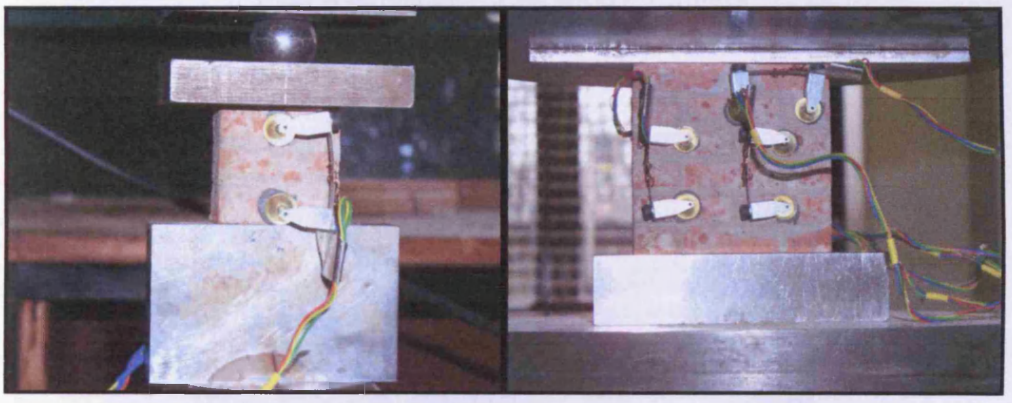

Plate 4.2- Set up for sixth scale triplet and wallette specimens respectively.

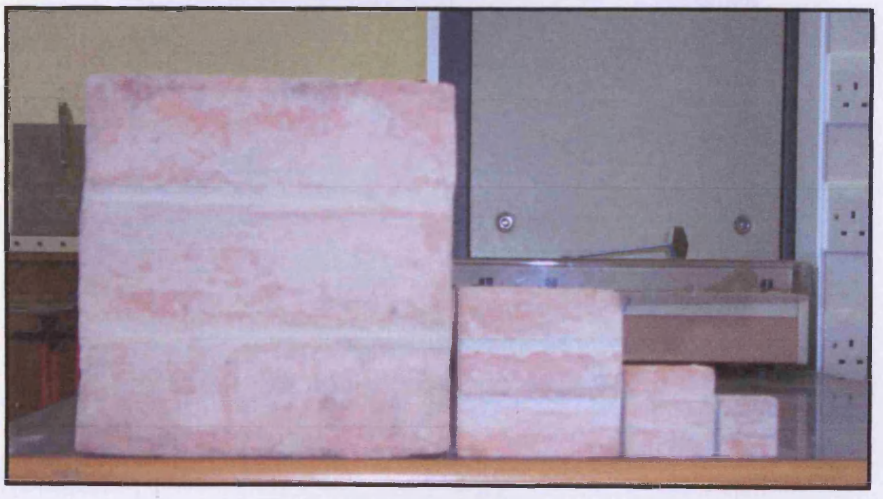

Plate 4.3- Triplet specimens in the four scales.

Plate 4.4- Set up for prototype wallette.

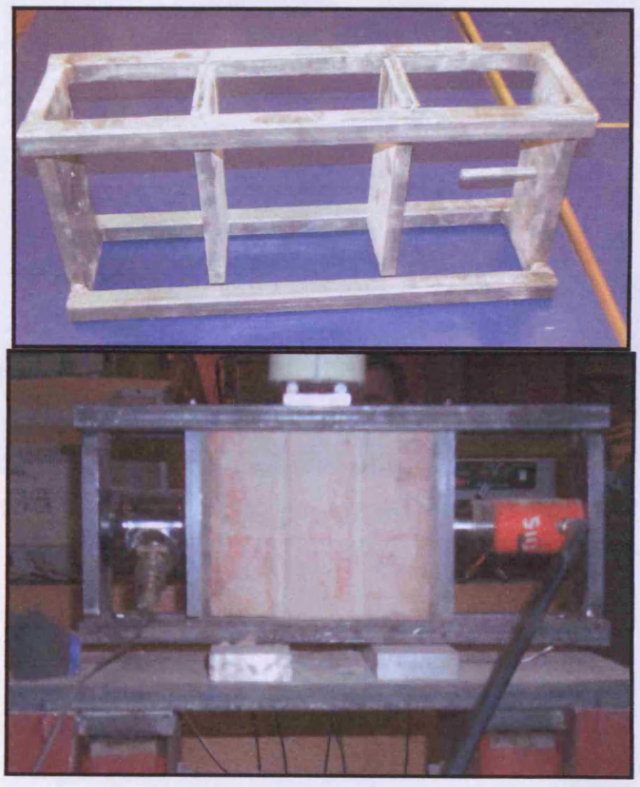

Plate 4.5- Set up for prototype shear strength test.

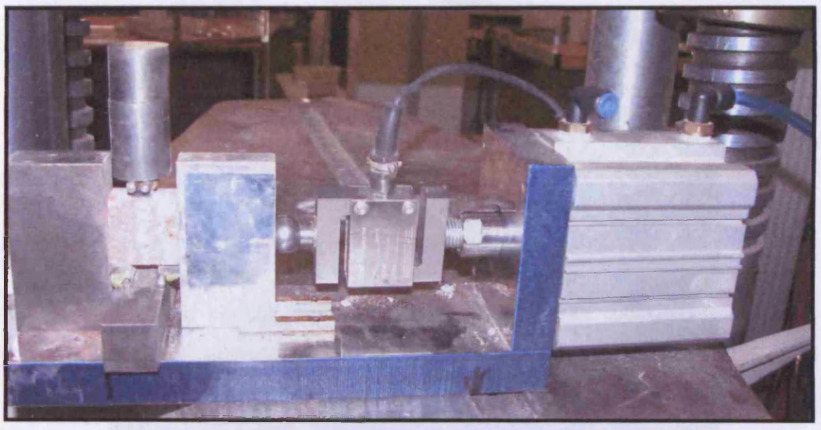

Plate 4.6- Set up for sixth scale shear strength test.

Plate 4.7- Set up for prototype flexural strength test.

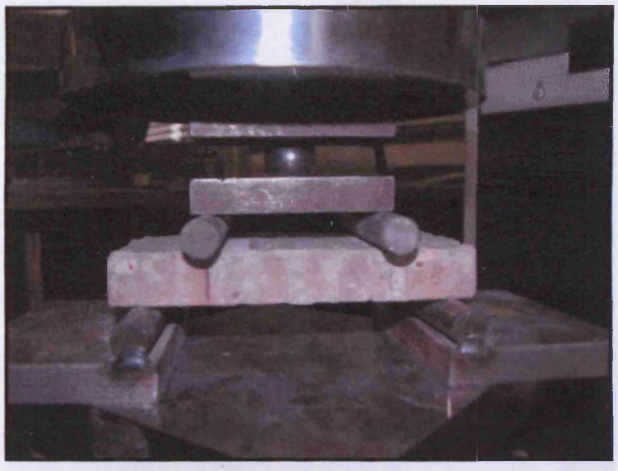

Plate 4.8- Set up for sixth scale flexural strength test.

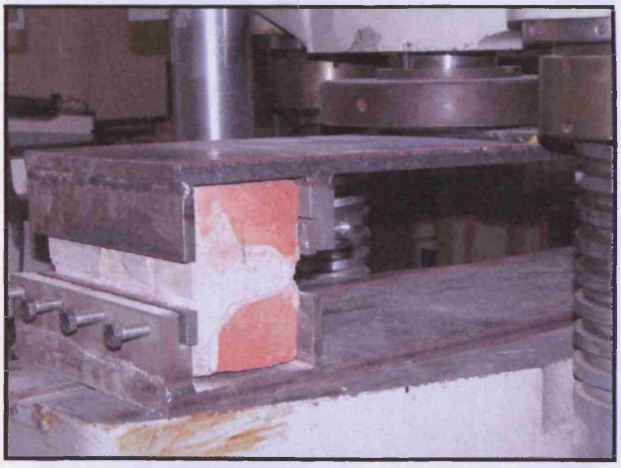

Plate 4.9- Set up for the prototype bond wrench test.

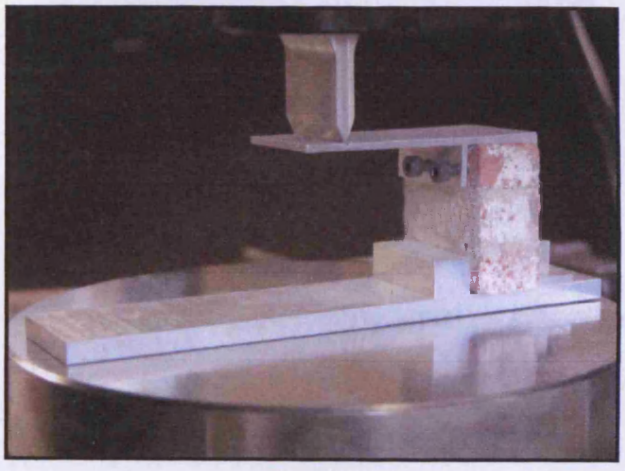

Plate 4.10- Set up for sixth scale bond wrench test.

Plate 4.11- Wooden panel used for carrying the prototype diagonal tensile strength test specimens.

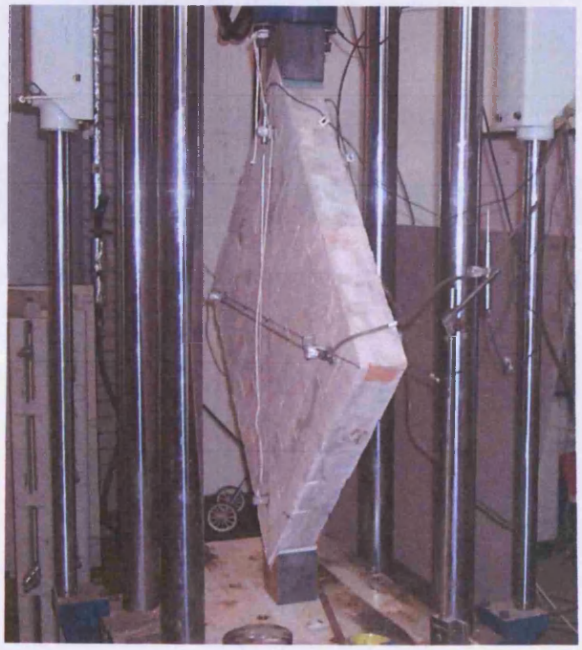

Plate 4.12- Set up for the prototype diagonal tensile strength test.

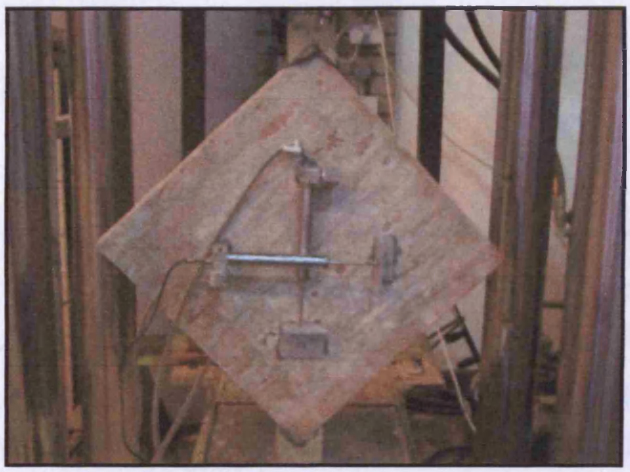

Plate 4.13- Set up for the half scale diagonal tensile strength test.

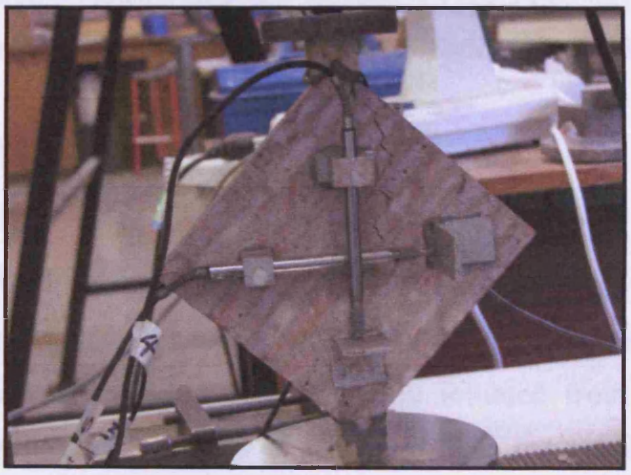

Plate 4.14- Set up for the sixth scale diagonal tensile strength test.

5 Masonry Tests at Different Scales Results and Discussions

In this chapter the results and discussion of the tests at different scales are presented and discussed. Discussions also look at the size effect analysis of the test data with respect to the two size effect laws; Size Effect Law, SEL and Multifractal Scaling Laws, MFSL. In the identification system used for the tests, the first number denotes the scale of the test followed by a letter denoting the type of test under consideration (C- compressive strength test, S- shear strength test, F- flexural strength test, B- bond strength test, D- diagonal tensile strength test) and the specimen number. For example 4D-A1 refers to the diagonal tensile strength test specimen 1 at the fourth scale.

5.1 Compressive test results

5.1.1 Triplets

5.1.1.1 Failure patterns

Plate 5.1 shows the typical failure patterns in the prototype triplets. The failure is characterised by vertical splitting cracks, usually initiated from the sides of the specimens and passing through the mortar bed. The failure is also sometimes characterized by spalling off of the front face of the units prior to failure. Specimens that have completely failed in the prototype tended to leave pyramidal shaped masses on the platens. The failure mechanism and cracks are also similar in the half and fourth scales with the typical tensile cracks at the sides of the specimens. Such similarity in the failure patterns is also seen in Plate 5.2, which shows the typical failure patterns in the sixth scale triplets. Therefore the failure mechanisms in the four scales are similar with all the models showing the typical failure patterns evident in the prototype.

5.1.1.2 Compressive strength

Most small scale masonry model tests to date have shown that the models are stronger than the prototypes, as seen in Egermann et al[51]. But current masonry theory assumes that if the mechanical properties of the brick and mortar are similar then

there should not be a significant strength difference between models and prototype[16, 51].

Table 5.1 shows the summary of the triplet compressive strength test results and Figure 5.1, shows the variation of the triplet compressive strength across the four scales. It can be seen from the Figure 5.1 and Table 5.1, that even though there is an increase of the compressive strength of masonry as the scale is reduced, there is wide scatter in the results. There is a 20% increase in the mean triplet masonry strength from prototype to half scale but this jumps to 150% in the fourth scale and drops to 120% in the sixth scale. Similar higher strengths at smaller scales have been seen in earlier tests by Egermann et al[51] and Hughes and Kitching[52], in the latter study there was a 84% increase in the masonry strength at sixth scale over the prototype for standard triplets made with type III mortar. Despite the high fourth scale strength results, the general trend as shown by the trend line in Figure 5.1 is for an increase in compressive strength as the scale is reduced.

The results here suggest that the masonry strengths are similar in the half and prototype scales on one hand and in the quarter and sixth scales on the other hand. As explained in the case of the compressive strength of the units and as noted in discussions from the tests carried to investigate the possible effect of strength anisotropy in the units, it is possible that the trend in the similarity of the masonry strength in the two sets of scales could also be due to anisotropy of the unit.

This behaviour could be due to the molecular structure of the clay compounds making up the brick which usually consist of aluminosilicates sheets arranged parallel to each other[122]. The parallel arrangement of these molecules may explain the strength differences seen in the bricks tested in the different orientations. Therefore some degree of anisotropy may be exhibited by a clay brick due to its molecular make up. A stronger factor could be the manufacturing process of extruded clay units in which the plastic clay is forced through a die as discussed in Chapter 3. Jessop et al[25] have also discussed the anisotropy of masonry with regards to their moduli properties, while Shrive and Jessop[24] have reported on the anisotropy of extruded clay units with respect to their strengths in orthogonal directions. But even this may not address the big increase of masonry strength at the smaller scales. Because the masonry strengths in the two smallest scales, that is the fourth and the sixth are more than twice the

strengths at prototype and half scales. While the average unit strengths difference in the two sets of scales (fourth/sixth over prototype/half) is about 1.5.

In order to reduce the effect of the unit strength on the masonry strength, Figure 5.1 is re-plotted with the masonry strength normalised with respect to their respective unit strengths in Figure 5.2. This figure shows a reduced rate of increase of masonry strength as the scale is reduced. This suggests there is still some additional factor that is responsible for the high increase in strength, apart from the effect of unit strength alone.

Studies of the fracture of brittle materials (mostly concrete) have shown that smaller sized specimens have higher strengths than larger specimens[87]. According to the Griffith theory of brittle fracture, the less the surface area of a material the stronger it is, since there is less probability of flaws occurring[13]. Therefore this size effect seen in testing brittle materials may also be one of the reasons for the strength differences. But curiously there is little scale effect seen in the half scale results. This suggests a possible interplay of two factors at the smallest scales; firstly a possible anisotropy with respect to strength due to the manufacturing process of clay brick and secondly the size effect phenomena.

For the brick under consideration here the half scale masonry strength shows very good correspondence to the prototype. Such close half scale model to prototype correspondence has been reported by Long et al [123] in testing grouted concrete block masonry.

The fourth scale compared to the prototype shows the highest percentage increase in strength, the reason for this is not clear. Even though the mean unit strength in the fourth scale is more than that in the prototype, it still is less than the mean unit strength in the sixth scale; nevertheless the fourth scale masonry strength is still the highest of the four scales. So far only the influence of the brick material has been discussed in relation to the masonry strength because its properties have the most effect on the masonry assembly. But of course the behaviour of masonry is also influenced by the mortar joint, because as stated by many authors the tensile stresses that cause failure in the brick are due to the stresses induced by the mortar joint. Again using the Griffith concept that smaller sized elements are stronger than larger ones, it would be expected that thinner joint should be able to withstand higher

stresses than thicker ones; consequently the brick would be able to carry higher tensile forces in masonry with a thinner joint. This has been corroborated by Porto et al[21] who found that prototype masonry with thin layer joints (1.3mm) were 20% stronger in compression than those with 12mm joints. This suggests that model masonry could show a stronger compressive strength due to the thinness of their joints alone. However this may be applicable to only the very small scales like the sixth and fourth scales in this study, because as we seen from the results, the half scale strength is similar to the prototype strength.

From Table 5.1 it can be seen that the mortar cube strengths for the tests are similar to each other. The highest cube strength of 4.9N/mm^2 was in the half scale test. This is marginally higher than the mortar cube strength in the prototype test by about 6% and fourth and sixth scale tests by about 4%. Therefore since the mortar strengths are comparable to each other in the four scales the difference in masonry strengths seen could be principally due to the unit properties and the size of the joints at the smallest scales.

5.1.1.3 Stiffness

Figure 5.3 shows the stress/axial strain curves for the prototype triplets while the summary of all the triplet test results is presented in Table 5.1. The curves reveal that in two of the tests, the plots are similar, whereas in the third test there is some variability. Unfortunately, because the deformation measurements could not be continued until failure of the specimens, the peak behaviour of the specimens was not captured. The transducers were removed before reaching of the peak loads so that they were not damaged during the failure of the specimen. However, continuing the measurements may not have shown much difference to the shape of the curve seen here because of the way the specimens failed, which was usually quite sudden. One problem encountered was that, even though two transducers were fixed (one each on either face of a specimen) to measure the vertical deformations, only measurements from one of the transducer was used because measurements from the other transducer were erratic and were therefore not used for the analysis. This happened despite having calibrated both transducers before the tests.

For the half scale tests, the complete stress strain measurements from a typical test are shown in Figure 5.4. The figure shows the stress/strain curves from the front (top)

surface, designated as (1), and back (bottom) surface, designated as (2), of a specimen as well as the average of the two strains. This identification system is also used for the other tests in this section. The top and bottom surfaces of the specimen are as defined in the last chapter and refer to the orientation of the faces during casting. It is seen that the average strain is very close to the other two lines, an indication that the strains were uniform on both faces of the specimen. From the figure the flattening of the peak portion of the graph, could suggest some ductility in the specimen. This feature is typical of most of the tests at this scale, as shown in Figure 5.5, which shows the stress/axial strain curves in all the tests. Near the failure load, because of cracking and spalling of masonry pieces from the specimens, there is usually some disturbance to the transducer positions and this is reflected in some of the tests shown in the figure, for example 2C-A5, which shows a reduction in strain near the peak stress. Despite this anomaly near the peak stress in some of the tests, there is still good agreement of the slopes of the curves in the tests at this scale.

Figure 5.6 shows the stress/strain curves from a typical fourth scale test, (4C-A3). It is seen in this case, that the strain from the top face denoted by (1) is stiffer than the strain from the bottom face. This feature is repeated in all the tests undertaken at this scale for measurements from that particular transducer. This behaviour could either be due to some problem with the transducer or due to some construction issues as will be discussed later. However as seen from the combined plots of all the tests in Figure 5.7, the slope of their elastic regions are similar an indication that their behaviour is similar.

The stress/strain curves at the smallest scale, the sixth scale, are shown in Figure 5.8 for a typical test. The curves show that the average strain is in reasonable agreement with the top and bottom strains, an indication that the tests conditions are reasonably uniform. The combined stress/strain curves in the three tests are shown in Figure 5.9, and it shows that the tests were similar as can be seen from their similar shapes and slopes. One observation from the stress/strain curves in Figures 5.4 and 5.8 is that the top strains were similar to the bottom strains. This shows that the construction method does not significantly affect the stiffness properties on the top and bottom faces of the specimens. The stiffness of the top strains from the fourth scale test as seen in Figure 5.6 is therefore most probably due to some problem with the transducer. Therefore the construction method employed here can be considered to be consistent and repeatable.

The concerns over the possible effects of the construction method on the top and bottom faces of the specimens because of the different curing conditions on the exposed top surface and the covered bottom surface have not materialised.

All the stiffness results are similar; the half and fourth scales stiffness were 6% and 2% more than the prototype stiffness, while the sixth scale stiffness was 9% more than the prototype stiffness. Even though we have seen substantial variations with regards to their strength properties their deformation properties are very similar. This is further illustrated in Figure 5.10, a combined plot of stress/strain curves for the four scales and in Figure 5.11, which shows the variation of stiffness of the masonry across the four scales. It is seen from Figure 5.10 that the slope of their elastic region are markedly similar. However results from other researchers[44, 51, 52] show a different trend. Their results show that reduced scale masonry models are softer than prototype by a factor approximately equal to the scale factor. This may be due to the manner in which the models were constructed in our case which is different to the way the other researchers made their specimens, that is, they all used conventional brick laying. Because in conventional brick laying the light weight of model bricks subject the mortar bed to a lower bedding stress than the heavier prototype bricks, as a result the bed joints in the model scales are compacted to a lower degree during curing than the bed joints in the prototype. Consequently the bed joints in scaled masonry models are less compacted which could lead to a softer masonry response under compression. Egermann et al[51] have suggested this as a possible reason for the softness of small masonry models and it has also been reported by Mohammed and Hughes[97]. By comparing it to the stiffness of its constituents elements, it is seen that the average stiffness of the masonry in the four scales; 5500N/mm^2 in this case is about half of the brick stiffness; 11500N/mm^2 and roughly similar to the mortar stiffness (6300N/mm^2 for prototype mortar and 6500N/mm^2 for benchmark mortar) determined in Chapter Three from Table 3.6. This shows the influence of mortar in determining the stiffness properties of masonry.

5.1.2 Wallettes

5.1.2.1 Failure pattern

Typical failure patterns are shown in Plate 5.3 for the sixth wallettes. The failure pattern in the prototype wallettes were also similar to the model wallettes,

characterised by vertical tensile splitting cracks at the sides and ends of the specimens. The cracks usually radiated from within the units, above and below the perpend joints at the ends. The cracks on the top surface of the specimens became visible to the eye at around 70-75% of the peak load reached. Near the peak load, there was also spalling of the surface of the units.

5.1.2.2 Compressive strength

Again it is seen from the summary of the compressive strength test results on the wallette specimens in Table 5.2 and in Figure 5.12, which shows the variation of the wallette strengths in the prototype and sixth scale, that the sixth scale compressive strength is greater than the prototype compressive strength. The percentage increase in masonry strength is 65% which is similar to the 64% increase in unit strength in the two scales. This suggests that the wallette strength is mainly influenced by the unit strength. This is better illustrated in Figure 5.13, which shows the variation of the wallette strength normalised, with respect to their respective unit strength, plotted against the scale. The figure seems to suggest that the difference in masonry strength here may be mainly due to the influence of the unit strengths.

In the prototype tests, the wallette strength of 10.2N/mm^2 is about 11% more than the prototype triplet strength, while in the sixth scale tests; the wallette strength is 21% less than the triplet strength. The reason for the difference in strength between the prototype and model wallettes and triplets is not certain but could be contained within the relatively higher COV of the model units over that of the prototype units as previously discussed.

5.1.2.3 Stiffness

The position of the gauges for the wallette and sixth model tests are as shown in Figure 5.14. Figure 5.15 shows a typical stress/axial strain curves for a prototype test. This shows that there is good agreement in the four strains, an indication that the tests conditions were uniform. This good correspondence in the axial strains is also seen in the stress/lateral strain curves for the same test, Figure 5.16, which shows that the curves are nearly identical. Figure 5.17 shows a summary of the axial and lateral stress/strain curves from the prototype tests and reveals that there is good consistency in the results.

For the sixth scale model tests, the stress/axial strain and stress/lateral strain figures are shown in Figures 5.18 and 5.19. In this case, the curves are not as consistent as in the prototype tests, nevertheless, the curves are similar. The summary of the axial and lateral stress/strain curves for the sixth scale tests are shown in Figure 5.20, and they show that curves have similar slopes in their elastic region which may be an indication that the tests were consistent. They reveal a higher load carrying capacity than the prototype tests; this can be seen from the comparison of typical stress/strain curves of the two scales in Figure 5.21.

Figure 5.21 shows a good agreement in the stress/strain curves for the two scales. It is seen that the slope of their elastic regions is quite similar. This shows that the sixth scale model not only exhibits similar behaviour and failure patterns to the prototype, it also models the deformation properties quite well. The curves also show the plasticity of the wallette near its peak stress. This is different to what was seen in the triplets, where the curves were characterized by a shorter plastic region. This may be due to the presence of the perpend joints in the wallettes. The sixth scale model stiffness of 6800N/mm^2 is about 20% stiffer than the prototype, which could be due to the stronger model bricks. Figure 5.22 shows the variation of masonry wallette stiffness with scale, from which the higher model scale stiffness is apparent. This is opposite to the effect seen in the triplets, where there was no net increase or decrease in stiffness across the four scales. The presence of the perpend joint in this case may have altered the way the masonry behaves and this could result in the difference seen in the stiffness.

The Poisson's ratio of 0.19 for the model wallettes (which is three times more than that for the prototype) makes it on the higher side possibly due to the constraints in accurately placing the gauges because of the small specimen size.

By comparing the masonry stiffness in the prototype tests, it can be seen that the triplet and wallette stiffnesses show a remarkable similarity. In fact they are exactly the same at 5500N/mm^2. While in the sixth model tests, the wallette stiffness is about 13% more than the triplet specimen. On the whole, the triplet tests do give a reliable and quick way of determining masonry properties as suggested by Shrive[88] and Edgell et al[124].

5.1.2.4 Characteristic strength of masonry

The characteristic compressive strength for the prototype wall and triplet specimens, evaluated on the basis of Equation 4.2, yields 8.5N/mm^2 and 7.7N/mm^2 respectively. These values were obtained by dividing the mean compressive strengths from Table 5.1 by a factor of 1.2 as prescribed by BS EN 1052-1[125].

In Eurocode 6(EC 6)[22], the characteristic strength for unreinforced masonry made with general purpose mortar is given as Equation 2.1, whose evaluation is based on the strength of the unit and mortar.

Using a K of 0.6 as given in EC 6 the characteristic compressive strength of the wall and triplet specimens are 13.1 and 12.6 N/mm^2 respectively. While using the formula suggested by Khalaf and Hendry[126] for the calculation of the shape factor (determined to be 0.74), the characteristic strength was found to be 12.0 N/mm^2 for the wall and 11.6 N/mm^2 for the triplet specimens.

It can be seen that Equation 2.1, for determining the characteristic strength of unreinforced masonry as given in EC 6, overestimates the value of the characteristic strength as found from the test results and evaluated on the basis of BS EN 1052-1[89], even though the formula is for use with masonry built in the conventional way. Since characteristic strength should be less than the mean, calculations based on the EC 6 formula have overestimated the characteristic strength of the specimens here. This may be significant for masonry that is prefabricated and cast in the horizontal plane as in this case. Perhaps there may be need for further investigation in this area in order to look at the applicability of formulae used for predicting masonry characteristic strength built in the conventional way, for predicting the characteristic compressive strength of prefabricated masonry panels cast horizontally.

5.1.2.5 Size effect analysis

The size effect analysis of the compressive strength data from the four scales is shown in Figure 5.23. The log plot of nominal strength, in this case, the actual compressive strength against the characteristic size, D (length of specimen), shows that the test data approximately follows the size effect laws. The Multi Fractal Scaling Laws (MFSL) agrees better with the data than the original Size Effect Law (SEL) of Bazant. However as discussed in Chapter 2, the SEL is not intended for use with notch-less specimens, rather Bazant's other law, Equation 2.11, which is identical to the MFSL

should be used. The intention behind comparing the MFSL to the SEL was to see if previous observations[72] that the MFSL agrees better with masonry data than the SEL, will be repeated here or not. From the results, both Equation 2.11 of Bazant and the MFSL agree with data more than the SEL. The graph reveals that there is a size effect which is consistent with the sizes under consideration; as discussed with reference to Figure 2.3 where most laboratory tests are shown not to exhibit a strong size effect. It is therefore seen that size effect laws seem to be applicable to masonry as has been suggested by Carpenteri[84] and Lourenco[72].

5.2 Shear test results

5.2.1 Failure mode

Typical failure of the prototype specimens is as shown in Plate 5.4, which shows a failure plane through the mortar bed. In the model scale specimens the failure is characterized by double shear lines; a failure line on either side of the middle brick. The line of failure was mostly through the mortar bed and not at the mortar/unit interface.

5.2.2 Initial shear strength and coefficient of internal friction

The initial shear strength is determined from the graph of the shear strength against the precompression stress as the intercept of the best fit line on the appropriate axis. The plot of the shear stress/precompression stress for the prototype test is shown in Figure 5.24, it reveals a similar degree of scatter in the shear strength results at the three levels of precompression stress. This may imply that the test conditions were uniform and consistent. However the shear stress/precompression stress plot for the half scale test in Figure 5.25 shows a different trend; it shows a similar degree of scatter in the shear strength result at precompression stress levels of $0.2N/mm^2$ and $0.6N/mm^2$ and a much narrower scatter in the shear strength results at $1.0N/mm^2$. This could be either due to the natural material variability in specimens or deviations in the boundary condition to achieve minimum bending in the specimen, as reported by Jukes and Riddington[30], the degree of bending in the triplet test has a significant effect on the shear strength. The shear stress/precompression plot for the fourth scale in Figure 5.26 and sixth scale in Figure 5.27, respectively, also reveal this dissimilar scatter in the shear strengths recorded at the three levels of precompression. However the plot for the sixth scale test, as seen in Figure 5.27, shows a greater consistency

than the other model tests. The variability in the results in the model tests could then be due to the natural material variability, because the model bricks are more variable than the parent prototype as seen in the consistently higher COV of the model bricks in the material tests.

Figure 5.28 shows the variation of the co-efficient of internal friction at the mortar-unit interface across the four scales. It reveals that there is no clear scale effect for this parameter. But it shows an increase in the friction coefficient as the scale is increased within the model scales. It may be difficult to see a clear scale effect in this case because of the different surface finishes of the bricks on the one hand and the sands on the other hand. However in the experimental design the different surface textures of the prototype and model bricks were not considered to be a mitigating factor because of the findings by Tauton[3] that showed no significant difference between the frictitonal properties of surfaces of prototype and cut model bricks.

The initial shear strength test results summarised in Table 5.3 show that the prototype specimens had the highest initial shear strength of 0.89N/mm^2, probably due to the different surface finishes of the prototype and model bricks. It is seen from Figure 5.29, which shows the variation of the initial shear strength across the four scales, that there is no clear trend in the initial shear strength across the four scales. This could be due to the wide scatter in the results as previously discussed. The figure also shows that within the model scale results there is a decrease in the initial shear strength as the scale is increased. Perhaps there is some scale effect in the shear strength but because of the different properties of the prototype bricks and mortar on one hand and the model bricks and mortar on the other hand it is difficult to quantify the effect.

5.2.3 Size effect analysis

The size effect analysis of the shear strength tests data from the four scales is presented in Figures 5.30 and 5.31 for a procompression stress of 0.2N/mm^2 and 1.0N/mm^2, respectively. The characteristic size was chosen as the depth of the specimen because it is over that length that shearing occurs. Figure 5.31 shows a greater size effect than Figure 5.30, probably because of the increased precompression stress in the former. However both figures show a very weak or no size effect even though their relative magnitudes differ. The negligible size effect seen here could be due to the way the specimens were constructed, which has eliminated any compaction

of the bed joint during curing. It has been discussed that the nature of masonry bond is more mechanical than chemical in nature; therefore any factor that would increase interaction between the joints and bricks (like greater compaction) could affect the nature of the bond. If this is case, then it is perhaps not unexpected that the size effect seen here is negligible. The trend in the figures however agrees with the suggestion in the size effect plot in Figure 2.3 that structures with relatively small values of the characteristic structural size, D should not exhibit a strong size effect.

In Figure 5.30 it is seen that the MFSL agrees better with the test data than the SEL as stated in the case of the compressive strength test. While in Figure 5.31, maybe because of the higher precompression stress, both the SEL and the MFSL are in close agreement.

5.3 Flexural test results

5.3.1 Flexural strength normal to bed joints

Failure of the flexural strength test normal to the bed joints in the prototype specimens was always in between the loading rollers and in the third or fourth joint from either support. Plate 5.5 shows typical failures in the half scale specimens, where failure was mostly through the fourth joint from either support but there were cases of two failure lines as well, all between the loading rollers. In the fourth scale, failure was usually in the fourth or fifth joint from either support with one case of failure in the fifth and second joints from a support. However, that test was still considered because the fifth joint failure is between the loading rollers. Plate 5.6 shows typical failure in the sixth scale specimens, where failure was usually in the fourth or fifth joint from either support.

A summary of the flexural strength normal to bed joint test results is shown in Table 5.4 and Figure 5.32, which shows the variation of the mean flexural strength normal to the bed joint. It is seen from the figure and table that there is no well defined trend in the flexural strength. Since the surface texture of the bricks has a significant influence on the flexural strength[94], it is therefore possible that there will be some degree of variability in the results because of the different surface textures of the prototype and model bricks as well as due to the different sand gradings in the model and prototype mortars.

5.3.2 Flexural strength parallel to bed joint

In the case of the flexural strength test parallel to the bed joints, for the prototype specimens, the failure line was mostly straight passing through a combination of joints and units. Plate 5.7 shows a typical failure in the prototype tests. This failure pattern was seen in most of the model scale tests except for the sixth scale, where there were also cases of joint rotation. In this case the failure lines were always through the joints (through the perpend and bed joints in a zigzag manner). As observed previously, the first type of failure is limited by the modulus of rupture of the units and is an indication of strong bond between the units and mortar while the second type of failure is governed by the shear strength of the mortar/unit interface and it suggest a less strong bond between the units and mortar. If this suggestion is correct, the flexural bond strength parallel to the bed joints would be weaker in the sixth scale.

A summary of the flexural strength parallel to the bed joints is provided in Table 5.5. It is seen from the Table and in Figure 5.33, which shows the variation of the flexural strength across the scales, that there is an indication of a trend in the mean flexural strength parallel to the bed joint. The figure shows that there is a slight decrease in the mean flexural strength parallel to the bed joint as the scale is reduced; in this case the modulus of rupture of the units is likely to have had a major influence on the flexural strength. This can be seen in Figure 5.34, which shows that there is direct relationship between the flexural strength parallel to the bed joint and the modulus of rupture of the units. The modulus of rupture of the prototype and model scale units is about twice the flexural strength parallel to the bed joint. It also seen that the sixth scale flexural strength is the lowest of the four scales, this collaborates the earlier suggestion made on the mode of failure in the sixth scale, which is characterised by cracking through the bed and perpend joints suggesting a possible low bond strength.

In terms of the relationship between the flexural strengths in the orthogonal directions as shown in Figure 5.35, it is seen that the flexural strength parallel to the bed joint is about 4.0 times more than the flexural strength normal to the bed joints in the prototype and sixth scale while this ratio is about 2.0 in the fourth scale and five in the half scale. Figure 5.36 shows the orthogonal ratio against the flexural strength normal to the bed joints, and it reveals the general trend reported in the literature[19], that the

orthogonal ratio decreases markedly with increase in the flexural strength normal to the bed joint.

5.3.3 Size effect analysis

Figures 5.37 and 5.38 show the logarithmic plot of the nominal strength (actual flexural strength) against the specimen depth for the flexural strength normal to the bed joints and the flexural strength parallel to the bed joints respectively. They both show that there is little or no noticeable size effect as seen in the case of the shear strength test. In the plot of the flexural strength normal to the bed joints, the MFSL agrees with the test data better than the SEL while in the graph of the flexural strength parallel to the bed joints, both of the laws agree with the test data. It may be because the latter failure is usually governed by the tensile strength of the unit (for failures through unit and perpend joints) for which the mechanics of the failure is different to the former, and therefore the crack propagation process agrees somewhat with the SEL. The trend seen in Figure 5.37 is different to the findings of Lourenco[58], who found that there is a strong size effect in the flexural strength normal to bed joint, characterised by a marked decrease in flexural strength as the specimen depth was increased. This could be due to the range of characteristic structure size D (specimen depth) used in his tests which is in the range of 100-300mm while the range in this study is 10.8-65mm. This suggests that the threshold structure size beyond which size effect becomes manifest may not have been reached in this study, because as seen from Figure 2.3 for small sizes of the D the strength criterion shows no apparent size effect. Size effect only becomes manifest beyond a threshold value of D that follows the size effect laws. This may be the reason for the suggestion by fracture mechanicians for the incorporation of size effect laws in design codes to guide in the extrapolation of the strength of real size structures from laboratory specimens. Presently design calculations are based on small specimen tests in laboratories without any extrapolations to determine the strength for real size structures, which could lead to over predicting the actual strength of a structure. However the dead load factor used in the codes compensates for this and therefore most designs are deemed to be safe according to Bazant[127].

5.4 Bond test results

5.4.1 Failure mode

The failure pattern in most of the cases in both prototype and model specimens was characterised by a clean failure plane between the brick and mortar. But there were also cases of a "rough" failure face characterised by a failure line through the mortar joint.

5.4.2 Bond strength

The results of the bond strength tests in the four scales are summarised in Table 5.6 and shown graphically in Figure 5.39, which shows the variation of the bond strength across the four scales. From this figure it is seen that there is no clear trend in the bond strength across the four scales, but there seems to be a gradual increase in bond strength as the scale is increased. However the validity of this trend is distorted by the relatively higher mortar cube strength in the half scale test over that of the fourth and sixth scale tests; the mortar cube strength in the half scale test is about 20% higher than those of the fourth and sixth scale tests. Since the bond strength in known to increase with mortar strength perhaps the higher bond strength in the half scale test may be due to the higher mortar strength in the test. But since the nature of the mechanical bond in masonry has been suggested to be due to the mechanical interlocking of the hydration products transferred into the surface pores of the unit, it may be that the surface finish of the units and the different sand gradings of model and prototype mortars may be more important in influencing the bond strength. Anderson and Held[15] have suggested that mortars having sands with fine gradings usually result in masonry with lower bond strength. This would mean that model tests would all have lower bond strength than the prototype test. Since this is not the case here, it may be that the scale of the tests or different surface finish of the model and prototype bricks may have resulted in the lack of clear trend seen in the results.

5.4.3 Bond strength test compared to flexural strength test

Figure 5.40 shows the relationship between the flexural strength normal to the bed joints and the bond strength test. It is seen from the figure that there is no clear relationship because of the wide scatter in the results. If the trend line were fixed to pass through the origin it gives a relation in which the mean flexural strength is half the mean bond strength. Both of the methods measure only the bond strength in

relation to out-of-plane failure by bending but the flexural strength test results are higher because of the influence of the normal stresses which have been neglected in the case of the bond strength. The ratio of the bond strength to the flexural strength in the prototype, half, fourth and sixth scales are 2.1, 3.0, 1.2 and 2.4 respectively.

5.4.4 Size effect analysis

The size effect analysis of the bond strength test results is shown in Figure 5.41. It shows that there is no noticeable change in the nominal strength of the specimens as their characteristic size (specimen width) is increased. This agrees with the effect seen in the shear strength and flexural strength tests. Again it is seen that the MFSL agrees with the test data better than the SEL.

5.5 Diagonal tensile test results

5.5.1 Failure mode

Typical failure of most specimens was by a shear failure in the direction of loading. The failure line usually passing through the joints in a zigzag manner whist passing through some units. Plate 5.8 shows a typical failure pattern in the half scale specimen. Occasionally there were cases of bond failure in addition to the usual shear failure as shown in Plate 5.9, which shows one of such cases in a sixth scale test. Most of the failures in the prototype, half scale and fourth scale were abrupt and sudden. While in the sixth scale most of the failures were more gradual with a few cases of sudden failures.

5.5.2 Diagonal tensile strength

A summary of the shear strength from the diagonal tensile strength tests is shown in Table 5.7 and the variation of the shear strength in the four scales is shown in Figure 5.42. They show that the sixth scale test has the lowest shear strength of 0.63N/mm^2 and also the least COV among the model scale tests. While the fourth scale test provided the highest shear strength of 0.96N/mm^2 and also the highest COV in all the scales. As a result of this lack of a clear trend, there is no net decrease or increase in shear strength across the four scales as shown in the figure. This is also similar to the effect seen in the initial shear strength test of masonry, which also showed no increase or decrease in the initial shear strength across the four scales. The initial shear strength in the sixth scale agrees closely with the shear strength obtained here, which

is also the case in the prototype test. For the prototype scale the shear strength obtained here is about 2% higher than the initial shear strength while in the case of the sixth scale, it is about 5% higher than the initial shear strength. But in the half and fourth scale tests, the percentage increase is about 280% and 192% respectively. The lack of a clear trend in the results could be due to the different surface textures of the units as well as the different properties of the prototype and benchmark mortars.

5.5.3 Stiffness

The shear stress/axial strain curves for a typical prototype specimen are shown in Figure 5.43. The deformation measurements from the top transducer designated as (1) was from the upward surface of the specimen as cast horizontally, while the deformation measurements from the bottom transducer designated as (2) was from the downward surface. The bottom strains show a stiffer response than the top strain. This could be due to some bending effect during the actual test, even though every care was taken to position the specimens as plumb as possible. The stress/lateral strain curves shown in Figure 5.44 are more similar to each other than the previous curves for the axial strain. However the summary of the shear stress/strain curves, which are shown in Figures 5.45 and 5.46 for axial strain and lateral strain in all the prototype tests reveal that the shear behaviour of the specimens is very similar as can be seen from the correspondence in their slopes. In one of the tests, 1D- A2, the failure stress is much lower than the other two. This could be due to a very fine crack along one the bed joints visible prior to testing. The abrupt nature of the failure as stated earlier, can be seen from the shape of graph, which is almost a straight line with no plasticity.

In the half scale test, the stress/strain curves shown for a typical test in Figures 5.47 and 5.48 for the axial and lateral strain respectively reveal a better correspondence of the curves in this test. This could be an indication that construction and test conditions were uniform. Figures 5.49 and 5.50 show the stress/strain relationship in the axial and lateral direction for the half scale specimens and indicate that some of the curves have abnormal shapes. This is usually due to disruption to the gauge positions caused by cracking etc. Nevertheless it can still be seen from the figures that the half scale specimen showed a softer response than the prototype.

Figures 5.51 and 5.52 show the shear stress/strain behaviour in a particular test in the axial and lateral directions respectively for the fourth scale test. It is again seen that,

as in the case of the prototype tests, the bottom strains are stiffer than the top strains. The variability in the results at this scale can be seen from the differences in the shape of the stress/strain curves in the axial direction in Figure 5.53. Surprisingly the strain in the lateral direction for the same tests in Figure 5.54 shows a much better correspondence. It may be that the different configurations of the units/joint in the axial and lateral directions bring about different behaviour under load.

In the sixth scale it is seen that there is a much better agreement of the stress/strain relationship in both the axial and lateral directions for the test shown in Figures 5.55 and 5.56 respectively. It is seen from the figures that there is very good correspondence in the top and bottom strains in the axial direction while they are not so dissimilar in the lateral direction. This feature is also repeated in the other tests at this scale, as can be seen from the good agreement of the stress/strain curves in both axial and lateral directions for the tests in Figures 5.57 and 5.58 respectively. The curves also reveal the more plastic response of the specimens under load. This behaviour is significant because of the numerous model scale shaking table studies that have been made in relation to the dynamic behaviour of masonry in earthquake regions. Because as seen here, a ductile model scale masonry response may not necessarily mean the same behaviour in a prototype.

A comparison of the stress/strain curves for all the scales is shown in Figure 5.59 for the axial direction and Figure 5.60 for the lateral direction. It is seen from the curves for the axial strain that their slopes in the elastic region, at about a third of the maximum stress reached, are similar. The close agreement of the curves is even more apparent in the case of the lateral strain. The discussion that has just proceeded regarding the more plastic response of the sixth scale is more apparent in the figures. While in the other scales failure was abrupt, in the sixth scale it can be seen that there is evidence of a more ductile and plastic response near the peak stress.

5.5.4 Size effect analysis

The size effect analysis of the diagonal tensile strength test data is shown in Figure 5.61. It shows, as seen in the case of the other tests, that except for the compressive strength test, there is no size effect seen when the limiting failure condition is the bond/shear characteristic of the masonry. Again it is seen that the MFSL agrees better with the test data than the SEL, although only a slight improvement.

5.6 Conclusions

The results of the masonry tests at different scales has shown that the strength of masonry triplet in compression was higher than the prototype in the fourth and sixth model scales but the similar to the prototype in the half scale. The same pattern was also repeated in the tests of the unit strengths, therefore indicating the strong influence of the unit in determining the masonry properties. There is evidence of anisotropy of strength in clay brick masonry possibly due to the manufacturing process of extruded clay units which therefore makes the direction of loading on a cut model brick important.

In terms of the wallette compressive strength, it was found that the sixth scale wallette strength is 64% more than the prototype wallette strength. This percentage increase is identical to the percentage increase between sixth scale and prototype unit strengths. Therefore is seems that in the case of the wallette compressive strength, the increase in the strength of the model test could be attributed to the stronger unit strength in the model scale.

It can then be suggested that the increase in model unit strength, could be attributed to two factors, namely; strength anisotropy and the energetic size effect in quasi-brittle materials. The compressive strength test data was also found to closely follow the size effect laws of fracture mechanics (MFSL and SEL) and shows a noticeable size effect with increase in scale, characterised by a decrease in the nominal strength with increase in scale.

It was found that triplet stiffnesses in the four scales were identical to each other and no scale effect was observed. The prototype masonry and model stiffness were in good agreement with the prototype and model mortar stiffness respectively. This may be attributed to the way the specimens were constructed, which has effectively cancelled any differential compaction of the joints due to the different weight of the unit bricks in the various scales. The good agreement in the stiffness of the four scales may be evidence of the importance of the mortar bed in determining the stiffness properties of masonry. This finding is very significant bearing in mind that model tests by other researchers showed a much softer model response to the prototype under axial compression.

The EC 6 empirical formula for the unreinforced characteristic strength of masonry overestimates the wallette and triplet characteristic strength evaluated on the basis of the tests by more than 50%. But there is need for further research to confirm this because the implications could be important in situations were masonry is constructed horizontally like in prefabricated and cast masonry panels.

In the initial shear strength test, there is no clear evidence of an increase in either the coefficient of friction or the initial shear strength as the scale was increased but within the model scales there seems to be an increase in the coefficient of friction and a decrease in the initial shear strength as the scale was increased. This suggests a possible scale effect within the model scales but it is difficult to conclude.

Both the flexural strength normal to the bed joint and parallel to the bed joint shows no clear effect of scale. But there is a slight increase in the flexural strength parallel to the bed joints as the scale was increased, perhaps because it is significantly influenced by the tensile strength of the units.

The bond strength test shows a possible increase in strength as the scale was increased within the model scales, but there is no clear trend across the four scales. This could be due to the different surface finishes on the model and prototype units on one hand and different sand gradings of the model and prototype mortars on the other hand.

The same lack of clear trend is also seen in the diagonal tensile strength tests, which shows there is no increase or decrease in the shear strength as the scale was increased. The stress/strain relationship showed that the sixth scale had a more plastic response than the other scales, characterised by a gradual and more restrained failure which is different to failure in all the other three scales, most especially the prototype tests. This may be significant in shaking table model tests that are used to simulate seismic effects on masonry, in that, a softer model response may not necessarily suggest similar behaviour at prototype scale.

The size effect analysis for the initial shear strength test, flexural strength tests, bond strength tests and diagonal shear strength tests shows no significant size effect in all these tests. This may be due to the general scale of the specimens in this study, because as suggested by Figure 2.3 most laboratory tests should not exhibit a strong

effect since they are in strength failure criterion range; which implies no size effect is seen. Generally the MFSL agreed better with the test data than with the SEL

It appears therefore, that the prototype compressive strength of masonry could be predicted through model tests more easily than the other strength properties. This may be because masonry compressive strength is mainly influenced by the unit compressive strength and thus prototypes and models with similar unit compressive strength should have similar masonry strength and vice versa. Hence masonry models of down to sixth scale could be used to predict prototype masonry compressive strength by taking into account the difference in unit compressive strength between models and prototypes. But in order to predict stiffness properties from models the effect of the weight of the units should be considered, because while setting, the mortar bed in a model are at a lower stress state than in a prototype. Consideration should also be made about the instrumentation for deformation measurements since the smallest scales may require specially made gauges.

The support conditions in the initial shear strength test are the most important considerations for a model test. Because of the size of the specimens in model tests, achieving the boundary conditions for minimum bending in the specimens may be challenging, and since achieving minimum bending is a perquisite for the validity of the Coulomb criterion, the initial shear strength test may be better suited for half scale and higher scales, where it is easier to achieve those boundary conditions.

The flexural strength test bond strength and diagonal tensile strength tests at model scales appear not to pose significant challenges with regards to actual test set up but rather with regard to the inherent properties of the constituent materials, for example the fine grading of the sand in the model tests could result in lower bond strength. Thus for modelling the bond strength of prototypes it is better to choose a scale that will not require using a fine grading of sand because of the size limitations of the joints. Therefore bond strength tests are best carried out on models that have similar gradings of sands to the prototype as well as similar surface finish of units.

Scale	Mortar Type	Bed thickness mm	Compressive Strength,N/mm^2	COV %	Stiffness N/mm^2	COV %	Mortar Cube Strength,N/mm^2
Prototype	MP-iii	10.0	9.2	10.8	5500	22.6	4.6
Half	M95-iii	5.0	11.0	9.1	5200	26.9	4.9
Fourth	"	2.5	23.0	9.1	5400	6.6	4.7
Sixth	"	1.6	20.3	11.6	6000	20.1	4.7

Table 5.1- Summary of triplet masonry compression test results in the four scales.

Scale	Mortar Type	Compressive Strength,N/mm^2	COV %	Stiffness N/mm^2	COV %	Poisson's Ratio	Mortar Cube Strength,N/mm^2
Prototype	MP-iii	10.2	2.7	5500	8.1	0.06	5.3
Sixth	M95-iii	16.8	5.4	6800	21.4	0.19	3.7

Table 5.2- Summary of wallette masonry compression test results in prototype and sixth scale.

Scale	Mortar Type	Initial Shear Strength,N/mm^2	Co-efficient of friction	Mortar Cube Strength,N/mm^2
Prototype	MP-iii	0.89	1.17	3.6
Half	M95-iii	0.27	1.76	6.6
Fourth	"	0.50	1.19	4.7
Sixth	"	0.60	0.85	5.5

Table 5.3 –Summary of masonry shear strength test results in the four scales.

Scale	Flexural Strength Normal to Bed Joint,N/mm^2	COV %	Mortar Cube Strength,N/mm^2
Prototype	0.54	33.9	6.5
Half	0.46	21.7	6.3
Fourth	0.86	18.6	5.1
Sixth	0.32	20.6	4.8

Table 5.4- Summary of masonry flexural strength normal to bed joints test results in the four scales.

Scale	Flexural Strength Parallel to Bed Joint,N/mm^2	COV %	Mortar Cube Strength N/mm^2
Prototype	1.91	20.5	6.1
Half	2.01	5.2	5.4
Fourth	1.72	14.6	5.7
Sixth	1.26	31.2	4.8

Table 5.5- Summary of masonry flexural strength parallel to bed joints test results in the four scales.

Scale	Bond Strength N/mm^2	COV %	Mortar Cube Strength,N/mm^2
Prototype	1.00	17.3	4.3
Half	1.27	31.6	4.3
Fourth	0.99	22.0	3.5
Sixth	0.73	28.1	3.6

Table 5.6- Summary of bond strength test results in the four scales.

Scale	Shear Strength N/mm^2	COV %	Mortar Cube Strength,N/mm^2
Prototype	0.91	0.41	3.92
Half	0.76	11.09	3.95
Fourth	0.96	37.63	4.47
Sixth	0.63	7.24	4.06

Table 5.7- Summary of diagonal tensile strength test results in the four scales.

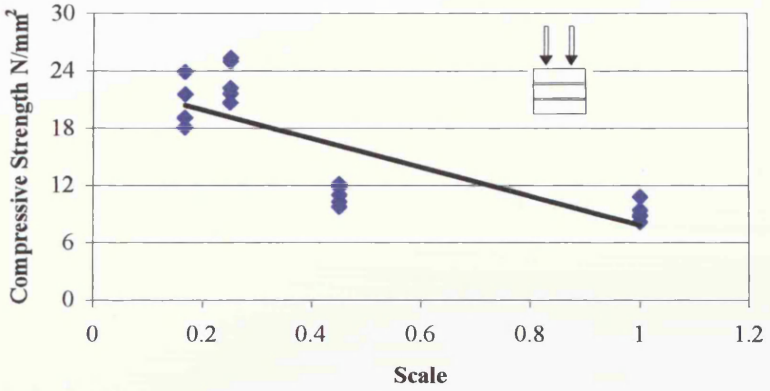

Figure 5.1- Triplet compressive strength in the four scales.

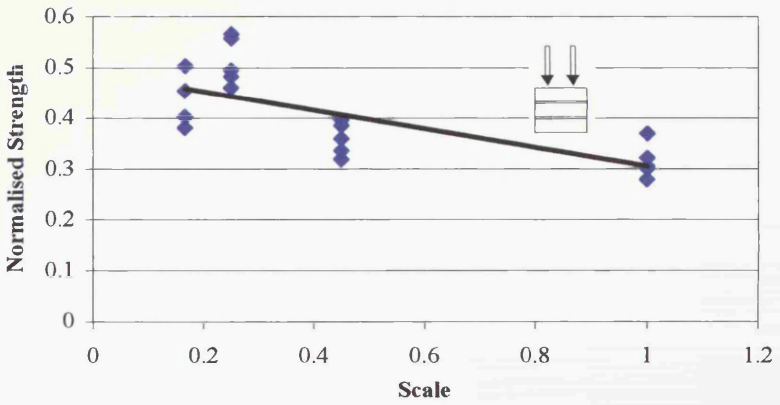

Figure 5.2- Normalised triplet compressive strength across the four scales.

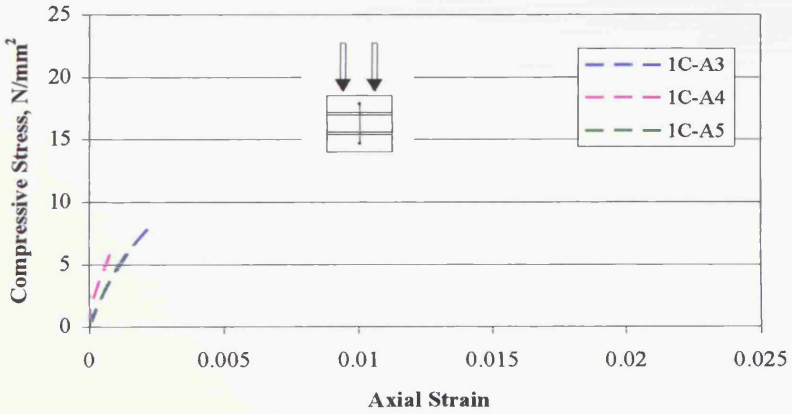

Figure 5.3- Summary of stress/axial strain curves for prototype masonry triplet tests.

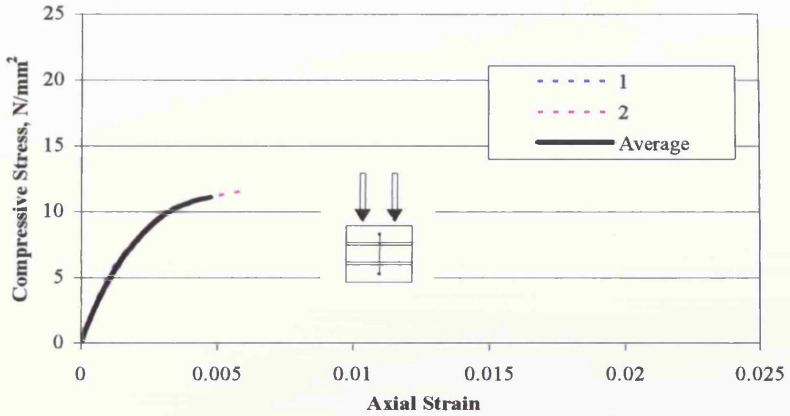

Figure 5.4- Typical stress/axial strain curves for half scale masonry triplets, test 2C-A2.

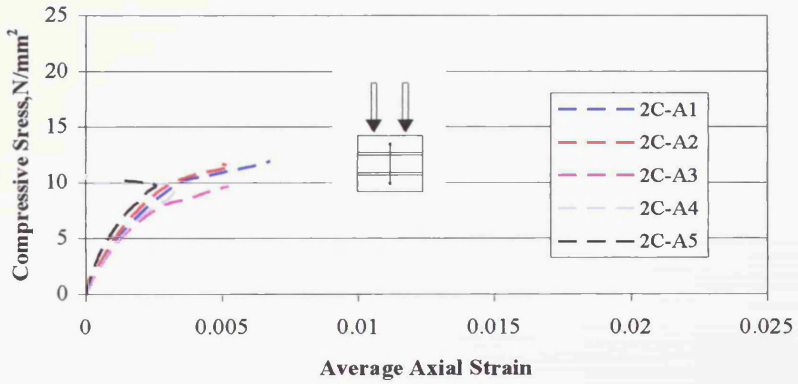

Figure 5.5- Summary of stress/axial strain curves in all half scale masonry triplet tests.

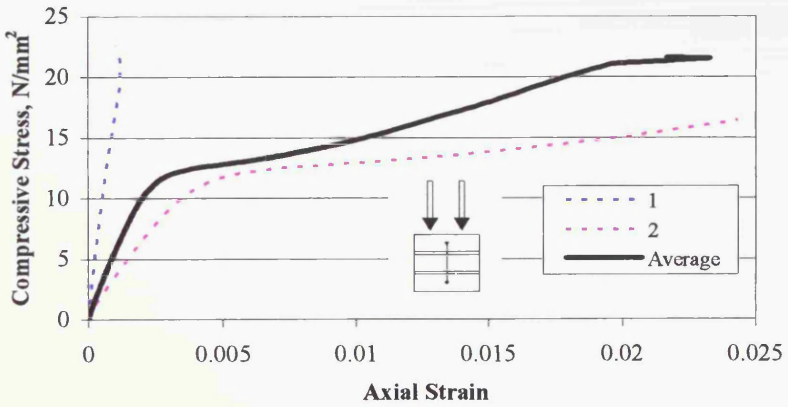

Figure 5.6 – Typical stress/axial strain curves for fourth scale masonry triplets, test 4C-A3.

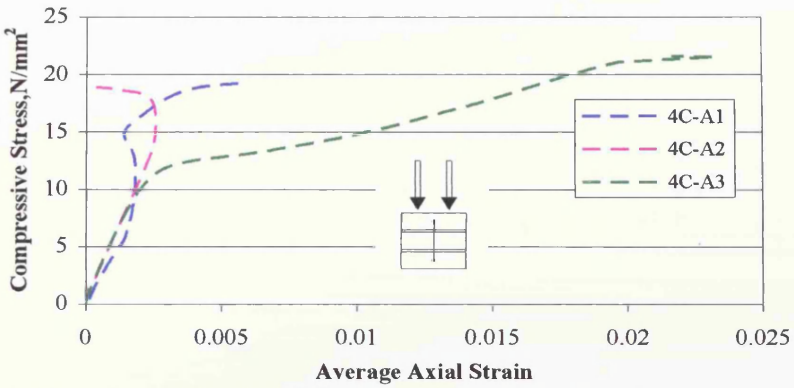

Figure 5.7- Summary of stress/axial strain curves for fourth scale masonry triplet tests.

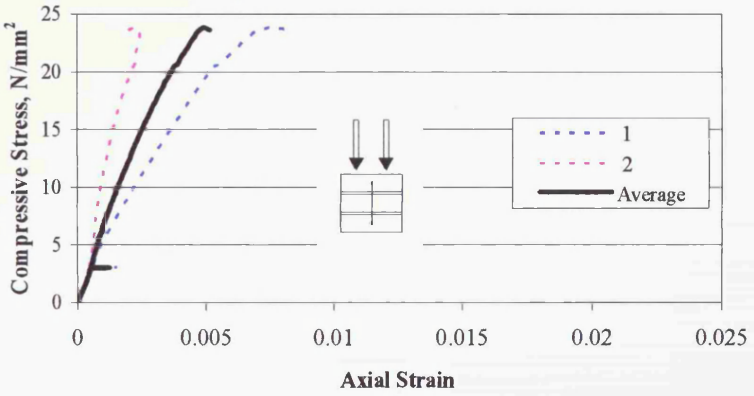

Figure 5.8- Typical stress/strain curves for sixth scale masonry triplets, test 6C-B4.

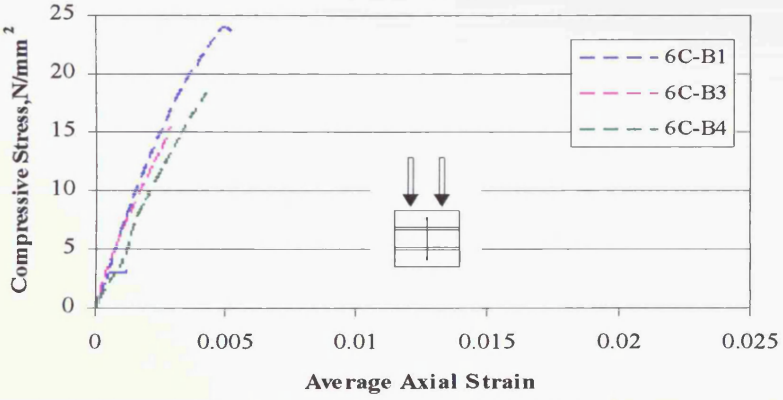

Figure 5.9- Summary of stress/axial stain curves for sixth scale masonry triplet tests.

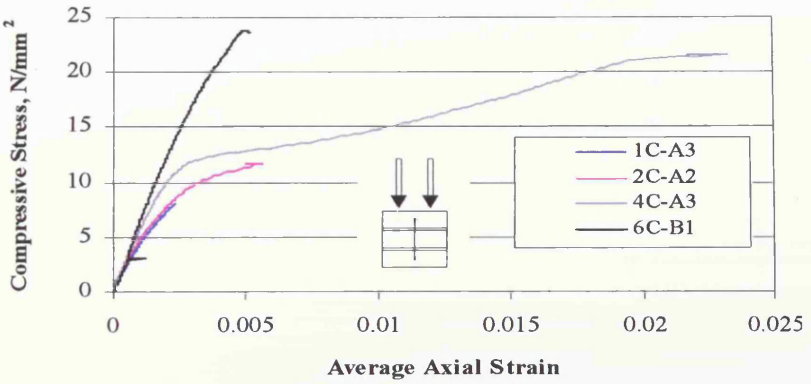

Figure 5.10- Stress/strain curves for selected triplet tests across the four scales.

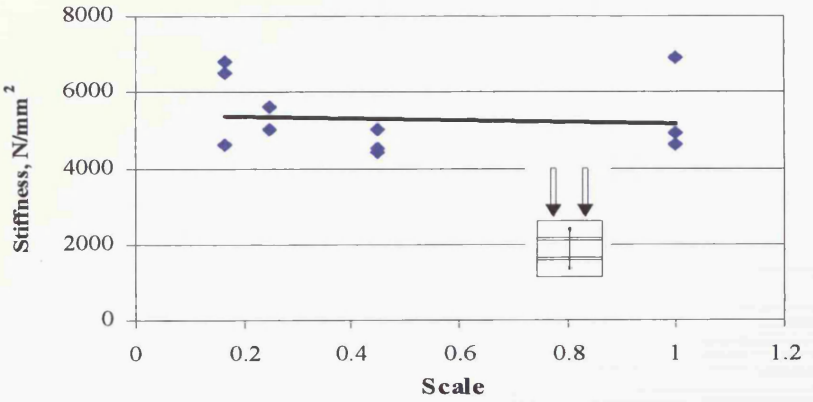

Figure 5.11- Stiffness of masonry triplets in the four scales.

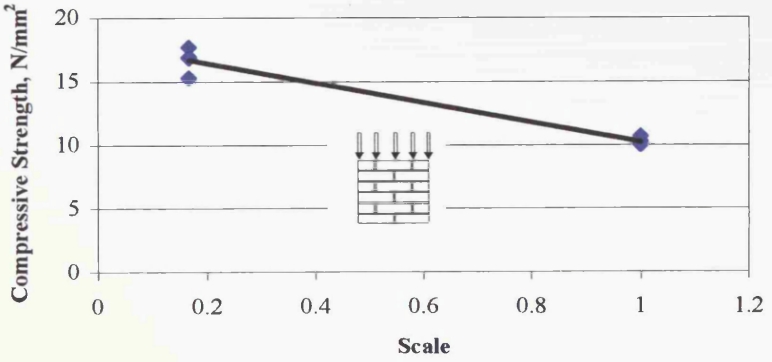

Figure 5.12- Comparison of prototype and sixth scale wallette compressive strength.

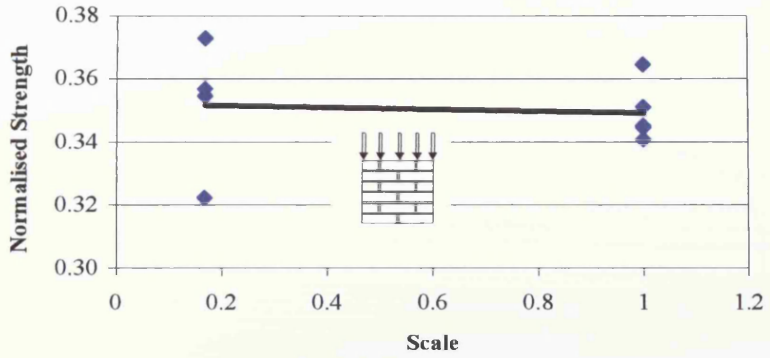

Figure 5.13- Comparison of normalised prototype and sixth scale wallette strength.

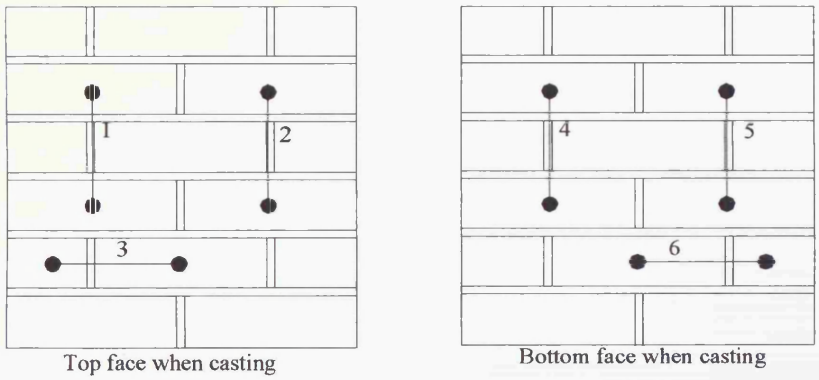

Figure 5.14- Position of transducers in prototype and sixth scale wallettes.

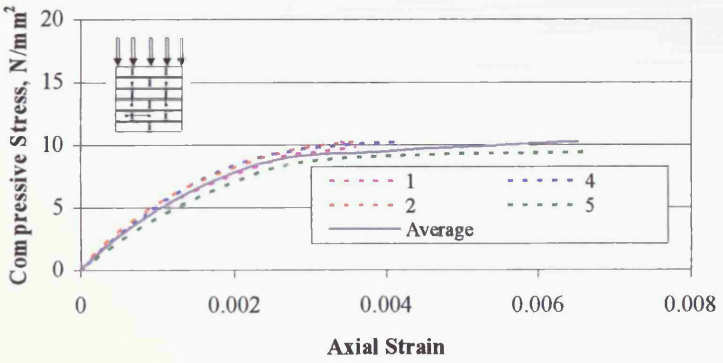

Figure 5.15- Typical stress/axial strain curves for transducer 1, 2, 4, 5 and their average strain as shown in Figure 5.14, prototype test 1C-B1.

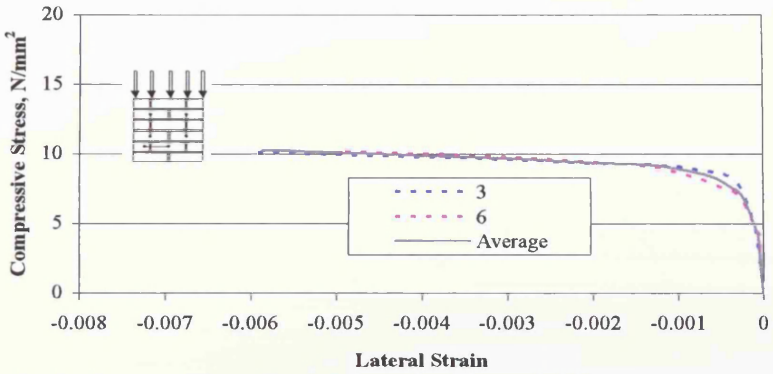

Figure 5.16- Typical stress/lateral strain curves for transducer 3, 6, and their average strain as shown Figure 5.14, prototype test 1C-B1.

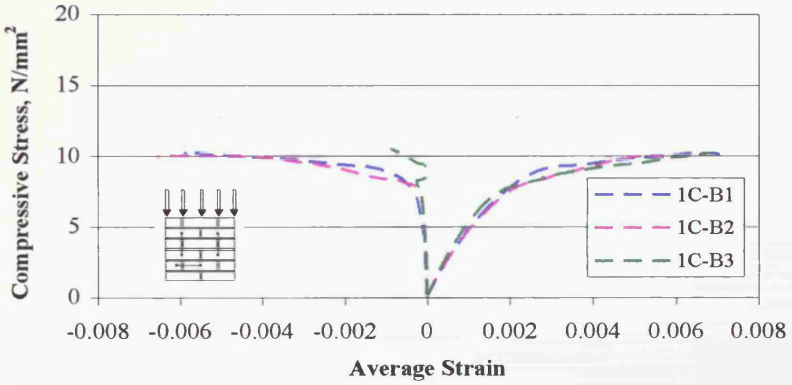

Figure 5.17- Summary of stress/strain curves in prototype masonry wallette tests.

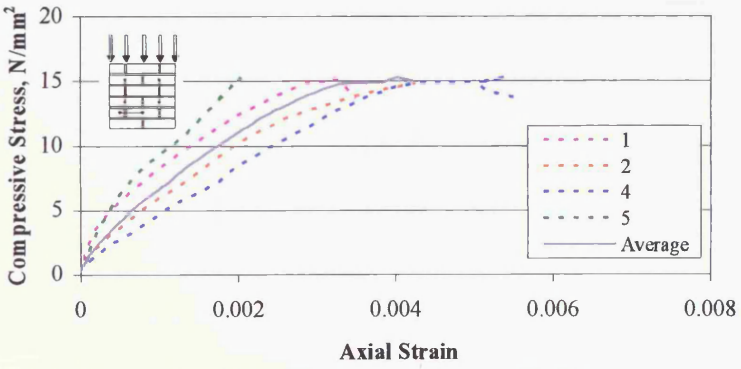

Figure 5.18- Typical stress/axial curves for sixth scale wallette for MMCG's 1, 2, 4 and 5 as shown in Figure 5.14, test 6C-I1.

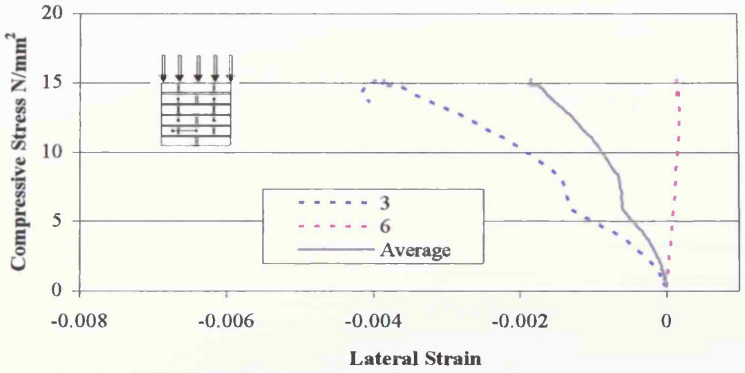

Figure 5.19- Typical stress/strain curves for sixth scale wallette for transducers 3 and 6 as shown in Figure 5.14, test 6C-I1.

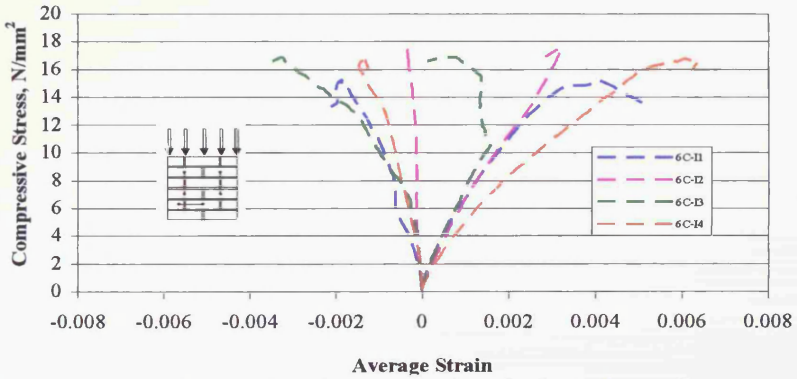

Figure 5.20- Summary of stress/strain curves for sixth scale wallette masonry tests.

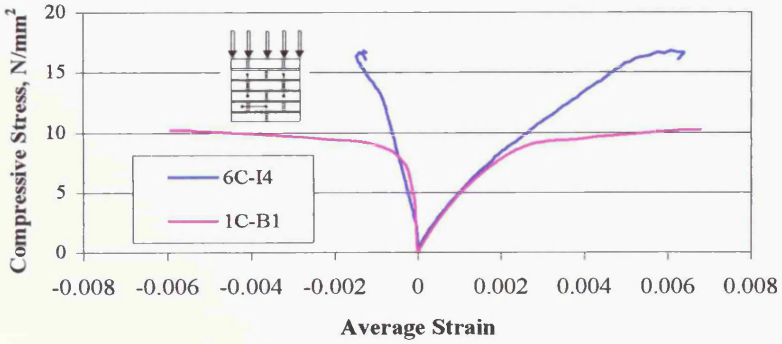

Figure 5.21- Typical stress/strain curves for prototype and sixth scale wallette specimens, tests 1C-B1 and 6C-I4.

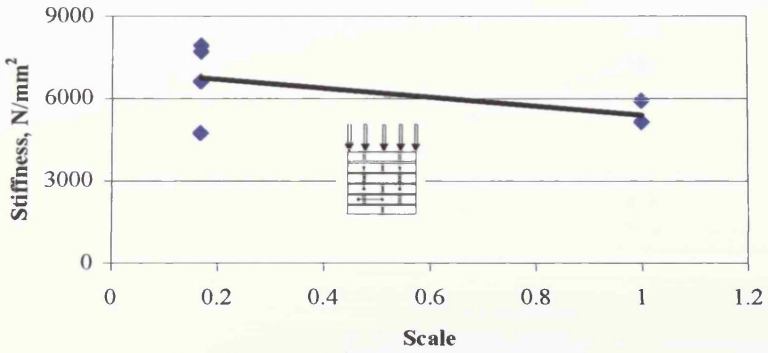

Figure 5.22- Variation of wallette stiffness with scale in prototype and sixth scale tests.

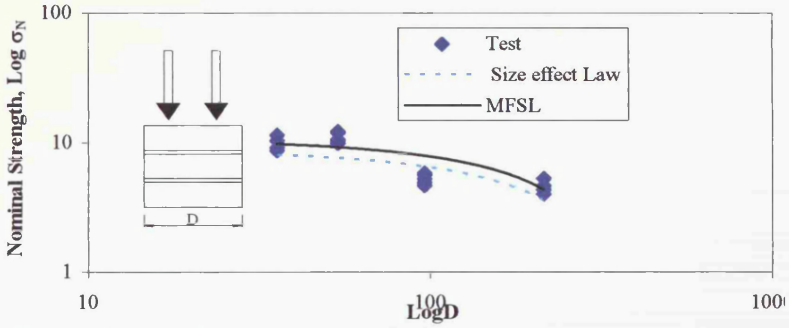

Figure 5.23- Size effect analysis of masonry compressive strength triplet test results.

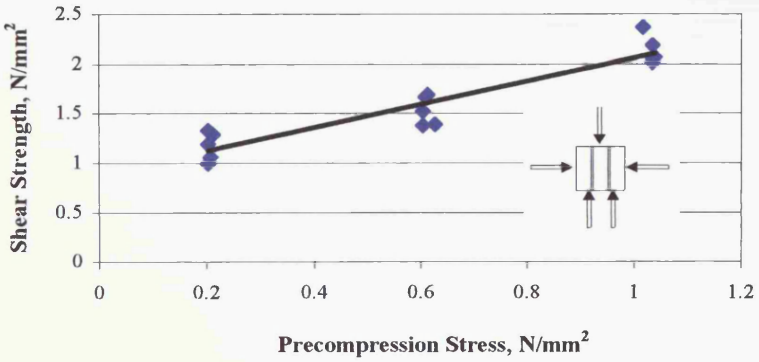

Figure 5.24- Shear stress/precompression stress relationship for prototype specimens.

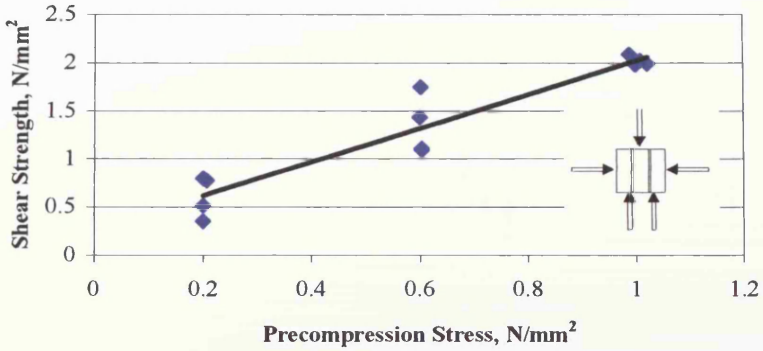

Figure 5.25- shear stress/precompression stress relationship for half scale specimens.

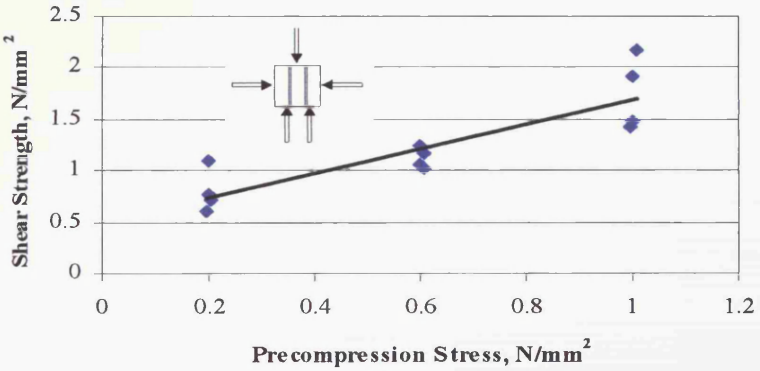

Figure 5.26- Shear stress/precompression stress relationship for fourth scale specimens.

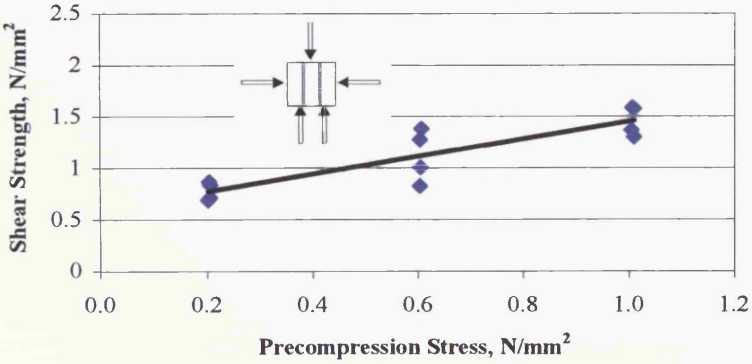

Figure 5.27- Shear stress/precompression stress relationship for sixth scale specimens.

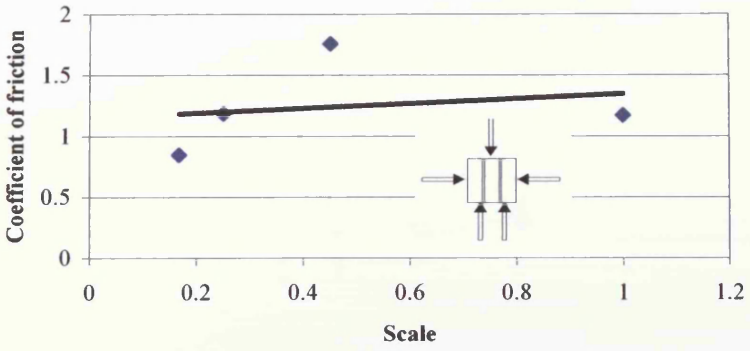

Figure 5.28- Coefficient of friction across the four scales.

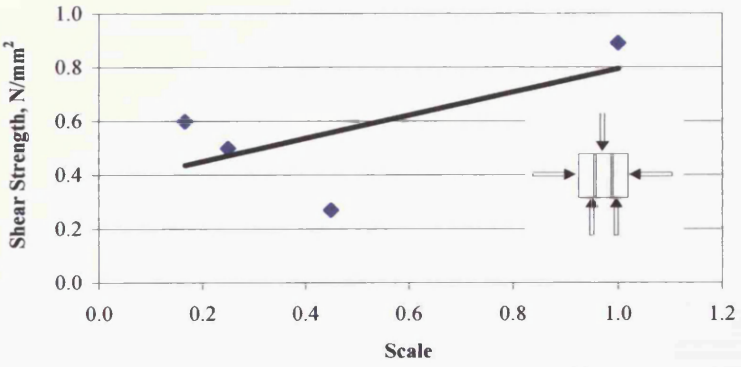

Figure 5.29- Initial shear strength across the four scales.

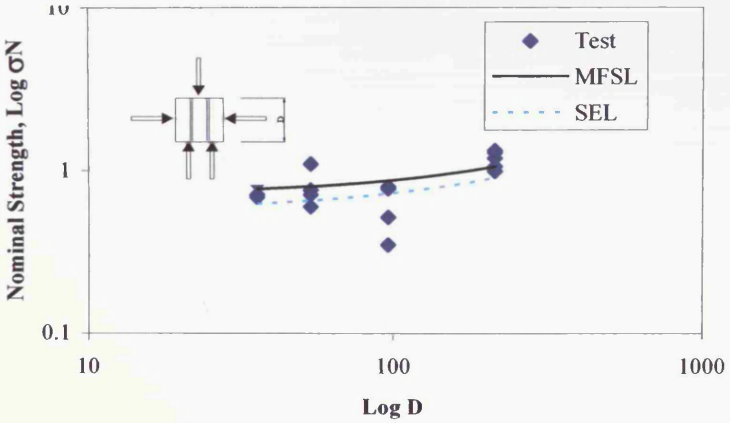

Figure 5.30- Size effect analysis of shear strength tests results at a precompression stress of 0.2N/mm^2

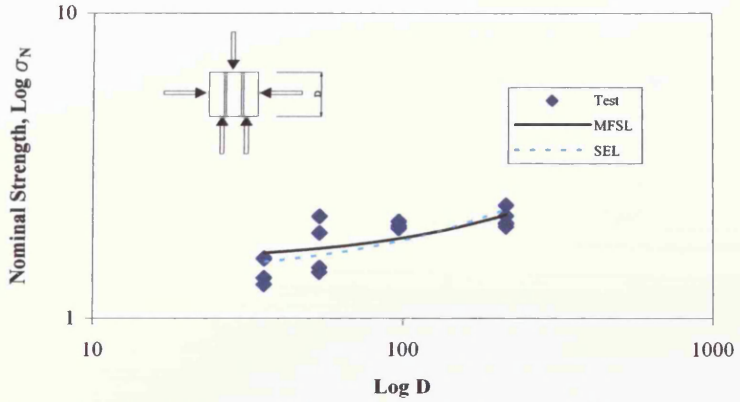

Figure 5.31- Size effect analysis of shear strength test results at a precompression stress of 1.0N/mm^2

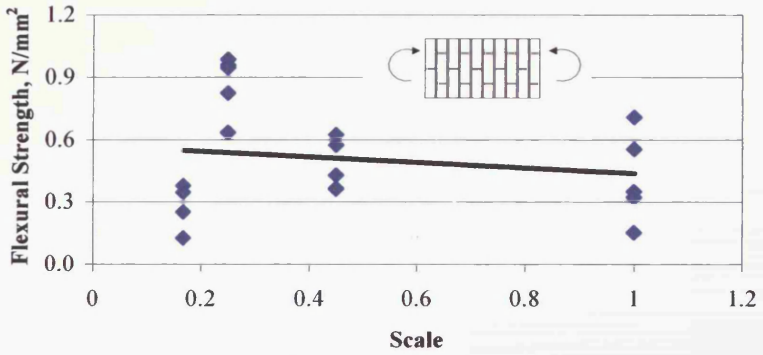

Figure 5.32- Flexural strength normal to bed joint across the four scales.

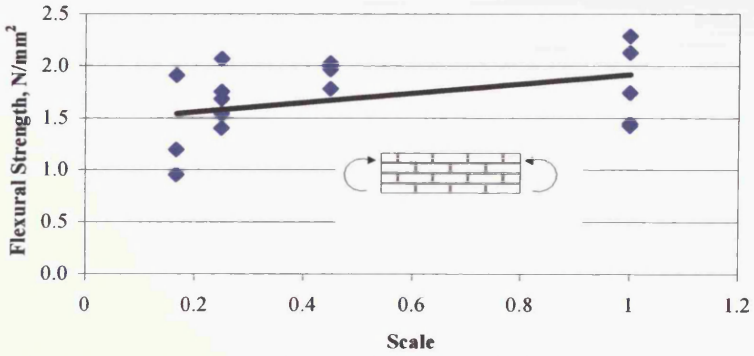

Figure 5.33- Flexural strength parallel to bed joints across the four scales.

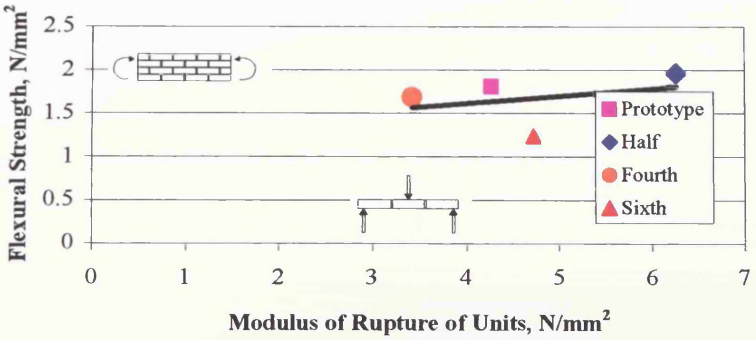

Figure 5.34- Flexural strength parallel to bed joint/modulus of rupture of units.

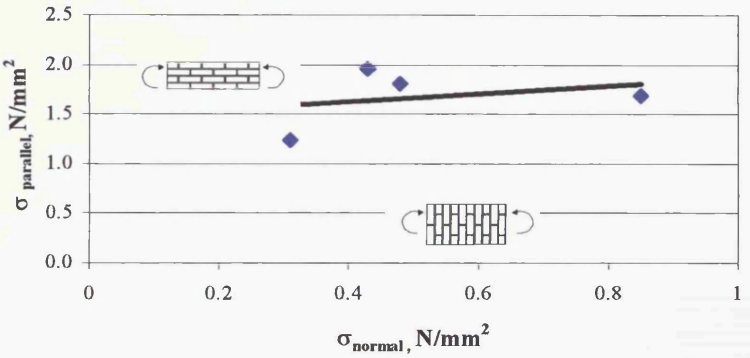

Figure 5.35- Plot of flexural strength in the orthogonal directions.

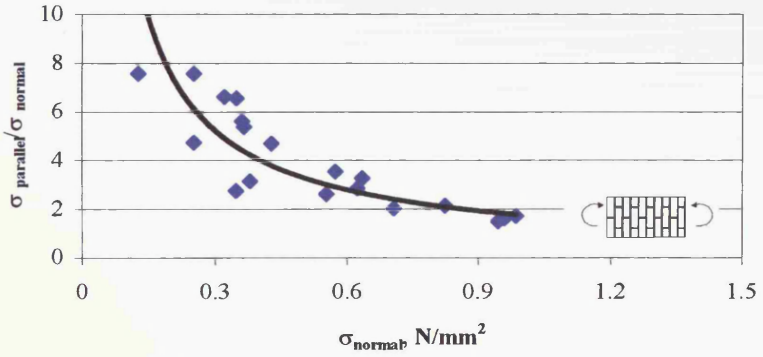

Figure 5.36- Relationship between the orthogonal ratio and σ_{normal}.

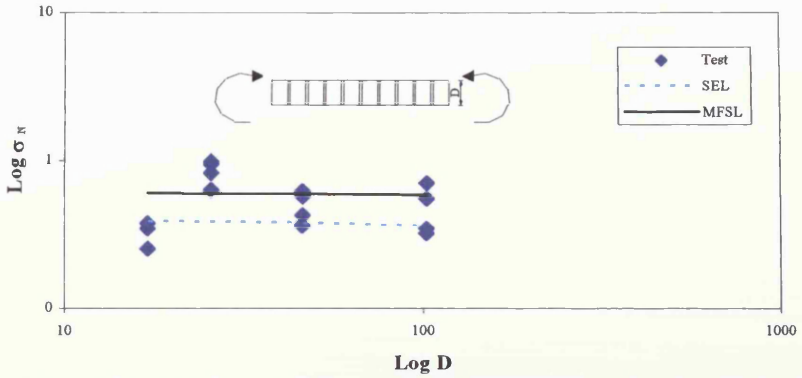

Figure 5.37- Size effect analysis of flexural strength (normal to bed joints) test data.

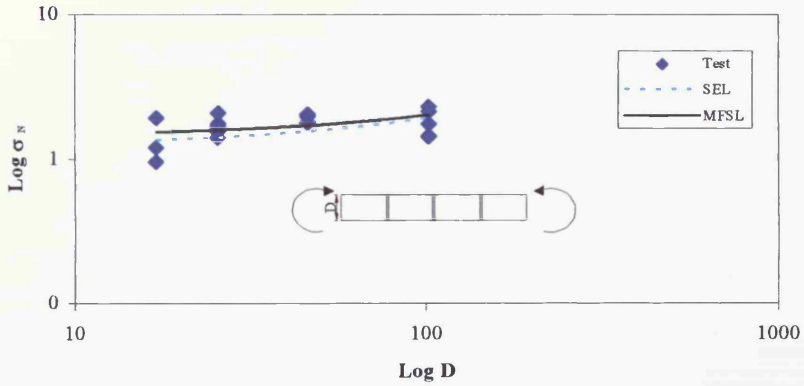

Figure 5.38- Size effect analysis of flexural strength (parallel to bed joints) test data.

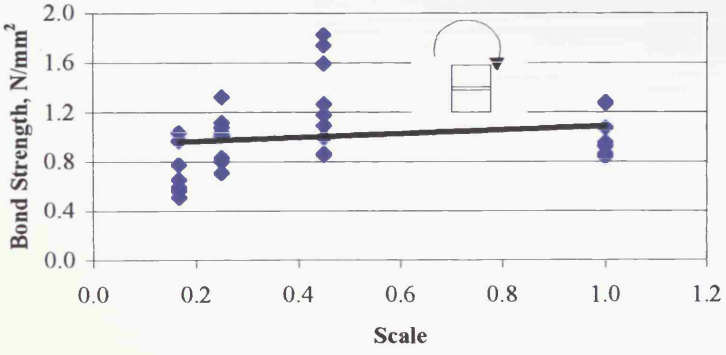

Figure 5.39- Variation of bond strength across the four scales.

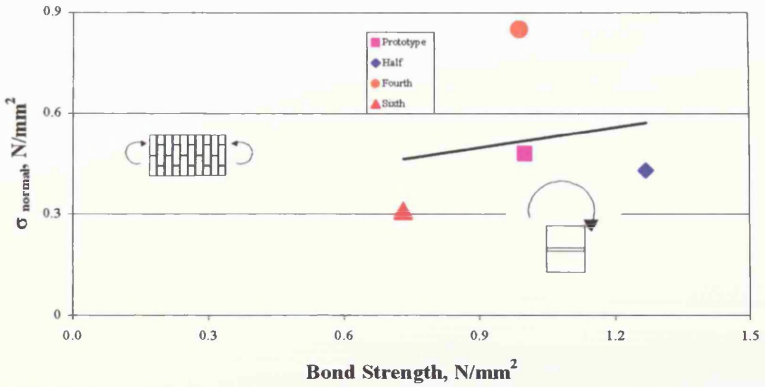

Figure 5.40- Relationship between flexural strength and bond strength in the four scales.

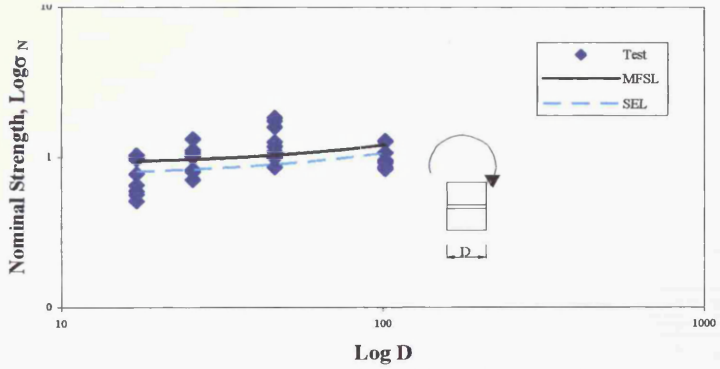

Figure 5.41- Size effect analysis of bond wrench test results.

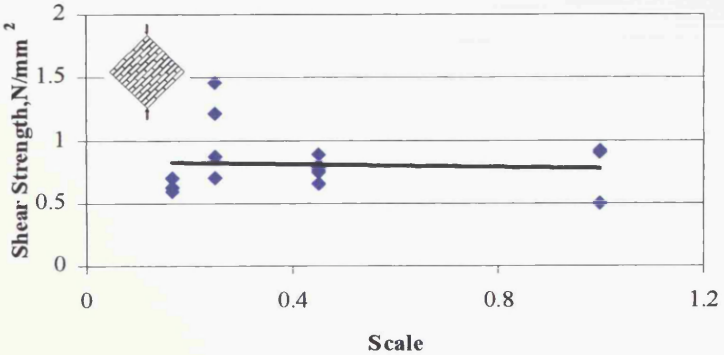

Figure 5.42- Variation of shear strength with scale in the diagonal tensile strength tests.

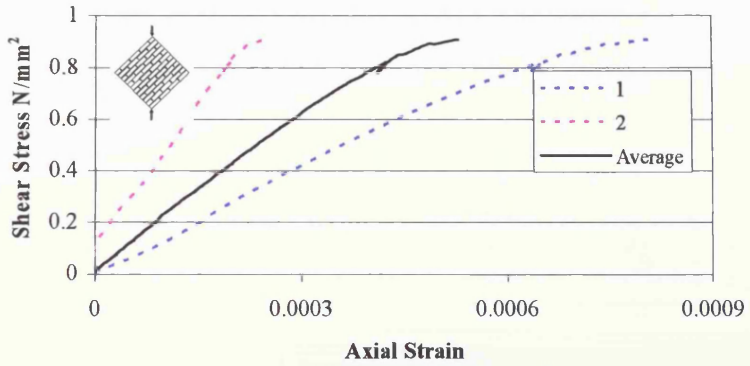

Figure 5.43 – Typical shear stress/axial strain curves in prototype diagonal tensile strength test 1D-A1.

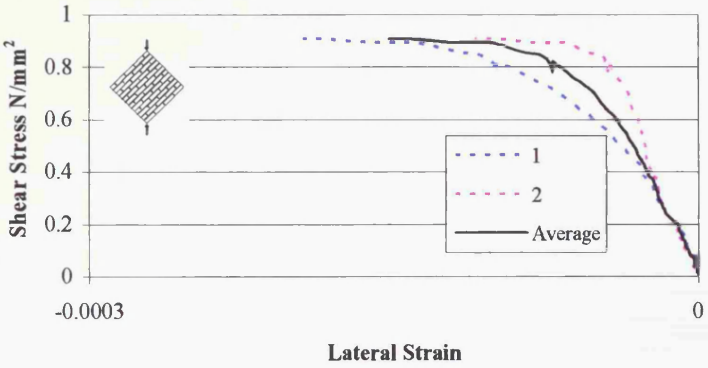

Figure 5.44- Typical shear stress/lateral strain curves in prototype diagonal tensile strength test 1D-A1.

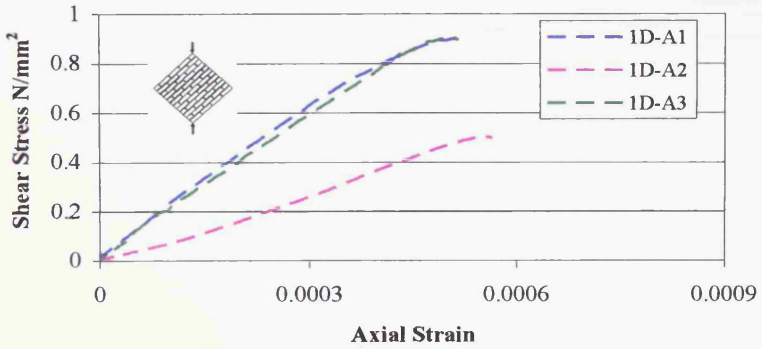

Figure 5.45- Summary of shear stress/axial strain curves for the diagonal tensile strength prototype tests.

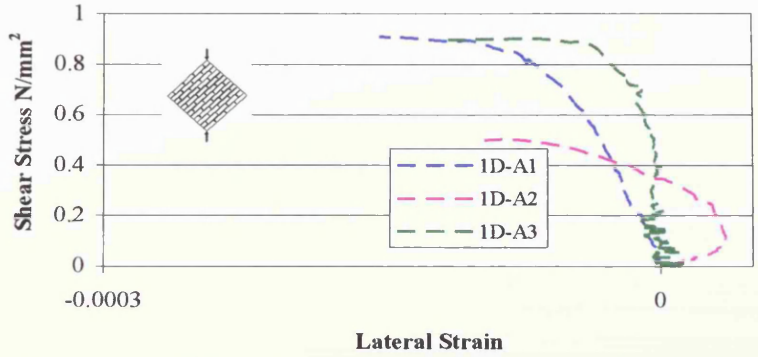

Figure 5.46- Summary of shear stress/lateral strain curves for the diagonal tensile strength test prototype tests.

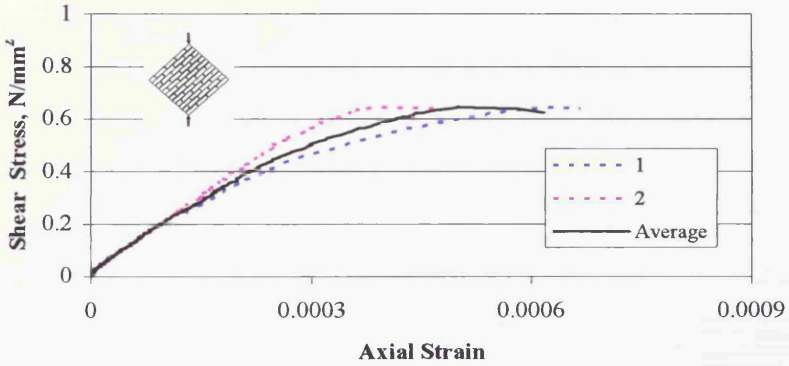

Figure 5.47- Typical shear stress/axial strain curves in half scale diagonal tensile strength test 2D-A5.

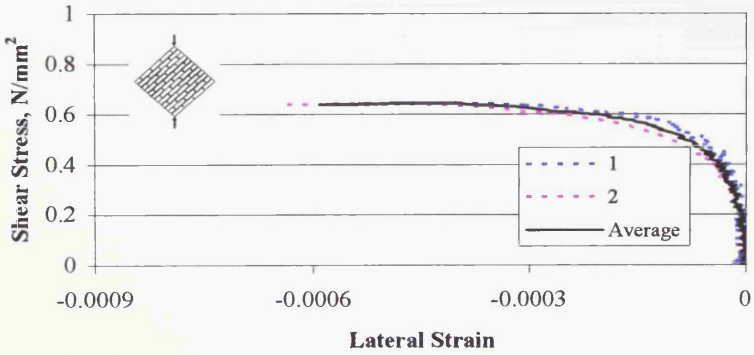

Figure 5.48- Typical shear stress/lateral strain curves in half scale diagonal tensile strength test 2D-A5.

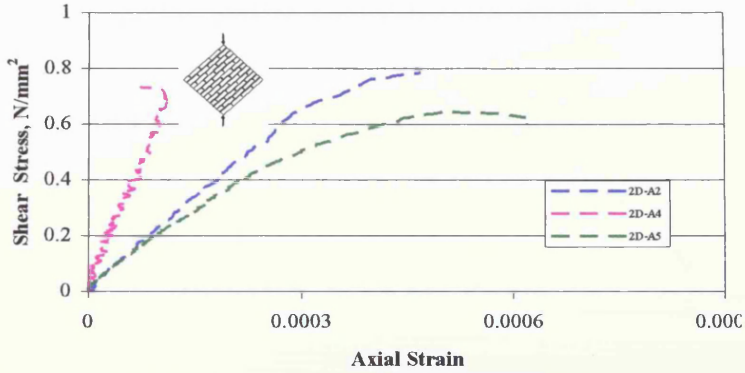

Figure 5.49- Summary of shear stress/axial strain curves for the half scale diagonal tensile strength tests.

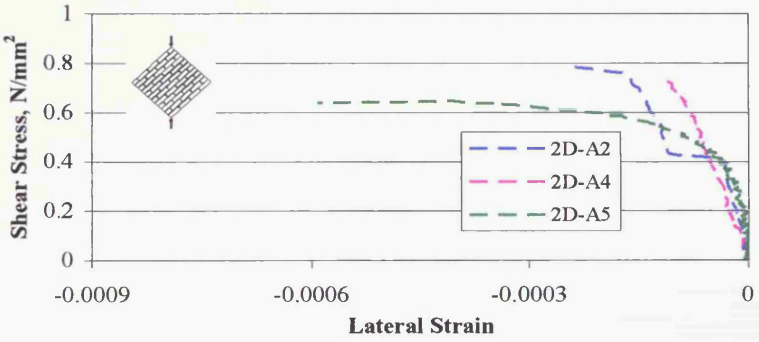

Figure 5.50- Summary of shear stress/lateral strain curves for the half scale diagonal tensile strength tests.

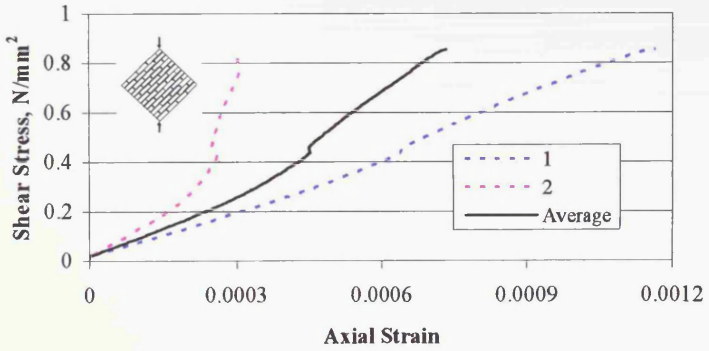

Figure 5.51- Typical shear stress/axial strain curves in fourth scale diagonal tensile strength test 4D-A2.

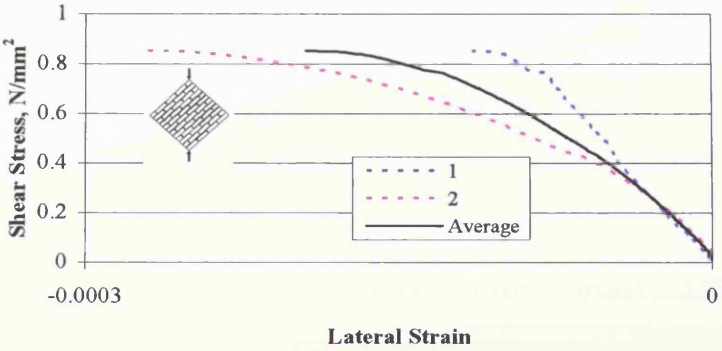

Figure 5.52- Typical shear stress/lateral strain curves in fourth scale diagonal tensile strength test 4D-A2.

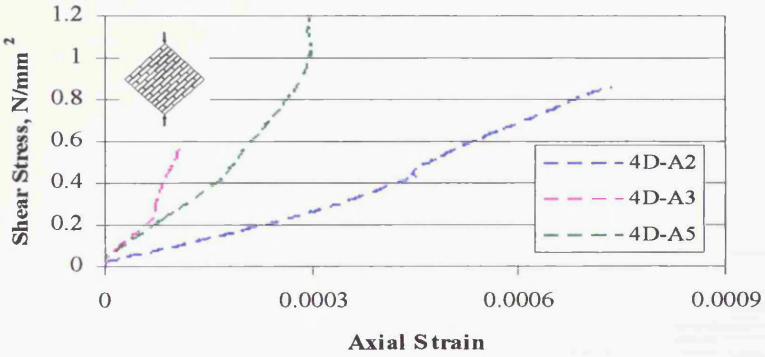

Figure 5.53- Summary of shear stress/axial strain curves for the fourth scale diagonal tensile strength tests.

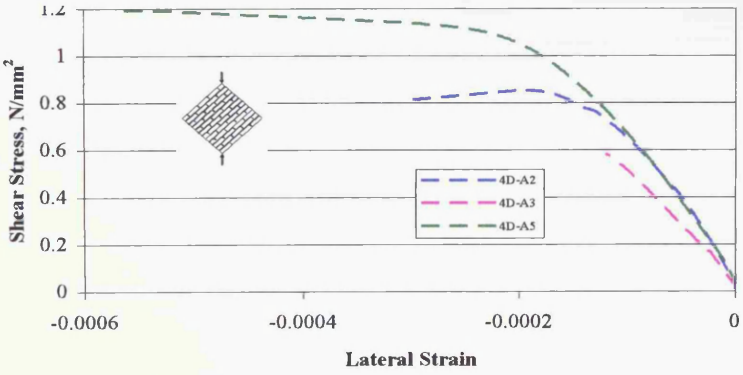

Figure 5.54- Summary of shear stress/lateral strain curves for the fourth scale diagonal tensile strength tests.

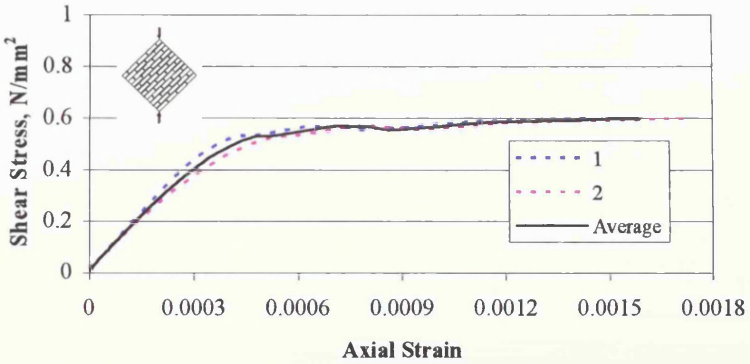

Figure 5.55- Typical shear stress/axial strain curves in sixth scale diagonal tensile strength test 6D-B1.

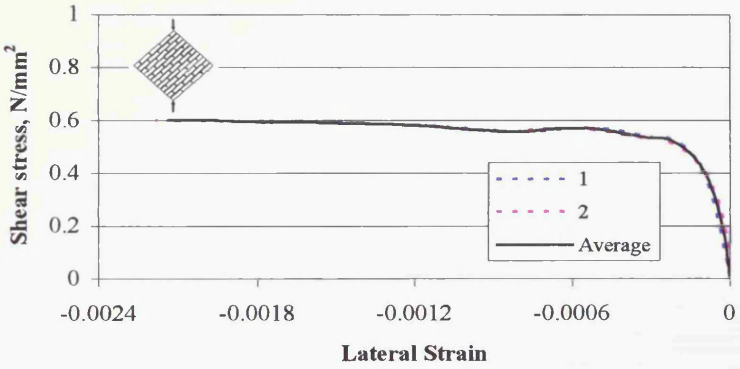

Figure 5.56- Typical shear stress/lateral strain curves in sixth scale diagonal tensile strength test 6D-B1.

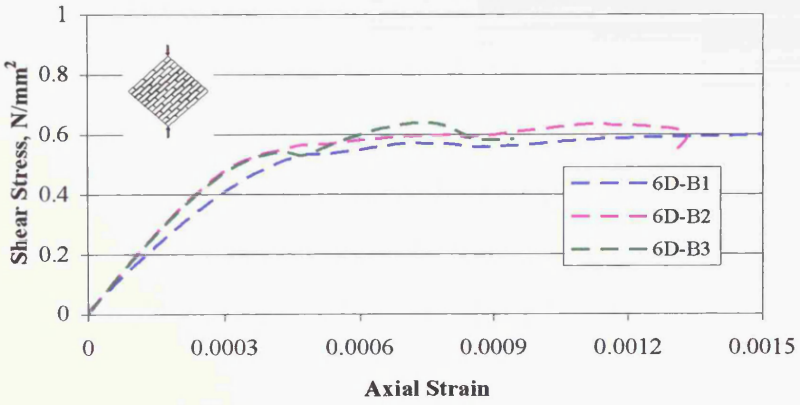

Figure 5.57-Summary of shear stress/axial strain curves for the sixth scale diagonal tensile strength tests.

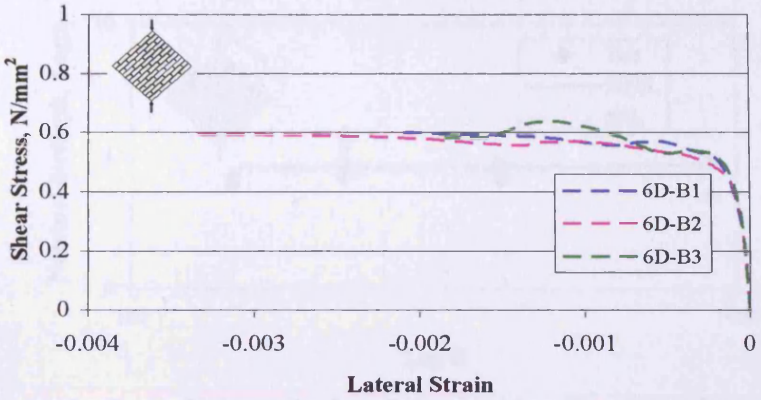

Figure 5.58- Summary of shear stress/lateral strain curves for the sixth scale diagonal tensile strength test.

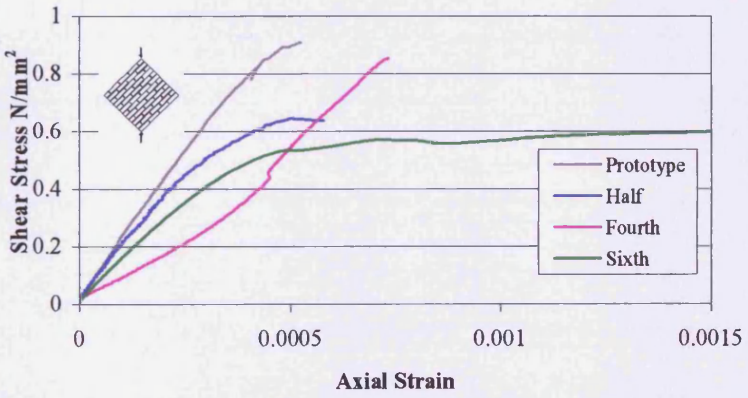

Figure 5.59- Comparison of typical shear stress/axial strain curves for the diagonal tensile strength tests in the four scales.

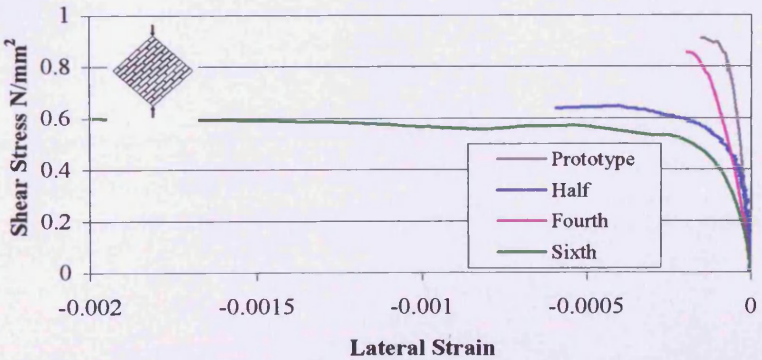

Figure 5.60- Comparison of typical shear stress/lateral strain curves for the diagonal tensile strength tests in the four scales.

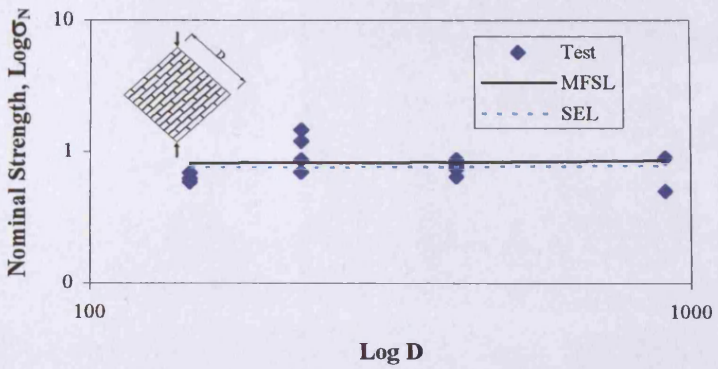

Figure 5.61- Size effect analysis of diagonal tensile strength test data.

Plate 5.1- Cracking patterns in prototype triplets.

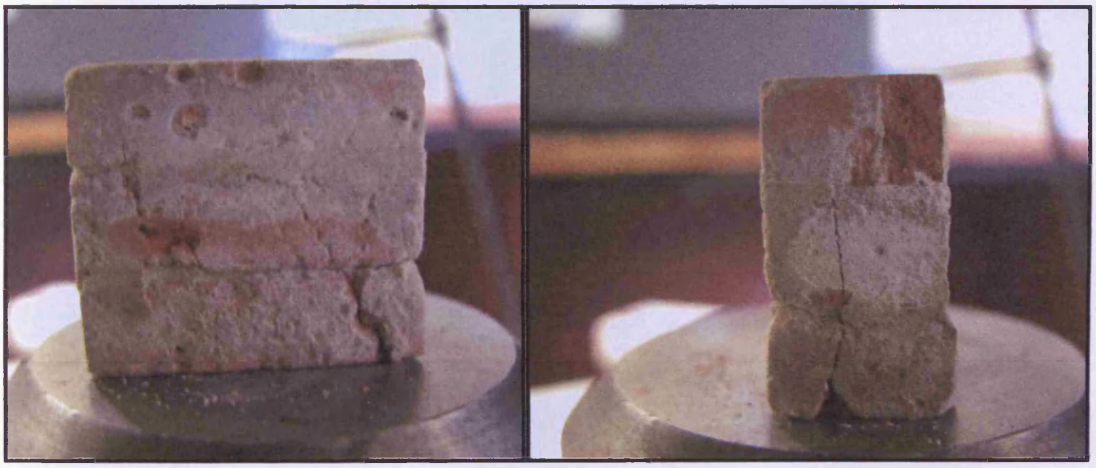

Plate 5.2- Cracking patterns in sixth scale triplets.

Plate 5.3- Cracking patterns in sixth scale wallettes.

Plate 5.4- Shear failure in prototype specimens.

Plate 5.5- Failure in half scale flexural strength specimens.

Plate 5.6- Failure in sixth scale flexural strength specimens.

Plate 5.7- Failure in prototype flexural strength specimens.

Plate 5.8- Failure patterns in half scale diagonal tensile specimens.

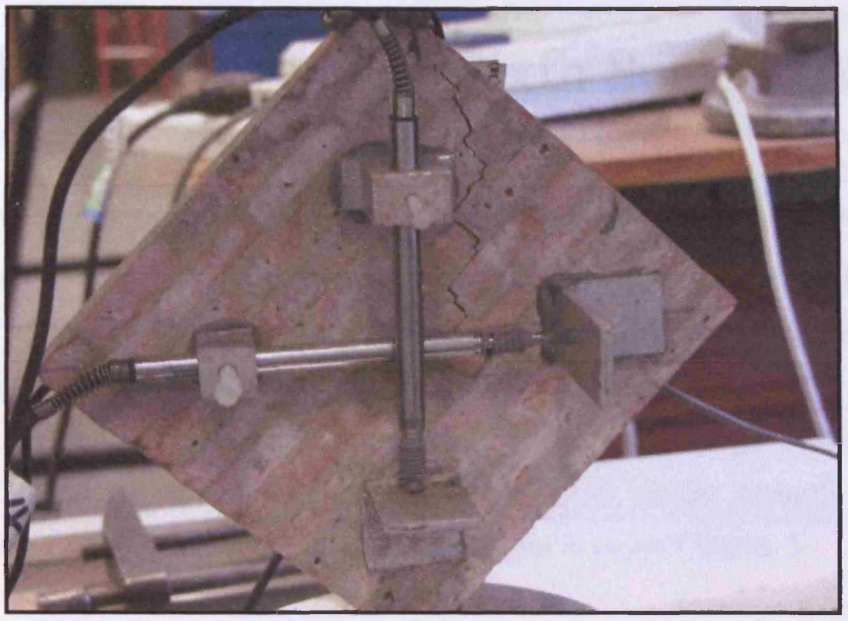

Plate 5.9- Failure pattern in sixth scale diagonal tensile specimens.

6 Masonry Tests at Sixth Scale Results and Discussions

This chapter presents the results and discussion of sixth scale tests looking at parametric effects of different joint thicknesses, different mortar grades and different sand gradings. The aim was to investigate the feasibility of using sixth models to determine the influence of these parameters on the compressive strength, shear strength, flexural strength, bond strength and diagonal tensile strength tests. The identification system used for the tests in this chapter is as per Chapter 5.

6.1 Compressive strength test

6.1.1 Varying joint thickness

Typical failure of the specimens was characterised by tensile cracks in the axial direction, at the sides and on the top and bottom faces and splitting cracks on the end faces as already shown in Plate 5.2. This failure pattern was seen in all the three joint thicknesses of 1.0mm, 1.6mm and 2.5mm. A summary of the compressive strength test results with varying joint thicknesses is shown in Table 6.1 and Figure 6.1 shows the variation of compressive strength with increasing joint thickness. It can be seen from the table that the mean compressive strength for the benchmark triplet (1.6mm bed joint) is the same as the mean strength (neglecting the lowest triplet strength) of the 1.0mm bed joint triplets. It is also seen that the mean strength of the benchmark triplet is just 1% higher than the mean strength of the 2.5mm triplet. The figure shows that there is no clear trend in the masonry compressive strength as the joint thickness is increased. The expectation was for an increase in the masonry strength as the joint thickness is decreased as reported by Francis et al[20] and others[19] from tests on stack bonded full scale masonry units. Since the mortar cube strengths for the tests are in good agreement as seen from the table, the expectation was to see an increase in the masonry strength as the joint thickness was reduced.

One possible explanation for the lack of a clear effect may be because at the very small scale of the test it is difficult to see the effect of increasing joint thickness for the range of bed joints used. Since, as it has been discussed previously in relation to

Figure 2.3, that at relatively small scales, the strength criterion applies, this may therefore imply that no size effect is seen in the masonry strength at small scales because of the size of the joints. It is also possible that the relatively higher COV (25.7%) of the 1.0mm tests as compared to the other tests masks the true structural response of the results in that test, because as seen from the figure, both the highest and lowest compressive strengths were recorded in the 1.0mm test. Therefore because of such a large variation in the strength of the model bricks it may be difficult to see the influence of the different joint thickness at this scale. It therefore seems that the mortar joint thickness does not appear to have a marked effect on the compressive strength at this scale, contrary to prototype results.

6.1.2 Effect of sand grading and mortar type

6.1.2.1 M95, Mortar designations ii, iii, and iv.

The cracking pattern in the M95 tests are characterised by the usual tensile cracking pattern as seen previously. The summary of the test results are shown in Table 6.1 and Figure 6.2. The mean triplet strengths for designation ii, iii and iv mortars were found to be 22.6 N/mm^2, 20.3 N/mm^2 and 16.7 N/mm^2 respectively. From the results it is seen that that there is an increase in masonry strength as the mortar strength is increased. There is about an 11% strength increase from designation iii to designation ii, and a 20% increase from designation iv to iii. This is also true for numerous other tests conducted at different scales, as detailed by Egermann et al[51]. The reason for the increase in masonry strength is because, as observed previously, the mortar becomes stiffer with increasing strength (increasing cement content) which therefore implies that more force is needed to create the frictional forces that induce the tensile stresses that cause failure in the units and ultimately the masonry. Just as an illustration, the EC6 formula for the characteristic strength of masonry (Equation 2.1) is also shown in the figure to see if the results will conform to the trend in the equation; the intention was not to see whether the characteristic strength prediction is accurate or not but rather to see how the test data fit the trend set by the formula. It is seen that the test results corresponds well to the general trend of Equation 2.1.

The stiffness results shown in Figure 6.3 also show that masonry stiffness increases with increasing mortar strength. The mean stiffness of the designation iii triplet was determined to be 6000 N/mm^2, while the mean stiffness for the triplets with

designation ii mortar was 53% more than that. The stiffness for the triplets with designation iv mortar is 30% less than the stiffness of the benchmark test. Remarkably, the mean masonry triplet stiffness for the specimens made with designation iii mortar is similar to the mortar stiffness from the material tests (Table 3.6); the mortar stiffness is about 8% higher than the masonry triplet stiffness. The correspondence of the masonry stiffness to the mortar stiffness is even closer in the tests made with designation iv mortar, the masonry stiffness is only 2% higher than the mortar stiffness. However there does not seem to be a good correspondence in the masonry stiffness in the tests made with designation ii mortar, the masonry stiffness is about 35% higher than the mortar stiffness in this case. But despite the lack of correspondence in this last result, the influence of mortar stiffness on the masonry stiffness can be seen as has already been seen from the masonry triplet results on different scales from Chapter 5, where the masonry stiffness in the four scales were also in good agreement with the mortar stiffness.

6.1.2.2 M60, Mortar designations ii, iii, and iv.

The failure of the specimens in the M60 tests were also characterised by tensile cracking patterns. The results from Table 6.1 and Figure 6.4 show that, as in the case of the previous test, there is clear trend of an increase in the masonry strength as the mortar strength is increased. In this case there is about an 8% increase from designation iii to designation ii mortar and about an 18% increase from designation iv to designation iii mortar. The percentage increases in this case from one designation to the other also agrees with those from the M95 tests, an indication that it is possible to use a sixth scale masonry model to look at the effects of increasing mortar strength. The figure also reveals that the test data corresponds well with the EC6 equation even though the trend line for the equation straddles the trend line for the test data.

6.1.2.3 Effect of different sand gradings

The combined plot for the variation of masonry strength with mortar strength for both M95 and M60 tests is shown in Figure 6.5. It is seen that the trend line for the M95 test is steeper than that for the M60 test. This may mean that the M95 tests are more receptive to changes in cement content because the sand grading is finer than in the M60 tests. Another interesting point from the plot is that even though the M60 mortars are stronger than the M95 mortars in all three designations; the masonry

strength is still stronger for the triplets made with M95 mortar. This may be because as the mortar bed is compressed, tensile stresses are induced in the unit because of their different stiffness properties. But since these stresses are initiated by the friction at the mortar-brick interface, it could be that a mortar with coarser sand grading might develop a higher friction than a mortar with finer sand grading, and consequently result in a lower failure stress in the unit. It has also been seen that the M95 test data follow the trend of Equation 2.1 much better than the M60 test data. All this implies that the grading of the sand is an important consideration in small scale modelling of masonry compressive strength since the results suggest that models made with coarser sands are likely to have a lower compressive strength than those made with mortars having finer sands.

6.2 Shear strength test

6.2.1 Varying joint thickness

Typical failure of the shear strength test specimens is by the pushing through of the central unit with two lines of failure on either side of the unit. The two failure lines were usually at the mortar/unit interface or through the mortar bed. The shear strength/precompression stress for the benchmark test (1.6mm), 1.0mm bed joint test and the 2.5mm bed joint test are shown in Figures 6.6, 6.7 and 6.8 respectively. The figures show that as the joint thickness is increased at a precompression stress of $0.2N/mm^2$, the mean shear strength increases slightly from the 1.0mm test to the 1.6mm test, and decreases marginally from the 1.6mm test to the 2.5mm test. While at precompression stresses of $0.6N/mm^2$ and $1.0N/mm^2$ the benchmark test recorded the highest shear strengths. The reason for this could be the relatively higher mortar cube strength in the benchmark test, as shown in a summary of the results for the shear strength test in Table 6.2. It is seen that the mortar cube strength in both the 1.6 and 2.5mm bed joint tests was $3.6N/mm^2$, while that of the benchmark test was 5.5 N/mm^2. Because of this the benchmark test could have recorded the highest initial shear strength of $0.6N/mm^2$, while the initial shear strength in the 1.0mm bed joint test was only marginally higher(about 3%) than the 2.5mm bed joint test. This is better reflected in Figure 6.9, the plot of initial shear with increasing joint thickness. It is seen in this figure that there is a lack of a clear trend because of the scatter in the results. However, there is a noticeable decrease in the co-efficient of friction with

increase in bed joint thickness even with the lack of correspondence in the mortar cube strengths as seen from Figure 6.10, which shows the variation of joint thickness with co-efficient of friction. This may imply that the co-efficient of friction is not as susceptible to mortar strength as the initial shear strength because it is dependent on the physical properties of the mortar-unit interface. The results in the next section should provide further evidence in relation to this preposition.

6.2.2 M95, mortar designations ii, iii, and iv.

Figures 6.11 and 6.12 show the shear strength/precompression stress response in the M95-ii and M95-iv tests, respectively. The figures show that there is some degree of scatter in the result most notably at the precompression stress of 0.6N/mm^2. The figures also show that the shear strengths recorded at the different precompression levels in the benchmark test are almost the same with the M95-ii test, even though the mortar cube strength in the M95-ii test was marginally higher than that in the benchmark test. Because of this, the plot of the initial shear with mortar cube strength in Figure 6.13 shows an unexpected trend, as seen from the fitted trend line, which shows a slight decrease in initial shear strength with increase in mortar cube strength. The plot of the co-efficient of friction with mortar cube strength in Figure 6.14 shows an increase in the friction co-efficient from the designation iv to the designation iii mortar followed by drop from the designation iii to the designation ii mortar. In fact the friction co-efficient is the same for the designation ii and designation iv mortar. This seems to agree with the earlier preposition that co-efficient of friction is not strongly influenced by different mortar strengths.

6.2.3 M60, mortar designations ii, iii, and iv.

The plot of shear strength/precompression stress for the M60-iii, M60–ii and M60-iv mortar tests are shown in Figures 6.15, 6.16 and 6.17 respectively. The figures again show some degree of scatter for the M60-iii and M60-ii tests but considerably less scatter for the M60-iv test. The figures also show that there is a gradual increase in the shear strength at the different precompression levels as the mortar strength was increased. In this case therefore, there is a clear trend of an increase in the initial shear strength as the mortar strength is increased, as seen from plot of initial shear strength with mortar cube strength in Figure 6.18. This is to be expected since there will be a better bond between the mortar and brick because of the higher cement content in the

stronger mortar grades which should increase the resistance to shear. The variation of the friction co-efficient with mortar strength is shown in Figure 6.19 and it reveals that mortar strength has no significant effect on the friction co-efficient as seen in the last section.

6.2.4 Effect of different sand gradings

Figure 6.20 shows the effect of sand grading on initial shear strength and it reveals that the influence of the sand gradings on the initial shear strength is different for the two sands. It is seen that, there is an increase in initial shear strength as the mortar strength is increased for the HST 60 sands while the reverse is true for the HST 95 sands, but the effect is not as marked as in the case of the HST 60 sands. However the real response may be masked by difficulties in accurately placing the loading and support rollers as a result of the small size of the specimens. Regardless, the HST 95 test showed higher initial shear strengths than the HST 60 test.

With respect to the friction co-efficient, Figure 6.21 shows how the sand gradings affect the friction co-efficient. It is seen from the figure that there is a just noticeable increase in the co-efficient as the mortar strength is increased for both HST 95 and HST 60 sands. In fact because of the very marginal rate of increase, it could be argued that there is no effect of the increase in mortar strength on the friction co-efficient. In this case however, the tests with HST 60 sand gave higher friction co-efficients than the tests with HST 95 sand. This could be because the grain size is coarser for the HST 60 sands.

6.3 Flexural strength test

6.3.1 Varying joint thickness

Typical failure of the flexural strength test specimens is as shown in Plate 5.7, which is characterised by a bond failure at the brick-mortar face in case of the flexural strength normal to bed joint test and a combination of joint-brick fracture for the flexural strength parallel to bed joint test. In the case of the 1.0mm and 2.5mm flexural strength normal to bed joint tests, the failure line was mostly through the 3rd joint from either the top or bottom face for the flexural strength normal to the bed joints. While in the case of the benchmark tests the failure was normally through the fourth or 5th joint from either face. Failure for the flexural strength parallel to bed

joint test was similar in all three test, but for two specimens that showed joint rotation in the benchmark test; which failed through the joints and not through a joint-brick failure as in the other cases.

The summarised results for failure normal to bed joints and failure parallel to the bed joints are shown in Tables 6.3 and 6.4 respectively. From the tables and from the plot of flexural strength with varying joint thickness in Figure 6.22, it is seen that there is slight increase in flexural strength parallel to the bed joint as the joint is increased but only marginally. A gradual decrease in flexural strength normal to bed joint is shown as the bed joint is increased, but because of the variability in the results, it is difficult to draw any definite conclusion on the effect of increasing joints thickness on flexural strength. Figure 6.23, the plot of the orthogonal flexural strength ratio($\frac{\sigma_{Parallel}}{\sigma_{Normal}}$) to the flexural strength normal to the bed joints reveals the expected trend that with increase in the latter the former reduces markedly as discussed by Hendry[19]. The orthogonal strength ratios are 4.4, 4.0 and 2.5 respectively for the 1.0mm, 1.6mm and 2.5 mm bed joints test, which again shows the lack of a clear trend in the results. This could be due to the general scale of the test as observed earlier with reference to Figure 2.3. The trend seen here does not correspond to tests conducted on prototype specimens by Sise et al[33], who found that the flexural bond strength is strongly influenced by the bed joint thickness, characterised by a decrease in flexural strength as the joint thickness was increased.

6.3.2 M95, mortar designations ii, iii, and iv.

Figure 6.24 shows the effect of increasing the M95 mortar strength on the flexural strength for the two specimen formats. In this case, despite the scatter there is a noticeable increase in both flexural strengths with increase in mortar strength. This is to be expected since the unit-mortar bond should increase with increasing mortar strength because of the increasing cement content. Again Figure 6.25, which is the plot of the orthogonal ratio to the flexural strength normal to the bed joints, shows the expected decrease of the former as the latter is increased.

6.3.3 M60, mortar designations ii, iii, and iv.

The graph of flexural strength with increasing M60 mortar strength is shown in Figure 6.26. It is seen from the figure that as in the case of the M95 mortars there is an

increase in the flexural strengths with increase in mortar strength. In this case however the scatter is less, as seen from the COV of their mean flexural strength from Tables 6.3 and 6.4. It also seen that the COV of the flexural strength normal to bed joints is much higher than that for the flexural strength parallel to the bed joints for both the M60 and M95 test. This may be because the failure in the flexural strength normal to the bed joints is governed by the weakest joint in the specimen, which is limited by two variables either the bond strength at the mortar-unit interface or the tensile strength of the mortar. While failure in the flexural strength parallel to the bed joints is mainly influenced by one variable, the modulus of rupture of the units of the units when there is strong bond between the bricks and mortar. Figure 6.27 also shows that the orthogonal ratio deceases with increasing flexural strength normal to the bed joint as expected.

6.3.4 Effect of different sand gradings

The effect of the different sands on the flexural strength parallel to the bed joints is shown in Figure 6.28. It is seen from the figure that even though the flexural strength is higher for the M60 mortars, the effect is negligible, possibly because the flexural strength parallel to the bed joint is mainly influenced by the tensile properties of the units. But in the case of the effect of the different sand gradings on the flexural strength normal to the bed joints as shown in Figure 6.29, there is a much more noticeable effect of the increase in flexural strength. This could be due to the presence of more cement per unit volume of M60 mortar than an equivalent weight of M95 mortar, because as observed in Chapter 3, the HST60 sands have a higher bulk density than an equivalent weight of HST95 sand. The extra cement could then result in increased bond between the mortar and unit which subsequently results in increased bond strength.

The plot of the orthogonal ratios for the two mortar types in Figures 6.24 and 6.27 also shows that the ratio is higher for the M95 tests than the M60 tests at lower values of the flexural strength normal to the bed joints. But as the flexural strength normal to the bed joints is increased the ratios for the mortars begin to correspond, and actually have similar ratios at about the flexural strength of $0.8N/mm^2$.

6.4 Bond Strength test

6.4.1 Varying joint thickness

Typical failure of the bond strength test specimens was in the top or bottom joint of the triplet specimen but in no particular order. A summary of the mean bond strengths is presented in Table 6.5 and the effect of joint thickness on bond strength shown in Figure 6.30. It can be seen from the results that there is no net effect of the varying joint thickness on the bond strength. The expectation was for a decrease in the bond strength as the joint thickness was increased, as reported by Sise et al[33] from tests on prototype specimens. Even though the 1.0mm and 2.5mm tests were constructed from the same batch of mortar and the benchmark test from a separate one, the mean bond strengths in the 1.0mm is only marginally higher than that in the 2.5mm test. The bond strength from the benchmark test was the lowest of the three because of the lower mortar strength in that test. The original benchmark test was discarded because it was gave misleading results, but even if the benchmark test was not considered, the figure still reveals a lack of a clear trend in the bond strength as the joint thickness is increased. This is further complicated by the scatter in the results as seen from the relatively high COV from the table. This seems to reinforce the earlier observation in the previous sections, that it is difficult to model the effect of varying joint thickness at small scales.

6.4.2 M95, mortar designations ii, iii, and iv.

The failure of the bond strength M95 test specimens was also as reported in the last section with failure in either the bottom or top joint of a triplet. The effect of increasing the M95 mortar strength on the bond strength is shown in Figure 6.31, from which it is clear that there is an increase in the bond strength as the mortar strength is increased. This is to be expected since the mortar strength increase is due to the increase in cement content. It follows therefore that this may also affect the brick-mortar bond which consequently results in higher bond strength, since a greater amount of force would be required to break the bond at the mortar-unit interface.

6.4.3 M60, mortar designations ii, iii, and iv.

Figure 6.32 shows the effect of increasing the M60 mortar strength on the bond strength. It is seen from the figure and Table 6.5 that there is an unexpected drop in the bond strength for the M60-iii test batch. However this does not affect the general

trend of the regression line, which shows that there is an overall increase in the bond strength as the mortar strength is increased.

6.4.4 Effect of different sand gradings

The effect of the different sands on the bond strength is shown in Figure 6.33. From which it can be seen that because of the low bond strength results from the M60-iii batch and relatively lower M60-iv bond strength (compared to M95-iv), the fitted regression line for the M95 mortars appears to be higher than that for the M60 mortars. It is therefore difficult to conclusively argue about the effect of the sand grading.

6.4.4.1 Flexural strength normal to bed joint compared to bond strength

The flexural strength normal to the bed joint is in actual fact a flexural bond strength since failure will always occur at the weakest joint. This can therefore be related to the flexural bond strength from the bond wrench test. The two values are of course not exactly the same since in the bond wrench test; individual joints are tested, while in the flexural strength test; failure occurs at the weakest joint. Fried et al[90] have reported that Lawrence[90] found that the bond strength obtained from testing single joints could be greater than that at which a single joint (the weakest) fails. Figure 6.34 shows the effect of the joint thickness on the flexural strength/bond strength relationship. As seen from the previous discussion on the effect the bed joint thickness has on the bond strength, the fitted regression line does not show the expected trend; that is, a direct relationship between the flexural strength and the bond strength.

In the case of the M95 tests, the relationship between the flexural strength and the bond strength seems to be linear, as shown in Figure 6.35. The plot again reveals a wide scatter in the results, despite that a correlation can still be made between the flexural strength and the bond strength. The regression line from the plot shows a positive intercept and also above the equality line, indicating that the flexural strength is greater than the bond strength for this set of tests. This does not correspond to the findings of Lawrence as stated earlier. But, as it has been previously stated, the normal stresses are neglected in the bond wrench calculations but not in the determination for flexural strength, which could lead to the lower bond strength, as seen here. The flexural strength/bond strength relationship for the M60 tests shown in Figure 6.36 also reveals a direct relationship between the two.

6.5 Diagonal tensile strength test

Typical failure of the diagonal tensile strength test specimens was by shear failure through the joints and in some cases combination of joints and units. The failure line usually occurred in the direction of the compression diagonal, but there were cases of shear-bond failure between the mortar bed and units along the bed joint. There were also cases of explosive and sudden failure of the specimens, although most specimens failed more gradually.

6.5.1 Varying joint thickness

The shear stress/strain curves for the 1.0mm, 1.6mm and 2.5mm test are shown in Figures 6.37, 6.38, 6.39 respectively. The curves show that there is good agreement between the curves for each of the tests, as evidenced by the slope of the curves. From Figure 6.40, which shows typical stress/strain curves on the same plot, it can be seen that the curves have similar slopes although the curves from the benchmark test have a less steep slope. The curves also reveal that failure is not abrupt after attainment of the maximum shear stress but are more plastic. This is more noticeable in the case of the benchmark test, in which it is seen that there is a greater plasticity at the maximum stress. In Figure 6.41 the effect of joint thickness on shear strength is shown and it reveals that there is a decrease in shear strength as the joint thickness is increased. The summary of the test results in Table 6.6 also shows that mean shear strength of the benchmark tests; 0.63N/mm^2 is the lowest of the three probably due to its lower mortar strength.

6.5.2 M95, mortar designations ii, iii, and iv.

Figures 6.42 and 6.43 show the stress/strain curves for the M95-ii and M95-iv test. Again the figures show that curves in each set of tests are similar to each other. The curves are more consistent for the benchmark test than for the M95-ii and M95-iv tests as seen from their higher COV in Table 6.6. In Figure 6.44, which compares typical stress/strain curves for the three mortar grades, it is seen that the specimens made with designation iii and iv mortars have a greater capacity to withstand deformation at the attainment of their respective maximum shear stresses, than specimens made with designation ii mortar. But the latter have a greater capacity to withstand higher shear stress. The effect of increasing mortar strength on shear strength is seen in Figure 6.45, and it shows, as expected, that there is an increase in

shear strength as the mortar strength increases. From Table 6.6 it is seen that even though the M95-ii cube strength is four times the M95-iv cube strength, the shear strength of the specimens made with the M95-ii mortar are about 2.3 times more than that made with the M95-iv mortar. This test underlines the importance of using the right kind of mortar designation to model masonry behaviour because as seen here their plastic responses can differ significantly.

6.5.3 M60, mortar designations ii, iii, and iv.

The stress/strain curves for the M60-iii, M60-ii and M60-iv tests are shown in Figures 6.46, 6.47 and 6.48 respectively. The curves again show that their slopes are similar, an indication that test specimens have identical characteristics in each particular set. However the curves in the M60-iii test are more variable than those in the other two tests as seen from the relatively higher COV in that test. The comparison of typical stress/strain curves for the three mortar designations is shown in Figure 6.49, from which it is seen that there is a softer response in the M60-iv test than either the M60-ii or M60-iii tests. The M60-ii test however shows a greater capacity to withstand shear than the other two. As expected the plot of shear strength against mortar strength in Figure 6.50 shows an increase in the shear strength as the mortar strength is increased. This is to be expected since there is more cement per unit area of bed joint as the mortar strength is increased, which consequently results in greater adhesion between the mortar bed and units. The mean shear strength of the M60-ii tests is about 2.8 times more than the mean shear strength of the M60-iv tests. However, even though the mean mortar cube strength of the M60-ii tests is more than twice the cube strength of the M60-iii test, the mean shear strength from the M60-ii tests is only about 1.2 times the shear strength in the M60-iii tests.

6.5.4 Effect of different sand gradings

The effect of different sand gradings on shear strength is shown in Figure 6.51. It reveals that the specimens made with the HST60 sands had slightly higher shear strength than those made with the HST95 sand. This, as observed earlier, could be due to the presence of more cement per unit volume of M60 mortar than an equivalent weight of M95 mortar. The additional cement could then result in increased bond between the mortar and unit which consequently manifests in increased shear strength. The different stress/strain curves for the two mortar types also show that

specimens made with the HST95 sand are more able to resist further deformations after the maximum shear stress was reached.

6.6 Conclusions

The results show that in the case of the compressive strength tests, there was no change in the masonry strength with increasing joint thickness due to the wide scatter in the results. However masonry strength and stiffness was observed to increase with increasing mortar strength. Significantly it was also observed that, even though the M60 mortar strengths were higher, the M95 masonry tests gave higher results.

The initial shear strength was observed to decrease marginally with increase in joint thickness in the shear strength tests. In the M60 mortar tests, the initial shear strength increases with increase in mortar strength while there was virtually no change in the shear strength for the M95 tests. But because of the effect of the different sand the M95 tests had higher initial shear strength than the M60 tests.

In the case of the joint thickness tests for the flexural strength there was a mixed picture; the flexural strength normal to the bed joint was seen to increase marginally with increase in joint thickness, while the flexural strength parallel to the bed joints was observed to decrease marginally with increase in the mortar bed thickness. But the picture was clearer in the other tests, as it was observed that the flexural strengths were both increasing with increasing mortar strengths. In this case however the M60 tests showed slightly higher flexural strengths.

In the bond strength tests, no net effect was seen on the bond strength with increasing joint thickness. However the bond strength was observed to increase with increasing mortar strength in both M60 and M95 tests. In terms of the effect of the different sand types, the M95 tests had higher bond strengths than the M60 tests.

The shear strength was found to decrease with increasing mortar bed thickness in the diagonal tensile strength test. In this case there was clear trend of decrease in shear strength with increasing joint thickness. The shear strength was also found to increase with increasing mortar strength in both M60 and M95 mortar tests. But in this case, the M60 tests gave higher shear strength values.

Overall, the results suggest that the effect of varying joint thickness is difficult to quantify at this scale while it is possible to see the effect of increasing mortar strength and different sand gradings.

Test Reference	Mortar Type	Joint thickness mm	Compressive Strength, N/mm^2	COV%	Stiffness N/mm^2	Mortar Cube Strength, N/mm^2
6C-A1-4	M95-iii	1.0	20.3	25.7	-	5.2
6C-B1-5	"	1.6	20.3	11.6	6000	4.7
6C-C1-4	"	2.5	20.1	8.9	-	5.2
6C-D1-4	M95-ii	1.6	22.6	4.6	9200	7.7
6C-E1-4	M95-iv	"	16.7	15.5	4600	1.7
6C-F1-4	M60-iii	"	18.0	13.6	-	7.3
6C-G1-4	M60-ii	"	19.5	7.7	-	9.9
6C-H1-4	M60-iv	"	15.3	23.8	-	1.8

Table 6.1- Summary of compressive strength test results.

Test Reference	Mortar Type	Joint thickness mm	Initial Shear Strength, N/mm^2	Co-efficient of Friction	Mortar Cube Strength, N/mm^2
6S-A1-12	M95-iii	1.0	0.35	0.78	3.6
6S-B1-12	"	1.6	0.60	0.85	5.5
6S-C1-12	"	2.5	0.34	0.65	3.6
6S-D1-12	M95-ii	1.6	0.58	0.65	6.1
6S-E1-12	M95-iv	"	0.24	0.65	2.0
6S-F1-9	M60-iii	"	0.19	1.16	4.7
6S-G1-12	M60-ii	"	0.55	1.27	6.4
6S-H1-9	M60-iv	"	0.16	1.15	1.7

Table 6.2- Summary of initial shear strength test results.

Test Reference	Mortar Type	Joint Thickness mm	Flexural Strength N/mm^2	COV %	Mortar Cube Strength, N/mm^2
6F-A1-5	M95-iii	1	1.13	44.3	5.5
6F-B1-5	"	1.6	1.24	31.6	4.8
6F-C1-5	"	2.5	0.99	18.0	5.0
6F-D1-5	M95-ii	1.6	1.76	13.9	6.2
6F-E1-5	M95-iv	"	0.88	13.6	1.4
6F-F1-5	M60-iii	"	1.34	18.1	4.1
6F-G1-5	M60-ii	"	1.89	16.9	7.0
6F-H1-5	M60-iv	"	0.74	7.9	1.5

Table 6.3- Summary of flexural strength parallel to bed joints test results.

Test Reference	Mortar Type	Joint Thickness mm	Flexural Strength N/mm^2	COV %	Mortar Cube Strength, N/mm^2
6F-I1-5	M95-iii	1	0.26	50.0	5.4
6F-J1-5	"	1.6	0.31	21.1	4.8
6F-K1-4	"	2.5	0.40	39.5	5.0
6F-L1-5	M95-ii	1.6	0.74	21.1	6.2
6F-M1-4	M95-iv	"	0.22	66.4	1.4
6F-N1-5	M60-iii	"	0.64	26.8	4.1
6F-O1-5	M60-ii	"	0.77	35.5	7.0
6F-P1-2	M60-iv	"	0.13	5.0	1.4

Table 6.4- Summary of flexural strength normal to bed joints test results.

Test Reference	Mortar Type	Joint Thickness mm	Bond Strength N/mm^2	COV %	Mortar Cube Strength, N/mm^2
6B-A1-8	M95-iii	1	0.93	25.7	5.1
6B-B1-7	"	1.6	0.73	28.1	3.6
6B-C1-8	"	2.5	0.88	35.5	5.1
6B-D1-7	M95-ii	1.6	0.89	24.3	5.2
6B-E1-8	M95-iv	"	0.57	34.0	2.0
6B-F1-7	M60-iii	"	0.48	30.7	4.4
6B-G1-7	M60-ii	"	1.04	12.5	7.7
6B-H1-8	M60-iv	"	0.50	20.2	1.7

Table 6.5- Summary of bond strength test results.

Test Reference	Mortar Type	Joint thickness mm	Shear Strength N/mm^2	COV %	Mortar Cube Strength, N/mm^2
6D-A1-4	M95-iii	1	0.94	22.6	5.1
6D-B1-4	"	1.6	0.63	7.2	4.1
6D-C1-4	"	2.5	0.67	18.5	5.4
6D-D1-4	M95-ii	1.6	0.92	26.3	6.7
6D-E1-5	M95-iv	"	0.40	39.0	1.6
6D-F1-5	M60-iii	"	1.02	26.2	4.4
6D-G1-5	M60-ii	"	1.21	13.5	9.8
6D-H1-4	M60-iv	"	0.44	11.0	2.0

Table 6.6- Summary of diagonal tensile (shear) strength test results.

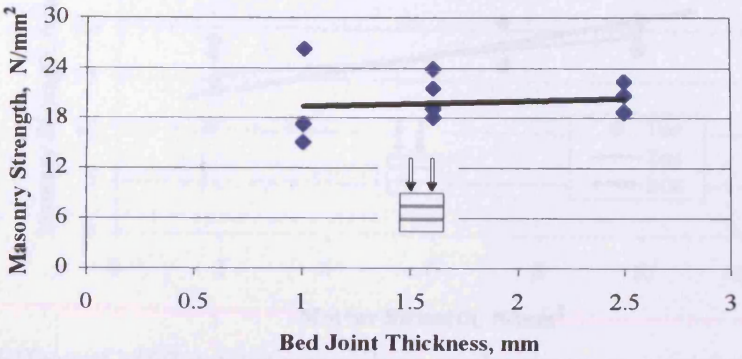

Figure 6.1- Effect of bed joint thickness on triplet masonry compressive strength.

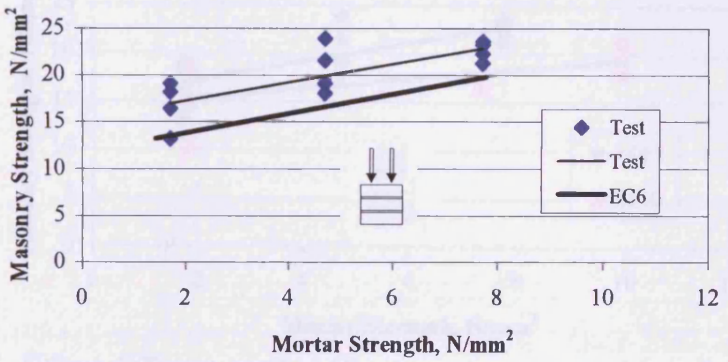

Figure 6.2- Effect of M95 mortar strength on triplet masonry compressive strength.

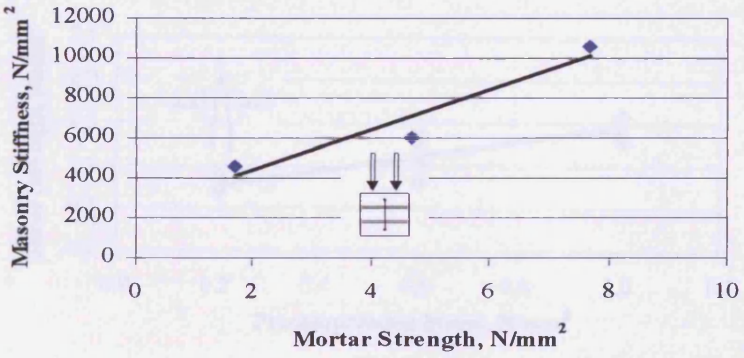

Figure 6.3- Variation of masonry stiffness with M95 mortar strength.

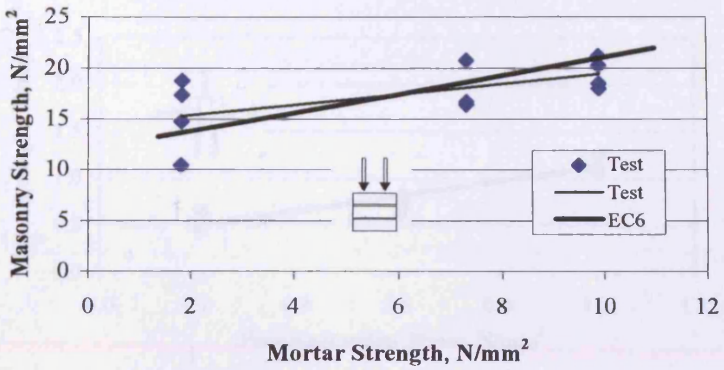

Figure 6.4- Effect of M60 mortar strength on triplet masonry compressive strength.

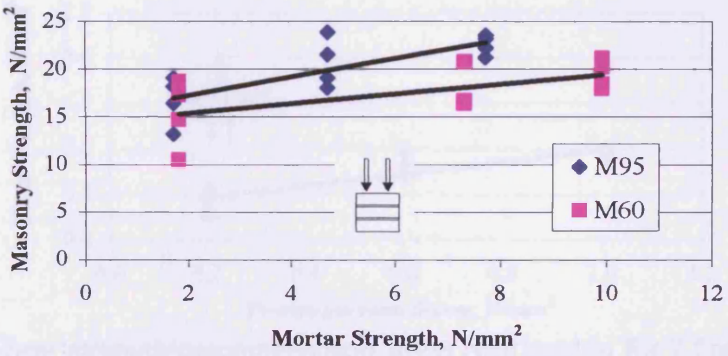

Figure 6.5- Effect different sand gradings on masonry compressive strength.

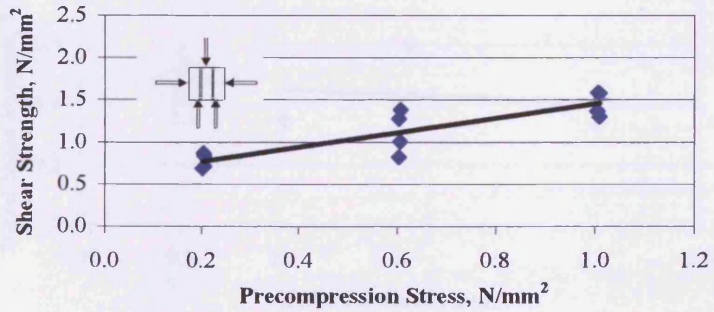

Figure 6.6- Shear strength/precompression stress relationship for benchmark test.

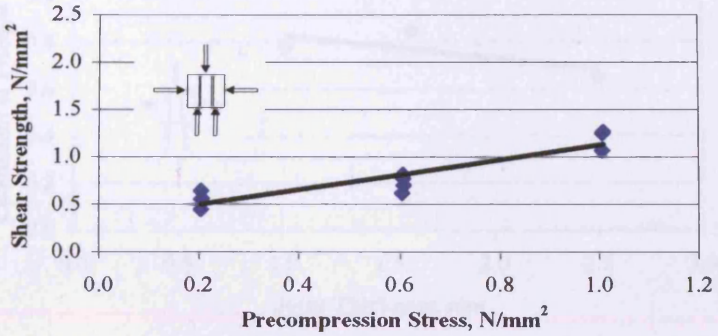

Figure 6.7- Shear strength/precompression stress relationship for 1mm bed joint test.

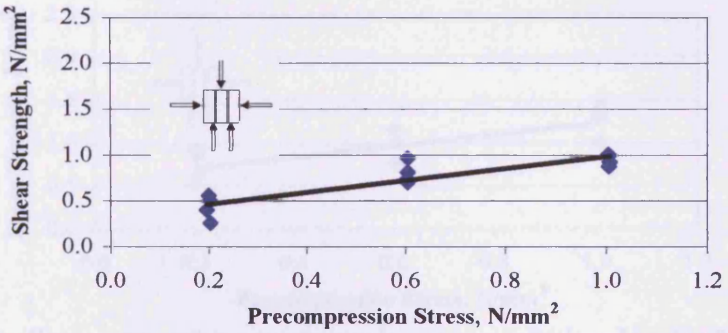

Figure 6.8- Shear strength/precompression stress relationship for 2.5mm bed joint test.

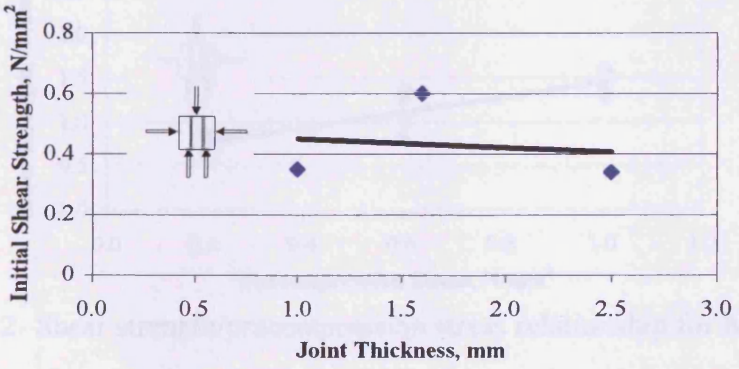

Figure 6.9- Variation of initial shear strength with joint thickness.

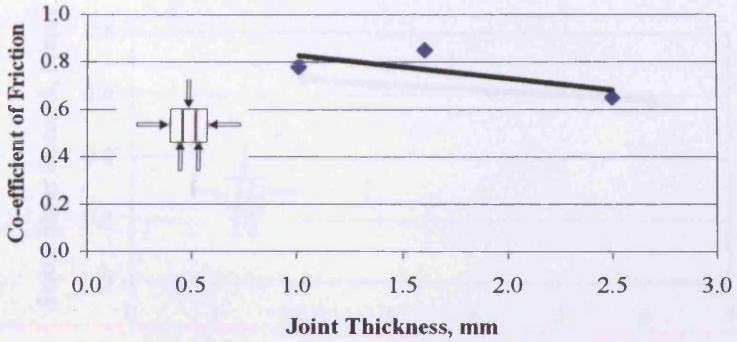

Figure 6.10- Variation of co-efficient of friction with joint thickness.

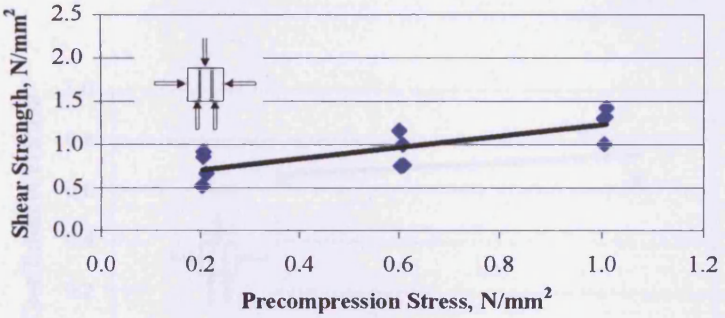

Figure 6.11- Shear strength/precompression stress relationship for M95ii test.

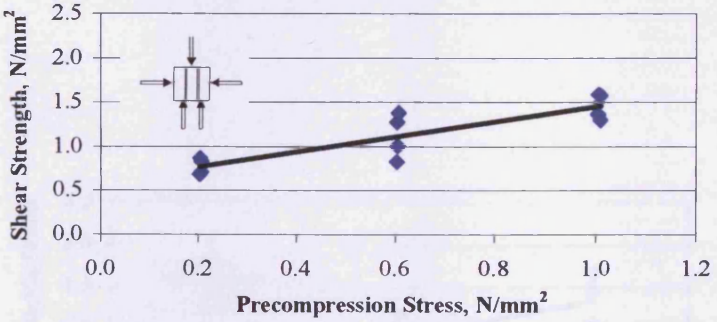

Figure 6.12- Shear strength/precompression stress relationship for M95iv test.

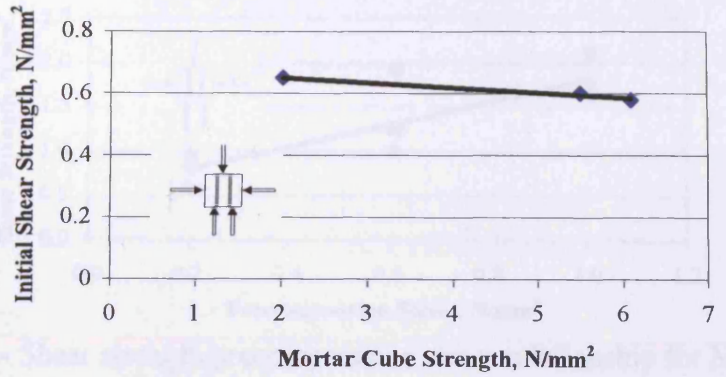

Figure 6.13- Variation of initial shear strength with M95 mortar strength.

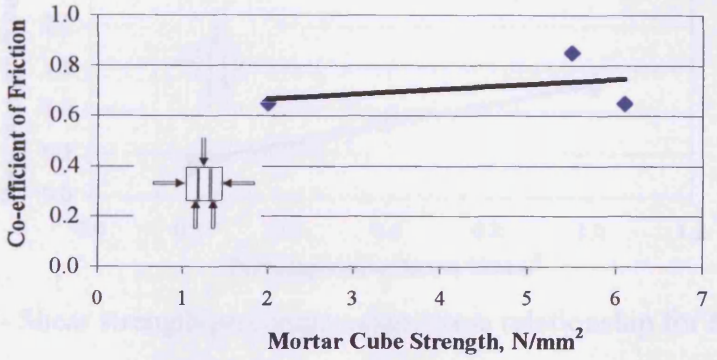

Figure 6.14- Variation of co-efficient of friction with M95 mortar strength.

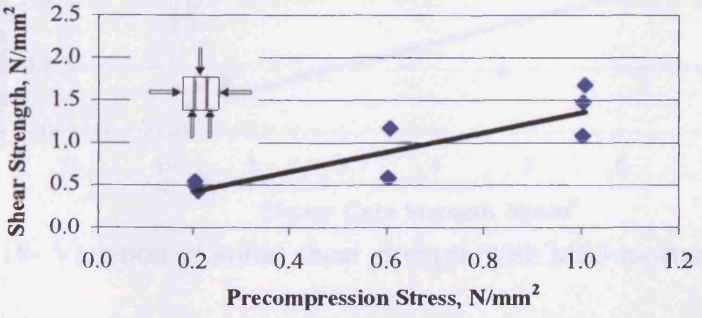

Figure 6.15- Shear strength/precompression stress relationship for M60iii test.

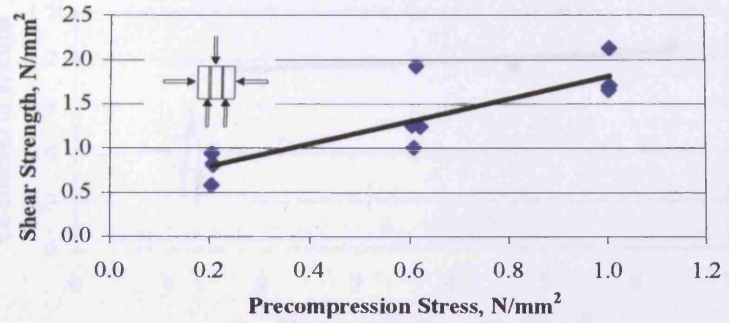

Figure 6.16- Shear strength/precompression stress relationship for M60ii test.

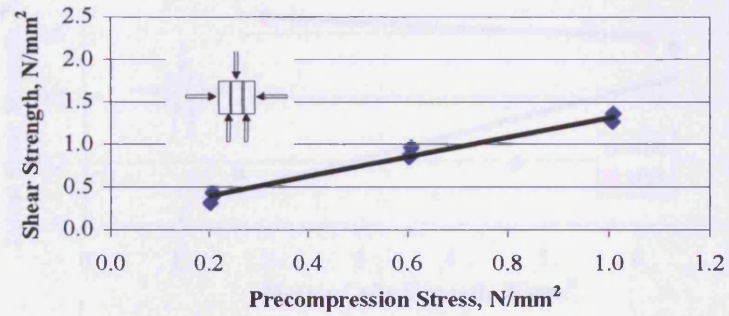

Figure 6.17- Shear strength/precompression stress relationship for M60iv test.

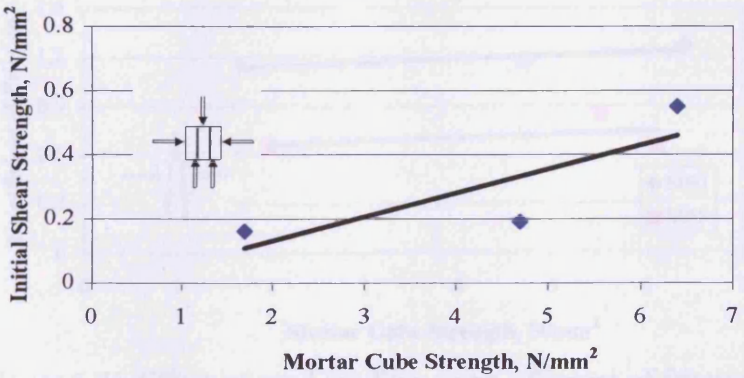

Figure 6.18- Variation of initial shear strength with M60 mortar strength.

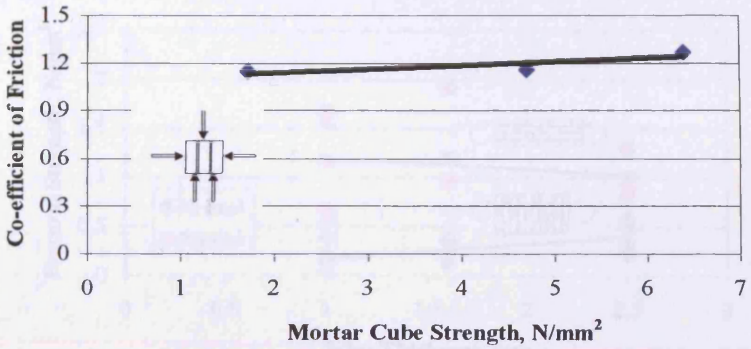

Figure 6.19- variation of co-efficient of friction with M60 mortar strength.

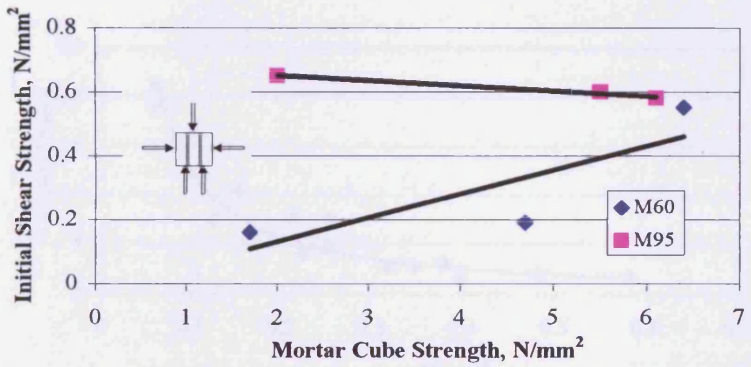

Figure 6.20- Effect of sand grading on initial shear strength.

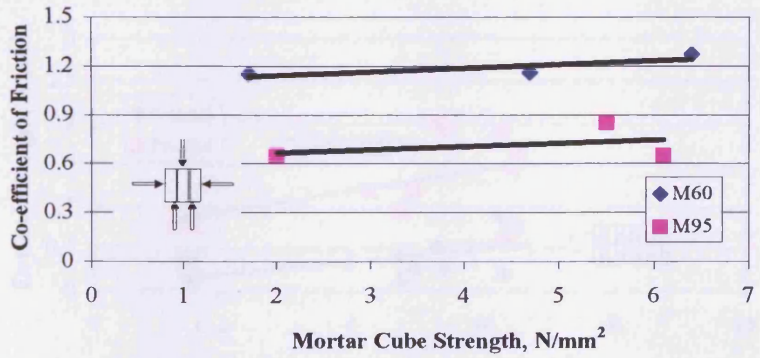

Figure 6.21-Effect of sand grading on co-efficient of friction.

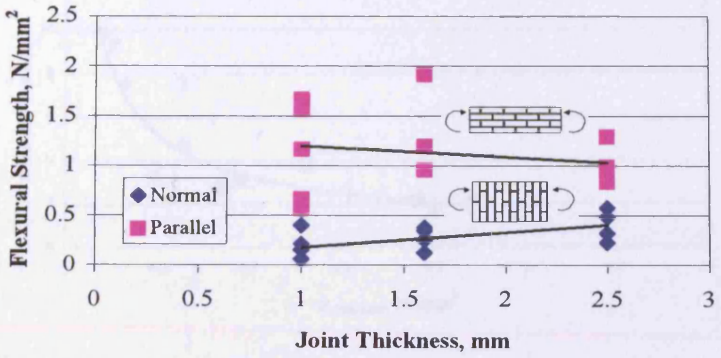

Figure 6.22- Effect of joint thickness on flexural strength.

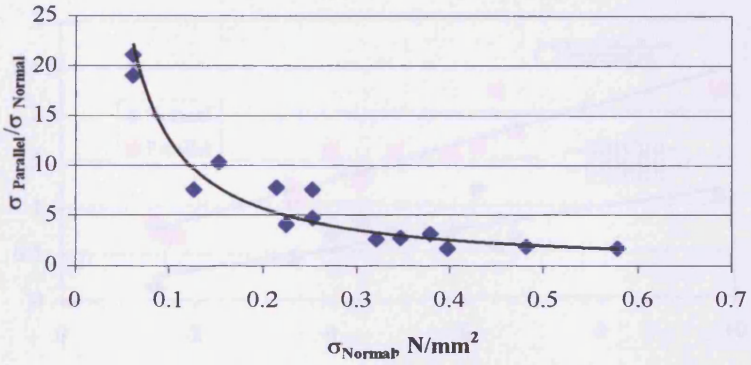

Figure 6.23- Ratio of moduli in orthogonal directions for different bed joints tests.

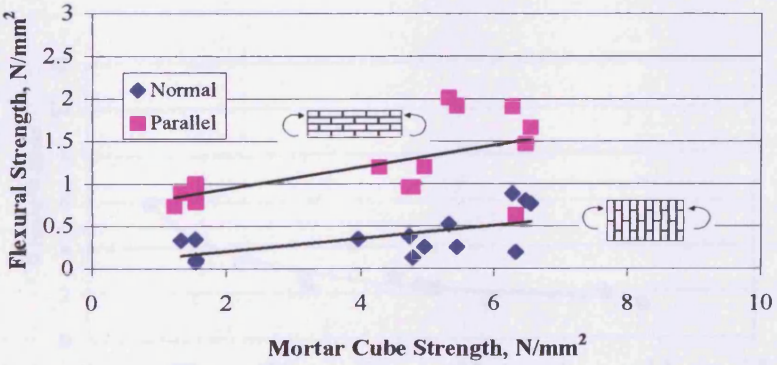

Figure 6.24- Effect of M95 mortar strength on flexural strength.

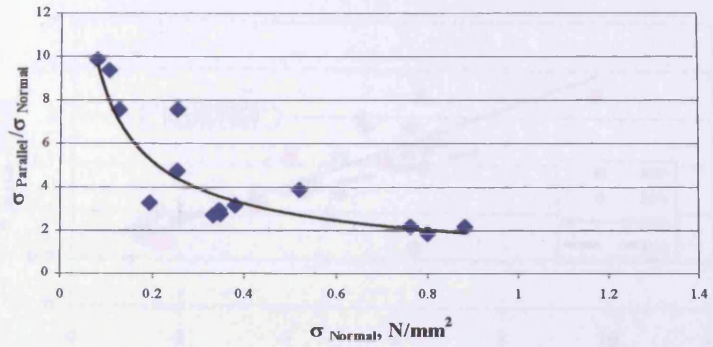

Figure 6.25 – Ratio of moduli in orthogonal directions for M95 mortar test.

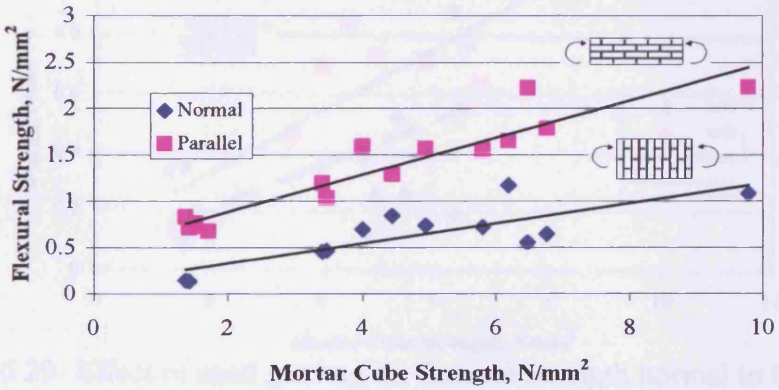

Figure 6.26- Effect of M60 mortar strength on flexural strength.

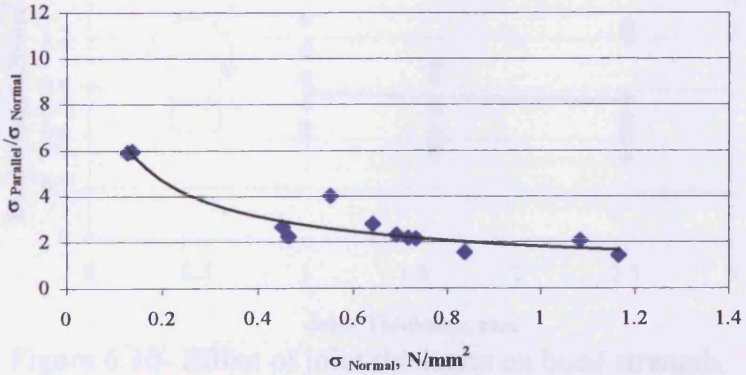

Figure 6.27- Ratio of moduli in orthogonal directions for M60 tests.

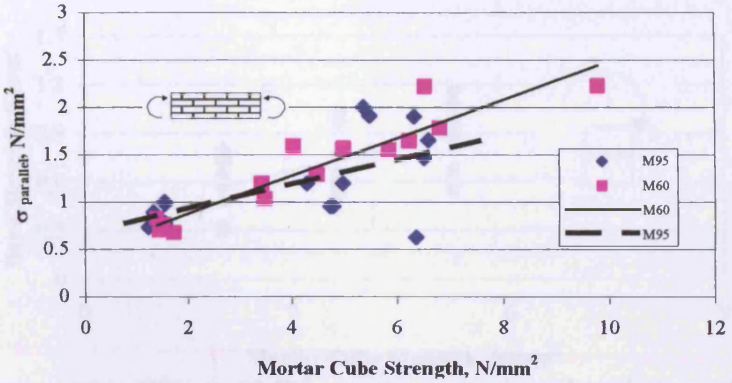

Figure 6.28- Effect of sand grading on flexural strength parallel to bed joint.

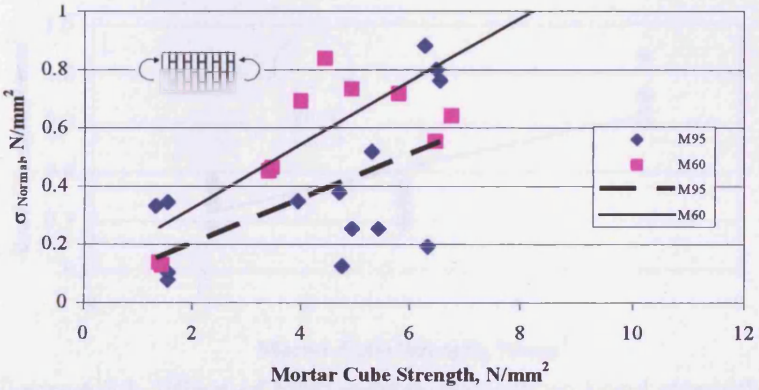

Figure 6.29- Effect of sand grading on flexural strength normal to bed joint.

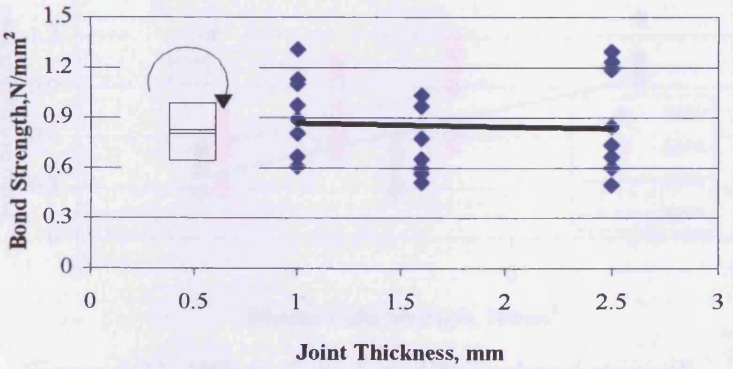

Figure 6.30- Effect of joint thickness on bond strength.

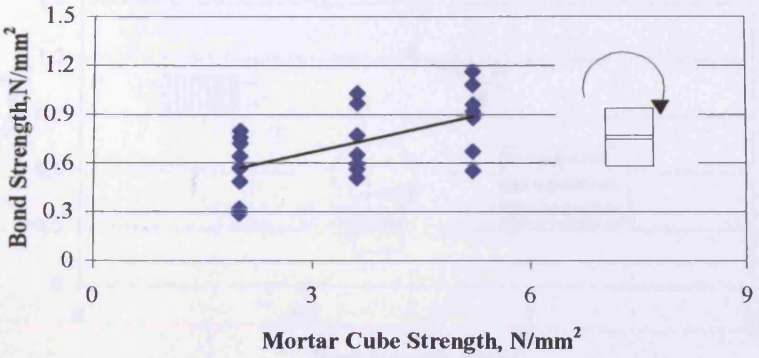

Figure 6.31- Effect of M95 mortar strength on bond strength.

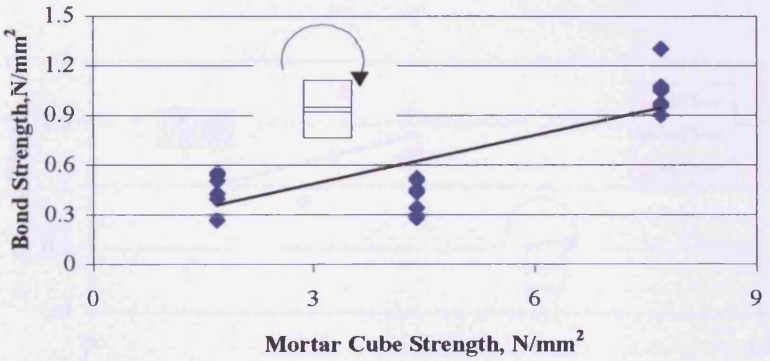

Figure 6.32- Effect of M60 mortar strength on bond strength.

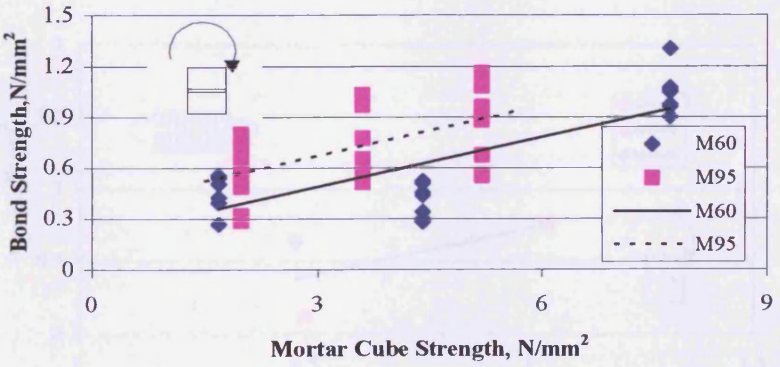

Figure 6.33- Effect of sand grading on bond strength.

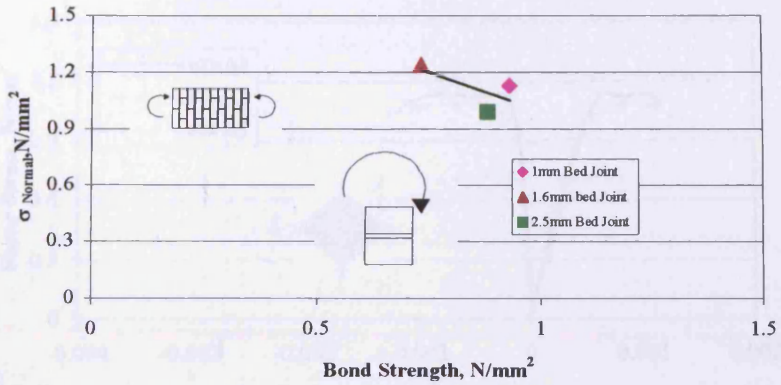

Figure 6.34- Effect of joint thickness on flexural strength/bond strength relationship.

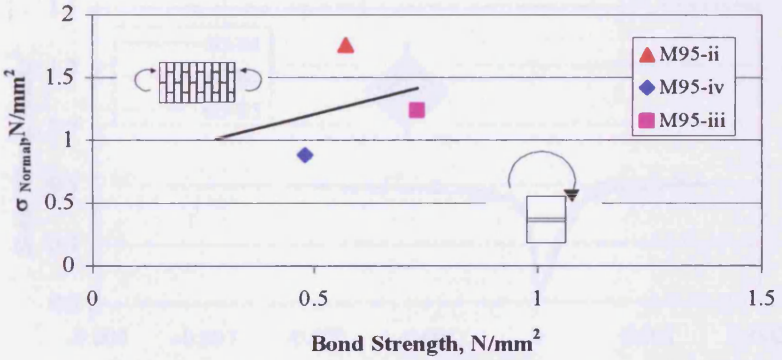

Figure 6.35- Effect of M95 mortar on flexural strength/bond strength.

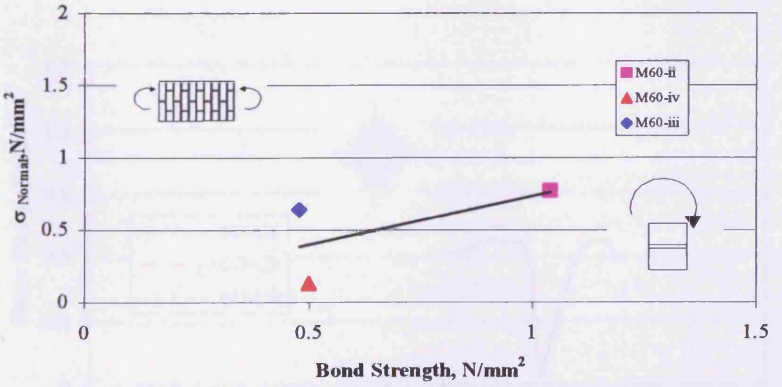

Figure 6.36- Effect of M60 mortar on flexural strength/bond strength.

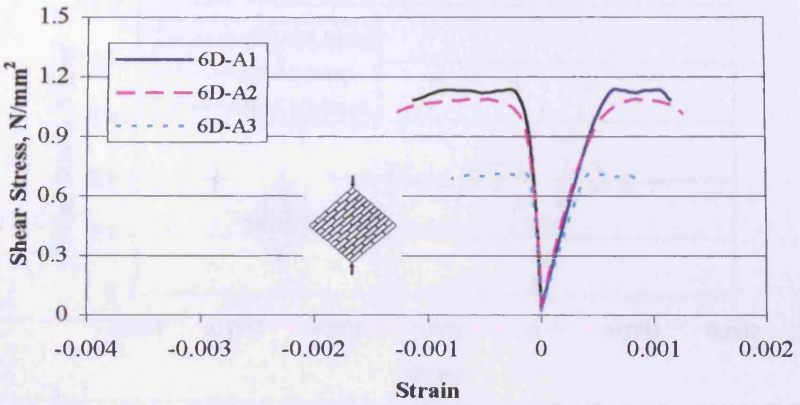

Figure 6.37- Summary of shear stress/strain curves for diagonal tensile strength 1mm joint test.

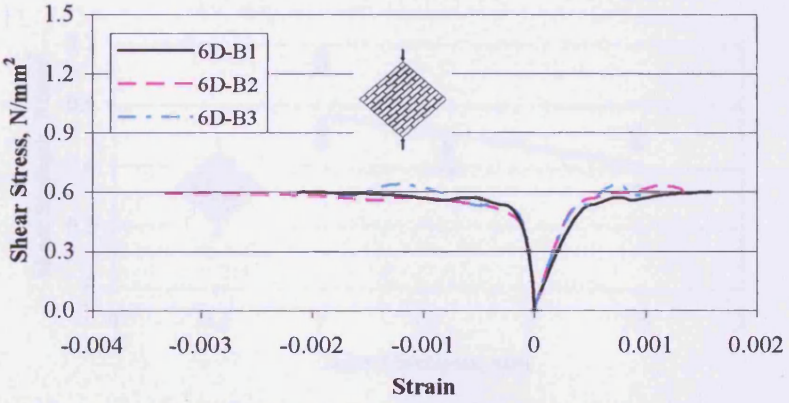

Figure 6.38- Summary of shear stress/strain curves for diagonal tensile strength benchmark test.

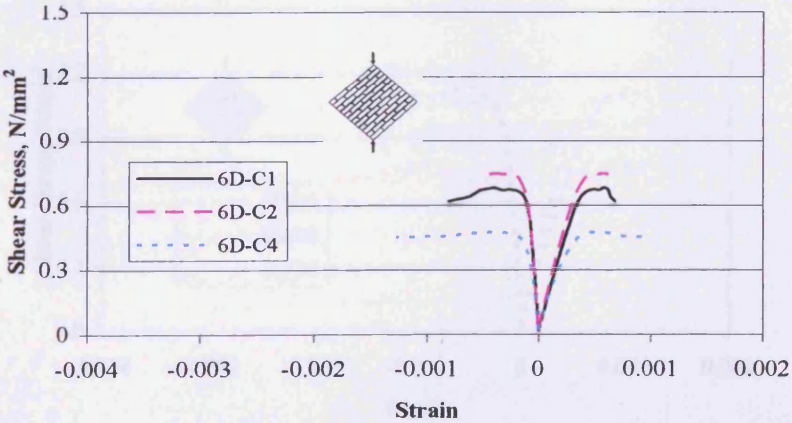

Figure 6.39- Summary of shear stress/strain curves for diagonal tensile strength 2.5mm joint test.

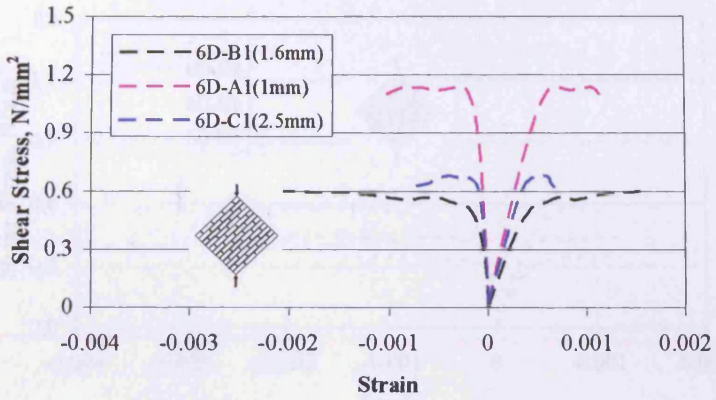

Figure 6.40- Shear stress/strain comparison for effect of joint thickness.

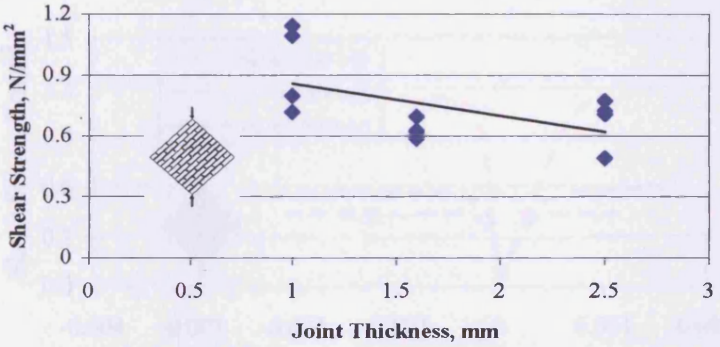

Figure 6.41- Effect of joint thickness on shear strength.

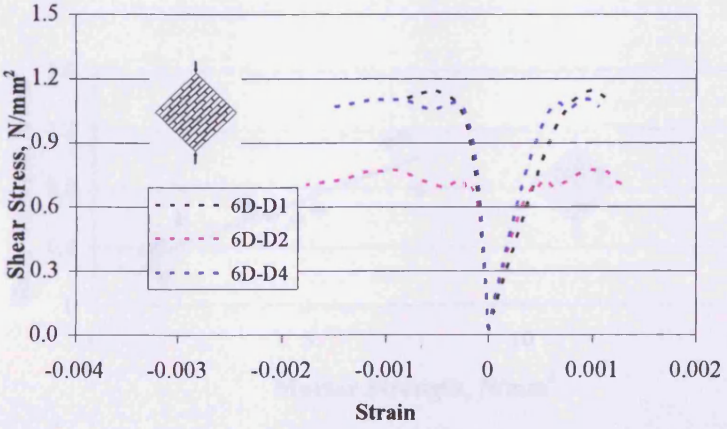

Figure 6.42- Summary of shear stress/strain curves for diagonal tensile strength M95-ii test.

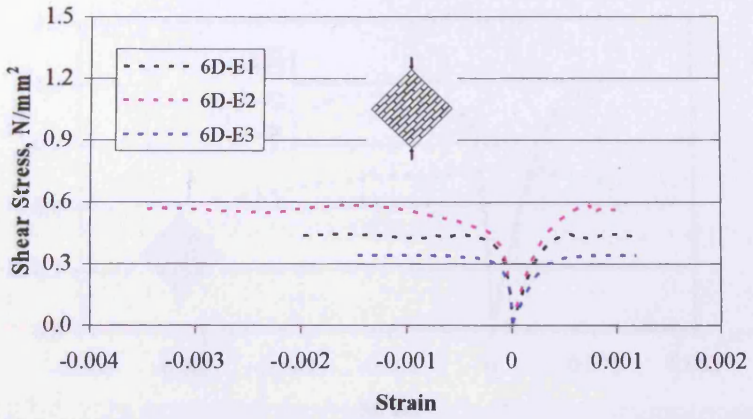

Figure 6.43- Summary of shear stress/strain curves for diagonal tensile strength M95-iv test.

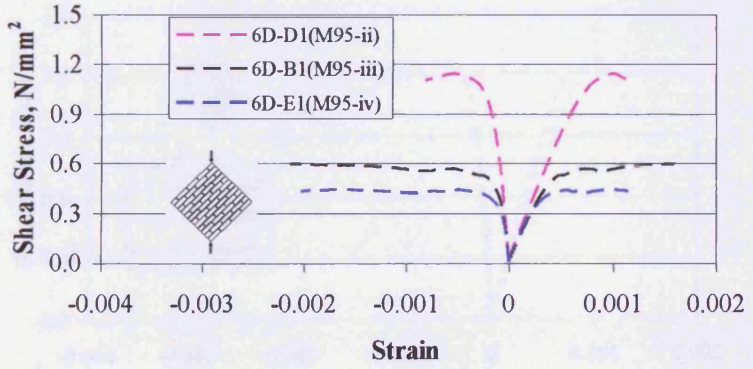

Figure 6.44- Comparison of shear stress/strain curves for the effect of varying grades of M95 mortar.

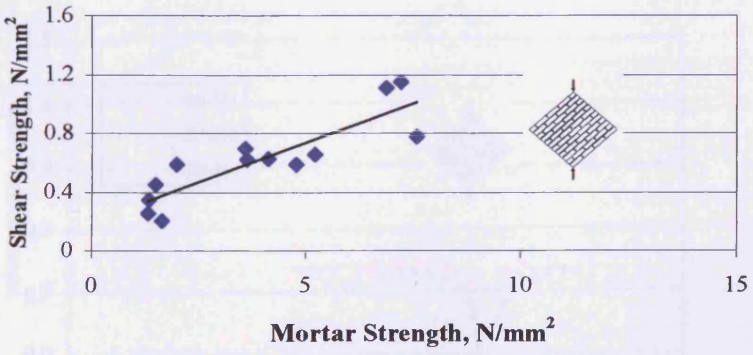

Figure 6.45- Effect of increasing M95 mortar strength on shear strength.

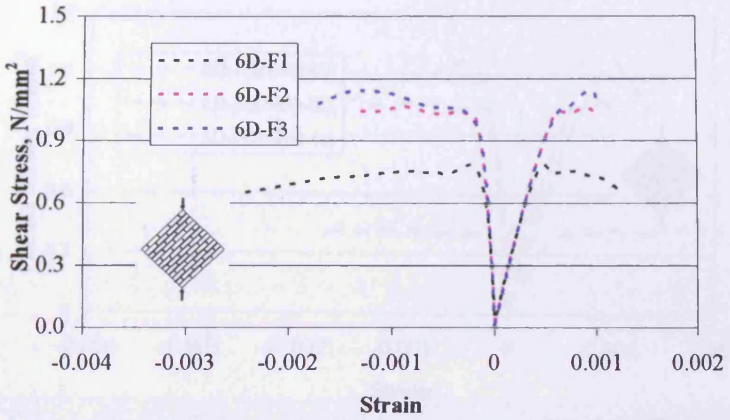

Figure 6.46- Summary of shear stress/strain curves for diagonal tensile strength M60-iii test.

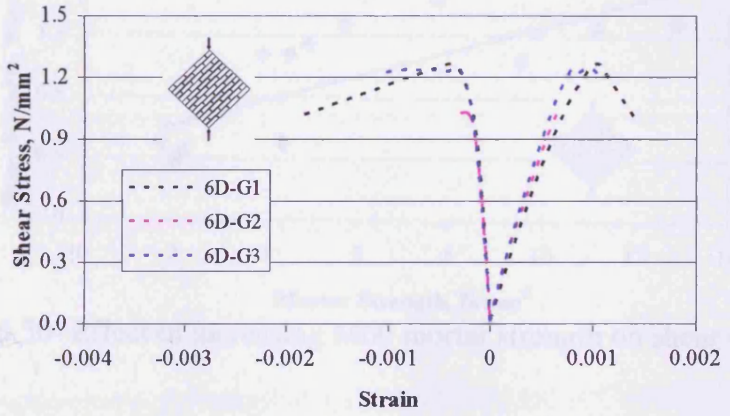

Figure 6.47- Summary of shear stress/strain curves for diagonal tensile strength M60-ii test.

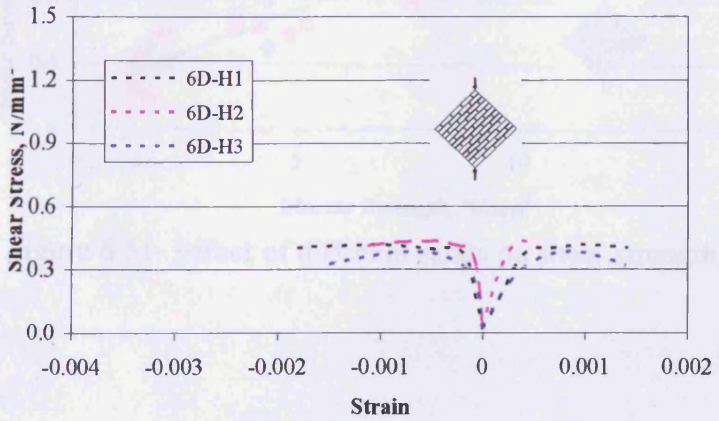

Figure 6.48- Summary of shear stress/strain curves for diagonal tensile strength M60-iv test.

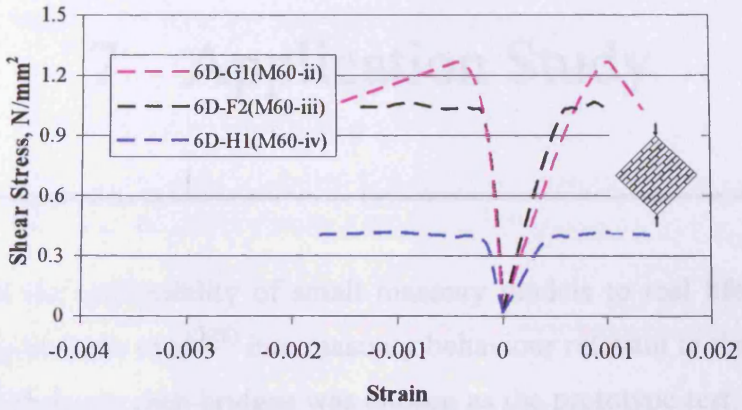

Figure 6.49- Comparison of shear stress/strain curves for the effect of varying M60 mortar grades.

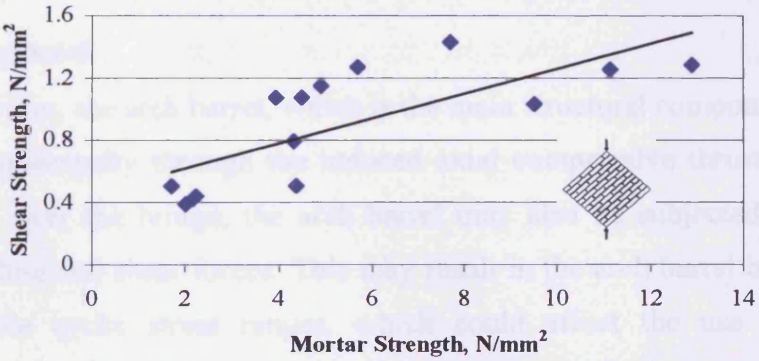

Figure 6.50- Effect of increasing M60 mortar strength on shear strength.

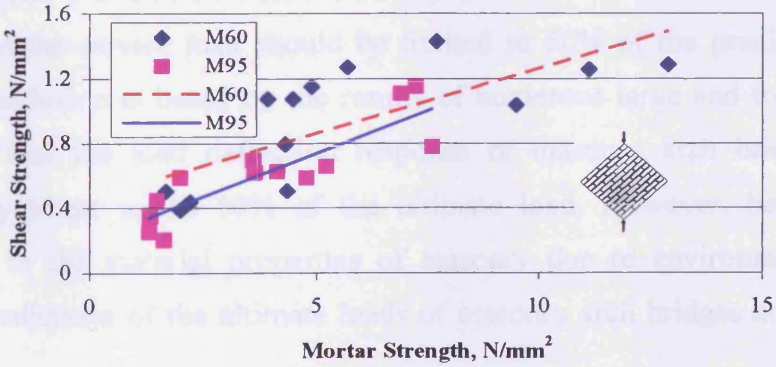

Figure 6.51- Effect of different sands on shear strength.

7 Application Study

In order to test the applicability of small masonry models to real life problems, an investigation by Roberts et al[128] into masonry behaviour relevant to the serviceability requirement of masonry arch bridges was chosen as the prototype test. The prototype test involved the testing of various arrangements of specimens in dynamic and static loading.

7.1 Background

In masonry arches, the arch barrel, which is the main structural component, carries the applied load principally through the induced axial compressive thrust. However, as traffic moves over the bridge, the arch barrel may also be subjected to significant reversed bending and shear forces. This may result in the arch barrel being subjected to considerable cyclic stress ranges, which could affect the use of the bridge adversely[129].

Recently there has been interest in the establishment of serviceability limits for masonry bridges, BD 21/97[130] and Boothby et al[131]. In BD 21/97 (1997), it is suggested that the service load should be limited to 50% of the predicted ultimate load. This conclusion is based on the results of numerous large and full scale tests, which show that the load deflection response of masonry arch bridges remains approximately linear up to 50% of the ultimate load. However, because of the uncertainties in the material properties of masonry due to environmental effects, theoretical predictions of the ultimate loads of masonry arch bridges are usually not reliable[129].

In masonry arches the compressive force will generally be eccentric and in approaching failure, the force on some units will be highly eccentric and these forces will generally be concentrated on a small part of the surface area of the unit and form a so called hinge[132]. Various prototype studies[133, 134] have shown that the compressive stress at failure under eccentric loading is greater than under axial loading and further enhancement to the apparent compressive strength have been

established under highly concentrated loads by other studies[132, 135]. Therefore the main objective of the application study was to investigate the effect of eccentric concentrated loading on sixth scale masonry with a view to comparing it to the prototype study by using static tests as a tool for the understanding of the overall behaviour of masonry arches.

7.2 Masonry specimens

Only representative masonry specimens were considered in the study, this corresponded to parts of an arch ring in a complete masonry arch. For the purpose of this study a five unit high, sixth scale masonry specimen as shown in Figure 7.1 was used. All the quality control and preparation procedures were as described for the sixth scale model tests in Chapter 3 but using two mortar designations; designation iv and designation v. These were weak mortars to better conform to existing old structures. The proportions of the constituent elements used in the mortar are as given in BS 5628[95] and the dry mass proportions in BS 4551[96] were used and are shown in Table 7.1. All mortars were made using HST 95 sand. All the specimens were allowed to cure normally in the laboratory after preparation and tested at or shortly after 28 days of curing.

Other specimen formats were also used in the original study[128], but for the purpose of the application study, only the five unit high stack bonded specimen was used. This was because the objective was to see if it was feasible to conduct such tests at sixth scale.

7.3 Testing

Testing was carried in a 20kN capacity testing machine under constant rate of displacement of 0.25mm/min. Load was applied via an arrangement of 6mm steel plates and 6mm steel bars as shown in Plate in 7.1. The specimens were also supported on similar arrangement of plates and bars as used in applying the loads in order to ensure uniform eccentricity from the centre of the specimens. Loads were applied at four eccentricities of 0, 5, 9, and 14mm from the centre of the specimens. This corresponds to e/d ratios of 0, 0.14, 0.25, and 0.39, where e is the eccentricity of the load and d the length of the transverse section of the specimens as defined in Figure 7.1.

7.4 Stress calculations

The assumed stress blocks used in calculations are shown in Figure 7.2. For concentric and eccentric loading within the middle third of the section the stress distribution is as shown in Figure 7.2 (a). In this case the maximum compressive stress f_m is given by Equation 7.1

$$f_m = \frac{P}{bd} + \frac{6Pe}{bd^2} \tag{7.1}$$

Where P is the applied compressive force and bd is the loaded cross-section area (width x depth)

When the eccentricity of load is beyond the middle third of the cross-section the cracked triangular stress block in Figure 7.2 (b) was assumed. For this distribution, equilibrium of external and internal forces entails that Equations 7.2 and 7.3 applies

$$\frac{f_m bh}{2} = P \tag{7.2}$$

$$\frac{f_m bh}{2}\left[\frac{d}{2} - \frac{h}{3}\right] = Pe \tag{7.3}$$

Substituting for P in (7.3) gives Equations 7.4 and 7.5

$$h = 3\left[\frac{d}{2} - e\right] \tag{7.4}$$

$$f_m = \frac{2P}{bh} \tag{7.5}$$

The cracked triangular no tension distribution was chosen for this solution because it gave an upper bound solution rather than the cracked parabolic no tension distribution (not presented here).

7.5 Discussion of results

In the prototype test failure of the specimens was initiated by crushing and squeezing of the mortar from the mortar joints followed by vertical splitting of the bricks as shown in Plate 7.2.

Figure 7.3 and 7.4 show the variation of compressive strength with load eccentricity for mortar designation v. Both of the figures show that the compressive strength is increased as the eccentricity is increases in line with findings by most authors, notably Page and Hendry[136] who have even suggested design rules for concentrated loads with varying eccentricities on masonry . The reason for the enhancement as suggested by Drysdale and Hamid[133] is due to the strain gradient effect on the compressive strength. They argued that the gradient of vertical compression strain across a brick due to eccentricity of load will be accompanied by a corresponding tensile strain gradient in the lateral direction. But because the tensile strength of masonry units are affected by strain gradient (as shown by the greater flexural tensile strength in comparison to the direct axial tensile strength), they concluded that the apparent compressive strength should be higher for eccentrically loaded brickwork.

Typical failure of the specimens in the model study was usually characterised by vertical splitting cracks under the load point as well as at the sides of the specimens. This was followed by crushing of the loaded point in some cases. Plate 7.3 shows a typical failure in one of the tests. In the case of the specimens with e/d of 0.39 there were cases in which tension debonding was noticeable at the edge furthest from the load point just before failure, in specimens made with both designation iv and designation v mortar. Plate 7.4 shows the debonding on the tensile side in one of the tests. This type of failure represents an elastic instability characterised by debonding on the tensile side for loads with high eccentricity according Sahlin[11].

The results as tabulated in Tables 7.2 and 7.3 for tests using mortar designations iv (test; S4) and v (test; S5) show a mixed picture as seen in Figures 7.5 and 7.6, which show the variation of maximum compressive strength with e/d ratio for tests using mortar designations iv and v, respectively. In Figure 7.5, it is seen that there is an initial increase in strength from the point of zero eccentricity to point e/d = 0.14. Followed by a decrease in strength from this point up to the last point e/d = 0.39. While in Figure 7.6, there is an increase in strength from the point of zero eccentricity up to the point e/d = 0.25 before decreasing at the last point e/d = 0.39. Therefore, as seen from the trend lines in both figures there is only a marginal increase in compressive strength as the eccentricity is increased for the eccentricities considered (neglecting e/d = 0.39). But the actual compressive strength in the model tests was

higher because of the higher model unit compressive strength, which is about 57% higher than the prototype unit strength.

Figure 7.7 shows a comparison of the effect of eccentricity in the prototype and model scale for the same mortar type. The vertical axis has been made dimensionless by normalising it with respect to their (both prototype and model) respective compressive strengths at zero eccentricity. It is seen from the figure that the fitted trend line for the prototype test is significantly steeper than that for the model test. The ratio of their gradients is 5.4 which is nearly equal to their scale ratio. From the foregoing it therefore seems that in the S4 model test for e/d ratios of 0.25 and 0.39 (outside the middle third of the section), the expected enhancement in compressive strength is not seen while in the S5 model test strength enhancement does not hold for the e/d of 0.39. However since in the prototype tests the highest eccentricity used was 0.33 it can still be argued that there is some agreement of the S5 test to the prototype test since there is strength increase with load eccentricity within their comparable range of eccentricities. The reason for the greater enhancement in the prototype over the model scale is not certain, but it could to be due to the elastic instability characterised by the cracking on the tension side of the model specimens before material failure in the units. But since the geometries of the test specimens and load eccentricities for the prototype and model tests are similar, the expectation was for a comparable enhancement factor in the model test. It therefore seems that there is better agreement between the failure mechanics of prototype and model specimens in axial compression than in eccentric loading. This may be because it is difficult to model mortar at very small scales because of the thinness of the joints. Because as we have seen in Chapter 6 effects with regards to joint thickness are difficult to model at sixth scale. The reason for this is not certain but it offers a possible area of further investigation in the future.

7.6 Conclusions

The application study somewhat agrees with the prototype study for low eccentricities therefore, strength enhancement is seen over the concentric compressive strength. However this does not apply at higher eccentricities as specimens were noticed to fail by elastic instability characterised by tension debonding of the top mortar joint.

Mortar Type	Proportions Cement:lime:sand	W/c ratio
iv	I:2:9	2.50
v	I:1.5:13	3.12

Table 7.1- Mortar proportions

Test Reference	e/d	Load, N	Masonry Strength,N/mm^2	Mean, N/mm^2	Mortar Strength,Nmm^2
S4-A1	0	9812	16.0		
S4-A2	0	8153	13.3		
S4-A3	0	6745	11.0		
S4-A4	0	6573	10.7		
S4-A5	0	8860	14.5	13.1(17.2)	1.7
S4-B1	0.14	4813	14.4		
S4-B2	0.14	6142	18.4		
S4-B3	0.14	7105	21.3		
S4-B4	0.14	5973	17.9		
S4-B5	0.14	5873	17.6		
S4-B6	0.14	6563	19.7	18.2(12.6)	3.0
S4-C1	0.25	3860	16.9		
S4-C2	0.25	4298	18.8		
S4-C3	0.25	3343	14.6		
S4-C4	0.25	4421	19.4		
S4-C5	0.25	4022	17.6		
S4-C6	0.25	2830	12.4	16.6(16.0)	1.9
S4-D1	0.39	1565	15.6		
S4-D2	0.39	1028	10.3		
S4-D3	0.39	1284	12.8		
S4-D4	0.39	1589	15.9		
S4-D5	0.39	1327	13.3		
S4-D6	0.39	1229	12.3	13.4(15.9)	2.1

Table 7.2 – Test results for specimens made with designation iv mortar, S4, with COV in brackets

Test Reference	e/d	Load, N	Masonry Strength,N/mm^2	Mean, N/mm^2	Mortar Strength,Nmm^2
S5-A1	0	7811	12.8		
S5-A2	0	6361	10.4		
S5-A3	0	8720	14.2		
S5-A4	0	8720	14.2		
S5-A5	0	5780	9.4		
S5-A6	0	7516	12.3	12.2(16.2)	1.1
S5-B1	0.14	7521	12.3		
S5-B2	0.14	4600	13.8		
S5-B3	0.14	4990	15.0		
S5-B4	0.14	5259	15.8		
S5-B5	0.14	6012	18.0		
S5-B6	0.14	2822	8.5	13.9(23.7)	0.9
S5-C1	0.25	3784	16.6		
S5-C2	0.25	3276	14.3		
S5-C3	0.25	2282	10.0		
S5-C4	0.25	3535	15.5		
S5-C5	0.25	2240	9.8		
S5-C6	0.25	5145	22.5	14.8(32.0)	0.8
S5-D1	0.39	1168	11.7		
S5-D2	0.39	638	6.4		
S5-D3	0.39	1643	16.4		
S5-D4	0.39	879	8.8		
S5-D5	0.39	708	7.1	10.1(40.7)	1.1

Table 7.3- Test results for specimens made with designation v mortar, S5, with COV in brackets

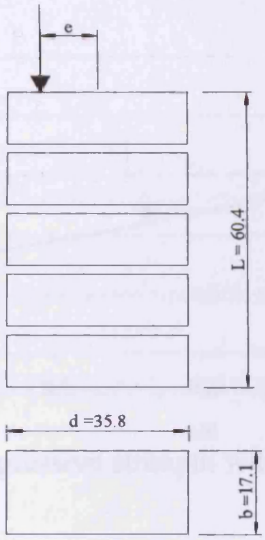

Figure 7.1- Dimensions of specimens in mm.

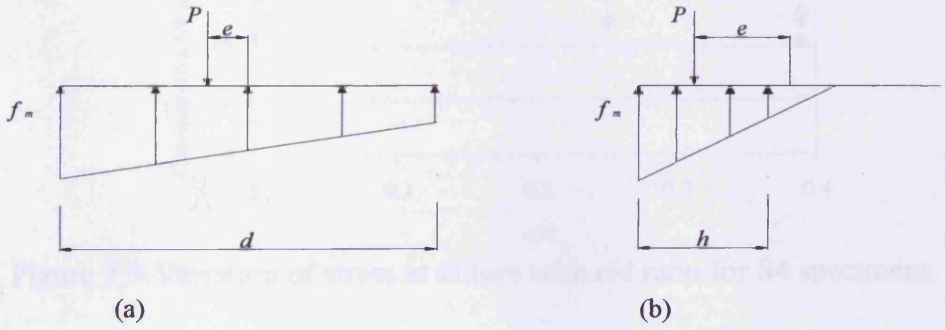

(a) (b)

Figure 7.2- Assumed stress distributions for eccentric loading (a) no tension (b) linear cracked.

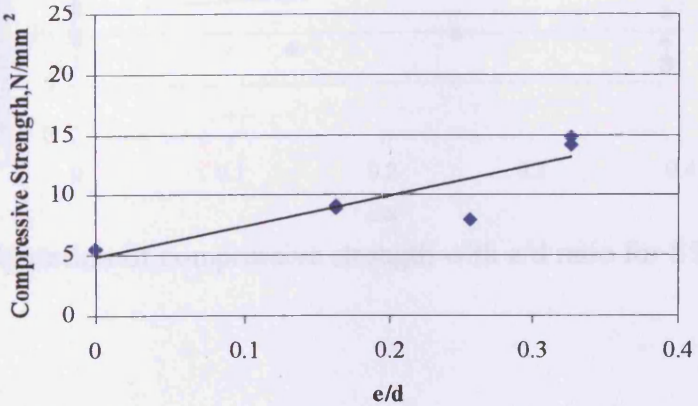

Figure 7.3-Variation of compressive strength with e/d ratio for prototype test 1

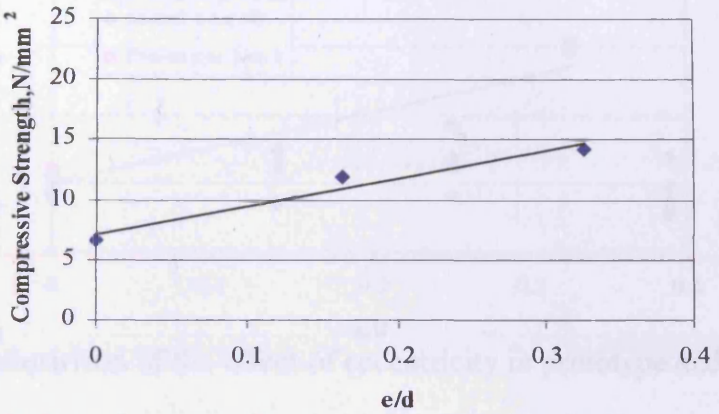

Figure 7.4-Variation of compressive strength with e/d ratio for prototype test 2.

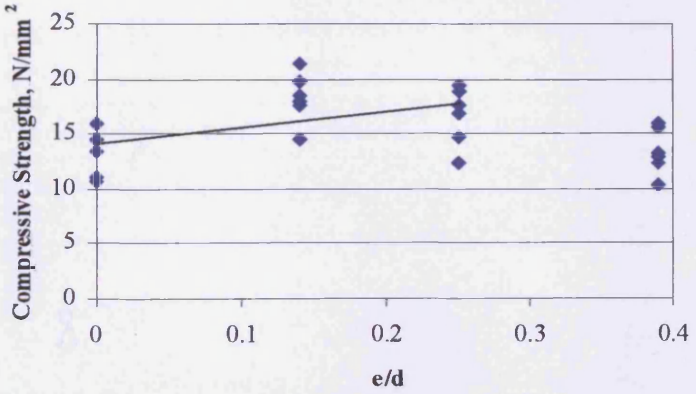

Figure 7.5-Variation of stress at failure with e/d ratio for S4 specimens.

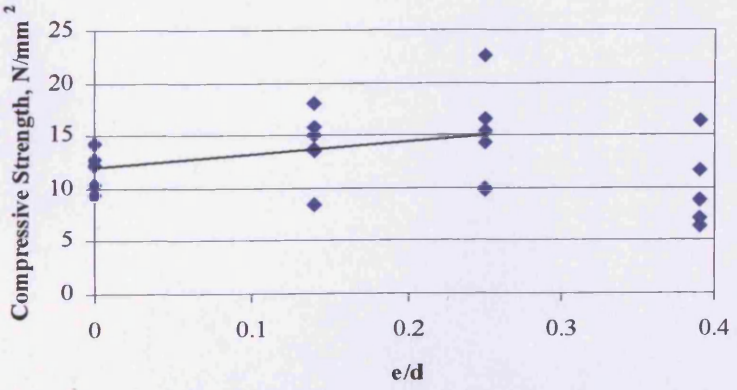

Figure 7.6- Variation of compressive strength with e/d ratio for S5 specimens.

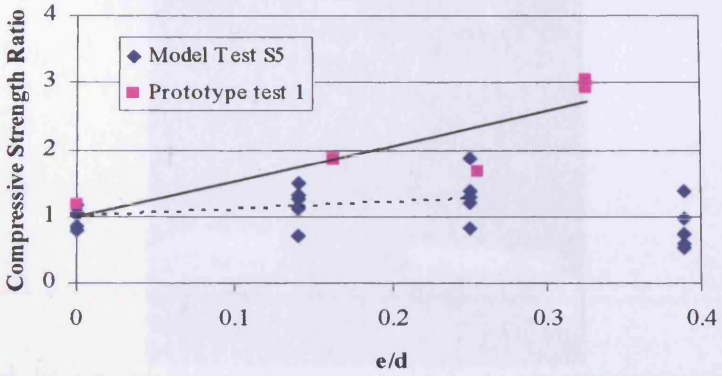

Figure 7.7- Comparison of the effect of eccentricity in prototype and model test.

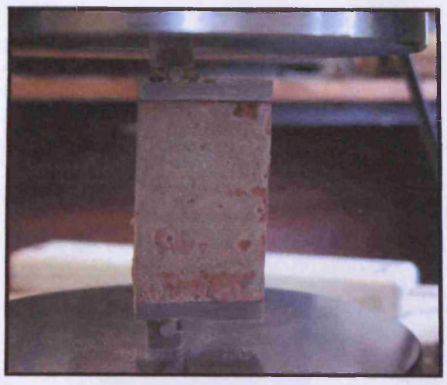

Plate 7.1- Set up of model test at an eccentricity of 0.25.

Plate 7.2- Typical failure pattern in prototype tests.

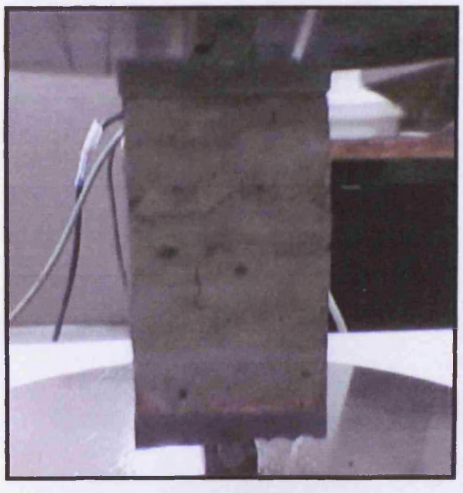

Plate 7.3 - Typical failure pattern in model tests.

Plate 7.4- Bond failure in top bed joint of model specimen at e/d of 0.39.

8 Conclusions and Recommendations

8.1 Conclusions

A programme of tests has been undertaken at various scales and under various loading conditions in order to understand the structural behaviour of model masonry by testing small masonry components with a view to determining the overall structural behaviour of real masonry structures. Firstly, various standard tests were considered on masonry at different scales, with a view to understanding masonry behaviour across the scales considered. Secondly a parametric study of some factors the affect masonry behaviour at model scale was considered at sixth scale. And finally an application study was undertaken at model scale in order to compare the results to a prototype study.

The tests have shown that model scale tests can be carried out in a repeatable manner using sawn model bricks from the prototype. And some agreement of prototype and model behaviour has been established.

In the compressive strength test, it was found that the masonry strength was primarily influenced by the unit compressive strength. And generally the unit compressive strength in the smallest model scales were higher than in the larger scales, resulting in higher masonry strength in the smallest scales. There was evidence of anisotropy of strength in clay brick masonry possibly due to the manufacturing process of extruded clay units which consequently makes the direction of loading on a cut model brick a significant factor.

Therefore the increase in the unit compressive strength in the smallest model scales could be due to strength anisotropy and or the energetic size effect in quasi-brittle materials like brick masonry. The compressive strength test data was also found to closely follow the size effect laws of fracture mechanics (MFSL and SEL).

The stiffness of the triplet specimens in the compressive strength in the four scales test, were similar to each other and no scale effect was observed. The prototype masonry and model stiffness were in good agreement with the prototype and model mortar stiffness respectively. This could due to the way the masonry specimens were

constructed, which has effectively negated any differential compaction of the joints due to the different weight of the unit in the four scales. The good agreement of the masonry stiffness in the four scales is significant because tests by other researchers showed a much softer model response to the prototype under uniaxial compression.

In all other masonry tests; shear strength, flexural strength, bond strength, and diagonal shear strength tests, no significant size effect was observed in the tests. This may be because in most of the tests, joint failure dominates, and because of the way the specimens were constructed, the scale effects were effectively cancelled. Another stronger reason could be that the general scale of the tests was in size range where the strength criterion applies which implies a zero size effect. The size effect laws were also found to be applicable to the data from all the tests which suggest a strong reason for the incorporation of size effect formulae in design codes to aid designers in predicting strengths of real structures from laboratory specimens.

In the parametric tests conducted at sixth scale to look at the effect of some factors on the strength of masonry, some of the more important findings were;

No noticeable effect was seen with regards to increasing mortar joint thickness in the compressive strength test, initial shear strength test, bond strength test and the flexural strength test, but there was a decrease in the shear strength as the joint thickness was increased in the diagonal shear strength test. Therefore it could be argued that different joint thicknesses do not significantly affect the strength of model masonry.

However, increasing mortar strength was found to increase the masonry strength in all the five tests and for both types of sands. The effect of the different sand gradings for the tests having mortar with finer grading of sand mainly resulted in a higher masonry strength in the compressive strength test, initial shear strength test and the bond strength test but slightly lower masonry strength in the flexural strength and diagonal tensile strength tests. Because of this mixed picture it is difficult to give a definite effect of the sand grading on all the tests, perhaps the effect of sand grading is different for the various tests.

In the application study, there was some agreement in the results for the comparable range of eccentricities in the prototype and model tests however the effect of eccentricity was far more significant in the prototype test by a factor of 5.4 which

happens to be somewhat close to the scale factor of 6, between the prototype and sixth scale model. Most prototype studies in this area have reported a marked increase in masonry strength with increasing eccentricity. This could be due to the model masonry developing high tensile stresses that could have resulted in an elastic instability before failure in the units. This may explain the observed bond failure in some specimens while there were no visible cracks in the units, in tests with the highest load to eccentricity ratios.

Overall the study has shown it is possible to model prototype behaviour at model scales of down to one sixth scale. And, that apart from the compressive strength of masonry which could be influenced by the energetic scale effect or anisotropy of units, all other tested strength properties, namely; flexural strength, initial shear strength, bond strength and shear strength seemed not to be significantly influenced by scale. The parametric study has also shown encouraging results on the effect of increasing mortar strength and different grading of sands. Which all suggest that masonry models can be used to provide useful strength properties that could be used to simulate structural behaviour of whole masonry structures (for example model bridges) by using numerical models.

8.2 Recommendations

- Because of constraints in accurately and consistently constructing the masonry, the horizontal laying technique was used in this case, it is suggested that a future study should look into specific areas covered in this study but using the normal way of constructing masonry in carrying out the masonry tests at different scales.

- It is suggested that more tests are carried out in the area of characterisation of masonry properties using fracture mechanics. Much stands to be gained from the fracture mechanics properties of masonry in areas like the mechanics of crack growth in masonry under compression, incorporating of size effect formula in design codes etc.

- Further research is also suggested into the modelling of concentred loads with different eccentricities at model scales in order to establish the possible reasons for the elastic instability of the specimen seen in the application study.

REFRENCES

1. Kerr R. Flood aftermath still being felt. 2006 [cited; Available from: http://news.bbc.co.uk/1/hi/england/cumbria/4583364.stm

2. Caglar A. Earthquake research groups seek lessons from Bam earthquake. 2004[cited; Available from: http://www.parstimes.com/news/archive/2004/washfile/quake_construction_codes.html

3. Taunton PR. Centrifuge modelling of soil/masonry structure interaction [PhD]: Cardiff University, UK; 1997.

4. Burroughs PO. A study of parameters that influence the strength of masonry arch bridges using a geotechnical centrifuge. [PhD]: Cardiff University, UK; 2002.

5. Baralos P. The small scale modelling of repair techniques for masonry arch bridges using a geotechnical centriguge. [PhD]: Cardiff University UK; 2002.

6. Miri M. Modelling of repair techniques for masonry arch bridges [PhD]. Cardiff: Cardiff University; 2005.

7. Sneck T. Dependence of masonry properties on the interaction between masonry units and mortar. Proceedings of the North American masonry Conference. Colorado; 1978. p. 21-1 to -12.

8. Brocken HJP, Spiekman ME, Pel L, Kopinga K, Larbi JA. Water extraction out of moratr during brick laying: A NMR study. Materials and Structures. 1998;31:49-57.

9. Harvey RJ. Creep of concrete masonry. Cardiff: Cardiff University; 1996.

10. Lenczner D. Elements of loadbearing brickwork. Oxford: Pergamon press; 1972.

11. Sahlin S. Structural Masonry. New Jersey: Prentice-Hall; 1971.

12. Harris B, Bunsell AR. Structure and properties of engineering materials. London: Longman; 1977.

13. Moss JB. Properties of Engineering Materials. London: Butterworth; 1971.

14. Hendry AW, Sinha BP, Davies SR. Design of masonry structures. 3rd ed. London: E & FN Spon; 1997.

15. Anderson C, Held LC. The effect of sand grading on mortar properties and the tensile bond of brickwork specimens. Proceedings of the British Masonry Society, No 1; 1986; Stoke on Trent; 1986. p. 1-5.

16. Hilsdorf HK. Investigation into the failure mechanism of brick masonry loaded in axial compression. In: Jonson FB, editor. Designing ,Engineering and Constructing with masonry Products; 1969. p. 34-41.

17. Berto L, Saetta A, Scotta R, Vitaliani R. Failure mechanism of masonry prism loaded in axial compression: computation aspects. Materials and Structures. 2005;38:249-56.

18. McNary WS, Abrams DP. Mechanis of masonry in compression. Journal of Structural Engineering. 1985 857-870;111(4).

19. Hendry AW. Structural Masonry. 2nd ed. London: Macmillan Press; 1998.

20. Francis AJ, Horman CB, Jerrems LE. The effect of joint thickness and other factors on the compressive strength of brickwork. In: West HWH, Speed KH, editors. Proceedings of 2nd International brick masonry conference; 1971; Stoke on Trent, UK; 1971. p. 31-7.

21. Porto Fd, Garbin E, Modena C, Valluzzi MR. Failure modes for in plane loaded masonry walls made with thin layer mortar. 10th Canadian Masonry Symposium 2005; Banff, Canada; 2005. p. 694-703.

22. CEN. Eurocode 6 : Design of Masonry Structures .ENV 1996 -1-1. Brussels: European Committee For Standardisation; 1995.

23. Plowman JM. The modulus of elasticity of brickwork. Proceedings of the British Ceramic Society; 1965; 1965. p. 37-44.

24. Shrive NG, Jessop EL. Anisotropy in extruded clay units and its effect on masonry behaviour. Proceedings of the 2nd canadian masonry Symposium; 1980; Ottawa; 1980. p. 39-50.

25. Jessop EL, Shrive NG, England GL. Elastic and creep properties of masonry. Proceedings of the North American Masonry Conference. Colorado; 1978. p. 12-1 to -7.

26. Brooks JJ, Baker BHA. The modulus of elastcity of masonry. Masonry International. 1998 58-63;12(2).

27. BSI. BS 5628. Code of practice for use of masonry: Part 2: Structural use of unreinforced masonry. British Standards Institution; 1995.

28. Knutsson HH, Nielsen J. On the modulus of elasticity of masonry. Masonry International. 1995;9(2):57-61.

29. Riddington JR, Ghazali MZ. Hypothesis for shear failure in masonry joints. Proceedings Institution of Civil Engineers. 1990;Part 2:89-102.

30. Jukes P, Riddington JR. The failure of brick triplet specimens. Masonry International. 2001;15(1):30-3.

31. BS EN 1052-3:2002 Methods of test for masonry- Part 3: Determination of initial shear strength.: British Standards Institution; 2002.

32. Lourenco PB. A review of out-of-plane behaviour of masonry. Masonry International. 2001;14(3):67-73.

33. Sise A, Shrive NG, Jessop EL. Flexural bond strength of masonry stack prisms. Proceedings of the British Masonry Society, Masonry (2); 1988 April 1988; 1988. p. 103-6.

34. Fried AN, Li S. The influence of unit moisture content on masonry flexural strength. In: Huizer NGSaA, editor. Proceedings of the 10th IB2MAC; 1994; Calgary; 1994. p. 939-45.

35. Taha MMR, Lucero JL, Ross TJ. Examining the significance of mortar and brick unit properties on masonry bond strength using bayesian model screening. 10th Canadian Masonry Symposium; 2005; Banff, Canada; 2005. p. 742-51.

36. Groot CJWP. Aspects of brick-mortar bond. Proceedings of the 8th IB2MaC; 1988; Dublin, Ireland.; 1988. p. 175-81.

37. Shrive NG, Taha MMR. Bond strength of clay masonry prisms constructed with normal and fly ash substituted mortars. Proceedings of the 13th IB2MaC; 2004; Amsterdam; 2004.

38. Jukes P, Riddington JR. A review of masonry tensile bond strength test methods. Masonry International. 1998;12(2):51-7.

39. BSI. BS EN 1052-5:2005: Methods of test for masonry- Determination of bond strength by the bond wrench method.: British Standards Institution; 2005.

40. Janney JR, Breen JE, Geymayer H. Use of models in structural Engineering. Models for concrete structures, ACI SP-24, American Concrete Institue, Detriot. 1970:1-18.

41. Harris GH, Sabnis GM. Structural Modelling and Experimental Techniques. 2nd ed. Florida: CRC Press LLC; 1999.

42. Collins AR. The origins and design of the attack on the German dams. Proceedings of the Institute of civil Engineers; 1982 June; 1982. p. 383-405.

43. Vogt H. Considerations and investigations on the basic principles of model tests for brickwork and masonry structures. Translated from German. Garston: Building Research Station; 1956. Report No.: Library communication No 932,.

44. Hendry AW, Murthy CK. Comparative tests on 1/3 and 1/6 scale model brickwork piers and walls. Proceedings of the British Ceramic Society, No 4; 1965. p. 45-66.

45. Sinha BP, Hendry AW. The effect of brickwork bond on the load bearing capacity of model brickwalls. Proceedings of the British Ceramic Society; 1968; 1968. p. Pp 55-67.

46. Sinha BP, Hendry AW. Further tests on model brickwork and piers. Proceedings of the British Ceramic Society, No 7; 1970 February; 1970. p. 83-95.

47. Khoo CL, Hendry AW. Strength tests on brick and mortar under comple stresses for the development of a failure criterion for brickwork in compression. Proceedings of the British Ceramic Society, Lad bearing brickwork; 1973; 1973. p. 51-6.

48. Samarashinghe W, Hendry AW. The strength of brickwork under biaxial and compressive stresses. Proceedings of the 7th International Symp Load bearing brickwork; 1980; London; 1980. p. 129-39.

49. Samarasinghe W, Page AW, Hendry AW. A finite element model for the in-plane behaviour of brickwork. Proceedings of the Institute of Civil Engineers; 1982 March; London; 1982. p. 171-8.

50. Page AW. The biaxial compressive strenth of brickwork. Proc Instn Civ Engrs; 1981; 1981. p. 893-906.

51. Egermann R, Cook DA, Anzani A. An investigation into the behaviour of scale model brick walls. Proceedings of the 9th International Brick/Block Masonry Conference; 1991; Berlin; 1991. p. 628-35.

52. Hughes TG, Kitching N. Small Scale testing of masonry. Proceedings of the12th International Brick Block Masonry Conference; 2000 25-28 June; Madrid,Spain; 2000. p. 893-202.

53. Murthy CK, Hendry AW. Model experiments in load bearing brickwork. Building Science. 1966;1:289-98.

54. Kalita UC, Hendry AW. An experimental and thoeretical investigation of the stresses and deflections in model cross-wall structures. Proceedings of the International brick masonry conference. Stoke on trent; 1970.

55. Sinha BP, Maurenbrecher AHP, Hendry AW. Model and full cale tests on a five-storey croass-wall structure undwer lateral loading. Proceedings of the second International brick Masonry Conference; 1970; Londom; 1970. p. 201-8.

56. Baker LR. Manufacture and testing of model brickwork wind panels. Structural Models conference,. Sydney , Australia; 1972.

57. Duarte RB, B.P.Sinha. Lateral strength of brickwork panels with openings. Proceedings Institution of Civil Engineers, Structure and Buldings, Vol 94; 1992; 1992. p. 397-402.

58. Lourenco PB, Barros JAO. Size effect on masonry subjected to out of plane loading. 12th International Brick/Block Masonry Conference. Spain; 2000.

59. Suter GT, Keller H. Reinforced brickwork lintel study utilizing small scale bricks. Proceedings of the North American masonry Conference. Colorado; 1978.

60. Daou Y, Hobbs B. An experimental investigation of post-tensioned brickwork in fin walls. Proceedings of the Instituion of Civil Engineers, Structures and Buildings; 1992 Nov 1992; 1992. p. 429-38.

61. Qamaruddin M, B.Chandra, Arya AS. Dynamic testing of brick building models. Proceedings of the Institution of Civil Engineers; 1984; 1984. p. 353-65.

62. Tomazevic M, Weiss P. Seismic behaviour of masonry buildings: reinforced versus unreinforced masonry. Proceedings of the 9th International Brick/Block Conference, Berlin; 1991; Berlin; 1991. p. 552-9.

63. Kwan AKH, Xia JQ. Shake table tests of large-scale shear wall and infilled frame models. Proceedings of the Institute of civil Engineers; 1995; 1995. p. 66-77.

64. Alexandropoulos S. An Experimental investigation of the static and dynamic behaviour of masonry assemblages using small scale models. London: University of London; 1996.

65. Zonta D, Zanardo G, Modena C. Experimental evaluation of the ductility of a reduced scale reinforced masonry building. Materials and Structures. 2001;Vol 34:636-44.

66. Hughes TG, Davies MCR, Taunton PR, Burroughs PO. Centrifuge testing of small scale masonry. Masonry International. 2002;Vol 15(No 3):80-6.

67. Sicilia C. A study of 3D masonry arch structures using centrifuge models and FE analysis.: PhD thesis, Cardiff University, UK; 2001.

68. Bazant ZP. Scaling of structural strength. London: Hermes Penton Ltd; 2002.

69. Sabnis GM. Size effects in material systems and their impact on model studies: A theoritical approach. Proceedings of SECTAM X conference. Knoxville, TN; 1980. p. 649-68.

70. Bazant ZP. Size effect. International Journal of Solids and Structures. 2000;37:69-80.

71. Bazant ZP. Size effect in blunt fracture: concrete, rock, metal. Journal of Engineering Mechanics, ASCE. 1984;110:518-35.

72. Lourenco PB. Two aspects related to the analysis of masonry structures: size effect and parameter sensitivity.: Delft University of Technology Faculty of Civil Engineering

1997. Report No.: 97-NM-R1533.

73. Carpenteri A, Chiaia B. Embrittlement and decrease of apparent strength in large-sized concrete structures. Sadhana. 2002;Part 4(27):425-48.

74. Bazant Z, Yavari A. Is the cause of size effect on structural strength fractal or energetic-statistical.? Engineering fracture mechanics. 2005(72):1-.31.

75. RILEM. RILEM TC QFS - Quasibrittle frcature scaling and size effect- Final report. Materials and Structures. 2004 October 2004;37:547-68.

76. Carpenteri A, Chiaia B. Multifractal scaling law for the fracture energy variation of concrete structures. In: Wittmann FH, editor. Proceedings FRAMCOS-2; 1995; Freiburg, Germany: Aedificatio Publishers; 1995. p. 581-96.

77. Carpenteri A. Fractal nature of material microstructure and size effects on apparent mechanical properties. Mechanics of materials. 1994(18):89-101.

78. Carpenteri A, Ferro G. Size effects on tensile fracture properties: a unified explanation based on disorder and fractality of concrete microstructure. Materails and Structures. 1994(27):563-71.

79. Karihaloo BL. Size effect in shallow and deep notched quasi-brtittle structures. International Journal of fracture. 1999;95:379-90.

80. Abdalla HM. Strength size effect in concrete structures. Cardiff: Cardiff University; 2003.

81. Karihaloo BL, Abdalla HM, Xiao QZ. Size effect in concrete beams. Engineering fracture mechanics. 2003;70:979-93.

82. Bocca P, Carpinteri A, Valente S. Fracture mechanics of brick masonry: size effects and snap-back analysis. Materials and Structures. 1989(22):364-73.

83. Olivito RS, Stumpo P. Fracture mechanics in the characterisation of brick masonry structures. Materials and Structures. 2001;34:217-23.

84. Carpenteri A, Chiaia B, Bocca P. Size dependence of strength and fracture properties of brick masonry. Journal of Engineering Mechanics, ASCE. 1997;123(8).

85. RILEM. FMC 1. Determination of the fracture energy of mortar and concrete by means of three-point bend tests on notched beams. RILEM. London: E & FN Spon; 1994.

86. Lourenco PB. Simulations of size effect in masonry structures. In: Mihasi H, Rokugo K, editors. Proceedings FRAMCOS-3; 1998; Freiburg, Germany; 1998. p. 2001-10.

87. Sabnis GM, Aroni S. Size effect in Material systems- The state of the art. Proceedings of the Southampton 1969 Civil Engineering Materials Conference. Southamptom; 1971. p. 131-42.

88. Shrive NG. The Prism test as a measure of masonry strength. Proceedings of the British Masonry Society, No 1; 1986. p. 117-21.

89. BS EN 1052-1:1999 Methods of test for masonry- Part 1: Determination of compressive strength. London: British Standards Institution; 1999.

90. Fried A, Anderson C. A comparative study of experimental techniques for determing the flexural strength of masonry. Proceedings of the British Masonry Society, Masonry (2); 1988 April 1988; 1988. p. 98-102.

91. BS EN 1052-2:1999 Methods of test for masonry- Part: Determination of flexural strength. British Standards Institution; 1999.

92. Jukes P, Riddington JR. A review of masonry joint shear strength tests methods. Masonry International. 1997;11(2):37-43.

93. RILEM. LUM B6 : Diagonal tensile strength of small wall specimens. RILEM Technical recommendation for the testting and use of construction materials. London: E & FN SPON; 1994. p. 488-9.

94. Lawrence SJ, Page AW. Bond studies in masonry. Proceedings of the 10th IB2MaC; 1994; Calgary, Canada.; 1994. p. 909-17.

95. BS 5628. Code of practice for use of masonry: Part 2: Structural use of unreinforced masonry. British Standards Institution; 1995.

96. BS 4551: Part 1:1998. Methods of testing mortars, screeds and plasters. London: British Standards Institution; 1998.

97. Mohammed A, Hughes TG. Comparison of prototype and 1/6th model scale behaviour under compressive loading. 10th Canadian masonry symposium; 2005 June 8-12, 2005; Banff, Canada; 2005. p. 454-64.

98. Eurocode 6 : Design of Masonry Structures .ENV 1996 -1-1. Brussels: European Committee For Standardisation; 1995.

99. BSI. BS EN 13139:2002. Aggregates for mortar. London: British Standards Institution; 2002.

100. BSI. BS EN 197-1:2000. Cement. Composition, specifications and conformity criteria for common cements. London: British Standards Insititution; 2000.

101. BSI. BS EN 459-1:2001. Building lime. Definitions, specifications and conformity criteria. London: British Standards Institution; 2001.

102. BSI. BS 3921:1985. Specification for clay bricks. London: British Standards Institution; 1985.

103. BSI. BS EN 772-1:2000. Methods of Tests for masonry units- Part 1: Determination of compressive strength. London: British Standards Institution; 2000.

104. RILEM. LUM A2. Flexural Strength of masonry units. RILEM technical recommendations for the testing and use of construction materials. London: E & FN Spon; 1994. p. 459-61.

105. RILEM. LUM A3. Indirect tensile strength of masonry units (splitting test). RILEM Technical Recommendations for the testing and use of construction materials. London: E & FN Spon; 1994. p. 462-4.

106. RILEM. LUM A4. Water absorption and porosity of masonry units. RILEM Technical Recommendations for the testing and use of construction materials. London: E & FN Spon; 1994. p. 465-6.

107. Taha MMR, El-Delb AS, Shrive NG. Sorptivity: A reliable measurement for surface absorption of masonry brick units. Materials and Structures. 2001 August-September;34:438-45.

108. Baker MG. Finite element analysis of masonry with application to arch bridges. [PhD]: University of Wales Cardiff; 1996.

109. Wittmann FH. Fracture mechanics of concrete Amsterdam: Elsevier; 1983.

110. BSI. BS EN 1015-11:1999. Methods of tests for mortar for masonry- Part 11: Determination of flexural and compressive strength of hardened mortar. London: British Standards Institution; 1999.

111. BS EN 13139:2002. Aggregates for mortar. London: British Standards Institution; 2002.

112. BS EN 1015-11:1999. Methods of tests for mortar for masonry- Part 11: Determination of flexural and compressive strength of hardened mortar. London: British Standards Institution; 1999.

113. Karihaloo B. Fracture mechanics and structural concrete. London: Longman; 1995.

114. Barr B, Lee M, Hansen EdP, Dupont D, Erdem E, Schnutgen SSB, et al. Round-robin analysis of the RILEM TC 162-TDF beam bending test: Part 2- Approximation of δ from the CMOD response. Materials and Structures. 2003;36:6221-630.

115. BSI. BS 4551: Part 1:1998. Methods of testing mortars, screeds and plasters. London: British Standards Institution; 1998.

116. RILEM. MR 2. Determination of mortar consistence. RILEM Technical Recommendations for the testing and use of construction materials. London: E & FN Spon; 1994.

117. RILEM. MR 3. Workability, consistence, plasticity of mortars. RILEM Technical Recommendations for the testing and use of construction materials. London: E & FN Spon; 1994.

118. Maurenbrecher AHP. The effect of test procedures on compressive strength of masonry prisms. Proceedings of 2nd Canadian Masonry Symposium; 1980; Ottawa; 1980. p. 119-31.

119. Templeton W, Edgell GJ. The compressive strength of clay bricks ground or mortar capped. Masonry International. 1990;4(2):66-7.

120. Edgell GJ, Vekey RCD, Dukes R. The compressive strength of masonry specimens. In: West HWH, editor. Proceedings of the British Masonry Society 4; 1990; 1990. p. 131-5.

121. RILEM. LUM B3: Bond strength of masonry using the bond wrench method. RILEM: Technical recommendations for the testing and use of construction materials. London: E & FN SPON 1994. p. 481-3.

122. MRSEC. Exploring the nano world with LEGO Bricks. The University of Wisconsin - Madison Materials Research Science and Engineering Center (MRSEC); 2001.

123. Long L, Hamid AA, Drysdale RG. Small-scale modelling of concrte masonry using 1/2 scale units: A preliminary study. 10th Canadian Masonry symposium; 2005; Banff, Canada; 2005. p. 484-93.

124. Edgell GJ, Arora SK, Vekey RCD. Analysis of results of compressive strength testing. Proceedings of the British Masonry Society, No 6; 1994. p. 147-64.

125. BSI. BS EN 1052-1:1999 Methods of test for masonry- Part 1: Determination of compressive strength. London: British Standards Institution; 1999.

126. Khalaf FM, Hendry AW. Masonry unit shape factor from test results. In: West HWH, editor. Proceedings of the British Masonry Society (6). Stoke on Trent; 1994. p. 136-9.

127. Bazant ZP, Frangpool DM. Size effect hidden in excessive dead load factor. Journal of Structural Engineering. 2002;128(1):80-6.

128. Roberts TM, Hughes TG, Dandamudi VR. Progressive damage to masonry arch bridges caused by repeated traffic loading- Phase 2. Cardiff: Cardiff University; 2004.

129. Roberts TM, Hughes TG, Goutis G. Progessive damage to masonry arch bridges caused by repeated traffic loading. Cardiff: Cardiff University; 2003.

130. BD 21/97 Design manual for roads and bridges. Vol 3: Sect 4: Part 3: The assesment of highway bridges and structures.: Department of Transport; 1997.

131. Boothby TE, Domalik DE, Dalal VA. Service load response of masonry arch bridges. Journal of Structural Engineering, ASCE. 1998;124(1):17-23.

132. Hendry AW. Masonry properties for assessing arch bridges.: Transport and Road Research Laboratory; 1990. Report No.: Contractor Report 244.

133. Drysdale RC, Hamid AA. Effect of eccentricity on the compressive strength of brickwork. Journal of Brtitish Ceramic Society. 1982;30:140-48.

134. Martinez JL, Martin-Caro JA, Leon J. Masonry compressive strength enhancement under eccentric axial load. In: Roca P, Molins C, editors. Arch Bridges IV; 2004; Barcelona; 2004. p. 405-12.

135. Arora SK. Performance of masonry walls under concentrated load. Proceedings of the British Masonry Society No 2, Masonry 2; 1988; London; 1988. p. 51-5.

136. Page AW, Hendry AW. Design rules for concentrated loads on masonry. The Structural Engineer. 1988;66(17):273-81.

APPENDIX A

SIZE EFFECT CALCULATIONS FOR COMPRESSIVE STRENGTH TEST

Considering D is the reference structural size, in this case the specimen width as shown in Figure A.1 and σ_N is the nominal load at failure as defined in Equation A.1.

$$\sigma_N = \frac{C_n P_u}{D^2} \qquad \text{Equation A.1}$$

Where C_n is a dimensionless constant taken as 1 and P_u is the ultimate load at failure. Also considering that, in section 2.6.3 it has been discussed that the SEL (Equation 2.6) can be represented in terms of Equations 2.7 and 2.8. Where $X = D$ and $Y = \frac{1}{(\sigma_N)^2}$

Using the data from the compressive strength test as represented in Table A.1, a plot of Y against X can be made as shown in Figure A1.2.

From which the intercept C and the slope A can be determined and from Equation 2.8 $D_o = C/A = 7.667$

By knowing D_o, $B_o f_t$ can then be evaluated from Equation 2.8.

$$B_o f_t = \frac{1}{\sqrt{A D_o}} = 20.85.$$

σ_N from Equation 2.6 can then be calculated, since $B_o f_t$ and D_o are now known. The SEL plot using Equation 2.6 for the compressive strength data is shown in Figure 5.23. A similar procedure was followed for determining the MFSL plot for the compressive strength test data in Figure 5.23 as well as for the other tests.

D	σ_N	$1/(\sigma_N)^2$
215	5.12	0.038
215	3.87	0.067
215	4.17	0.058
215	4.22	0.056
215	4.46	0.050
96.8	5.77	0.030
96.8	5.61	0.032
96.8	4.64	0.046
96.8	5.23	0.037
96.8	4.89	0.042
53.8	12.07	0.007
53.8	10.29	0.009
53.8	10.56	0.009
53.8	11.89	0.007
53.8	9.83	0.010
35.8	11.40	0.008
35.8	9.11	0.012
35.8	10.29	0.009
35.8	9.12	0.012
35.8	8.63	0.013

Table A.1

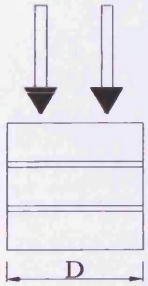

Figure A.1- Triplet compressive strength specimen

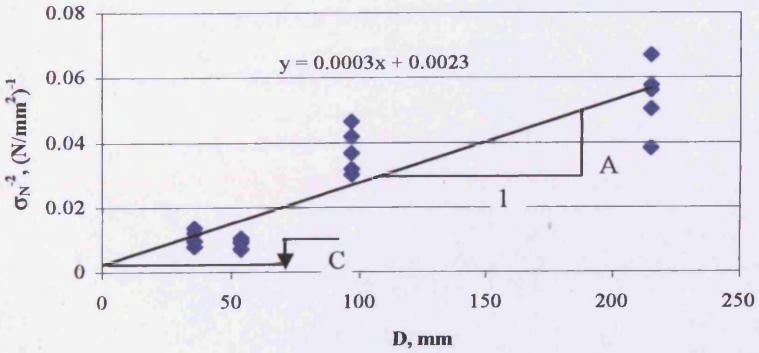

Figure A.2- Determination of *A* and *C* using the SEL.